Optimal Operating Parameters for Performance Improvement of a Biogas Fueled Spark Ignition Engine

A thesis

Submitted in Partial Fulfillment of the Requirements for the Award of the Degree of

DOCTOR OF PHILOSOPHY

By

SANTOSH KUMAR HOTTA

(146151007)

SCHOOL OF ENERGY SCIENCE AND ENGINEERING

INDIAN INSTITUTE OF TECHNOLOGY GUWAHATI

July 2023

In The Memory

of

My Beloved Father

Late Kishore Chandra Hotta

DECLARATION

I hereby certify that the work compiled in this dissertation is the outcome of the research work, performed by myself, else stated, under the guidance of **Prof. Niranjan Sahoo** and **Prof. Kaustubha Mohanty.**

Any part of this work has not been submitted for the award of any degree, diploma, associate-fellowship, fellowship or its equivalent to any university or institution.

Santosh Kumar Hotta

Registration No. 146151007
School of Energy Science and Engineering
Indian Institute of Technology Guwahati

CERTIFICATE

It is certified that the work contained in the thesis entitled **"**Optimal Operating Parameters for Performance Improvement of a Biogas Fueled Spark Ignition Engine**"** by **Mr. Santosh Kumar Hotta**, a student, in the School of Energy Science and Engineering, Indian Institute of Technology Guwahati, India, for the award of the degree of the Doctor of Philosophy, has been carried out under our supervision and, that this work has not been submitted elsewhere for the degree.

Date: 06/07/2023

Dr. Niranjan Sahoo
Professor
Department of Mechanical Engineering
Indian Institute of Technology Guwahati
Guwahati-781039, Assam, India

Dr. Kaustubha Mohanty
Professor
Department of Chemical Engineering
Indian Institute of Technology Guwahati
Guwahati-781039, Assam, India

Acknowledgements

"*Every successful work requires a lot of effort & support from many people, and this work has no difference.*"

This preface is to express the author's gratitude to all those individuals who, with their generous co-operation, guided him in every aspect to make the thesis work successful.

In presenting this thesis, the author would like to express his sincere gratitude and indebtedness to his thesis advisers **Prof. Niranjan Sahoo,** Department of Mechanical Engineering and **Prof. Kaustubha Mohanty,** Department of Chemical Engineering, IIT Guwahati, Assam for their valuable suggestion and requisite guidance in various aspects of this project work. It was a great pleasure for me to work under their supervision. This has been a precious opportunity for me to learn skills and approaches towards the work. They inspired me and remained a constant catalyst throughout the work. The constant motivation and the emotional support extended by my supervisors during my critical medical condition are unforgettable. The author is also profoundly obligated to the Director of Indian Institute of Technology Guwahati to provide such pleasing circumstances for the inception of research career.

Besides supervisors, the author would like to acknowledge the doctoral committee members, **Prof. Pinakeswar Mahanta, Prof. Vinayak Kulkarni**, **Prof. Animes Golder** for their valuable recommendations and insightful remarks throughout research activities, which has constantly engaged him towards undertaking a meaningful thesis work.

The author would like to convey his regards to the HOS, School of Energy Science and Engineering and HOD, Department of Mechanical Engineering to facilitate the administration, which helped in smooth conduction of the experimental work.

The author would like to convey his esteems to **Dr. Pankaj Kalita, Prof. U.K. Saha** for his suggestions as and when required.

Further, the author would like to express special appreciation to the senior technician and support staff of the School of Energy Science and Engineering and the Department of

Mechanical Engineering for their valuable help. The author also likes to thanks the central workshop team for their support and co-operation. The author would sincerely thank all his fellow lab-mates in the Gasdynamics Laboratory: **Dr. Jnyana Ranjan Pati, Dr. Ramesh Chandra Mishra, Dr. Asish Chaudhary, Dr. Sumit Agarwal, Dr. Soumya Ranjan Nanda, Dr. Menelik Walle**, **Dr. Abinash Mohapatro, Dr. Anil Kumar Rout, Mrs. Priyanka Dash**, **Mr. Abhishek Kamal, Mr. Anand Verma, Mr. Nikki Rajaura, Mr. Sashank Kulkarni** for all the enriching and valuable discussions and sleepless nights spent working together. Without this group, the journey perhaps would have been less fun.

The author would like to rejoice in the support from all his batch mates and colleagues from the School of Energy Science and Engineering, namely, **Dr. Sanjeev Mishra, Dr. Bidhu Bhusan Makut, Dr. Deep Bora, Dr. Praveen Tiwari, Mr. Debarshi Baruah.** The author also owes thanks to his seniors, fellow mates and Utkalika family members.

This Ph.D. journey was made smoother due to the homely atmosphere created by a few families especially providing delicious foods and arranging many memorable gatherings. The author would like to convey his gratitude to **Nibedita Madam, Sana**, **Saukhyada Madam, Mihika**, **Anita Madam**, **Lipsa Madam, Dr. Prakash Sahu and Dr. Jayashree,**

As a special mention, the author would like to convey his love to **Mrs. Kamala Kumari Hotta**, **Mrs. Rameswari Sadangi and Mr. Adwait Kumar Hotta** for their unconditional support. Last but not least, the author owes his profound gratitude towards **Dr. Krushna Prasad Sadangi**, **Mr. Sujit K. Hotta**, **Mrs. Anuradha Hotta**, **Mr. Subhransu K. Hotta, Mr. Ankit K. Hotta**, **Ms. Araydhya Hotta, Mr. S. N. Sadangi, Mrs. R. N. Sadangi** and **Dr. Debasish Sadangi** for being the constant supporting force throughout.

Santosh Kumar Hotta

Indian Institute of Technology Guwahati
March, 2023

List of Publications

Journals:

1. **Hotta, S.K.**, Sahoo, N., Mohanty, K. and Kulkarni, V., 2020. Ignition timing and compression ratio as effective means for the improvement in the operating characteristics of a biogas fueled spark ignition engine. Renewable Energy, 150, pp.854-867.
   DOI: https://doi.org/10.1016/j.renene.2019.12.145
2. **Hotta, S. K.**, Sahoo, N., and Mohanty, K., 2019. Comparative assessment of a spark ignition engine fueled with gasoline and raw biogas, Renewable Energy, 134, pp.1307-1319.
   DOI: https://doi.org/10.1016/j.renene.2018.09.049
3. **Hotta, S. K.**, Sahoo, N., Mohanty, K., 2019. Ignition Advancement Study for Optimized Characteristics of a Raw Biogas Operated Spark Ignition Engine. International Journal of Green Energy, 16(1), pp.101-113.
   DOI: https://doi.org/10.1080/15435075.2018.1544901
4. **Hotta, S. K.**, Sahoo, N., Mohanty, K. and Mahanta, P., 2018. Effect of compression ratio on the performance of a constant speed spark ignition engine operating on raw biogas. Journal of Energy and Environmental Sustainability, 5, pp. 53-57.

Conferences:

1. **Hotta, S. K.**, Rout, A. K., Sahoo, N., Mohanty K., Effect of compression ratio on the thermal efficiency and cycle by cycle variation of a raw biogas operated spark ignition engine**,** International Conference on Thermofluids-2020, Jan 23-24, 2020, KIIT, Deemed to be University, Bhubaneswar, India.
2. **Hotta, S. K.**, Sahoo N., Rout A.K., Mohanty K., and Mahanta, P., Effect of compression ratio on the cyclic variability and thermal efficiency of a biogas fueled spark ignition engine, 7nd International and 45th National Conference on Fluid Mechanics and Fluid Power, December 10-12, 2018, IIT Bombay, India
3. **Hotta, S. K.**, Sahoo, N., Mohanty K., Mahanta, P., "Effect of compression ratio on the performance of a constant speed spark ignition engine operating on raw biogas", 2nd International Conference on Sustainable Energy and Environmental Challenges, Jan 01-03, 2018, IISc, Bangalore, India.
4. **Hotta, S. K.**, Sahoo, N., Mohanty K., Mahanta, P., Choudhari, A. J., "Effect of compression ratio on the performance and emission characteristics of a raw biogas fueled spark ignition engine", 6th International Conference on Advances in Energy Research, Dec12-14, 2017, IIT Bombay, India.
5. **Hotta, S. K.**, Sahoo, N., Mohanty K., Mekonen, M. W., "Effect of air-fuel ratio on the performance and emission characteristic of a biogas fuelled spark ignition engine", 7th International Conference on Theoretical, Applied, Computational and Experimental Mechanics, Dec 28-30, 2017, IIT Kharagpur, India.
6. **Hotta, S. K.**, Sahoo, N., Mohanty K., Mahanta, P., "Comparative assessment of a spark ignition engine fuelled with petrol and raw biogas", Proceedings of the 24th National and 2nd International ISHMT-ASTFE Heat and Mass Transfer Conference (IHMTC-2017),Dec 27-30, 2017, pp.1455-1462, BITS Pilani, Hyderabad, India.
7. **Hotta, S. K.**, Singh, R., Sahoo, N., Mohanty K., Mahanta, P., "Design of a venture type biogas mixer for a four stroke spark ignition engine," 5th International Conference on Advances in Energy Research, Dec10-12, 2015, 998-1005, IIT Bombay, India

Abstract

The environmental concerns and the uncertainties associated with the future availability of fossil fuel are driving the interest of utilizing renewable biofuels in the internal combustion (IC) engines. Consideration of renewable gaseous fuels are advantageous compared to the liquid fuels due to higher hydrogen to carbon ratio and wider ignition limits. Among the renewable gaseous fuels, biogas is an attractive source of energy in rural areas and is mainly composed of CH_4 (50-70%), CO_2 (25-50%), H_2 (1-5%), N_2 (0.3-3%) with traces of H_2S.

For the large-scale utilization of biogas, it is essential to have a suitable energy conversion device such as an IC engine to efficiently convert the available energy of biogas into required mechanical or electrical forms. Most of the present applications of the commercial gaseous engine are limited to medium or high-power multi-cylinder engines. However, a significant number of small or low power single-cylinder engines are being used worldwide for different applications and are being fueled with diesel, gasoline, and kerosene. Further, the commercially available single-cylinder engines are usually gasoline or diesel-based engines and do not operate efficiently with biogas. Because of properties such as higher self-ignition temperature, higher resistance to auto ignition and knock, direct use of biogas as a standalone fuel in CI engine is almost impossible. But, the physical and chemical characteristics of biogas have a great resemblance on the octane fuels in higher compression ratio (CR) SI engines. Hence, the 'CI modified SI engine' are one of the alternative solutions to accommodate biogas and operate independently in premixed spark ignition mode. However, the conversion methodologies are quite complex and the performance of such engines (CI modified SI) deteriorate and result in derating of engine power, poor fuel conversion efficiency, poor emission-quality and higher cyclic variation. The commercial SI engines are designed to operate with the octane fuels and the combustion is initiated by means of spark ignition. Further, the method of conversion from a 'gasoline-fueled SI engine' into a gas or biogas powered SI engine is comparatively more convenient than the 'CI modified SI engine'. Hence, the 'SI converted gas/biogas engines' are the most convenient solution to use biogas as a standalone fuel in commercial SI engines.

Although SI engines are best suitable for renewable or non-renewable high-octane fuels, they need special attention to accommodate renewable gaseous fuel like biogas. The combustion process in a SI engine is greatly influenced by the operating parameters such as, compression ratio (CR), spark timing or ignition timing (ST/IT), air-fuel ratio (AFR), exhaust gas recirculation (EGR), variable valve timing (VVT), engine speed, combustion chamber design and composition of the fuel. Therefore, very precise techniques are required to efficiently operate the available commercial SI engine with raw biogas. In accordance with this fact, many researchers have proposed different approaches to convert the existing commercial CI or SI engines to operate exclusively with biogas in SI mode. Various techniques like alteration in CR and IT, preheating, pre-chamber ignition, etc. were proposed to enhance the performance, combustion and emission characteristics of the biogas fueled SI engine. Thus, one of such techniques, with proper optimization of operational parameters, can be employed to develop an efficient biogas-based SI engine.

The current research is mainly focused on the biogas fueled retrofitted SI engines. It is highly desirable to improve the performance of a variable speed SI engine if it is operated with biogas. Such engines are potential prime movers for machinery such as pump and generators used commonly in Indian farms and can also be implemented in transport sector. However, the commercial SI engines are generally gasoline or CNG based engines, which do not operate at their best when fueled with biogas. After an extensive literature survey, *the theme of this thesis is framed to determine the optimal operating parameters (optimum compression ratio, maximum brake torque timing, throttle position and optimum air-fuel ratio) of a biogas fueled SI engine through a multi fuel, variable compression ratio (VCR), spark ignited research engine setup for effective implementation in a commercial SI engine.* The theme of the thesis is being achieved through a predefined sequence of objectives.

The preliminary investigation of the study was started with a commercially customized biogas fueled constant speed SI engine (Engine 1) of rated capacity 4.4 kW. The rated power, speed, CR and IT of the engine are 4.4 kW, 1500 rpm, 13.94:1 and 15.88° CA bTDC, respectively. In this investigation the CR of the engine was further altered and operated at CR 10.52, CR 11.96, CR 13.94 and CR 15.92 with the corresponding MBT timing obtained through series of trial runs. The engine was further assessed under dynamic loading condition. Operating the engine at the rated CR (13.94) and maximum brake load

condition (74.8%) declines the rated speed of the engine by 9.3% and deteriorate the engine power by 34.5%. The maximum achievable BP and BTE of the commercial biogas engine was observed 2.88 kW and 14.84%, respectively at the rated CR.

The issues and inefficiency identified with customized commercial biogas engine (Engine1) motivated to explore the possible techniques to convert and optimize the efficiency of the existing SI engines for biogas application. Hence, further in this investigation a variable speed VCR SI engine (Engine 2) of rated capacity 4.5 kW (at 1800 rpm and CR10) has been retrofitted with a specially designed biogas induction mechanism, variable compression ratio (VCR) and variable ignition timing (VIT) mechanism to operate the engine with a wide range of CR, IT, N and ER combination. Further, before optimizing the operating parameters to have an efficient biogas fueled SI engine, the baseline investigations are carried out in the VCR SI research engine (Engine 2) to evaluate the performance of the engine with gasoline, methane and biogas. The motives behind selection of these fuels (gasoline, methane) are to establish a base line for the further investigation of the engine with biogas. The base line experiment was conducted in two stages. In the 1st stage, the optimum IT for the methane and biogas fueled engine are evaluated and reported, 40^{o} and 45^{o} CA bTDC. In the 2nd stage the comparative assessment of gasoline, methane and biogas fueled the VCR SI engine at CR 10 at WOT revealed that, the biogas fueled SI engine produced an average of 17.5% and 4.5% less BP than that of the gasoline and methane fueled SI engine respectively at WOT operating condition.

Further to determine the near optimal operating parameters (CR, IT, throttle position and ER) of the biogas operated VCR SI research engine, the investigation was planned in three stages. At the 1st stage, the influence of operating ITs are inspected at different operative CR and speed range of the engine. The IT is progressively advanced from 23^{o} to 55^{o} CA bTDC for each operating CR and engine speed configuration while the operating ER is maintained constant (ϕ =0.79~0.80). The CR and engine speed are progressively varied from CR 8 to CR 14 and 1400 to 1700 rpm, respectively. Based on the overall performance of the biogas fueled engine, the optimum ITs are identified for each operative CR and speed range of the engine. Similarly, at the 2nd stage of investigation, the influence of the operating CR over the speed range of the engine is analyzed with the respective MBTs. The CR is progressively advanced from CR 8 to CR 14 for each operating speed of the engine by retaining the ER almost constant (ϕ = 0.80~0.83). The optimum CR

is identified over the operating speed range of the engine based on the overall performance of the engine.The MBT timings of biogas fueled engine are reported 53^{o}CA, 49^{o}CA, 45^{o}CA, 39^{o}CA, 33^{o}CA, 29^{o}CA and 25^{o}CA bTDC, respectively at CR 08, 09, 10, 11,12, 13, and 14. The optimum CR was reported CR 12. The maximum BP, BTE of the engine with the optimum CR and IT configuration was reported 3.5 kW and 30.3%, respectively. Further, at the 3rd stage of the investigation, the influence of operating ER (ϕ) over the operating speed range of the engine is identified for the optimum CR and IT setting of the engine. The ER is progressively varied from 0.744 to 1.109 (A/F ratio: 5.11 to 7.16) over the operating speed range for the optimum CR and IT configuration. Based on the overall performance, the optimum ER is identified and reported 0.92.

Further, in the process of developing a biogas fueled SI engine, the optimized operating parameters (CR, IT, TP and ER) attained through series of experiments in the VCR SI research engine setup was incorporated in a commercial SI engine (Engine 3) (Make: Honda, Model: GX 200) commonly used for the stationary power generation application. The particular model (Honda, GX 200) variable speed SI engine with a fixed CR (8.5:1) and rated capacity of 3.7 kW at 3600 rpm. However, due to manufacturing constraints, the operating CR of the commercial SI engine (Engine 3) could not be enhanced beyond 9.5:1 even after the alteration Hence, The CR and IT of the commercial SI engine has been set to CR 9.5:1 and 50°CA before bTDC. The maximum achievable BT and BP of the engine are reported 11.97 N-m and 2.94 kW, respectively at 2347 rpm and WOT condition of the engine. Due to biogas mode operation, the rated power of the engine (3.7 kW@ 3600 rpm) was derated and dropped by 20.54%. However, the drop is quite acceptable due to the lower calorific value of biogas. The average fuel consumption of the engine was also estimated as 2.05 kg/h (1.84 m^3/h) and 1.16 kg/h (1.04 m^3/h) at WOT and PT operating condition of the engine, respectively. The maximum achievable brake thermal efficiency of the engine was found 30.37% at 2347 rpm at WOT condition.

Contents

Abbreviations

ACP	Average Cylinder Pressure
AFR	Air-Fuel Ratio
AKI	Anti-Knock Index
BIS	Bureau of Indian Standards
BMEP	Brake Mean Effective Pressure
BP	Brake Power
BS	Bharat Stage
BSEC	Brake Specific Energy Consumption
BTE	Brake Thermal Efficiency
CA	Crank Angle
CC	Combustion Chamber
CCV	Cycle-by-Cycle Variations
CDI	Capacitive Discharge Ignition
CHP	Combined Heat and Power
CHRR	Cumulative Heat Release Rate
CI	Compression Ignition
CNG	Compressed Natural Gas
CO	Carbon Monoxide
CO_2	Carbon Dioxide
COV	Coefficient of Variations
CR	Compression Ratio
CR	Compression Ratio
DAS	Data Accusation System
DI	Direct Injection
DIS	Direct Ignition System
ECU	Electronic Control Unit
EGR	Exhaust Gas Recirculation
ER	Equivalence Ratio
ES	Emission Sensor
IA	Ignition Advance

IAS	Idle Air Sensor
IC	Internal Combustion
IEA	Internal Energy Agency
IMEP	Indicative Mean Effective Pressure
IP	Indicated Power
ISFC	Indicative Specific Fuel Consumption
IT	Ignition Timing
ITE	Indicative Thermal Efficiency
LNG	Liquid Natural Gas
LPG	Liquefied Petroleum Gas
LPM	Liter per Minute
LPMGT	Location of the Peak Mean Gas Temperature
LPNHRR	Location of the Peak Net Heat Release Rate
LPP	Location of the Peak Pressure
MBT	Maximum Brake Torque
MFB	Mass Fraction Burnt
MGT	Mean Gas Temperature
MN	Methane Number
MN	Methane Number
MON	Motor Octane Number
NG	Natural Gas
NHRR	Net Heat Release Rate
NO_X	Nitrogen Oxides
PCP	Peak Cylinder Pressure
PFI	Port Fuel Injection
PM	Particulate Matter
PMGT	Peak Mean Gas Temperature
PNHRR	Peak Neat Heat Release Rate
PS	Pressure Sensor
PT	Part Throttle
RAFR	Relative Air-Fuel Ratio
RBA	Rapid Burn Angle

RON	Research Octane Number
SA	Spark Advance
SFC	Specific Fuel Consumption
SI	Spark Ignition
TCD	Thermal Conductivity Detector
TCI	Transistor Coil Ignition
TP	Throttle Position
TPS	Throttle Position Sensor
TS	Temperature Sensor
UHC	Unburnt Hydrocarbons
V_C	Clearance Volume
VCR	Variable Compression Ratio
VE	Volumetric Efficiency
VIT	Variable Ignition Timing
V_S	Swept Volume
VT	Valve Timing
VVT	Variable Valve Timing
WOT	Wide Open Throttle

List of Figures

List of Tables

CHAPTER 1

Introduction

Overview

Since last few centuries internal combustion (IC) engines have been widely adopted as the power source for many engineering systems and subsystems due to their high-power density and efficiency. The combustion process is one of the efficient energy conversion methods where the chemical energy of the fuel is directly converted to heat. Therefore, it can be underlined that, the human activity is greatly influenced by and rely on the fossil fuel energy. However, the exponential growth of population over the last decades has led to immense growth in fossil energy demand. In order to meet the current fossil energy demand, the usage of alternative and renewable fuels along with efficient combustion systems are the subjects of investigation by many researchers. Waste to energy is a popular concept for generating energy in developed countries. Biogas production from organic waste is one of the possible methods for producing energy from waste. Hence, the present chapter starts with the current energy scenario and the role of conventional fossil fuels in the IC engines at different sectors around the world. This section also includes the issues and limitation that arises due the extreme use of these natural resources and suggests the potential renewable alternative fuels (alcohols, vegetable oils, natural gas, liquefied petroleum gas (LPG), hydrogen, biogas, and producer gas) that can be effectively used to address the needs and issues raised by the conventional fossil fuels. Further, in this section the importance and the application of biogas has also been highlighted and suggested as a suitable alternative to gasoline in SI engines through its composition and physicochemical properties. The SI engines available for biogas application are explicitly discussed. Along with this, the shortfalls are also highlighted followed by the methods suggested for enhancing the performance of the biogas fueled SI engines. This section also includes the existing emission norms implemented by the international and national agencies followed by the summary of the chapter.

1.1 Motivation

The exponential growth of the world's population and the strongly increased technological development in the mechanized and fast-moving world led to a complex situation in the field of energy supply. The demand for energy is set to increase significantly, driven by increase in prosperity in the developing world. As per the literature, the global energy demand in the 'Reference Scenario' is projected to increase by 53% between 2004 and 2030, with an average annual growth rate of 1.6% (Birol, 2006). Similarly, the global energy demand in the 'Evolving Transition (ET) Scenario' is projected to increase by 47% between 2000 and 2040 with an average annual growth rate of 1.6% (Dudley, 2019). Most of this energy demand is expected to be contributed by the fastest growing developing non-OECD (Organization for economic cooperation and development) countries, led by India and China, as shown in **Fig. 1. 1**. As an estimate, over 70% of this increase is expected from the developing countries from which the combined share of India and China is assumed to reach 29.5% of the global energy share by 2040 (Dudley, 2019). Therefore, an amicable solution is essential in global prospective to meet the required energy demand. In that context "energy autonomy" is considered as a key factor for sustainable development in the developing countries and can be achieved by diversification of energy sources (Jaramillo et al., 2018). However, much of the global energy demand is still being achieved by fossil fuels in the form of petroleum oil, natural gas, and coal. The current share of fossil fuel in the global energy demand is 86.6% and is expected to reduce by a small percentage to 73.6% by 2040 (Dudley, 2019). Therefore, fossil fuels are assumed to remain as a dominant source of primary energy in global scenario and will be replaced by renewable forms of energy gradually.

Amongst the various sources of global energy demand, a major share is contributed by the industrial and transportation sectors. According to the report published by *BP Energy Outlook 2019*, the industrial sector (mining, manufacturing, agriculture, and construction) holds the largest share and accounts for more than 42% of the global energy demand over the entire projection period. The energy demand of the global industrial sector is expected to increase by 89% from 2000 to 2040. Similarly, the transportation sector also holds an appreciable share percentage in the global energy market and accounts for almost 21%. The energy demand of

the world transportation sectors is expected to increase by 78% from 2000 to 2040 (Dudley, 2019). Although the industrial sector remains the largest energy demanding sector throughout the projection period, energy demand in all other sectors grows more quickly than that the industrial sector both in the ET and reference scenario (IEO, 2017; Dudley, 2019). The average growth of the energy demand in the industrial sector is 1.8% per year, whereas it is expected to grow by 2.1% per year in the transportation sector. Hence, the energy demand in the transport sector should be considered seriously. In the ET scenario, the share of oil in the transport sector is estimated to decrease to 86% by 2040 from 95% in 2010.The transportation sector, an essential part of our modern society, represents the largest part of the petroleum-based fuels consumption. Its importance has continuously grown at a very fast rate over the last century (Dagaut and Cathonnet, 2006).

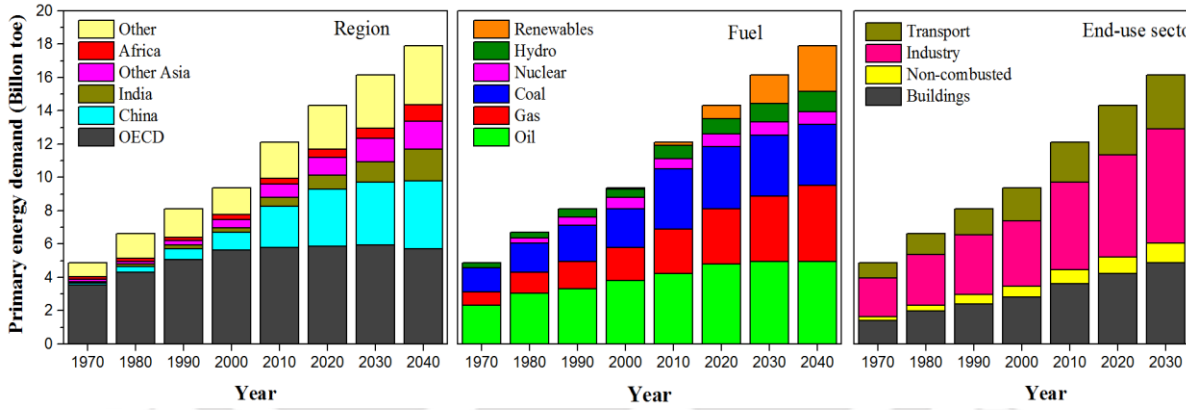

Fig. 1. 1: World energy transition through three different lenses (Dudley, 2019)

Different fuels contribute in a significant way for the transportation sector. Natural gas, electricity, and biofuels together account for more than half of the increase inenergy used in transport, with each contributing around 5% of transport demand by 2040. Despite the increasing use of natural gas, electricity and biofuels, the energy consumption in the transport sector is continuously dominated by oils (Dudley, 2019) as shown in **Fig. 1.2**. Petroleum based fossil fuels (oil and gas) are mainly used for transportation, agriculture and power generation activates by the internal combustion (IC) engines. Majority of transportation vehicles are propelled with IC engine power. As an estimate, at the beginning of the 21st centuries, more than 600 million vehicles are engaged in transportation (Cholakov, 2010). The world reserve of fossil fuel is undoubtedly limited and decaying at a faster rate due to its increased demand

(Ravi et al., 2017).Due to the extreme use of these natural resources, there is a growing concern that the world may run out of the petroleum-based fuel recourses. As of today, fossil fuels contribute about 86% of energy expenses, and among them, petroleum fuel played the dominant role and held a share of 56%, as shown in **Fig. 1. 2**. Hence there is a need to conserve petroleum resources by its judicious use and substituting it by other alternatives wherever possible.

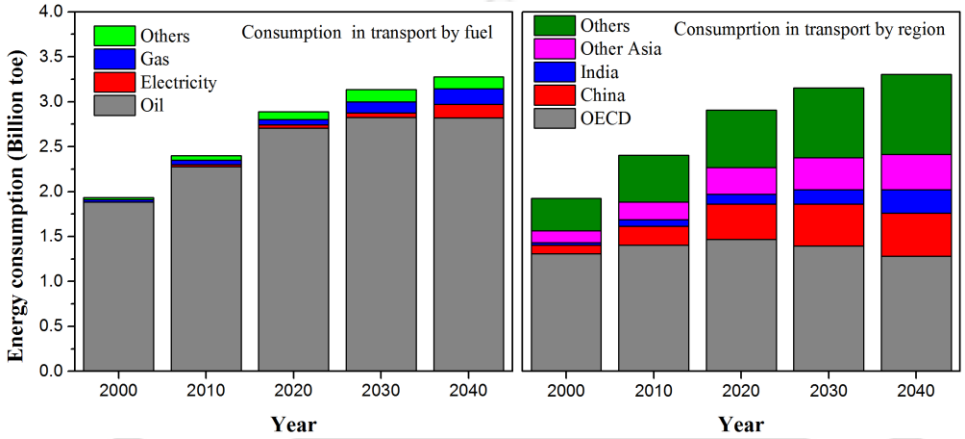

Fig. 1. 2: World energy consumption in the transport sector (Dudley, 2019)

Apart from petroleum conservation, there is a worldwide threat to the environment due to the pollutants from sources burning conventional fossil fuels. Considering the transportation sector in recent times, large quantities of fossil fuel have been used and polluted the global environment with harmful emissions by automobiles (Qian et al., 2017). During the stages of production and use of these fuels, the negative impact on the environment is an important factor (Kemal and Sayin, 2014; Pan et al., 2014). The most harmful pollutants are carbon monoxide (CO), carbon dioxide (CO_2), particulate matter (PM), nitrogen oxides (NO_X), sulfur oxides (SO_X), and unburnt hydrocarbons (UHC). Combustion of these fossil fuels also increase the global CO_2 level. In the ET scenario, the cumulative CO_2 emission of all sectors due to the combustion of fossil fuel is 33.6 Gt in 2017. The power, industry and transport sectors are the major contributor to the rise in global CO_2 level and hold a share of 37%, 27% and 24%, respectively as shown in **Fig. 1. 3**. As predicted, the global CO_2 level may grow by 7.9% in 2040, with a major share of 39%, 27% and 24% in power, industry and transport sector, respectively (Birol, 2006).According to the report published by *Internal Energy Agency (IEA)*,

China and United States are the major CO_2 contributors and account almost 28% and 15%, (Birlo, 2018) respectively to the global CO_2 emission as shown in **Fig. 1. 3**. Further, the environment is being polluted due to continuous emission of methane (CH_4) from sources such as anaerobic decomposition of organic wastes in landfills and natural wetlands, burning of biomass, emission from the livestock production system, fossil methane emission during the exploration and transport of fossil fuels (Heilig, 1994). Emissions of methane from these sources are even more potent as a pollutant and considered as the worst greenhouse gas than the CO_2 emitted from the combustion of fossil fuel. As a consequence of increased CO_2 and CH_4 level in the global environment, the global average temperatures increases (Aydin et al., 2010). The overreaching goal of Paris climate agreement aims to hold the increase in global average temperature to well below 2° C and pursue efforts to limit the temperature increase to 1.5° C above industrial levels (Rogelj et al., 2016), thus prevent the emission of greenhouse gases. Because of the global policy change, renewable energy researchers are to be reoriented to decrease the carbon footprint (Kwon et al., 2017). To address the issues of environmental degradation and the uncertainties associated with the future availability of conventional fossil fuel, the major research aspect of combustion and engine development are oriented towards exploring efficient combustion systems and renewable sources of energy (Sahoo et al., 2009).

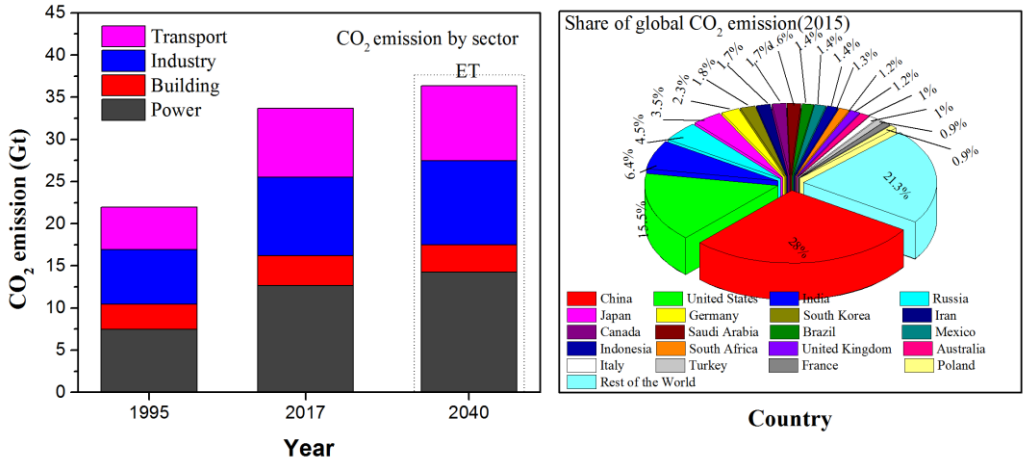

Fig. 1. 3: Share of global carbon dioxide emission from fuel combustion (Birol, 2006; Dudley, 2019; IEO, 2017)

Liquid fuels like alcohols and vegetable oils, gaseous fuels such as natural gas, liquefied petroleum gas (LPG), hydrogen, biogas, and producer gases are the promising

sources of energy and are alternatives to gasoline and diesel in conventional IC engines (Porpatham et al., 2012). Natural gas and LPG are the readily available petroleum-based fuels, while hydrogen, biogas and producer gas can be obtained from renewable sources. Uses of gaseous fuels in IC engines are more advantageous because of their higher hydrogen to carbon ratio compared to the liquid fuels. Additionally, gaseous fuel has the competence to form a homogenous mixture and has a wider ignition limit compared to that of liquid fuels. Moreover, very low levels of pollutant emissions reported when gaseous fuels are effectively utilized in spark ignition (SI) and compression ignition (CI) engines. Among these renewable gaseous fuels, biogas is an attractive source of energy in rural areas. It can be produced from various raw materials by thermochemical or biochemical conversion methods (Qian et al., 2017). The most common sources of biogas are the landfill and digester gas, which are the byproduct of anaerobic digestion of organic and plants matters (such as cow dung, animal manure, rice straw, leaves, and water hyacinth) under controlled conditions (Huang and Crookes, 1998b; Montoya et al., 2015). Most of these raw materials are renewable and are readily available in the county side. The application of such renewable fuel circulates CO_2 between the air and the fuel, and thus do not affect the net CO_2 in the environment (Porpatham et al., 2008; Qian et al., 2017). Research carried out on anaerobic digestion of verity of biomass, agricultural waste, and cooked waste indicates that there is great variability in the composition of the biogas generated. Biogas primarily consists of 50-70% of methane, 30-40% of carbon dioxide along with traces of other gases such as hydrogen (H_2), nitrogen (N_2) and hydrogen sulfide (H_2S) (Huang and Crookes, 1998b).Anaerobic digestion not only offers an effective way to manage manure by addressing the principal problem of odor control, but it also opens an opportunity to create energy from the conversion of biogas with a system of combined heat and power (CHP). Hence, it is considered to be an alternative option to alleviate the problems of fossil fuel depletion and environmental pollution.

For the largescale utilization of biogas, it is essential to have suitable energy conversion device such as an IC engine to efficiently convert the available energy of biogas into required mechanical or electrical forms. As reported in the literature, commercial CI or SI engines have been retrofitted and fueled with compressed natural gas (CNG) (Mello et al., 2006; Sahoo et al., 2009; Ma et al., 2012), LPG (Lee and Ryu, 2005; Selim et al., 2008; Pana et al., 2010; Ravi

et al., 2017) and hydrogen (Das et al., 2000a; Das, 2002, 1990; Sadiq Al-Baghdadi, 2004; Thurnheer et al., 2009)for use in transportation, power generation and agricultural applications in the recent years. Such engines are limited to medium or high-power rating with multi-cylinder configuration along with specially designed combustion and exhaust gas treatment systems. However, a significant number of small or low power single cylinder engines are being used worldwide for different applications. The uses of this kind of engines are significant in rural or remote areas of developing countries. Presently biogas is being utilized in a limited scale in dual fuel engines which partially utilize the diesel fuel. Because of some properties like, higher self-ignition temperature, higher resistance to auto-ignition and knock, direct use of biogas as a standalone fuel in CI engine is almost impossible (Porpatham et al., 2012; Bora et al., 2014; Jaramillo et al., 2018). However, biogas can be used in a CI engine with dual fuel approach along with a pilot spray of diesel-like fuel that has a low self-ignition temperature (Porpatham et al., 2007).As reported, the pilot fuel substitution is around 80-90% (Bora and Saha, 2015a, 2016; Jaramillo et al., 2018), allowing the premixed combustion of the lean mixture to dominate over diffusion combustion and decreases soot emission. Since the dual fuel engines depend on the pilot fuel injection to ignite the air-biogas mixture, their use in remote and rural areas with "poor diesel substitution" can be an infeasible solution for power generation or agricultural application. But, the physical and chemical characteristics of biogas have a great influence on the application of biogas specifically in higher compression ratio (CR) SI engines (Porpatham et al., 2007; Qian et al., 2017). At one end, considering biogas as a fuel, the presence of CO_2 remains an issue, since it is an incombustible diluent gas and its presence in biogas lowers the heat of combustion (Pan et al., 2014). On the other hand, the presence of CO_2 in biogas combustion lowers NO_x emission and permits the engine to operate at higher CR (Huang and Crookes, 1998b). Thus, lower NOx emissions, higher octane rating, higher auto ignition temperature, higher anti-knock index, and large-scale availability make biogas as a suitable fuel for the SI engines. However, due to certain drawbacks such as derating of engine power (Bora et al., 2014), poor fuel conversion efficiency, poor emission quality (Chaudhari et al., 2019), higher cyclic variation triggered by the diversified composition of biogas (Kwon et al., 2017), the cold starting issue and the difficulty in manufacturing biogas engine are the key demerits (Surata et al., 2014).

Although SI engines are best suitable for renewable or non-renewable high-octane fuels, they need special attention to accommodate renewable gaseous fuel like biogas, due to the enhanced complications of associated systems. The combustion process is characterized by the combustion duration, combustion completeness, and the form factor in an engine (Carrera et al., 2013). CR, spark timing or ignition timing (ST/IT), air-fuel ratio (AFR), exhaust gas recirculation (EGR), variable valve timing (VVT), engine speed, combustion chamber design and composition of the fuel are some of the important factors which influence the combustion phasing and evaluate the performance and efficiency of a SI engine (Porpatham et al., 2013a; Alagumalai, 2014; Corti et al., 2014). Therefore, very precise techniques are required to efficiently operate the available commercial SI engine with raw biogas. In accordance with this fact, many researchers have proposed different approaches to convert the existing commercial CI or SI engines to operate exclusively with biogas. Various techniques like alteration in CRand IT (Huang and Crookes, 1998b; Huang and RJ, 1998; Porpatham et al., 2008, 2012; Montoya et al., 2015), preheating (Alasfour, 1998; Azpiazu et al., 1990), pre-chamber ignition (Roubaud et al., 2002; Roethlisberger and Favrat, 2002a, 2002b), etc. were proposed to enhance the performance, combustion and emission characteristics of the biogas fueled SI engine. Thus, one of such techniques, with proper optimization of operational parameters, can be employed to develop an efficient biogas fueled SI engine.

1.2 Liquid and Gaseous Fuels for SI Engines

Fossil fuels are always at the center of growth and trade since industrialization reorganized economics to manufacturing goods (O'sullivan and Sheffrin, 2002). In many applications, petroleum-derived fossil fuels displaced coal and also dominating as major fuel in the transport sector. IC engine is the major backbone of the transport sector and can be powered by different forms of fuel such as liquid, gaseous, and even solid fuels (Ganesan, 2015). The characteristics of the type fuel used have a significant influence on the design, efficiency, output, and particularly the reliability and durability of the engine. Further, the characteristics of the fuel also play a vital role in the atmospheric pollution caused by the IC engines used in automobiles. As of today, most of the modern IC engines are powered by liquid and gaseous fuels which are commonly the derivatives of liquid petroleum. Gasoline, diesel,

compressed natural gas (CNG) and LPG are the commonly used fossil fuel derived petroleum resources. The most notable of these is gasoline, usually used as a liquid fuel in SI engines. It is a complex mixture of hydrocarbons that includes aromatic, naphthenic, olefin and paraffin compounds containing five to twelve carbon atoms with boiling point ranging from 30 to 200°C. This mixture results in incomplete combustion and formation of partially oxidized compound (Mello et al., 2006) when used in conventional SI engines. However, the unleaded gasoline is quite greener and produces lesser CO emission compared to the normal gasoline. Apart from this, resistance to knock is an extremely important characteristic of the fuels used in SI engines. These fuels differ widely in their ability to resist knock depending on their chemical composition and are defined by research octane number (RON) or motor octane number (MON). Indian companies such as BPCL, IOCL, HPCL, IBP red and Shell supply different graded gasoline to power vehicles driven by SI engines. The higher graded gasoline has comparatively higher octane rating and costs more (Chaudhari, 2017). The octane rating reflects the quality, purity, refinement, efficiency, and heat bearing capacity of gasoline. Hence, there is different graded gasoline for different application ranging from road to spacecraft. The recommended specification of gasoline/petrol approved by the Govt. of India is listed in **Table 1. 1** (Chaudhari, 2017)**.** The Physio-chemical properties of selected fuels such as gasoline (Heywood, 1988; Yüksel and Yüksel, 2004; Balki and Sayin, 2014; Bae and Kim, 2017; Ravi et al., 2017), methanol (Ryan III and Lestz, 1980; El-Emam and Desoky, 1985; Heywood, 1988; Balki and Sayin, 2014; Bae and Kim, 2017), ethanol (Liu et al., 2007; Balki and Sayin, 2014; Bae and Kim, 2017), LPG (Porpatham et al., 2012; Bae and Kim, 2017; Ravi et al., 2017), hydrogen (Porpatham et al., 2012; Bae and Kim, 2017; Ravi et al., 2017), CNG (Das et al., 2000a; Porpatham et al., 2012; Ravi et al., 2017), methane (Porpatham et al., 2008; Bae and Kim, 2017) and biogas (Jeong et al., 2009; Porpatham et al., 2012) as mentioned in the cited literature are represented in **Table 1. 2**. Besides, increasing fossil fuel price based upon the type of the gasoline being used, emission of greenhouse gases, the energy security and diversity are forcing the global community to search for renewable and alternative sources of fuel that can be utilized in SI engines.

Table 1. 1: Indian gasoline specification (Kisan et al., 2017, 2008)

Sl. No	Characteristics	Unit	BS II	BS III	BS IV	BS VI
1	Color, Visual		As decided by Refiners / Marketers			
2	Density,15°C		710-770	720-775	720-775	720-775
3	Distillation					
A	Recovery upto 70°C (E 70)	% vol	10-45	10-45	10-45	10-45
B	Recovery upto 100°C (E 100) percent by volume	% vol	40-70	40-70	40-70	40-70
C	Recovery upto 150°C (E 150) percent by volume, Min	% vol	-	75 min	75 min	75 min
D	Recovery upto 180°C (E 180) percent by volume, Min	% vol	90	-	-	-
E	Final boiling point, Max	°C	210	210	210	210
F	Residue max	% vol	2	2	2	2
4	Research Octane Number (RON), min		88			
A	MG 91		-	91	91	91
B	MG 95		-	95	95	95
5	Anti knock index (AKI)/MON, min		84(AKI)			
A	MG 91		-	81	81	85
B	MG 95		-	81	81	95
6	Sulphur, total max	mg/kh	0.05%	150	50	10
7	Lead content (Pb), max	g/l	0.013	0.05	0.005	0.005
8	Vapor pressure max	kPa	35-60	60	60	60
9	Benzene content	% vol	-	1	1	1
A	Metros		3			
B	For the rest		5			
10	Olefin content, Max	% vol				
A	MG 91		-	21	21	21
B	MG 95		-	-	18	18
11	Aromatic content, Max	% vol	-	42	35	35

The alternative fuels, also known as non –conventional or advanced fuels are defined as the fuels, which can be effectively utilized in IC engines except diesel and gasoline. The alternative fuels are anticipated to produce power with economical fuel consumption and minor emission of pollutant. Further, they should be safe enough to handle, store and transport both for stationary and mobile applications. Provision of local production and easy distribution through local market turn out alternatives fuels to be more attractive to use. Further, an alternative fuel is acceptable when any combination of engine technology and fuel meets the

prescribed vehicular emission norms as far as environmental perspective is concerned (Thipse, 2010). The alternative fuels are mainly classified into three categories. The petroleum fuel with non–petroleum additives namely ethers fall in this first category. Other non-conventional solid and liquid fuels fall into the second kind, and the non-petroleum fuels such as alcohols, biofuels, biogas, producer gas, hydrogen, etc. are listed in the third category of alternative fuels (Krylov and Tonkonogov, 2005). Among these alternatives, biofuels and biogas are seemed to have a significant role in the present-day scenario of energy crises because both of them can be produced locally from renewable sources. This helps in generating employment and support the local economy by eliminating the drainage of national currency spent on petroleum import. Further, for the ease of understanding, the alternative fuels used in SI engines are classified as non-renewable octane fuel and renewable octane fuel.

1.2.1 Non-renewable octane fuels

An octane fuel derived from resources that cannot readily be replaced by natural means to meet the rate of consumption is known as non-renewable octane fuel. Liquid fuel such as gasoline, gaseous fuels such as liquefied petroleum gas (LPG), natural gas (NG) and compressed natural gas (CNG) are some of the examples of non-renewable octane fuel.

The liquid petroleum gas (LPG) is a promising non-renewable gaseous and alternative fuel used widely in SI engines and also known as AUTOLPG gas. LPG as a byproduct of petroleum refining mainly consists of propane (C_3H_8) and butane (C_4H_{10}) in a specific ratio. Although propane and butane are the main constituents in LPG, it may also include iso-butane and n-butane in various proportions. It can be also produced from natural gas and shell gas. It is generally stored in the cylindrical vessel as liquid at a pressure in the range of 10-15 bar which eliminates the requirement of the fuel pump in SI engines (Ravi et al., 2017). Its calorific value (LHV- 47.5 and HHV- 49.53 kJ/kg), greater flame velocity (38.25 $cm.s^{-1}$), wider ignition limit (1.4-7.6 vol% in air) and higher octane number (103-105) make LPG as a better fuel than gasoline in SI engines (Ravi et al., 2017). Further, the higher auto ignition temperature and research octane number (RON) of LPG enables the SI engine to operate at higher CR and thereby increases the thermal efficiency of the engine. However, the energy density of LPG (26 $MJ.\ L^{-1}$) is lower than that of gasoline, as its relative density is lower and about 0.557 $kg.m^{-}$

^{3} compared to 737 kg.m^{-3} for gasoline. Hence the equivalent fuel consumption is higher in LPG fueled SI engines. Although, LPG is a remarkable alternative to gasoline, the advantageous of LPG can fully exploit when it is used in gasoline engines with well-developed technologies of conversion application. For, example, LPG fueled cars having fuel system converted from gasoline cannot take advantages of higher-octane rating of LPG because of no change in the structural component of the engine. Similarly, LPG provides less lubrication in the upper cylinder than that of gasoline or diesel. Hence the LPG fueled engines are more prone to valve wear, if they are not suitably modified. Only those which are specifically manufactured for the LPG application would have higher CR and can achieve higher thermal efficiency.

Natural gas is a naturally occurring, non-renewable fossil fuel formed due to decomposed plant and animal matter when exposed to intense pressure and heat under the surface of the earth for a million years. It is primarily composed of methane (CH_4) up to 94% followed by traces of other hydrocarbons such as ethane (C_2H_6), propane (C_3H_8), butane (C_4H_{10}), carbon dioxide (CO_2) and nitrogen (N_2) (Bae and Kim, 2017; Das et al., 2000b). It is generally stored as compressed natural gas (CNG) in high-pressure storage tanks (20- 25 MPa) at ambient temperature and as liquid natural gas (LNG) at supercooled condition (-120 to -170°C) in nearly atmospheric pressure. LNG has a higher cost of production and storage as compared to CNG due to the specific requirement of the expensive cooling system and cryogenic tank. However, CNG requires a higher pressure and much larger volume to store energy equivalent to gasoline. As a consequence, LNG is generally used for transporting NG over large distances over ships and trains, where it is further re-gasified and converted to CNG before distribution to the end. The physical properties and its typical composition are shown in **Table 1. 2.**

CNG has been used frequently as an alternative to gasoline in SI engines due to its favorable physio-chemical properties. CNG is an octane fuel and has a very high octane rating (RON: 120-130) compared to gasoline (RON: 83-93) (Das et al., 2000b). Further, the simple, stable molecular structure and the absence of long carbon-carbon chain allows the engine to operate without knocking even at high CR and increases the BTE (Bae and Kim, 2017). The LHV of CNG is 14% greater than that of gasoline. Hence, the BSFC of CNG fueled engines is

less than that of gasoline throughout the speed range of the engine. The higher hydrocarbon ratio and the homogenous mixture formed by the CNG engine produces lower CO, non-methane HC emission, and expected to reduce the CO_2 and particulate matter (PM) emission (Aslam et al., 2006; Mello et al., 2006). However, more than 90% of the unburnt HC emission is methane, and it has a higher potential for global warming than that of CO_2. Further, due to the higher cylinder temperature, the NO_x emission of the CNG fueled engine is higher than that of gasoline (Jahirul et al., 2010). Hence, the methane and NO_x emission have to be taken care for CNG fueled SI engine. Additionally, the traditional gaseous fuel induction mechanism implemented in CNG engines reduces the volumetric efficiency and results 16% drop introduced torque as compared to gasoline engine (Cho and He, 2007). Hence, direct injection (DI) or port fuel injection (PFI) techniques have to be integrated for better efficiency and optimized operation of CNG fueled SI engines.

1.2.2 Renewable octane fuels

Octane fuels produced or derived from renewable sources are termed as renewable octane fuels. Liquid fuel such as alcohols (methanol and ethanol), gaseous fuels such as compressed natural gas (CNG), hydrogen, methane, and biogas produced from renewable sources are the promising renewable octane fuels.

Methanol (CH_3OH) is an alternative, sustainable, and remarkable octane fuel and has a significant effect on the performance of a gasoline-fueled SI engine (Seko et al., 1986). It can produced from a wide variety of renewable energy sources such as gasification of wood, coal, straw plant stalks, and combustible trashes (Vancoillie et al., 2013). It can also be synthesized during gasification combined cycles. Because of simple chemical structure and enhanced physicochemical properties (Yanju et al., 2008; Vancoillie et al., 2013) the use of methanol in SI engines results in improved brake power (BP), enhanced brake thermal efficiency (BTE) (Vancoillie and Verhelst, 2010; Vancoillie et al., 2013) and volumetric efficiency (VE) (Gong et al., 2016) and reduce the regulated emission such as CO, CO_2, HC and NO_X under specified operating condition (Brinkman, 1977; Ryan III and Lestz, 1980). However, the uses of pure methanol in SI engine are still not popularized because of the unavailability of compatible SI engines, increased NOx and formaldehyde emission. But, the uses of methanol-gasoline blends

are being recommended in the available commercial gasoline engine with or without minor modifications (Abu-Zaid et al., 2004; Liu et al., 2007). Hence, a lower fraction of gasoline-methanol blends (M3 to M30) have resulted in lower engine power and torque, and achieve higher brake mean effective pressure (BMEP) and BTE along with reduced CO and HC emission (Bilgin and Sezer, 2008; Elfasakhany, 2015) compared to gasoline.

Among the alcohols, ethanol (C_2H_5OH) has been endorsed as a good nominee as a renewable alternative octane fuel for vehicles equipped with SI engines because of similarity in the physical and combustion properties with gasoline (Kemal and Sayin, 2014). It can be produced from ethylene or from the fermentation of grain and sugar. Much of it is made from corn, sugar cane and even cellulose (wood and paper). Ethanol has a higher-octane number, oxygen ratio, flammability limit, and low carbon to hydrogen ratio. The SI engine needs minute modification for the use of ethanol (Li et al., 2010) and can even operate at higher CR without any chance of knocking and produce lower emission than the gasoline-fueled SI engines (Yousufuddin and Nawazish, 2008). Further, the higher heat of vaporization in methanol cools the intake air to the engine and increases the volumetric efficiency and power output (Xie et al., 2013). However, cold starting and lower calorific value is an issue with this kind of fuel when used alone in SI engine. Hence, blended ethanol-gasoline mixture with E85 (85% ethanol) and E10 (10% ethanol or gasohol) are recommended to be used in SI engine. E85 is basically an alcohol fuel with 15% of gasoline added to eliminate the cold stating and tank flammability issue. Similarly, E10 reduces the use of gasoline without any modification in the gasoline engine. Though the present cost of ethanol production is very high, it could be tackled with popularity, promotion and mass production of this kind of fuel. However, a very high production will lead to food –fuel competition and result in high cost of both. Hence, the use of alcohols as a standalone fuel by eliminating gasoline seems to be very difficult in the current scenario and needs further attention in this regard by the research community.

Similarly, hydrogen is the simplest and most abundant element in the earth as a fuel. Thus it offers a virtually limitless supply, that can be mass produced from renewable resources (biomass, agricultural products, and waste) or non-renewable fossil fuels (coal and natural gas) via steam reforming processes or can also be produced through electrolysis of water with

solar-generated electricity (Pan et al., 2014; Niaz et al., 2015). It is widely used fuel in industries and transport and even aerospace field due to its higher energy density in mass basis, higher flame speed, and a wider range of ignition limit as shown in **Table 1. 2**. It can be favorably used as an alternative to gasoline in SI engine due to the above-mentioned properties. The higher-octane number (120-130) and the auto ignition temperature (858 K) of hydrogen enable the engine to operate at higher CR and increases the BTE. The higher laminar flame speed (1.85 $m.s^{-1}$) and diffusion velocity (< 2.0 cm^{-1} at NTP) are the distinct combustion characteristics of hydrogen and are faster than the hydrocarbon fuels (0.3-0.5 $m.s^{-1}$). Further, the wide range of flammability limit (4-75 vol% in air) of hydrogen enables the un-throttled operation of the engine with lean combustion (Das and Khas, 1991; Bae and Kim, 2017; Ravi et al., 2017). Hydrogen is clean burning fuel and does not produce toxic products such as HC, CO, CO_2, SO or SO_2 and organic acids (Das and Khas, 1991). However, NOx is the only non-trivial engine out emission in case of hydrogen-fueled SI engines and can be eliminated by the establish approaches (White et al., 2006) such as ultra-lean combustion with lean equivalence ratios lower than 0.45 and by using a lean NO_x trap or three-way catalytic converter. The minimum ignition energy of H_2 (0.02 mJ) is much lesser than that of equivalent gasoline-air mixture (0.24 mJ) and may initiate backfire and pre ignition due to the engine hotspots (Verhelst and Wallner, 2009). Hence, the commercialization of hydrogen fueled engines are challenging due to the high knock tendency and higher NO_x emission due to high combustion temperature. The issue of hydrogen storage and handling is a major challenge and need further research and development to popularize the use of hydrogen as an alternative fuel in SI engines.

Among these renewable gaseous fuels, biogas is an attractive source of energy in rural areas. It can be produced from various raw materials by thermochemical or biochemical conversion methods (Qian et al., 2017). It can be used as a promising alternative fuel by substituting a considerable amount of fossil fuel. It is produced through anaerobic digestion of organic matters and consists of approximately 50-70% of methane (CH_4), 25-50% of carbon dioxide (CO_2), 1-5% of hydrogen (H_2), 0.3-3% of nitrogen (N_2) and traces of other impurities, notably hydrogen sulfide (H_2S) (Huang and Crookes, 1998b; R. J. Crookes, 2006). Typically, it consists of 50-70% of methane and 30-40% of carbon dioxide. However, the percentage of methane and carbon dioxide in biogas varies with the maturities of feedstock, temperature,

water content, the feed rate of raw material and bacterial action (Bari, 1996). Their abundant availability is due to the presence of non-fossil carbon resources like cattle dung, kitchen/agricultural waste, and other biomasses. Most of these raw materials are renewable and are readily available in the county side. The application of such renewable fuel circulates carbon dioxide (CO_2) between the air and the fuel, and thus do not affect the net CO_2 in the environment (Porpatham et al., 2012, 2008; Qian et al., 2017). The main constituents of the biogas can be classified into two categories: combustible components and non-combustible components. The combustible components of biogas are CH_4, CO and H_2 whereas, CO_2 and N_2 are non-combustible (Qian et al., 2017). Biogas is a possible solution for the replacement of conversational fossil fuel and has relatively higher availability. But, CO_2 is an incombustible diluent gas and its presence in biogas lower the combustion enthalpy and combustion rate of the mixture in the engine cylinder (Pan et al., 2014). The CO_2 content in biogas reduces the laminar flame speed and leads to lower fuel conversion efficiency. On account of the higher CO_2 content, the calorific value (17 $MJkg^{-1}$), density (1.11 $kg.m^{-3}$), flame velocity (25 $cm.s^{-1}$) and flammability range (7.5-14) of the biogas is lower than that of natural gas (Porpatham et al., 2012; Qian et al., 2017). The main influence of CO_2 in biogas combustion is to produce lower NO_x emission and permit the engine to operate at a higher compression ratio (CR) (Huang and Crookes, 1998b). An increasing proportion of CO_2 in biogas deteriorate the indicated power output and triggers the cyclic variation of the engine (Huang and Crookes, 1998b). Karim et al. reported that the presence of CO_2 in biogas affects the performance of the engine by increasing the average period of combustion duration and ignition lag timing (Chandra et al., 2011). Biogas with CO_2 proportion higher than 40% resulted in unusable operation of the engine. However, Biogas with CO_2 proportion of 30% has notably improved the engine performance (Bari, 1996; Midkiff et al., 2001). Methane in biogas readily mixes with air and forms a homogenous mixture and has a higher octane rating (RON- 130) (Chandra et al., 2011). Methane number (MN) is a resistance to knock quantification methodology for gaseous fuel. Like octane number uses a mixture of isooctane and n-heptane as the reference fuel, methane number is quantified with reference to the mixture of methane (CH_4) and hydrogen (H_2) (Leiker et al., 1972). The methane number of biogas (138.5-139.7) is higher than that of natural gas (NG) (59.3-59.7) (Malenshek and Olsen, 2009; Montoya et al., 2015).

Additionally, the self-ignition temperature (650°C-700°C) and the anti-knock index of biogas are very high and hence resist knock in SI engine (Qian et al., 2017). Methane and biogas are quite stable against knocking and hence can accommodate higher CR than that of the petrol fueled engines. With an increasing proportion of methane, biogas fuelled SI engine notability enhances the performance by diminishing the hydrocarbon emission, extending the flammability limit and enhancing the flame speed (Moreno et al., 2012). So, Biogas is considered as a suitable fuel for spark ignition engines. Hence, biogas fueled SI engines are allowed to operate at higher CR compared to NG and leads to higher thermal efficiency and increased NO_x emission. Biogas also contains a small percentage of hydrogen sulfide, which may lead to corrosion in metal parts of the engine. But, biogas from the renewable fuel category still stands as a promising candidate for spark ignition engines since its merits override the limitations.

Table 1. 2: Physio-chemical properties of conventional and other alternatives fuels for SI engine (accepted values from the literatures)

Properties	**Gasoline**	**Methanol**	**Ethanol**	**LPG**	**CNG**	**Hydrogen**	**Methane**	**Biogas**
Molecular formula/ Composition	$C_nH_{1.87n}$	CH_3OH	C_2H_5OH	C_3H_8- 40% C_4H_{10}- 60%	CH_4- 85% C_2H_6- 7% C_3H_8- 2% CO_2- 5% N_2- 1%	H_2	CH_4	CH_4- 55.6%# CO_2- 42.3# N_2- 2.1#
Physical state	Liquid	Liquid	Liquid	Liquid/Gas	Gas	Gas	Gas	Gas
Density at 15°C (kg/m^3)	720-775	790-792	785-790	557 (l) 2.21 (g)	0.79	0.08-0.09	0.72	1.11#
Carbon to hydrogen ratio	0.44-0.50	0.25	0.333	0.38	0.33	0	0.25	0.25-0.5
Lower heating value (MJ/kg)	43.55#	19.6-19.9	26.95	45.7	44.24-50	120	50	17#
Heat of vaporization (MJ/kg)	0.33#	1.16-1.17	0.838-0.923	0.385-0.426	-	-	0.509	0.5
Stoichiometric A/F ratio	14.7*	6.5	9.0	15.5	17.3	34.2	17.23	5.67*
Research octane number (RON)	92-98	109	107	103-105	120	120-130	120	110
Auto ignition temperature (°C)	257#	455-470	363	488-502	540	585	540-600	650
Flammability limits Leaner-Richer (vol. % in air)	1.4-7.6	5.5-36.5	3.5-15	1.9-9.7	5-15	4-75	5.45-23.41 (Cui et al., 2016)	7.5-14
Flame Speed (cm/s)	37-43	43-52.3	39-41	38.25	34	185-275	38	25
Storage and handling	Easier	Easier	Easier	Easier	Difficult	Difficult	Easier	Easier
Availability	Limited	Diverse reserve		Limited	Limited	Abundant diverse reserve		
Renewability	Non-R	R	R	Non-R	Non-R/ R	R	R	R

* Calculated, # Experimental value, R- Renewable, Non-R – Non-renewable, n = 8 to 12

1.3 Performance Improvement Methods

The SI engine with different octane fuels needs to be utilized effectively to attain their optimum performance. To achieve this, it becomes necessary to rethink the structural alterations during the running of the vehicle as per the operating condition of the engine. Further, the operating parameters such as CR, IT, AFR, and TP play a vital role to enhance the efficiency and reduce the pollutant emission from the SI engines. In this thesis, a few techniques have been adopted and exercised for the performance improvement of the engines and these are explained in the subsequent sections.

1.3.1 Variable compression ratio

Higher fuel economy, improved thermal efficiency and lower emission levels are the major challenges in the automotive engine technology, which in turn are strongly dependent of the operating CR of the engines. Most of the commercial-conventional SI engines are operated at a fixed CR and lies in between 8 to 9:1(Asthana et al., 2016). Mathematically, CR is represented by *Eq. 1.1*, where, 'd' is the cylinder bore diameter, 'l' is the stroke length of the piston and 'Vc' is the clearance volume.

$$CR = \frac{\left(\pi/4 \times d^2 \times l\right) + V_c}{V_c} \qquad \textbf{(1.1)}$$

The CR is mainly governed by the quality of the fuel and knocking tendency at full load operating condition of the engine. However, in real world application most of the SI engines operate at a relatively lower speed or part throttle (PT) at part load condition and hence lead to lower thermal efficiency along with lower fuel economy. Further, the onset of detonation at wide open throttle (WOT) leads to decrease in the maximum applicable value of CR and are not applicable for part load condition due to lower in-cylinder temperature and pressure. This leads to noticeable drop in the efficiency of majority of the SI engines in the real world as they operates on part load for maximum duration of operation (Shaik et al., 2007; Asthana et al., 2016). Hence, the concept of variable compression ratio (VCR) engine comes into picture which addresses the solution to the above stated problems.

The technique of variable compression ratio (VCR) is quite old since 1920 where Harry Ricardo developed an engine with varying CR. He paid attention to the variation of clearance volume inside the combustion chamber. In doing the work, Ricardo introduced the octane rating system for the fuel which is still being used. But the VCR engine development was not successful due to mechanical complexity in manufacturing and difficulty of controlling all of the parameters. The advantages of the increase in CR increase the power output and efficiency. This is due to higher pressure intern higher temperature of compressed fuel-air, causing complete combustion of the fuel-air mixture in the cylinder. The optimum CR may vary for different octane fuels, load conditions, and speed as reported by different researchers based on their exhaustive experimentations (**Table 1. 3**). So, it is a challenge to find the optimum compression ratio which gives maximum power, efficiency with lower bsfc, and lower emission.

Table 1. 3: Optimum CR with varying octane rating of gasoline

Octane Rating	72	81	87	92	96	100	104	108
Compression ratio	5	6	7	8	9	10	11	12

For a specific fuel there always exist a maximum CR beyond which the engine may initiate knock (R J Crookes, 2006). The renewable fuels and non-renewable fuels discussed above such as petrol of different grades (MG 91, MG 95), and the gaseous fuels (LPG, CNG, Methane, Hydrogen, raw biogas) consist of various compositions of hydrocarbon along with different additives. This fact suggests that, there is a unique engine combustion environment for maximum performance with each fuel. The VCR is one of the techniques by which the CR can be optimized for each fuel in the same SI engine (Cerri et al., 2013). The advantage of this fact is the high specific power output accompanied with good reliability and longer engine life.

The optimum CR for different liquid and gaseous fuels reported by authors is tabulated in **Table 1. 4**. It is very clear from the discussion that the CR variation is important in SI engine with respect to the fuel being supplied. For the SI engines, the CR is made fixed at a particular optimum location with respect to the fuel supplied to the engine. However, when the engine operates, there are certain other parameters which need to be accommodated for optimizing

the CR. The applied load on the engine is one such parameter which defines the optimum CR of an engine. From the reported literatures, it was observed that with the lower engine load, the optimum CR could be higher as compared to the high load condition. The high peak pressure problems occur at high load conditions and may induce knock in the engine. Hence, it is recommended to reduce the operating CR at high load conditions. Whereas, during part load or cold starting condition higher CR is recommended. Hence, it is a challenging task to find out the optimum CR which gives maximum power, efficiency with lower BSFC, and emission. For the targeted fuel, there exist a limiting value of CR, beyond which rise in CR don't reflect any positive sign either in the BT and BP of the engine (Crookes, 2006). The method of continuous variation of CR adjusting the clearance volume and the swept volume of the combustion chamber will achieve the maximum performance from the engine. Many researchers investigated in this regard but still the vehicle with VCR implemented technology is a dream. The various methods developed for implementing the VCR technology is listed below and shown in **Fig. 1. 4**– **Fig. 1. 9**.

a. ***Moving the cylinder head****:* The concept of moving cylinder head or tilting block method was first introduced by Larsen (Larsen, 1991) and implemented by the Saab automobile (Haraldsson et al., 2002; Shaik et al., 2007). It comprises of a cylinder head with integrated cylinder which is known as the mono head. The mono head is pivoted at the crankcase and its slope can be adjusted up to 4° in relation to the engine block by means of a hydraulic actuator. The lower half of the block consist of the crank case along with the engine mounts and includes the crank shaft, gear box, oil cooler and other auxiliaries. Whereas, the upper half includes the cylinder, cylinder liner, and the camshaft along with an integrally cast cylinder head. The pivoting mono head adjust the slope of the upper part in relation to the lower part of the engine, thus changing the combustion chamber volume at piston top dead center. Because of this, the top and bottom parts of the engine were separated and each required its own cooling system. The technique of moving cylinder head or the tilting block method varies CR from 8 to 14 by means of the actuator and linkage mechanism.

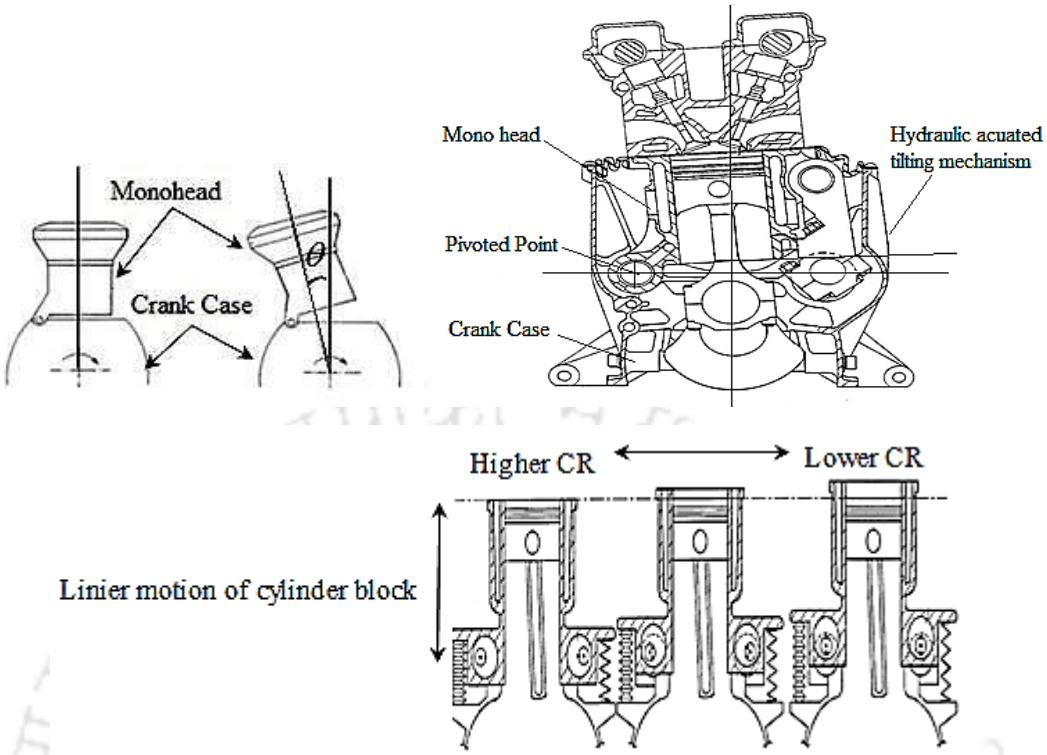

Fig. 1. 4: Moving cylinder head VCR mechanisms

(Haraldsson et al., 2002; Larsen, 1991; Shaik et al., 2007)

b. Moving the crankshaft axis: VCR can also be achieved by altering the rotational axis of the crankshaft as shown in **Fig. 1. 5**. In this method the crankshaft bearings are carried in an eccentrically mounted carrier that can rotate to raise or lower the TDC position of the of the piston in the cylinder (Asthana et al., 2016; Shaik et al., 2007).

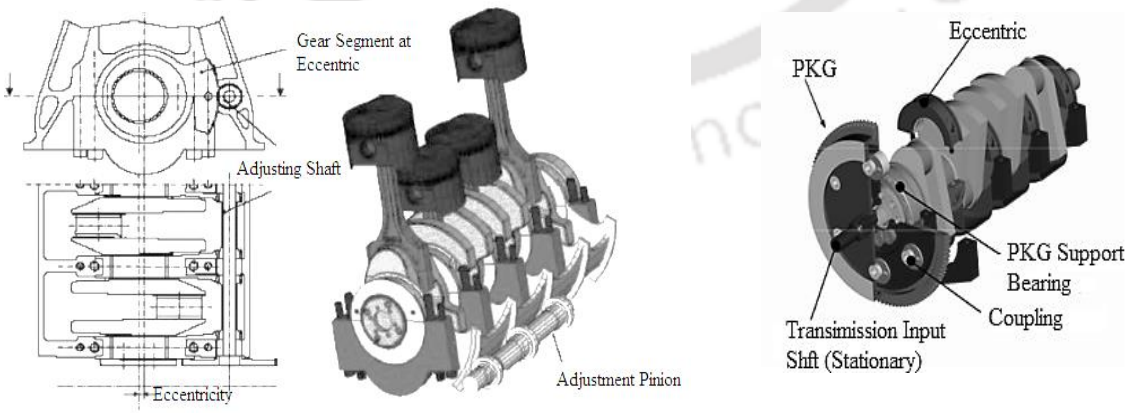

Fig. 1. 5: Eccentric crankshaft mounting (Asthana et al., 2016; Shaik et al., 2007)

The CR of the engine can be altered by altering the rotation of the eccentric carrier. Since the crankshaft is moveable, a fixed output shaft along with a coupling is required to transmit the torque in this case. The CR in this case can be varied from 8 to 14 approximately by altering the rotation of the eccentric carrier through 55°.

c. ***Variation in geometry of the connecting rod****:* The variation of connecting rod geometry alters the CR of the engine either by eccentric or multi linkage systems. In this method a multi-linkage system as shown in **Fig. 1. 6** was inserted between the connecting rod and the crankshaft (Moteki et al., 2003; Aoyama et al., 2013). The multi linkage system was controlled by a linkage and is actuated by the actuator arm driven by a harmonic driver. This system can be incorporated in conventional multi cylinder engine without major modification in the engine block.

d. ***Variation of combustion chamber volume using a secondary piston or valve****:* The volume of the combustion chamber can also be varied with the help of a secondary piston or valve as shown in **Fig. 1. 7**. The secondary piston could be maintained at an intermediate position, corresponding to the optimum CR for a particular condition. To increase the CR, the volume of the combustion chamber have to be reduced by allowing the secondary piston to extend into the combustion chamber (Clarke and Tabaczynski, 1943).

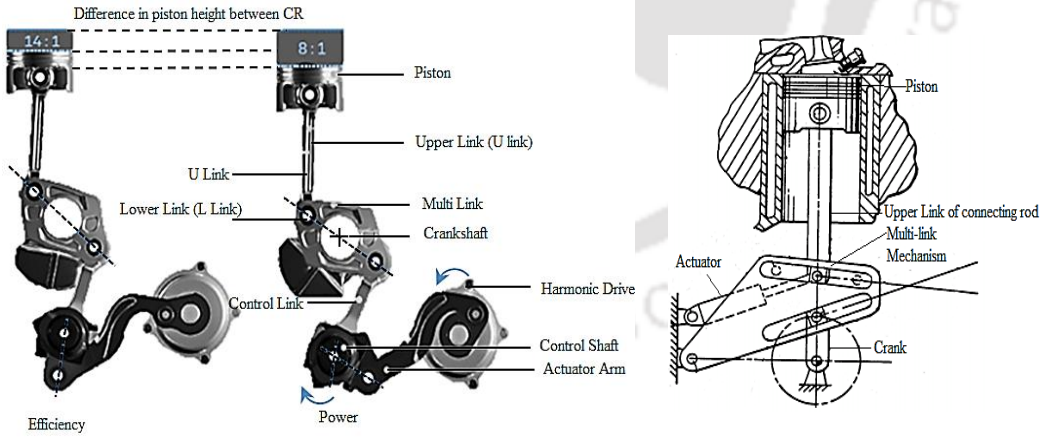

Fig. 1. 6: Multi-link VCR configuration by varying the connecting rod geometry (Moteki et al., 2003; Aoyama et al., 2013)

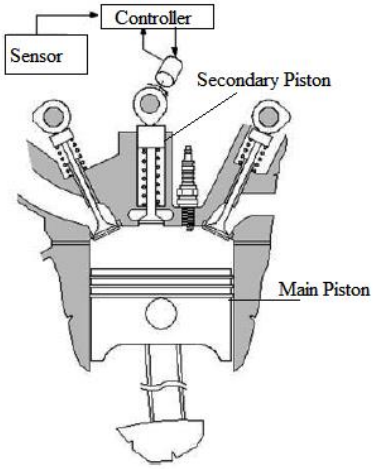

Fig. 1. 7: Secondary piston-based VCR mechanism (Clarke and Tabaczynski, 1943)

e. Variation of piston deck height: The variation in compressive height of the piston offers possibly the smartest method to produce VCR engine, since it requires minor changes to the base engine configuration relative to the other existing methods of VCR mechanism. In this method, a hydraulic piston was engaged to alter the piston deck height with response to the in-cylinder pressure. The CR was changed due to the variation of the relative position of an outer and inner piston and was made possible by supply of oil to the upper and lower chamber made in the inner piston. This is also called as the pressure reactive piston and developed by the University of Michigan (Assanis et al., 2018).The pressure reactive piston consists of a piston crown and a piston skirt along with the a set of springs housed in between them as shown in **Fig. 1. 8**. The configuration of the piston allows the piston crown to deflect in response to the high cylinder pressure. As the piston crown deflects, the clearance volume increases and lowers the effective CR of the engine.

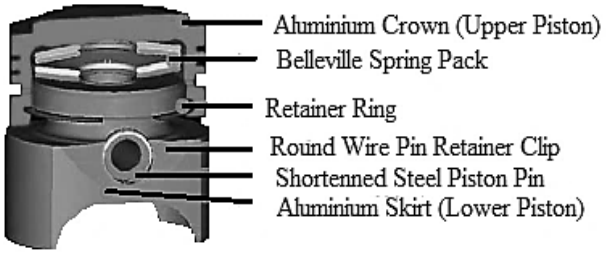

Fig. 1. 8: Secondary piston-based VCR mechanism (Assanis et al., 2018)

f. ***Moving the crankpin****:* The stroke length of the engine can also be altered by the eccentric movement of the crankpins. **Fig. 1. 9** shows the Gomecsys VCR engine in which the moveable crankpins form an eccentric sleeve around the conventional crankpins and are driven by a large gear (Roberts, 2002). The difference in TDC position may vary up to 10 mm with a rotation of the ring gear of only 40˚. While the crankshaft is at the TDC position (at the end of compression stroke), the piston of the eccentric can be lifted or lowered by rotating the ring gear slightly to the right or to the left. However, lifting the eccentric at one TDC automatically lowers the other TDC.

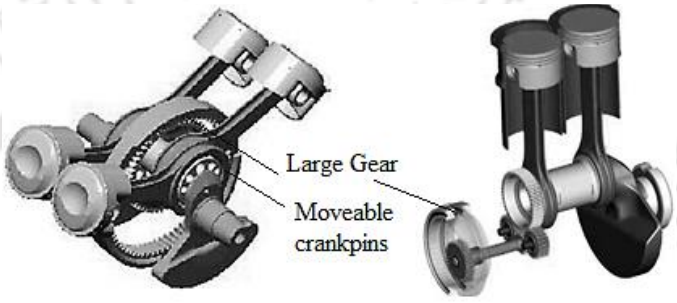

Fig. 1. 9: Gomecsys VCR Engine (Roberts, 2002)

Table 1. 4: The optimum CR for variety of fuels and engines reported by researchers

Sl No	Type of Engine	Fuel used	Optimum CR	Reference
01	12.78 kW Ricardo E6 SI engine at 3000 rpm	Simulated biogas	13	(Crookes, 2006)
02	3.5 kW CI converted SI engine at 1500 rpm	Raw biogas	13	(Porpatham et al., 2012, 2007)
03	3.5 kW CI converted SI engine at 1500 rpm	Simulate biogas Methane Raw biogas	12 13 13	(Chandra et al., 2011)
04	58.88 kW, 1.4 ltr SI engine at 1200-2300 rpm	Gasoline, RON 91 Gasoline, RON 93 Gasoline, RON95.5	8 8 8	(Sayin et al., 2007)
05	12.78 kW Ricardo E6 SI engine at 3000 rpm	Power gas ($CO+H_2$)	8	(Mustafi et al., 2006)
06	191 kW, SI engine at 2300 rpm	Biogas with hydrogen	10.5	(Park et al., 2011)
07	107 kW, 4-stroke, 5 cylinder FIAT engine at 6100 rpm	LPG	10	(Masi, 2012)

1.3.2 Variable ignition timing or spark timing

"Ignition timing (IT)" is the process of setting the time for initiating combustion (just before the end of compression stroke) relative to piston position and crankshaft angular velocity (Zareei and Kakaee, 2013). The IT of a specific fuel-air mixture is important for the best performance of the engine. Ideally it is assumed to be the spark timing of the spark plug. However, the actual combustion in the engine cylinder initiates later after the spark initiation and varies for different fuel. Further, the IT is not only dependent on the type of fuel, but also dependent on other factors such as mixture strength (air-fuel ratio), CR, throttle position (Wide open or part throttle), engine speed and load. Hence, the IT may be advanced or delayed to achieve the best performance of the engine for a particular operating condition. Generally, the combustion in SI engine is divided in four different phases namely, spark ignition, early flame development, flame propagation and flame termination. IT plays a dominant role to initiate these stages of combustion (Heywood, 1988). If the combustion is progressively advanced before the top dead center (bTDC), the compression stroke work transfer increases. With early ignition, the peak pressure and temperature may be sufficient to cause knock. If the end of the combustion process is progressively delayed by retarding the spark timing, the peak cylinder pressure occurs later in the expansion stroke and reduces the expansion work transfer. Hence, the optimum timing at which the magnitude of these opposing trends offsets each other is called as "maximum brake torque (MBT)" timing (Heywood, 1988; Stone, 2012). Therefore, the optimum spark timing is very important. Depending upon the type of fuel (liquid or gaseous) the ignition timing may be optimized. Even the octane rating matters a lot for optimizing the spark timing. Higher octane fuels need to settle the ignition timing to avoid knock causing vibrations and shocks. In this regard, the engine control management advances or retarded the ignition timing based on the signal provided by knock sensors fixed at different places inside the combustion chamber. The method of advancing and retarding the ignition timing is known as variable ignition timing (VIT) or variable spark timing.

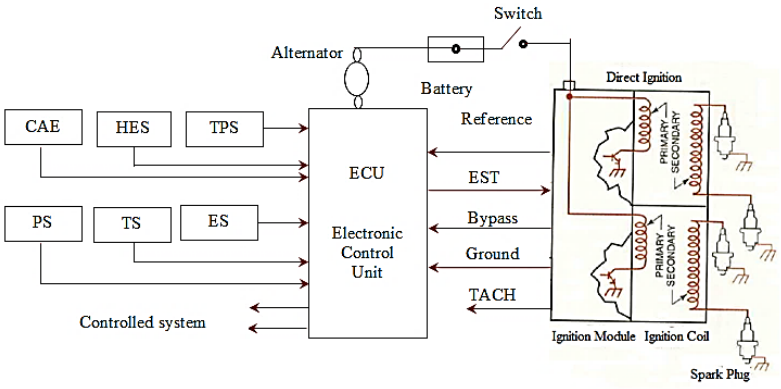

Fig. 1. 10: ECU controlled ignition system

Most of the advanced ignition system are distributor less and controlled by a programmable or a re-programmable electronic control module (ECM) or electronic control unit (ECU). **Fig. 1. 10** shows a typical ECU controlled ignition system. The ECU contains array of data consisting of the optimum ITs for various operating conditions (speed, fuel composition, air-fuel ratio, load, in cylinder temperature and pressure, throttle position, and emission level) of the engine. The ECU controlled ignition system uses a crankshaft position sensor (crank angle encoder). The crankshaft sensor is mounted on the engine shaft. However, some distributor less systems has a second sensor (hall- effect/ magnetic sensor) on the camshaft. The advantage of this system is the elimination of the distributor or assembly, rotor, and distributor cap. The electrical signal generated by the crank angle encoder and the hall-effect sensor are sent to the ECU to determine the position of the piston in the engine. Similarly, few auxiliary sensors such as throttle position sensor (TPS), idle air sensor, temperature sensor, piezo pressure sensor, and emission sensors are mounted on the engine in the respective positions to observe the throttle opening, air flow rate, in-cylinder temperature, pressure and emission levels and feed it back to the ECU for effective control of the IT based on the input signals. The sensor inputs are used by the ECU to govern engine speed and the ignition advance. The distributor less ignition creates a high voltage spark using the ignition coils and are connected the spark plugs through conventional resistor plug wires.

1.3.3 Fuel enrichment method

Method of fuel enrichment is used to improve the performance of the gaseous-fueled engine having impurities with the fuel such as CO_2, H_2S, and moisture as in case of biogas. It

is a mixture of 50 to 70% methane (CH_4) and 20 to 50% CO_2 with 5 and 3 % of hydrogen and nitrogen respectively. The concentration of impurities (carbon dioxide, water, hydrogen sulfide, nitrogen, ammonia, siloxanes and particles) in biogas is dependent on the composition of substrates from which biogas is produced. However, in order to prevent corrosion and improve the efficiency of the engine, it is advantageous to clean the gas before upgrading as fuel for IC engine. Scholars (Papacz, 2011) suggested different methods to remove water vapor from biogas. Cooling, compression, absorption, and adsorption are different methods to remove water vapor. Water will condensate from the biogas and can be removed by increasing the pressure or decreasing the temperature; cooling can be simply achieved by burying the gas line equipped with a condensate trap in the soil. Water can also be removed by adsorption using molecular sieves, SiO_2, or activated carbon. Other technologies for water removal are absorption in glycol solutions or the use of hygroscopic salts. The concentrations of hydrogen sulfide in the biogas can be eliminated either by precipitation in the digester liquid or by treating the gas either in a standalone vessel or while removing carbon dioxide. Addition of Fe_2^+ ions or Fe_3^+ ions in the form of $FeCl_2$, $FeCl_3$ or $FeSO_4$ to the digester precipitates the almost insoluble iron sulfide that is removed together with the digestate. Similarly, the CO_2 present in biogas can be scrubbed by methods such as physical absorption, chemical absorption, adsorption on a solid surface, membrane separation, cryogenic separation and chemical conversion method (Kapdi et al., 2005). Water scrubbing is a simple, continuous, and less expensive method for CO_2 removal from biogas for Indian conditions. It also simultaneously removes H_2S. After removal of CO_2, biogas becomes enriched in methane and equivalent to natural gas. It can be used for all such applications for which natural gas is being used viz. as a fuel for vehicles, CHP, electricity generation, etc. Methane enrichment in the biogas significantly improves the engine performance and reduces the emission of hydrocarbons. The methane enriched biogas by removal of CO_2 from raw biogas increases the methane and oxygen concentration in the charge and thus leads to faster combustion and higher power output as compared to CNG at a given equivalence ratio (Porpatham et al., 2008; Chandra et al., 2011). The presence of carbon dioxide in biogas up to 30-40%, do not deteriorate the engine performance. Further, the power output is almost equivalent to that developed by CNG in the same engine (Bari, 1996).

1.3.4 Exhaust gas recirculation

The exhaust gas recirculation (EGR) is the process, where part of the exhaust gas is feed into the combustion chamber along with the fresh intake air. The EGR rate refers to the volume fraction of exhaust gases found at the intake as a percentage of the total inlet charge. The exhaust gas recirculation (EGR) is an attractive means of improving the fuel economy and reducing the NO_x and HC emission in SI engines. It offers the benefits of charge dilution (lower pumping and cooling losses) by retaining the stoichiometric air-fuel mixture at the intake manifold of the engine (Neame et al., 1995). The percentage of excess air and the temperature of the combustion are reduced by introducing the exhaust gas in the intake manifold and results in lower NO_x emission. The schematic diagram of EGR mechanism attached to a SI engine is shown in **Fig. 1. 11**, where the dark lines represent the path of untreated EGR and dotted lines represents the path of catalytic treated EGR to the engine cylinder.

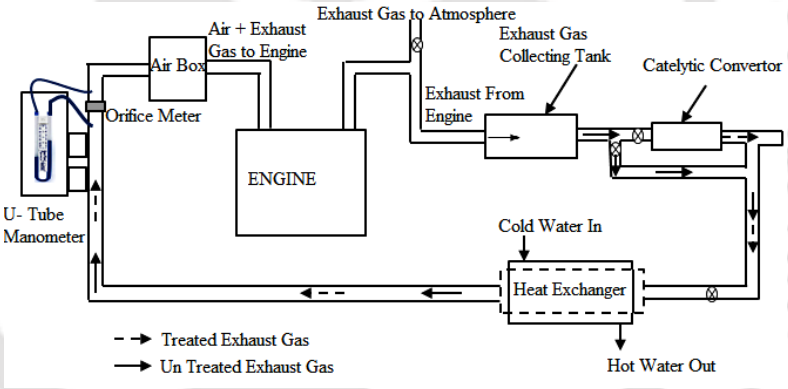

Fig. 1. 11: Exhaust gas recirculation system with catalytic converter

1.4 Emission Control Norms

The emission control norms came into force with the idle emission norms in 1984. Mass emission norms were introduced in 1991 and 1992 for petrol and diesel vehicles, respectively. Following the EURO norms, the Bharat Stage (BS) norms are developed, according to the atmospheric conditions in India. The BS norms are updated narrowing the gap with that of EURO norms. EURO 2 equivalent BS II was in force throughout the country from the year 2005. Further, EURO 3 and EURO 4 equivalents BS III and BS IV were implemented

throughout the Indian cities in the years 2010 and 2017, respectively. EURO 6 equivalent BS VI emission norm first came into picture in the year 2018 in India and was only implemented in NCR and was proposed to be implemented by April 2020 throughout the country. The structure of European standards as applied for Indian climatic conditions are shown in **Table 1. 5 and Table 1.6** ("Emission Standards: India," 2019; ICCT, 2016; Urdhwareshe, 2017; Williams and Minjares, 2016) and reflects the norms and limiting emission levels for passenger cars, three-wheelers and two-wheeler in India.

Table 1. 5: Indian emission standards for four wheelers

Standard	Reference	Date	Region
India 2000	Euro 1	2000	Nation wide
BS II	Euro 2	2001	NCR*, Mumbai, Kolkata, Chennai
		April 2003	NCR*, 11 Cities$
		April 2005	Nationwide
BS III	Euro 3	April, 2005	NCR*, 13 Cities$
		April 2010	Nationwide
BS IV	Euro 4	April 2010	NCR*, 13 Cities$
		April 2017	Nationwide
BS V	Euro5	To be skipped	
BS VI	Euro6	April, 2018	Delhi
		April, 2019	NCR
		April,2020(proposed)	Entire country
* National Capital Region (Delhi) $ Mumbai, Kolkata, Chennai, Bangaluru, Hyderabad, Ahmedabad, Pune, Surat, Kanpur, Lucknow, Solapur, Jamshedpur and Agra			

Table 1. 6: Emission standards for city cars, 3-wheel and 2-wheel petrol vehicles, g/km

		Year of assessment						
		1996	1998	2000	2005[$]	2010[$]	2010[$]	2018
Reference		-	-	Euro1	Euro2	Euro3	Euro 4	Euro 6
Emission (Gross vehicle weight ≤ 3500 kg), g/km	CO	8.68-12.4	4.34-6.20	2.72-6.90	2.2-5.0	2.3 4.17 5.22	1.0 1.81 2.27	1
	HC	-	-	-	-	0.20 0.25 0.29	0.1 0.13 0.16	0.1
	HC+ NO_x	3.00-4.36	1.50-2.18	0.97-1.70	0.5-0.7	-	-	0.17
	NO_x	-	-	-	-	0.15 0.18 0.21	0.08 0.10 0.11	0.06
Emission for 3-wheel petrol vehicles, g/km	CO	6.75	-	4.0	2.25	1.25	-	0.440
	NO_x	-	-	-	-	-	-	0.130
	HC+ NO_x	5.50		2.00	2.00	1.25	-	0.435
Emission for 2-wheel petrol vehicles, g/km	CO	5.5	-	2.0	1.5	1.0	-	1
	HC	-	-	-	-	-	-	1
	NO_x	-	-	-	-	-	-	0.06
	HC+ NO_x	3.60	-	2.22	1.5	1.0	-	-

+ for catalytic converter fitted vehicles
$ Mumbai, Kolkata, Chennai, Bangaluru, Hyderabad, Ahmedabad, Pune, Surat, Kanpur, Lucknow, Solapur, Jamshedpur and Agra

1.5 Summary

The demand for IC engines has grown over the years because of its ability to provide safe and reliable power. However, the SI engines are generally designed and configured for a specific kind of fuels and hence their performance with any other fuel remains below the optimum value. In addition to this, SI engines with alternative fuels produce adverse impact on environment and human health in terms of emissions. In order to improve the efficiency with controlled emissions using renewable fuels (such as biogas), some techniques such as VCR, VIT, fuel enrichment and exhaust gas recirculation have been reviewed which can

ultimately meet the growing energy demand. It is understood that there is a scope for improvement in the efficiency and emission of biogas fueled SI engines by determining the optimum operating parameters, with suitable VCR and VIT techniques. Hence, in the present work it has been thought of identifying these optimized operating parameters for the biogas fueled SI engine by suitable techniques followed by incorporation of these optimized parameters in a commercial SI engine. Hence the literature related to the existing biogas engines along with the conversion methodologies are studied in detail. Along with this, the influence of operating parameters on the performance, combustion and emission characteristics of the biogas fueled SI engines are reviewed in detail and reported in **Chapter 2**.

CHAPTER 2

Literature Review

Overview

This chapter includes the detailed review of the existing literature on the conversion methodologies of the conventional SI and CI engines for biogas, and methane enriched biogas operation in SI mode. However, the performance enhancements of these retrofitted engines running on gaseous octane fuel are the major challenging areas and are positively influenced by the operating parameters of the engine. Hence, the current chapter also includes the extensive literature on the influence of the operating parameters (effect of CH_4 enrichment, operating CR, IT, relative air-fuel ratio, equivalence ratio, engine speed, throttle position and, combustion chamber geometry) on the performance, combustion and emission characteristics of the biogas fueled SI engine. Further, the computational and analytical understanding in connection with the performance improvement techniques of the biogas fueled SI engine is also summarized in the current chapter. Thus, present chapter delivers a thorough review of the literature and their limitations to make a platform for proposed objectives. Further, this chapter includes a summary of the literature and scope of work, followed by the intended objectives and organization of the report.

2.1 Preface

Internal combustion (IC) engines are the machines that convert the heat produced from the combustion of fuel into mechanical work and are considered as the lifeline of the human race for generating power. They have been widely used as the power sources for transportation, electricity generation, irrigation, construction, and in other industrial application. The IC engines are usually powered by the combustion of conventional fossil fuels. Lack of consistent fuel was a significant drawback in the development and design of IC engines up to early 1859. Further, the discovery of crude oil in Pennsylvania made available the development of modern IC engines. However, the enriched hydrocarbon products, gasoline, lubricating oil, and the IC engine evolved together in the 1860s. The early development of the modern spark-ignited IC engine occurred dated back in the 1860s by J. J. E. Lenoir. The Lenoir double-acting, non-compression engine was operated on a two-stroke cycle and had efficiency and power output up to 5% and 4.5 kW, respectively (Heywood, 1988). The further successful development was a spark ignited atmospheric engine developed by Otto and Langen in 1867 and had an overall efficiency of 11%. Although the engine developed by Otto and Langen showed an improved efficiency, it had certain loopholes like higher weight to power ratio, lower mechanical efficiency and lower speed. After continuous research and understanding the shortcoming of Otto and Langen engine, Otto proposed an SI engine with four-piston stroke and the developed prototype was launched in 1876. This development was a breakthrough in the IC engine industry because of the improved efficiency (14%), and the enormous reduction of the engine weight to volume (Pulkrabek, 1997). In 1887, Atkinson developed an engine with variable engine strokes from complex crankshaft which had prolonged expansion than compression stroke and had higher efficiency at the cost of reduced engine power compared to Otto cycle engine. The CR of the engines was limited to less than 4:1 to avoid knock with the available fuels. Further, the development of suitable carburation and ignition system result in the progress of high-speed gasoline engines.

In all those inventions, fuel played a significant impact on engine design and development. Petroleum-based fossil fuels are mostly used for transportation and power generation activities by the IC engines. These fossil fuels (gasoline and diesel) are non-

renewable and decaying at a faster rate and are the primary sources of pollutant emission when combusted in IC engines. To address the uncertainty associated with the future availability of fossil fuel and environmental degradation, the fundamental research aspect of combustion and engine development has reoriented towards exploring efficient combustion systems and parallel sources of renewable energy. Liquid fuels such as alcohol, biodiesel, and gaseous fuels such as LPG, hydrogen, biogas, and producer gases are the parallel sources of alternatives to conventional fossil fuels. But, the use of gaseous fuels in SI engine is beneficial because of higher hydrocarbon ratio, wider ignition limit and formation of the homogenous air-fuel mixture as compared to the liquid fuels. Natural gas and LPG are the widely used petroleum-based alternative fuels but are non-renewable. On the other hand, hydrogen, biogas, and producer gas can be obtained from renewable resources (Porpatham et al., 2012). Further, the issues associated with handling, storage, and NO_x emission of hydrogen (Pulkrabek, 1997) and lower calorific value of producer gas (Sridhar, Mukunda., 2001; Arunachalam and Olsen, 2012) makes it quite challenging to use hydrogen and producer gas as the alternatives to gasoline in SI engine. However, biogas is a promising alternative as well as a renewable octane fuel and is produced through anaerobic digestion organic and plant matters. Most of these resources are renewable and plentily available in the countryside. It typically consists of 50-70% of methane and 30-40% of carbon dioxide (Huang and Crookes, 1998a) and can be used effectively as a fuel both in CI and SI engines with relevant modification in the fuel induction, injection/ignition systems (Mustafi et al., 2006; Qian et al., 2017). Presently biogas is being utilized in a limited scale in dual fuel CI/ HCCI engines with a pilot spray of diesel or biodiesel (Porpatham et al., 2012; Bora et al., 2014; Jaramillo et al., 2018), but the direct use of biogas as a standalone fuel in CI engine is almost impossible (Porpatham et al., 2007). However, it can be positively used as an independent fuel for SI engine (Qian et al., 2017). Further, the commercial SI engines available for the conventional fossil fuel do not operate at their best when fueled with biogas. Hence, the operating parameters such as CR, IT, Air-fuel (AFR)/ equivalence ratio (ER), inlet and exhaust valve timing (VT), operating speed, geometry of combustion chamber and rate of EGR of the commercial SI engine has to be reconfigured and optimized for biogas along with an appropriate fuel induction mechanism suitable for the engine application (Porpatham et al., 2013a; Alagumalai, 2014; Corti et al., 2014). Therefore,

precise techniques are required to operate the available commercial SI engine efficiently with raw biogas. In this regard, this chapter discusses the research so far carried out in the area of developing biogas fueled SI engine and the methodologies adopted to optimize the operating parameters for the enhancement of the performance, combustion and emission characteristics of the engine. Further, this section also includes the applied research of few renewable and non-renewable gaseous fuels in SI engine by many authors.

2.2 Application of Biogas as a Fuel in IC Engine

Biogas is one such fuel and attractive source of energy especially for rural areas because of the abundant availability of non-fossil carbon resources like cattle dung, kitchen west, agricultural waste, municipal waste and other biomasses (Huang and Crookes, 1998b; Montoya et al., 2015). Biogas can be effectively used as an alternative fuel both in CI and SI engines and considered as a replacement to diesel and gasoline, respectively. Because of higher self-ignition temperature and heterogeneous mode of combustion, biogas could not be used as a standalone fuel in CI engine; preferably it could be used in CI engine with dual fuel approach along with a pilot spray of diesel-like fuel that has a low self-ignition temperature (Porpatham et al., 2007).Presently biogas is being used on a limited scale in dual-fuel engines with 60-70% pilot fuel (diesel) substitution. Although the pilot fuel substitution in this kind of application has been improved and is around 80-95% in some cases with optimized CR and injection timing in biogas fueled dual fuel diesel or biodiesel engines (Bora and Saha, 2015a, 2016; Jaramillo et al., 2018), the technology is still under research and not commercialized due to associated complications. Further, the dual-fuel engines depend on the pilot fuel injection to ignite the air-biogas mixture. Hence, the CI converted dual-fuel engine, with reduced fuel substitution is an infeasible solution for this kind of application. However, the physiochemical characteristics (higher octane rating and auto-ignition temperature) of biogas has a significant influence as a standalone fuel on the application of biogas especially in high compression ratio (CR) spark ignition (SI) engines (Porpatham et al., 2007). The application of biogas as a standalone fuel in SI engines does not require the assistance of pilot fuel as in the case of dual fuel CI engines. SI engines with premixed combustion are best apposite for high octane fuels and need special attention (Midkiff et al., 2001; Qian et al., 2017). It is quite easy to use the

alternative liquid octane fuels in the conventional SI engine whether it is a carburetor engine or a manifold injection engine. But if the octane fuels are gaseous, then uses of such fuel are complicated in terms of the supply system, fuel metering, fuel quantity as per load and spark timing.

2.3 Conversion Methodologies for Gas/ Biogas Engines

The use of biogas in the IC engines is a long-established and consistent technology. As reported, engine capacity ranging from 45 kW to several MW was successfully operated on swage works, landfill sites, and other biogas installations. Further, medium or large SI and dual-fuel engines along with gas turbines of rated capacity 0.5 MW to 4 MW were successfully operated with landfill gas for power generation (Mustafi et al., 2006). However, the small engines are significantly used for decentralized power generation and agricultural activity in the rural or remote areas of the developing countries. Further, most of these low powered small single cylinder engines are fueled with diesel, gasoline and kerosene. The abundantly available biogas resources in those areas initiates the necessity of operating these low powered single cylinder engines with biogas. Moreover, the available single cylinder engines are usually gasoline or diesel-based engines, and do not operate efficiently with biogas. Hence, they need special attention to be modified into biogas fueled SI engines and are explained in the below mentioned sections.

2.3.1 Method of conversion from CI into gas/biogas SI mode

The compressed ignition (CI) systems operate at a relatively higher CR (16 - 20) with a heterogeneous mode of combustion (Ganesan, 2015). This mode of ignition is suitable for the less volatile cetane fuels which have low self-ignition temperatures such as diesel and biodiesel. The CI mode of combustion uses a fuel injection system which injects the pressurized (~210 bar) liquid fuel into the combustion chamber towards the end of the compression stroke of the engine (Bora et al., 2014). However, the gaseous octane fuel such as biogas has a higher auto-ignition temperature (650° C) and has a comparatively higher-octane number (RON-110). Therefore, SI mode with premixed combustion is essential and suitable for high octane gaseous fuel (Govil, 2006; Jeong et al., 2009; Qian et al., 2017). The

air and biogas are homogenously premixed and inducted into the engine cylinder in the intake stroke. The charge is further compressed and ignited by a spark plug just before the end of the compression stroke. The power output of the engine is controlled utilizing a throttling device which controls the supply of the air-biogas mixture to the engine. Further, the engine output power in case of biogas fueled SI engine can also be controlled by means of the operating CR. The CR of the gasoline fueled SI engines is normally restricted in between 8 to 10. However, biogas has a higher antiknock index in terms of its methane contentment and higher auto ignition temperature (Montoya et al., 2015). Hence, the biogas fueled SI engines can be operated at much higher CR than that of the normal gasoline fueled engine.

The diesel-fueled commercial CI engines can accommodate biogas in two different modes. One is the dual-fuel mode, and the other one is the CI converted SI mode. The former one is the method, where biogas is being used as the primary fuel and diesel or biodiesel are used as the pilot fuel. The pilot fuel substitution in those dual-fueled biogas engines are in the range of 60-80% and are still dependent on the conventional fossil fuel (Jeong et al., 2009; Bora and Saha, 2016, 2015a; Jaramillo et al., 2018). Further, the overheating issue of the injector nozzle and exhaust valve are the prime issues in the biogas-diesel dual-fuel engines and are the main reason for uneven combustion and detonation (Mitzlaff, 1988). However, the point of interest in the present investigation is the later method of converting the commercial CI and SI engines into gas/biogas Otto (SI) engines. This modification involves a major operation on the CI engine and is quite complicated. The methodology adopted for the conversion of a CI engine into an equivalent spark ignition engine requires the following alternations and are summarized below.

a. Removal of the fuel pump and fuel injection system.
b. Mountings with an appropriate ignition system with ignition distributor (angular gear), ignition coil and spark plug.
c. Modification of the engine intake system by incorporating a suitable mechanism (gas carburetor/ venture mixer/ pneumatic control valve) for supplying a correct air-fuel mixture to the engine.

d. Modification of the governing system of the engine based on the application (constant or variable speed) of the engine.
e. Modification of the combustion chamber (if essential) and reduction of the CR of the engine as recommended for the fuel.

2.3.2 Method of conversion from SI into gas/biogas SI mode

Because of the higher-octane rating and superior anti-knock index, biogas is considered as a suitable and alternative standalone fuel for the commercial SI engines. Although SI engines are ideal for renewable or non-renewable high octane fuels, they need special attention to accommodate renewable gaseous fuel like biogas, due to the associated complications in the fuel induction system (Carrera et al., 2013; Porpatham et al., 2013b). Since the commercial SI engines are designed to operate with the premixed air-fuel mixture and the combustion is initiated by means of spark ignition, the method of conversion from a gasoline-fueled SI engine into a gas or biogas powered SI engine is comparatively more comfortable than the CI modified SI engine. The primary modification is the provision of a biogas-air mixer/ a biogas carburetor or/ a biogas injector instead of a conventional carburetor used for gasoline engines (Mitzlaff, 1988; Mihic, 2004). The power and speed control of the engine is performed by variation of the air-fuel mixture supplied to the engine by operating the butterfly valve placed between the biogas mixer and engine intake system. The mixing device has to ensure the provision of constant air/fuel ratio irrespective of the actual amount sucked into the engine, i.,e. irrespective of the butterfly valve position. This is achieved by adequate design of the mixing device along with the precise control of the butterfly valve (Mitzlaff, 1988). An increase in operating CR of the commercial SI engine seems to be desirable for the biogas operation, as it increases brake thermal efficiency (BTE) and brake power (BP) and decreases specific fuel consumption (SFC) (Chandra et al., 2011; Hussain and Pradesh, 2012; Porpatham et al., 2012; Kemal and Sayin, 2014). Biogas has a comparative lower laminar flame speed (~ 0.25 m/s), and the combustion event must be properly located relative to the TDC to obtain the maximum power or torque. Hence, the “ignition timing” has to be advanced relative to gasoline. Further, to completely utilize the fuel energy and obtain a good combustion process with pressure peak optimality after TDC, it is necessary to advance the ignition/spark timing (IT/ST) in the SI engine, when

biogas is directly used (Von Mitzlaff, 1988). The methodology adopted for the conversion of a gasoline-fueled SI engine into a gas or biogas fueled SI engine is summarized herein in the below-mentioned section.

a. Provision of a biogas-air mixer/ a biogas carburetor or a biogas injector instead of a conventional carburetor used for gasoline engines. (Basic modification)
b. Enhancement of the operating CR of the convectional SI engine up to the optimum point. (Optional to enhance the performance)
c. Modification in the ignition timing (adjustment of the point of ignition) of the conventional SI engine to the optimum point with reference to the CR and operating speed of the engine. (Optional to enhance the performance)

A venturi mixer operates on the same principle as that of a standard carburettor. The mass flow rate and velocity of the airflow at the inlet section causes a pressure drop at the channel contraction which in turns affects a change inflow of the fuel to the venturi section and further mix with the mainstream of air at a required proportion. The design of a biogas-air mixer for a particular engine mainly depends on its rated power, specific fuel consumption, speed, volumetric efficiency, swept volume, and manifold connection diameter (Von Mitzlaff, 1988). In most of the cases, a T-junction gas mixer is preferred. The biogas mixer proposed by researchers has two inlets, one for gas and other for air and has one outlet of the air-gas mixer. The gas inlet either makes an angle 90^{o}or $45^{o}$with the air inlet or placed parallel along with the air inlet and the exhaust is connected to the inlet manifold of the engine. This simple design creates a huge energy loss because of the collision made by the two-stream of fluid and is unable to asymmetric mixing of the two-fluid streams. Similarly, the air-biogas mixer proposed by Huang et al., consisted of a flanged pipe inserted with two biogas inlet tubes and was located in the air stream immediately upstream of the carburetor (Huang and Crookes, 1998a) as shown in **Fig. 2. 1**.

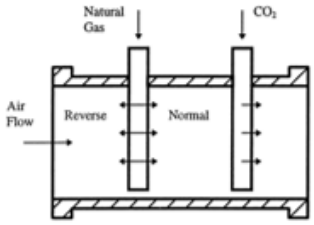

Fig. 2. 1: Venturi type air-biogas mixer proposed for biogas fueled SI engines (Huang et al., 1998)

Surata et al., (2014) reported a simple conversion method from gasoline to biogas fueled small engine to power an electric generator. The biogas obtained from the digester was desulfurized by using annealed, and compacted steel waste chips and H_2O content was reduced up to zero level for easy starting of the engine. The upgraded gas was compressed up to 6 bar before admitted into the engine cylinder. A single-cylinder, four-stroke SI engine with CR 8.5 was modified by replacing the carburetor of the gasoline engine with the only component of the air-fuel mixer. As reported, the engine speed was increased up to the maximum limit with the composition of 80% biogas and 20% LPG (Surata et al., 2014). Similarly, a single-cylinder, four-stroke SI, Ricardo E6 research engine with poppet valve was successfully modified to operate with simulated biogas in SI mode (Huang and Crookes, 1998a; Huang and RJ, 1998). The standard carburetor of the SI engine was replaced by a mixing device, as shown in **Fig. 2. 1** and the engine was tested with simulated biogas with a speed range of 1500 - 3000 rpm along with the relative air-fuel ratio ranging from rich to lean misfire limits and CR ranging from 8-15 where 15 was marked as the onset of detonation. A wide-open throttle setting was used with optimum spark timing ranging from 40^o to 50^o Crank Angle (CA) before the top dead center (bTDC). Further, a 2.3 L gas engine initially designed to run with liquefied petroleum gas (LPG) was successfully modified and operated with biogas (Jeong et al., 2009). The size of the intercooler was enlarged for effective cooling of the compressed intake air, which was compressed by a turbocharger. A larger fuel-air mixer with a larger size fuel supply line was used to supply biogas along with an anti-backfire valve installed in the intake line. The CR and maximum break torque (MBT) spark timing was set to 13 and 16^obTDC respectively. Likewise, a gasoline-fueled SI engine (GX 200) with a rated power output of 4.1 kW at 3600 rpm was retrofitted and successfully operated with simulated biogas with the help of a tri-fuel

conversion kit for biogas induction (Kwon et al., 2017). The tri-fuel conversion kit is composed of a regulator and an adapter and makes it possible to operate an SI engine on gasoline, propane and natural gas. The regulator regulates the steady flow of biogas at a constant pressure and the adapter connected to the regulator supplies the simulated biogas into the engine intake manifold.

Whenever a liquid-fueled CI (diesel/biodiesel) or SI (gasoline) engine is retrofitted for the use of a gaseous fuel, specifically a diluted gaseous fuel such as biogas which contains only 55-60% combustible constituents viz. methane (CH_4) and the rest is carbon dioxide (CO_2), there occurs necessarily reduction in the maximum power output of the engine (Vijay et al., 2005; Govil, 2006; Mello et al., 2006; Moreno et al., 2012). This is called derating the engine power. The main reason for this derating is as follows.

a. The biogas fueled SI engines modified from a gasoline-fueled SI engine produces less power as compared to the gasoline version (Ando et al., 2005; Shah et al., 2010). This is due to the reduced volumetric efficiency as the gaseous fuel occupies a higher volume fraction of the air-fuel mixture sucked into the engine cylinder than the liquid fuel (Mitzlaff, 1988).
b. Further, the liquid fuels (diesel/ gasoline) have higher volumetric energy content than that of gaseous fuel (biogas) (Bora and Saha, 2015a) and also cools the air-fuel mixture when evaporated in the intake manifold. As a result of which, the mass density of the supplied air-fuel mixture increases and hence the quantity of the air-fuel mixture inducted in the engine cylinder is higher on a mass basis (Mitzlaff, 1988).
c. Similarly, because of difference in calorific values of liquid (diesel ~ 43 MJ/kg; gasoline ~ 43.55 MJ/kg) and gaseous fuel (biogas ~ 17 MJ/ kg), the energy available in the charge per cycle is reduced (Bora and Saha, 2015b; Chaudhari et al., 2019).
d. To some extent, reduction also occurs because of the decrease in efficiency due to the comparatively slower combustion of biogas (Porpatham et al., 2008; Qian et al., 2017); even though, the air-fuel ratio required for biogas is much lesser (~ 5.67 to 6) as compared with diesel (~ 20), which is an advantage for power output per cycle for biogas engine on the whole.

2.4 Influence of Engine Operating Parameters

Biogas is a renewable gaseous fuel and attractive source of energy specifically for rural and urban communities. It can be produced by anaerobic digestion of the organic and plant matters, such as cow dung, animal manure, rice straw, leaves, water hyacinth, etc. It approximately consists of two-third of methane (CH_4) by volume and the rest is carbon dioxide (CO_2) along with traces of hydrogen (H_2), nitrogen (N_2) and hydrogen sulfide (H_2S). However, the composition and the content of the biogas is mainly influenced by factors such as the method followed for biogas production, environmental condition, feedstocks used, loading rate and maturity of the feedstock, and bacterial action (Bari, 1996; Porpatham et al., 2012). Hence, because of the diversified composition of the biogas, the difficulty in manufacturing biogas fueled SI engines still becomes a problem that yields in the high price of the biogas fueled engines (Surata et al., 2014).

Compression ratio (CR), spark timing/ ignition timing (ST/IT), air-fuel ratio (AFR), exhaust gas recirculation (EGR), variable valve timing (VVT), engine speed, combustion chamber design and composition of the fuel are some of the important factors which influence the combustion phasing and evaluate the performance and efficiency of a SI engine (Alagumalai, 2014; Corti et al., 2014). The combustion process of biogas fueled SI engine is characterized in terms of the combustion duration and is greatly influenced by the geometrical parameters such as the CR and operating parameters such as engine speed, equivalence ratio (ER), spark timing (ST/IT) and biogas composition (Carrera et al., 2013). Further, the stringent emission norms imposed by the government agencies drive the research community to innovate and implement efficient engine operating modes to meet the emission requirements, but the existing technologies are either relay on the catalytic exhaust gas after-treatment (for natural gas or purified biogas operation) or on lowered compression ratios. Gas engines operating with non- purified biogas do not use catalytic after treatment due to the sulfur and heavy metal content in the exhaust gas, which rapidly derates the catalytic. Hence, the use of purified biogas is recommended, but the process of purification is neither economic nor reliable. So the method remained is to use low CR engines for combustion of these fuels, but, the problem still persists with lower thermal efficiency and brake power output (Roubaud and

Favrat, 2005). The CO_2 content in biogas reduces the laminar flame speed and leads to lower fuel conversion efficiency. However, with optimized operating parameters a fast burning engine can be developed with improved performances (Huang and Crookes, 1998a; Huang and RJ, 1998; Midkiff et al., 2001).

2.4.1 Effect of biogas composition

Methane and carbon dioxide are the two main constituents of biogas. Typically, the proportions are 60% of methane and 40% of carbon dioxide. But it also contains traces of nitrogen, hydrogen, oxygen, hydrogen sulfide and siloxane. However, the concentration of the above constituents in biogas is the functions of the composition of substrates, the maturity of the feedstock, temperature, water content, loading rate of raw materials and bacterial actions (Huang and Crookes, 1998b; Papacz, 2011). Biogas is a possible alternative SI engine fuel that has relatively high availability but has a low enthalpy of combustion. The larger quantity of CO_2 present in biogas drops its volumetric energy density, calorific value, flame velocity and flammability range. However, on account of the higher CO_2 concentration, the biogas fueled SI engines can operate at higher CR and improves the performance of the engine. Further, the autoignition temperature of biogas is very high, hence it resists knocking even at higher operating CR in a SI engine (Porpatham et al., 2008, 2012).The removal of CO_2 also increases the flame velocity and calorific value of biogas (Porpatham et al., 2008). The hydrogen sulfide (H_2S) concentration in biogas corrodes the metal parts and thereby reduces the lifespan of the engine and biogas storage tank. Hence, it was recommended to upgrade the biogas to zero level H_2S impurity and moisture free before using as a fuel for IC engines (Surata et al., 2014). So to prevent corrosion and improve the efficiency of the engine, it is advantageous to clean the biogas before upgrading it as a fuel for the IC engine (Papacz, 2011).

On the performance characteristics of SI engine

The performance of a biogas operated SI engine is greatly influenced by the CH_4 and CO_2 concentration in the fuel. Methane enrichment in the biogas significantly improves engine performance and reduces the emission of hydrocarbons. The methane enriched biogas increases the methane and oxygen concentration in the charge and thus leads to faster

combustion and higher power output in biogas fueled SI engine as compared to CNG at a given equivalence ratio.

Methane in biogas can readily mix with air and has a higher-octane rating. Hence it can be considered as a SI engine fuel (Jeong et al., 2009). Methane has higher hydrogen to carbon ratio which results in reduced CO_2 emission as compared to gasoline. The octane number is also higher which allows larger CR, which in turn enhances the maximum achievable efficiency when used in SI engines. Furthermore, when used in SI engine it reduces the cold start and low temperature emission along with compatibility with lean burn technology. However, it has also some disadvantages like range limitation, reduced volumetric efficiency and lower heat release rate compared to gasoline (Thurnheer et al., 2009).

Biogas with CO_2 proportion higher than 40% resulted in unusable operation of the engine. However, biogas with CO_2 proportion of 30% has notably improved the engine performance (Bari, 1996; Midkiff et al., 2001).Further, the reduction of CO_2 concentration in biogas significantly increases the BTE and ultimately improves the BP output of the engine (Porpatham et al., 2008). Because of the lower energy density, biogas fueled SI engines produce lesser power output compared to liquid-fueled engines (Ferguson and Keck, 1977; Korakianitis et al., 2011).

On the combustion characteristics of SI engine

The presence of CO_2in biogas reduces the peak cylinder pressure and the rate of pressure rise. As the concentration of CO_2in biogas is increased, the peak cylinder pressure shifts away from the TDC and appears later in the expansion stroke(Huang and Crookes, 1998b; Huang and RJ, 1998; Roubaud and Favrat, 2005; Mustafi et al., 2006). The presence of CO_2 in biogas reduces the flame speed and affects the performance of the engine by increasing the average period of combustion duration and ignition lag timing (Bari, 1996; Karim and Wierzba, 2010).

An increasing proportion of CO_2 in biogas derates the indicated power output and triggers the cyclic variation of the engine. Huang et al., found an optimum CR of 13:1 for a

biogas mixture composed of about 40% CO_2. Above this CO_2 concentration, the engine efficiency is reduced, all emissions rose and detonation started to occur (Huang and Crookes, 1998b). But, with reduced CO_2 concentration in biogas, the peak cylinder pressure increases significantly because the faster combustion resulted in improved thermal efficiency and power output in the case of lean mixtures (Porpatham et al., 2008). The decrease in CO_2 concentration enhances the flame velocity and lean limit of combustibility of the inducted fuel air mixture and hence lowers the COV of IMEP (Porpatham et al., 2008). With an increasing proportion of methane in biogas, biogas fueled SI engine notability enhances the performance by diminishing the hydrocarbon emission, extending the flammability limit and enhancing the flame speed (Moreno et al., 2012).

The physical and chemical characteristics of biogas have a great influence on the application biogas in SI engines. With increasing CO_2 content in biogas, the turbulent combustion rate is decreased (Whiston et al., 1992) and reduced the engine knock (Anand et al., 2006). Increasing CR and improving the ignition timing can improve the thermal efficiency of the engine (Papagiannakis and Zannis, 2013). But, due to the high inert gas ratio, the heat value and the flame propagation velocity of biogas decreases and thereby leads to combustion instability. The presence of inert gas in biogas can improve the thermal efficiency and reduce the NOx emission. However, the HC emission and cyclic variation increases.

On the emission characteristics of SI engine

The presence of carbon dioxide (CO_2) in biogas reduces the NO_x emission but lowers the cylinder pressure, which reduces the engine power and thermal efficiency with an increase in the level of unburnt hydrocarbon (HC) emission (Chandra et al., 2011). As reported, because of the lower combustion temperature, NO_x emission fell off significantly with increased concentration of CO_2 in the fuel mixture at a relative air-fuel ratio (RAFR) of 0.98 and 1.05. However, the unburnt HC emission was increased with rise in the CO_2 content in the simulated biogas (Huang and Crookes, 1998b).As the reduced CO_2 concentration in biogas enhances the combustion chamber temperature, the peak cylinder temperatures reach about 1425–1450 ^oC for different CO_2 levels in the fuel. The dissociation of CO_2 into CO and O_2 becomes

significant beyond 1000^{o}C (Ganesan, 2012). Hence the CO level increases with decrease in the amount of CO_2 inducted at high equivalence ratios. The CO emission was lowered with lean mixture operation and reported to increase minutely with the variation of CO_2 fraction above 25%. But, with rich mixture condition, the CO emission increased significantly after the fraction of CO_2 was increased above 30%. This may because of the lower burning rate and lower oxygen availability inside the engine cylinder (Huang and Crookes, 1998b).

2.4.2 Effect of operating CR of the engine

The compression ratio (CR) of an engine is defined as the ratio of volumes of its combustion chamber from its largest capacity to its smallest capacity (Heywood, 1988). It plays a critical role to optimize the efficiency and permitting the IC engines to confirm the emission targets and standards. The benefit of the increased CR enhances the pressure and temperature of the compressed charge in the engine cylinder and thus increases the expansion work in the ideal case. Even though the efficiency and brake power output of a SI engine is directly proportional to the operating CR, there always exists a limiting CR (optimum CR) beyond which the rise in CR do not reflect any positive sign either in the BP or in the BTE of the engine. This may be due to the pre-ignition condition (knocking) that arises because of the auto ignition temperature achieved much earlier in the compression stroke when operated beyond the limiting CR (Huang and Crookes, 1998a; Huang and RJ, 1998). The biogas fueled SI engine can accommodate higher operating CR as compared to the gasoline, LPG and CNG fueled engines (Porpatham et al., 2008, 2013a, 2012) due to the higher self-ignition temperature (650°-700°C) and the anti-knock index of biogas (Qian et al., 2017).Even though biogas fueled SI engines are not knock prone at higher operating CR, there still exist a limiting CR that further depends on the fuel composition and operating parameters of the engine. Thus, the limiting CR is the optimum condition (Optimum CR) with which the engines need to operate to have maximum work output. However, the limiting CR is also dependent on the various operating condition of the SI engine, such as octane rating of the fuel, equivalence ratio (ER), ignition timing (IT), throttle position (TP) and load. Hence, the operating conditions should be taken care of while evaluating the limiting CR of any SI engine. Variable compression ratio (VCR) is a method, by which the operating CR of the SI or CI engines could

be altered to a range of values so that the efficiency of the engine can be optimized for a particular fuel at different loading conditions by optimizing the operating CR (Chaudhari, 2017). The followings are the pros and cons of the VCR method as discussed in the open literature (Boretti, 2013).

i. The fuel efficiency could be enhanced due to the complete combustion of the fuel-air charge.
ii. The engine can be used with alternative fuels having higher research octane rating attaining maximum efficiency by adjusting at a higher CR.
iii. The emissions such as CO and HC could be reduced with the optimum CR for the particular fuel.

Certain disadvantages are also there which restricts its application in the commercial engine yet. However, the enlisted disadvantages could be addressed with proper research and development.

i. The engine structure may not able to sustain the pressure with an increase in the CR. So, there is a limiting value beyond which the operating CR of an engine cannot be increased.
ii. Due to complete combustion, the temperature of combustion is increased which increases the harmful emission of NO_x in the atmosphere. However, there are techniques by which this could be reduced to a certain extent.
iii. The user may not able to calculate the optimum CR, which may damage the engine.

The limiting CR plays a key role to identify the optimum operating conditions of a biogas fueled SI engine. Hence, a detailed review of the existing literature reporting the effects of operating CR on the performance, combustion and emission characteristics of the biogas fueled SI engine are described in this section.

On the performance characteristics of SI engine

CR is an important factor that affects engine performance and directly proportional to the thermal efficiency. However, when the CR is too high, the engine knocks and degrades the

performance of the engine. Methane number (MN) is a resistance to knock quantification methodology for gaseous fuel. Like the octane number uses a mixture of isooctane and n-heptane as the reference fuel, MN is quantified concerning the mixture of methane and hydrogen (Leiker et al., 1972). The MN of biogas is higher than that of natural gas, hence biogas fueled SI engines are allowed to operate at higher CRs compared to natural gas and lead to higher thermal efficiency and increased NO_x emission (Malenshek and Olsen, 2009). CR is considered as a critical parameter when biogas is used as a fuel in the SI engine (Kwon et al., 2017)**.** However, due to the higher self-ignition temperature, biogas fueled SI engines are not knock prone even at higher operating CRs (Mitzlaff, 1988).

Hung and Crooks (1998), studied the effect of operating CR on the performance of a variable speed VCR Ricardo E6 single-cylinder SI engine fueled with simulated biogas. The tests were performed under variable speed ranging from 1500 to 3000 rpm, relative air fuel ratio (RAFR) ranging from rich to lean misfire limit (0.98 to 1.05), variable CO_2 concentration (10% to 40% of vol.) and VCR ranging from 8 to 15 at wide-open throttle (WOT) condition with optimum IT for each CR ranging from 40^o to 50^oCA bTDC. As reported, when the engine was operated with simulated biogas having CO_2 fraction of 37.5 % at 2500 rpm and RAFR of 0.97, the brake mean effective pressure (BMEP) and BTE values increased steadily with the rise in CR up to a critical value of 13. Traces of detonation were also noticed at CR 15 (Huang and Crookes, 1998a).Though the emissions were all reduced, power and thermal efficiency were noticed to be lowered for the leaner mixture. Increased CR is an effective means of enhancing the performance of biogas fueled engine when CO_2 is present in the biogas (Chandra et al., 2011). However, the presence of CO_2 in biogas suppresses the knocking tendency of the fuel when burnt in the SI engine, hence the operating CR of a biogas fueled SI engine should be higher than the normal SI engine. CR ranging from 11 to 13 are reported suitable for operation without knock (Crookes, 2006; Porpatham et al., 2008). Montoya et al., (2015) reported the performance of a 7 kW, constant speed (1800 rpm), CI converted SI engine fueled by biogas, biogas enriched with 25% and 50% of methane. The engine was operated at a constant compression ratio of 15.5:1 and equivalence ratio of 0.95, but the ITs were different and are set at 20°, 16° and 12° CA bTDC. The maximum BP and BTE achieved were 7 kW and ~28%, respectively for full load and full throttle operating condition of the engine when

fueled with the mixture of 50% biogas and 50% methane at 1800 rpm. Whereas, the output power of the engine was de-rated by 17.6% due to conversion from CI to SI mode. The optimum operating conditions of the engine with the biogas-methane mixture (50% biogas and 50% methane) were recommended to be 15.5 for CR, 0.95 for ER, and 12°CA bTDC for IT without the possibility of knocking (Montoya et al., 2015). Further, because of higher auto-ignition tendency in the end-gas, biogas fueled SI engine operated at higher CR (15.5) contributes to the reduction of the higher load limit but enables the increase in BTE of the engine(Jaramillo et al., 2018). However, when biogas is burned in a SI engine partial or total misfire at low load condition counteracts the benefits achieved at high load conditions thus reduces the knocking in combustion.

The variation of BP with a range of equivalence ratios (ER) at CRs ranging from 9.3 to 15 and 11 to 15 has been reported for a constant speed (1500 rpm) biogas fueled SI engine at full throttle (100%) and part throttle (25%) conditions, respectively (Porpatham et al., 2012). As reported due to the improved BTE; the peak power of the engine increases with increased CR irrespective of the ER at full throttle condition. However, there was a minute improvement in BP and BTE of the engine beyond the critical CR of 13. However, there was no significant effect of CR on output BP and BTE of the engine irrespective of ER at part throttle condition. Hence, it was confirmed that the rise in CR has a significant effect at full throttle condition as compared to the part throttle operating condition for biogas fueled SI engine (Porpatham et al., 2008, 2012). It was also suggested that, the rise in CR improves the BP and BTE but reduces the BSFC of biogas fueled SI engine. As reported, a Honda made gasoline-fueled SI engine (GX 200) with a maximum power output of 4.11 kW at 3600 rpm was modified and operated at three different CRs (8.01, 9.09 and 9.22) with the help of a tri-fuel conversion kit for biogas induction. The rise in CR from 8.01 to 9.22 enhanced the BP and BTE of the engine from 2.2 kW to 2.68 kW and 22% to 29.8%, respectively at 3600 rpm. However, the BSFC of the engine was reduced from 290.6 g/h.PS to 218.6 g/h.PS. It was also reported that the maximum engine power was obtained with the lowest carbon dioxide dilution in biogas (Kwon et al., 2017).

Increasing the CR in a SI engine could make it possible for the replacement of gasoline by biogas, but the SI engine operation with biogas contains significant fractions of inert gases

such asCO_2 and N_2. Hence, it exhibits a decrease in the performance of the engine compared with natural gas or gasoline. To overcome the issue, Surat et al., (2014) proposed a simple method of conversion from gasoline to biogas fueled small engine without altering the CR and IT of the original SI engine. As reported, a gasoline-fueled single-cylinder, 196 cc, four-stroke SI engine having a non-contact type transistor coil ignition (TCI) system and CR of 8.5 was operated with a desulfurized and dehumidified biogas containing a substantial part of CO_2. However, the speed of the engine was found unstable. Further, the speed of the engine was improved and enhanced by optimizing the fuel composition by mixing up to 80% of biogas with 20% LPG (Nindhia et al., 2013; Surata et al., 2014).

On the combustion characteristics of SI engine

The combustion process in a SI engine typically consists of exothermic subsonic flame propagation through a homogeneously premixed air-fuel mixture. Further, the flame front propagation is greatly amplified by the induced turbulence, swirl and squish within the engine cylinder (Pulkrabek, 1997). Further, the process of combustion is intensely reliant on the speed and turbulence level in the vicinity of the combustion chamber at the time of spark ignition and is also influenced by the pressure, temperature, and the homogeneity of the charge in the engine cylinder (Mokrane C, 2018). As reported, the combustion processes in a SI engine can be divided into four distinct phases. Such as spark ignition, early flame development, flame propagation and flame termination (Heywood, 1988). Further, to characterize the combustion process, it was typically divided into three different stages; (1) Flame development angle: This is the CA interval between spark discharge and the time when a small but significant fraction of the air-fuel mixture has burned or fuel chemical energy has been released. Usually this fraction is considered as 10%, though another fraction such as 1-5% has been used and this angle is sometimes referred as ignition delay, (2) Rapid burn angle: The CA interval between the end of the flame development stage (usually 10% of the mass fraction burned) and the end of the flame propagation process (usually 90% of the mass fraction burned), (3) Overall burning angle: This is the overall burning process and is the sum of flame development angle and rapid burning angle (Heywood, 1988; Pulkrabek, 1997; Carrera et al., 2013).As reported,

the combined duration of the flame development and propagation stage is typically in-between 30^o - 90^o CA (Heywood, 1988).

The performance and efficiency of a SI engine are mainly dependent on the combustion phasing and are influenced by factors such as compression ratio (CR), spark advance (SA) or ignition advance (IA), air-fuel ratio (AFR), exhaust gas recirculation (EGR), variable valve timing (VVT), combustion chamber design and composition of the fuel (Porpatham et al., 2013a; Alagumalai, 2014; Corti et al., 2014). While investigating the combustion process of biogas fueled SI engine, Carrera et al., (2013) numerically studied the effect of geometrical parameter and operating parameters on the combustion characteristics of the SI engine. As reported, the combustion process of biogas fueled SI engine was characterized by the combustion duration, combustion completeness, and the form factor and was greatly influenced by the operating parameter such as; CR, engine speed, ER, IT and biogas composition (Carrera et al., 2013).

As reported, the rise in CR (9.3-15) of a lean burn (Φ=0.78) biogas fueled SI engine significantly improved the peak cylinder pressure due to the enhanced flame propagation rate at WOT condition**.** However, at rich burn (Φ=1.04) condition, the rise in peak cylinder pressure was found insignificant with the increased CR due to the retarded IT. Whereas, at lower equivalence ratios (Φ< 0.78), the peak cylinder pressures were decreased irrespective of the CR (Porpatham et al., 2012). As reported, at the lean burn (Φ=0.78) operating condition, the rise in CR retarded the MBT timing to have maximum heat release rate at the crank angle (CA) where the energy conversion efficiency was maximum. Further, the effect of increasing CR on the in-cylinder pressure and temperature of a simulated biogas fueled SI engine has been studied at a fixed engine speed (2500 rpm), with the RAFR and CO_2 fraction held at 0.97 and 37.5%, respectively. As reported, there was a significant improvement in combustion pressure and temperature with increase in operating CR of the engine. For the CR variation from 8 to 15, the maximum cylinder pressure (P_{max}) was increased from 2.63 to 8.51 MPa. However, detonation started to appear at CR 15. Since this phenomenon reduced the operating efficiency and durability of the engine, the permissible upper limit of operating CR was specified to be 13 for biogas operation (Huang and Crookes, 1998b).

Faster flame front propagation, higher heat release rate and lower COV_{IMEP} are also the essential combustion characteristics to enhance the thermal efficiency of an engine. The use of higher operating CR in the SI engine enhanced the average in-cylinder pressure and temperature, reduced the cyclic variability (COV) levels and combustion duration. Further, the SI engine operating with higher CR (15) resulted in enhanced BTE and enabled the use of fuels, that have a higher resistance to auto ignition (biogas). However, the use of higher operating CR enhanced the auto ignition tendency of such fuel-air mixture and restricted the stable operating limit of the engine by initiating knocking. The abnormal combustion in the SI engine is mainly described by knocking and is initiated due to the rapid compression of the end gases (unburned charges) by the advanced flame front within the engine cylinder. Higher operating CR increased the knocking intensity and the cyclic variations in biogas fueled SI engines at advanced IT (Jaramillo et al., 2018).

Similarly, Porpatham et al., (2013) investigated the effect of intensified swirl on combustion characteristics of biogas operated SI engine at CR 13 with a range of ER for full (100%) and part throttle (25%) condition. The cylinder peak pressure and heat release rate with masked valve configuration was reported higher throughout the operating range as compared to normal valve configuration at full throttle condition. The increase in swirl level in the biogas reduced the combustion duration particularly with lean mixtures but the ignition delay was remained unaltered at full throttle condition. However, the ignition delay was quite significant in part throttle condition and decreased by 4^{o}CA in masked valve configuration (Porpatham et al., 2013b).

On the emission characteristics of a SI engine

Biogas is quite stable against knocking due to the higher methane number and anti-knock index. Hence, the biogas fueled SI engines can accommodate higher CR as compared to the gasoline and natural gas fueled engines (Chandra et al., 2011; Montoya et al., 2015). Increased CR is an effective means of enhancing the thermal efficiency of a biogas fueled SI engine. The leading impact of CO_2 in biogas combustion is to produce lower NO_x emission and permit the engine to operate at higher CRs. However, with increased CR, biogas fueled

engine emits higher HC and NO_x (Huang and Crookes, 1998a; Porpatham et al., 2012; Papagiannakis and Zannis, 2013). The increased CR boosts the in-cylinder temperature and results in higher NO_x emission. But, the rise in NO_x level was reported dominant beyond the critical CR (13). Whereas, the lower cylinder temperature after the expansion process (reflects in the exhaust gas temperature) results in incomplete combustion and release higher unburnt HC. However, the CO emission was not remarkably affected by the change in CR rather sensitive to the biogas composition or mixture fraction. As reported, the CO levels are very low in the leaner than the stoichiometric ratio range. In the rich region, the CO level shoots up due to incomplete combustion (Huang and Crookes, 1998a; Huang and RJ, 1998; Porpatham et al., 2012). As recommended, the preferable operating CR of the biogas fueled SI engine (37.5% of CO_2 fraction, 0.97 of RAFR, 2500 rpm) should be 13 to have minimal emission. The NO_x, CO and HC emission are noticeably increased beyond the critical CR (13) (Huang and RJ, 1998). Similarly, Crookes, experimentally investigated the performance and emission characteristics of SI engine (Ricardo, E6) fueled by simulated biogas. The engine was operated at a constant speed of 2000 rpm with wide-open throttle (WOT) condition, CR ranging from 11 to 13 (before the onset of detonation) with optimum IT ranging from 40^o- 50^o CA bTDC and the ER ranging from lean to rich misfire limit. As reported, the increased CR increases the in-cylinder temperature, NO_x and HC emission. Nevertheless, the CO emission was predominantly affected by the air-fuel ratio. However, the NOx emission can be controlled by biogas inert diluent (CO_2 and N_2) except a higher fraction of N_2. But, the presence of diluent also affects the performance of the engine (Crookes, 2006). The reasons behind higher HC emission, in a WOT throttled biogas fueled SI engine at increased CRs may also be due to an increased amount of unburnt fuel in the cylinder crevices and reduced post oxidation rate of HC in the exhaust due to lower exhaust temperature. However, the lower cylinder temperature and higher charge dilution at part throttled condition considerably increases the HC emission even at higher operating CR of the engine. In order to have lower HC and CO emission, the biogas fueled SI engine should be operated at CR 13 while maintaining the ER in between 1.08 to 0.95 (Porpatham et al., 2012). Similarly, Chandara et al., (2011) reported higher CR leads to maximum combustion temperature and resulted in grater NO_x and unburnt HC emission. Presence of CO_2 in biogas reduces the NO_x emission but lowers the cylinder pressure, which

reduces the engine power and thermal efficiency with an increase in the level of unburnt HC emission. However, an adequate control of IT and CR could be resulted in controlled exhaust emission of the engines operating at higher CRs (Chandra et al., 2011). Biogas can also be used as a substitute for natural gas in SI engines. As reported, reduction of greenhouse gases can be as much as 100% if biogas will be used as a fuel in SI engines (Bari, 1996). Almost 100% reduction in CO_2 emission can be achieved when biogas produced from manure is utilized as a vehicle fuel. SI engines operated with upgraded biogas reported lower NO_x and SO_x emission (Papacz, 2011).

2.4.3 Effect of ignition timing

The air-fuel mixture in a SI engine is usually ignited through the spark generated in a spark plug. The ignition timing (IT) or spark timing (ST) plays a critical role to further define and control the combustion process in the SI engine. Ignition timing (IT) is the process of setting the time for initiating combustion (just before the end of compression stroke) relative to the piston position and crankshaft angular velocity (Zareei and Kakaee, 2013). It is one of the most important parameters which permit the control of complete combustion. Thereby, it allows the engines to confirm future emission targets and standards for optimizing efficiency and emission. Improper IT may increase the instability (knock intensity and cyclic variability) in combustion, loose thermal efficiency and increases the level of pollutant emission (Jaramillo et al., 2018). Mainly the combustion process in the SI engine is divided into four different phases namely, spark ignition, early flame development, flame propagation and flame termination. IT plays a dominant role to initiate these stages of combustion (Heywood, 1988). If the combustion process is progressively advanced by advancing the IT before the top dead center (bTDC), the compression stroke work transfer increases. If the IT is advanced too much, the increase in work during the compression stroke (from the piston to the cylinder gas) is greater than the increase in work done on the piston during the expansion stroke. Further, with early ignition, the peak pressure and temperature may be sufficient to cause knock. If the end of the combustion process is progressively delayed by retarding the IT, the peak cylinder pressure occurs later in the expansion stroke and reduced the magnitude of expansion work. The optimum timing at which magnitude of these opposing trends offsets each other is called

"maximum brake torque (MBT)" timing (Heywood, 1988; Mehrnoosh et al., 2012; Stone, 2012). Hence to optimize the efficiency and emission of a SI engine the IT has to be controlled accurately. The IT which is advanced or retarded from its optimum value (MBT) results in lower torque and brake power. The optimum IT or MBT is mainly influenced by factors such as the rate of flame development and propagation, the length of flame travel path across the combustion chamber and the details of flame termination process after it reaches the wall. However, these factors are mainly governed by the combustion chamber design, engine operating conditions and properties of the fuel, air and burned gas mixture. So, the study of obtaining the MBT and analyzing its effect on the performance, combustion and emission characteristics are considered significant to have an optimized performance of a SI engine.

On the performance characteristics of SI engine

Ignition advance (IA) is an effective tool, which directly influences the combustion phasing in a SI engine. The optimal values of IA are usually determined through calibration procedures carried out at a steady-state condition on the engine by changing the IT while monitoring the performance indicators. Since, the calibration process is time consuming with exhaustive tests, followed by off-line data analysis, researchers (Corti et al., 2014) suggested a dynamic calibration methodology for reducing the calibration duration. The use of gray-box extreme seeking techniques to design a controller for real-time optimization of the spark advanced in alternative fueled SI engines has been proposed (Mohammadi et al., 2014). By performing quasi-dimensional computer simulation and finite-time thermodynamic analysis, Cutro-Risso et al., (2009), concluded the optimal dependency of the IT on the engine rotational speed to get maximum thermal efficiency at any fixed power requirement. Similarly, the effects of varying IT on a gasoline engine operated with methanol were studied where the significant improvements in the engine performance parameters were reported at optimal IT (MBT) (Li et al., 2010). However, to utilize the fuel energy in an effective manner and to obtain a good combustion process with pressure peak optimally after TDC, it is necessary to advance the IT in SI engines fueled by biogas (Mitzlaff, 1988).

The laminar flame speed of biogas (~ 0.25 m/s) is comparatively lower than that of gasoline. Moreover, the combustion chemistry of biogas is also different from gasoline due to

its chemical composition. The lower laminar flame speed and slower flame front propagation rate of biogas delayed in initiation, development, and propagation of the flame front in a SI engine after the spark ignition. Because of these reasons, the peak cylinder pressure appears much later in the expansion stroke and reduces the expansion work in biogas fueled SI engines. To effectively utilize the expansion work, the IT has to be properly configured and the combustion event must be precisely located relative to the TDC to obtain the maximum power or torque. Hence, the IT has to be advanced relative to gasoline in biogas fueled SI engine. IA of 40-45^{o} CA bTDC was reported as the optimum IT range for the variable speed biogas fueled SI engine operating with CR ranging from 8 to 15 (Huang and Crookes, 1998b; Crookes, 2006). Porpatham et al., (2012) investigated the effect of CR in biogas fueled SI engine for the critical operating CR (13) where the MBT timing was varied between ~34.9^{o} to ~16.1^{o} CA bTDC for the ER ranging from 0.69 to 1.1. Similarly, the MBT timings for the recommended operating ER range (0.95 - 1.08) were reported to be ~16.8^{o}-18.9^{o} CA bTDC for the optimal operating CR (Porpatham et al., 2012, 2013a).Roubaud et al., (2002) reported the positive aspect of higher IA is to attain higher fuel conversion efficiency due to higher peak cylinder pressure. To achieve higher fuel conversion efficiency (>36%) along with lower NO_x and CO emission, the IA of the simulated biogas fueled SI engine equipped with combustion pre-chamber should be operated in between 10^{o}-13^{o} CA bTDCat CR 13.3 and 10.5^{o}-12^{o} CA bTDC at CR 12 and RAFR in between 1.54 to 1.57 (Roubaud et al., 2002; Roubaud and Favrat, 2005). Similarly, Jatana et al.,(2014) reported 42^{o}CA bTDC is the optimal IT for the biogas fueled SI engine operating at CR 9.2:1 both in fuel injection and premixed mode operation (Jatana et al., 2014).

Increased proportion of CO_2 content in biogas demands advanced IT to have the best torque in SI engines. As reported, with CO_2 concentration of 20% the IT has to be retarded to 11^{o}bTDC for best performance against 18^{o}bTDC for raw biogas (CO_2-41%) operation with ER of 0.95 at CR 13:1 and WOT condition of the engine (Porpatham et al., 2008). Stone at al., (1993) evaluated the effect of CO_2 dilution on the burn duration and MBT IT of biogas fueled SI engine and reported moderately advanced MBT and prolonged burn duration because of slower flame propagation rate of biogas. Hence, it was recommended to use relatively advanced IT for biogas compared to NG and gasoline in SI engine (Stone et al., 1993; Mustafi et al., 2006).

Similarly, researchers (Fleming, 1985; Jang et al., 2002; Li et al., 2010; Kakaee et al., 2011; Ma et al., 2012; Mehrnoosh et al., 2012; Zareei and Kakaee, 2013; Corti et al., 2014; Mohammadi et al., 2014) investigated the effect of IT and reported the MBT for gasoline and various alternative fueled (LPG, LNG, NG, Hydrogen and producer gas) SI engine to obtain maximum BTE and lower emission levels.

On the combustion characteristics of a SI engine

The state of pressure and temperature of the gas mixture in the engine cylinder strongly influence the combustion process and is primarily dependent on the IT. An advanced IT initiates the combustion process much before the TDC and reduces the combustion duration. As the combustion starts before the piston riches to TDC, the fresh charges are being pushed by the piston towards the developing flame front as a result of which the rate of flame front propagation was increased and reduced the combustion duration. Whereas, if the combustion was initiated at the TDC, the flame front and fresh charges move in the same direction and decreased the rate of flame front propagation, thus increased the combustion duration. The increased pressure and temperature of the end gas in the engine cylinder at higher operating CR retarders the optimum IT in a SI engine. Similarly, operating the engine with leaner or richer mixture tends to advance the optimal IT irrespective of operating CR due to the prolonged ignition delay and slower flame propagation (Sadiq Al-Baghdadi, 2004). Advancing the IT by 40^{o} CA bTDC was reported suitable for the biogas fueled SI engine operating with CR 14 at 3000 rpm and fuel-air equivalence ratio of 1.5 (Carrera et al., 2013). Engine operating with advanced IT initiates a greater proportion of the combustion process mostly during the compression stroke and resulted in increased pressure and temperature in the cylinder. However, it may initiate knocking and increases COV_{IMEP} in some cases. But, with more advanced IT, the in-cylinder pressure and temperature are dropped which resulted in higher cyclic variation in flame development and propagation stage during the combustion process. Biogas engine operating with leaner ER (Φ=0.6) reported an improved combustion process with advanced IT (335^{o} CA). However, due to the reduced cylinder pressure and temperature, the cyclic variation was increased significantly with delayed ITs (338^{o} CA and 348^{o} CA) at ER 0.6. Biogas –air mixture with comparatively higher ER (Φ=0.85 and 1) reported lower cyclic

variations (COV_{IMEP} below 2%) at an IA of ~347° CA. However, with advanced IT the presence of knock increased the cyclic variations (Jaramillo et al., 2018). Similarly, irrespective of the operating CR the peak cylinder pressures were decreased by the retarded ITs. Coefficient of variations (COV) was greatly influenced by the initial period of flame development. It significantly reduced the COV and was found minimum only within the region of MBT IT. The advanced IT lowered the initial flame speed and resulted in higher COV in the phase of flame development.

The reduced flame speed and the increased combustion duration also affect the MBT timing. On the other hand, with overly retarded IT, the mixture temperature in the end zone could drop below the misfire temperature in a lean burn engine due to the expansion and quenching phenomenon. This can result in occasional misfire and poor combustion with increased hydrocarbon emission. Therefore, stable combustion is achievable by using lower equivalence ratio and advance IT at part load as compared to leaner equivalence ratio at full load condition (Cho and He, 2007). Hence, the IT under lean operating condition must be advanced compared to stoichiometric operation with a particular limit up to "knock". In the meantime, further advancing the spark timing extends the lean limits while maintaining higher thermal efficiency. Although the MBT timing is advanced with leaner air fuel mixture but with increased load on the engine, the higher cylinder pressure and temperature promotes the flame propagation and the MBT timing is retarded (Hassaneen et al., 1998).

On the emission characteristics of a SI engine

The formation of thermal NO_x in SI engine is primarily governed by the Zeldovich Mechanism and is predominantly dependent on the average combustion temperature and local oxygen excess ratio. Increased IA initiates the combustion process relatively earlier in the compression stroke, thus positively affect the combustion rate of gaseous fuel specifically in the initial stages of combustion and leads to higher in-cylinder temperature. Hence, advancing the IT relative to the point of normal spark advance (MBT) resulted in increased specific NO_x emission. Further, advancing the IT at increased CR also resulted in drastic increase in NO_x (Kakaee et al., 2011; Papagiannakis and Zannis, 2013). Similarly, the CO formation rate primarily depends on the air to fuel excess ratio. The unburned gaseous fuel in the engine

cylinder and the cylinder charge temperature are also equally responsible for the formation of CO as well as control the rate of fuel decomposition and oxidation. An advanced IT increased the maximum cylinder temperature, which supported the CO formation mechanism. However, at the same time, the increased IA also reduced the time interval of the expansion phase for which the higher temperature was maintained in the cylinder and thus reduced the CO oxidation rate. Hence, the average CO emission was increased with advanced IT (Papagiannakis and Zannis, 2013; Zareei and Kakaee, 2013).

Midkiff et al. reported the peak NO_x emission of the SI engine operating with NG and various compositions of simulated biogas at CR 11 and MBT timing appeared near Φ=0.88-0.9. However, the extent of NO_x emission varies with fuel composition. IT also plays a vital role to control the NO_x emission in the SI engine. Even the modest level of delay in IT also substantially reduced the NO_x emission. Retarded IT reduces the in-cylinder pressure and resulted in lower combustion temperatures, thus lowered the NO_x emission at retarded IT. Further, the retarded IT did not have any significant effect on the unburnt HC and CO emission for the simulated biogas powered SI engine for all throttle settings and speed range of the engine. However, when operated with MBT, the emission of unburnt HC were fall between 2.3 to 2.5 g/bhp-h at Φ=0.8 to 1, respectively (Midkiff et al., 2001). SI engine operating with simulated biogas (60% CH_4, 40% CO_2) and lean mixture (ϕ = 0.9) condition at CR 6.23 reported reduced NO_x and CO_2 emission in between 10^o to 20^o CA bTDC of IA (Mokrane C, 2018). At an IT of 8^oCA bTDC, the emissions of CO and NO_x in a biogas fueled SI engine operating at CR 12 are reported well below the Swiss limits. The peak pressure in the engine cylinder was increased with advanced IT and appeared earlier in the engine cycle. The peak pressure induced higher combustion temperature and stimulated the formation of thermal NO_x. Further, the higher in-cylinder pressure trapped more fresh charge in the crevice volume during the early stage of combustion and resulted in higher CO emission due to secondary oxidation with increased IA. However, the reported HC emission was lower with advanced IT due to the stable combustion (lower COV_{IMEP}) in the expansion phase (Roubaud et al., 2002). Generally, the advanced IT leads to reduced THC and increased NOx emission for high energy density fuels such as NG and gasoline. However, in case of biogas the NO_x formation was significantly reduced and THC was considerably increased along with the increased proportion of N_2 in

biogas. Similarly, irrespective of the air-fuel ratio, H_2 addition produced higher NOx and lesser THC emission due to high adiabatic flame temperature and improved combustion characteristics. However, the THC emissions were increased with leaner mixtures (EAR> 1.2) (Min et al., 2002; Park et al., 2011).

2.4.4 Effect of relative air/fuel or fuel/air equivalence ratio

The engine performance evaluation mostly includes the measurements of air and fuel mass flow rates. The ratio of these mass flow rates is useful in defining the limit of engine operating conditions. The effect of mixture composition on the engine performance parameters are usually discussed in terms of the air/ fuel or fuel/air ratios. However, the relative proportion of air and fuel can be represented more commonly in terms of fuel/air equivalence ratio (Φ) $\left((F/A)_{actual}/(F/A)_{stoichiometric}\right)$ or relative air/fuel ratio (λ) $\left((A/F)_{actual}/(A/F)_{stoichiometric}\right)$. The combustion characteristics of fuel-air mixture and the properties of the combustion products govern the performance, efficiency and emission of the engine and can be correlated best for a wide range of fuels relative to the stoichiometric mixture proportion (Heywood, 1988). In order to achieve low-emission and the best fuel conversion efficiency in SI mode, it is highly recommended to maintain the accurate CR, air fuel ratio and IT, when the engine is fueled with biogas. Hence to meet current low-emission technology standards, precisely control of air-fuel ratio is desired (Alagumalai, 2014; Corti et al., 2014).

On the performance characteristics of SI engine

Experimenting with a constant speed SI engine operating at CR 12.65 and three different IT, Chandra et al., (2011) reported the operating range of the relative air-fuel ratios (RAFRs) of the engine fueled by CNG, methane enriched biogas and biogas. The operating ranges of RAFRs were reported 0.5-0.7, 0.5-0.8 and 0.5-0.9 raw biogas (65% CH_4) at an IA of 30^o, 35^o and 40^o CA bTDC respectively. The SI engine fueled with raw biogas was supplied with rich mixture at all selected IAs. However, the BP output and brake load development was comparatively reduced from the other fuel composition because of the lower calorific value, higher CO_2 content and reduced VE of the engine. Hence, it was recommended to supply right air-fuel mixture to have higher BTE for the raw biogas operated engine (Chandra et al., 2011).

The lean misfire limit of combustion of raw biogas under actual engine operating conditions gets considerably extended with increase in CR. The lean limit indicated by misfire was at ERs of 0.64 and 0.77 for CRs 15 and 9.3, respectively at WOT condition. Further the rise in CR also enhanced the BTE of the engine even at leaner ERs. As reported, the maximum BP (4.8 kW) and BTE (26.8%) of the raw biogas engine operating with CR 15 was reported at an ER of 1.02 and 0.94, respectively at WOT condition (Porpatham et al., 2012). A constant speed biogas fueled SI engine operating at CR 13 and MBT, produced maximum BP (5.4 kW) and BTE (30.4%) at an ER of 0.95-1.02 and 0.91, respectively when operated with reduced CO_2 concentration (20%) at WOT condition (Porpatham et al., 2008). Similarly, Huang and Crookes (1998) reported the BMEP and the brake BTE of a biogas fueled SI engine approached the limiting value as the RAFR changed from the lean misfire limit to the rich side for biogas mixture containing 37.5% CO_2 at CR 13 and 2500 rpm. The highest BMEP was observed at a RAFR of about 0.95 and the maximum BTE was noticed at a RAFR of about 1.05. Mixtures richer or leaner than this point triggered incomplete combustion and dropped the flame front propagation rate and hence reduced the BTE of the engine (Huang and Crookes, 1998a). Midkiff et al., (2001) studied the effect of ER in a gaseous fueled SI engine at CR 11 and WOT condition. As reported the increased air/fuel ratio (decreasing value of ER) gradually declined the BP and supplied a lower proportion of the fuel to the engine. The loss of BP was reported due to the higher BTE or lower brake specific energy consumption (BSEC) for reduced ER of the engine. Similarly, it was also verified that for a constant operating ER, the BP of the engine was dropped with increasing proportion of diluent (CO_2, N_2) in the NG (Midkiff et al., 2001).

On combustion characteristics of SI engine

The chemical composition of the fuel plays a vital role in the occurrence of the combustion process. Mixtures with lower ER and higher inert content have low reactivity and tend to slow down the burn rate thereby produce incomplete combustion and higher cyclic variability. However, mixtures with higher ER have high reactivity and tend to produce faster burning cycles and resulted in higher knock intensity with specific operating environments. Further, an incomplete combustion results into greater variability in cylinder pressures which leads to rapid fluctuation in output torque and power, thereby disturb the engine performance.

Hence, it was recommended to identify the moderate range of ER for safe operating range of a SI engine.

Jaramillo et al., (2018) implemented an interactive control strategy to evaluate the combustion stability and safe operating limit of a simulated biogas fueled SI engine at CR 15. The highest cyclic variability (COV_{IMEP}) of the engine was reported 7.74% and identified at Φ=0.6 with an IT of 334^o CA. Whereas, the lowest cyclic variability of IMEP was reported 0.61% and was identified at Φ=1 with an IT of 348^o CA (Jaramillo et al., 2018). Similarly, the laminar burning speed of the biogas consisting of 60% NG and 40% CO_2 was reported where slower flame propagation rate of biogas increased the combustion period, ignition lag timing and reduced the burning rate. The MBT ITs for the biogas was obtained by increased advance in the ITs with decreased ERs of the engine and were reported 40^o, 41^o, 43^o and 58^o CA bTDC at Φ=1, 0.9, 0.8 and 0.65, respectively (Midkiff et al., 2001). Further, the COV of the biogas fueled engine was remained below 4% within the specific range of ER (0.7<Φ>1) and rose sharply as the lean misfire limit approached. Porpatham et. al., (2012) reported SI engine operating with leaner mixture of biogas reflected a significant rise in peak cylinder pressure at CR 13. However, the rise in peak cylinder pressure was insignificant with richer mixtures for the same composition of biogas. Further, the COV_{IMEP} was reported maximum at the lean misfire limit (0.58) and increased with leaner ERs. As reported, the rise in CR of the engine fueled with leaner biogas-air mixture increased the rate of HRR and shifted the curve closer to TDC. However, with rich mixture at higher operating CR (15), the entire combustion process initiated in the expansion stroke and thus lowered the HRR (Porpatham et al., 2008, 2012).

Combustion duration is a function of flame factor and closely dependent on the operated ER range of the SI engine. The predicted combustion duration of the CNG fueled engine was reported lowest in between the ER range of 1 to 1.1. As reported, the combustion was most efficient for the ER of 1 to 1.1 and therefore the duration of combustion to release the fuel energy is minimum (Mehrnoosh et al., 2012). Similarly, Sadiq Al-Baghdadi (2004) addressed the uncontrolled pre ignition problem of hydrogen fueled SI engine and reported the operational limit of the engine for different CR. With increased engine speed, the operational

limit of pre-ignition was reduced and the reported limit of ER was 0.9-1.15 for 25 rps at CR 11 (Sadiq Al-Baghdadi, 2004).

On the emission characteristics of SI engine

Biogas engine functional closer to the stoichiometric air-fuel ratio resulted in lower level of toxic gases. As reported, the reduced CO_2 concentration in biogas significantly reduced the HC emission and extended the lean operating limit as well. SI Engine operating with leaner biogas-air mixture with RAFR (λ) in the range of 0.8-0.9 resulted in improved performance and reduced HC emission at CR 12.65 and MBT (Chandra et al., 2011; Porpatham et al., 2008). Similarly, it was reported biogas fueled SI engine operating at CR 13 and MBT with WOT condition release minimum level of HC (1150 ppm) at an ER (Φ) of 0.95**.** But with biogas-air mixture leaner than 0.95 (Φ< 0.95) revealed an increase in HC level due to the effects flame quenching and incomplete combustion. Whereas, the increased temperature of the combustion chamber (1425-1450^{o}C) dissociated the CO_2 molecules in to CO and O_2 and became significant with rich mixture. Hence, emits increased level of CO at higher ER (Φ> 0.95). Further, the peak NO emission was observed with leaner than stoichiometric mixture and reported decreasing with leaner biogas-air mixtures (Porpatham et al., 2008). Similarly, Huangs and Crookes (1998) observed, biogas fueled SI engine produced the peak NOx and minimum HC emission at the point of best thermal efficiency and was reported at λ=1.05 with CR of 13 and 2500 rpm (Huang and Crookes, 1998a)**.** Further, to minimize the HC and CO emission, it was recommended to operate the engine by limiting the CO_2 content of biogas below 40% at CR 13 and RAFR in between 1.05 to 0.95. However, the NO_x emission of the engine can be controlled at the expanses of performance indices at λ>1.2. Hence, to maintain the balance between the thermal efficiency along with NO_x and HC emissions, fastest and lean burning engine design technologies with biogas scrubbing and exhaust gas after treatment need to be adopted. Similarly, Mokrane at al., (2018) reported the fuel/air ER is the governing factor which controls the CO emission in SI engines. With increased ER, CO concentration in the exhaust emission was increased gradually for biogas rich mixtures due to the lack of O_2 and presence of unburnt CH_4in SI engines. However, for fuel lean mixtures, the CO concentrations

in the exhaust varied marginally with ER and reported in the order of 10^{-3} mole fraction (Mokrane, 2018).

Similarly, Midkiff et al., estimated the average combustion chamber temperature during the flame propagation period and reported the temperatures are closely parallel to the dependence of NOx levels on ERs. For leaner ERs ($\Phi < 0.8$), the reported HC emission was gradually increased and found maximum at the misfire limit (Φ=0.65) (Midkiff et al., 2001). Furtherer, it was reported for leaner ERs (Φ<0.8), the formation of NO is mainly governed by quenching of formation reaction in the expansion stroke, while for richer ERs (Φ>0.8), the NO emission was primarily dependent on the quenching of decomposition reaction. Hence, the NOx concentration in the exhaust emission was decreased for richer and leaner ERs, respectively due to the insufficient and abundance oxygen at the respective conditions (Sadiq Al-Baghdadi, 2004).

2.4.5 Effect of engine speed

The engine speed plays an important role to define the operational limit for pre-ignition, misfire and knocking in SI engine. Further the operating speed range of the engine is also responsible for defining the other limiting value of the engine operating parameters such as CR, IT and ER. It mainly affects the combustion process and hence should be taken care while engine modeling and design. Researchers (Stewart, 1997; Huang and Crookes, 1998a; Mustafi et al., 2006; Jahirul et al., 2010; Chandra et al., 2011; Mehrnoosh et al., 2012; Moreno et al., 2012; Ozcan and Yamin, 2008; Sadiq Al-Baghdadi, 2004) have studied the effect of engine speed on the performance, combustion and emission characteristics of SI engines fueled by gasoline, methane, hydrogen, NG, CNG, LPG and biogas. However, the field has not been explored much in line with the combustion and emission analysis and most importantly biogas fueled engines are hardly being investigated in this direction.

On the performance characteristics of SI engine

Huang and Crooks, investigated the effect of engine speed in a simulated biogas fueled SI engine at CR 13 and reported that the reduced air mass flow rate lowered the BMEP and BTE at higher speed (3000 rpm) of the engine. Increased engine speed also squeezed the operating

ER range of the engine for biogas operation (Huang and Crookes, 1998a). Further, Jahirul et al., investigated the effect of engine speed on the performance characteristics of retrofitted CNG engine operating in the range of 1500-5500 rpm at CR 9.5 for 50% and 80% throttle opening conditions. The BP output of the engine was increased with increasing speed of the engine at 80% throttle. The difference in power was mainly attributed due to the variation of fuel/air ER due to the operating throttle position (Jahirul et al., 2010). Investigating the effect of engine speed in a CNG operated SI engine Mehrnoosh et al., also reported, higher IP at increased engine speeds is due to the increased number of cycles per unit time. Further it was reported, the indicative specific fuel consumption (ISFC) was decreased with increasing speed of a CNG fueled SI engine and was attributed due to the increased indicative thermal efficiency (ITE) (Mehrnoosh et al., 2012). In the same way, Mustafi et al., (2006) studied the effect of engine operating speed on few performance parameters of some base line fuels such as gasoline, NG and power gas (composed of CO and H_2 in specific ratios). As reported, the BT in every case gradually declined as engine speed was increased from 1000 to 2000 rpm. The BSFC of NG fuel was remained invariant throughout the operating speed range of the engine, but for gasoline and power gas, the BSFC reflected a mild increase along with the increased engine speed.(Mustafi et al., 2006).

On the combustion characteristics of SI engine

Chandra et al., (2011) investigated the effect of brake load on the engine speed and reported, the engine speed was decreased with increasing brake load. The engine speed was always greater in methane enriched biogas due to more power developed by the engine and was attributed with higher calorific value per unit volume of the gas. The observed engine speed was found lowest on raw biogas and it was more than 1200 rpm. However at engine speed more than 1200 rpm or at higher compression ratios, the cycle to cycle variation is less evident (Chandra et al., 2011). The increased engine speed enhanced the turbulence in the engine cylinder and leads to an increased flame speed which further enhanced the rate of mass burnt fraction. Therefore, the time required for complete combustion was reduced and produced higher peak pressure and temperature in the cylinder which resulted in unstable combustion. Hence, the turbulent flame front propagation rate was reported highly sensitive to the engine

speed, pressure and temperature in the engine cylinder (Sadiq Al-Baghdadi, 2004). Similarly, the effect of speed on cylinder pressure and temperature of combustion were studied by Ozcan and Jehad, (2008) for LPG a fueled SI engine at for various stroke lengths. They found that with increased engine speed the in cylinder pressure and temperature during combustion was increased irrespective of the engine stroke length due to the improved turbulence and reduced burn duration (Ozcan and Yamin, 2008). Similarly, Stewart et al., reported when the engine speed is increased for a fixed engine torque, the role of diffusional or turbulent premixed combustion processes becomes more important. This may be a limiting factor for modern high-speed direct-injection engines (Stewart, 1997).

On the emission characteristics of SI engine

Sadiq Al-Baghdadi et al., (2004) reported that higher engine speed increased the peak cylinder temperature with abundant of oxygen and reduced the time required for dissociating NO to N_2 and O_2in hydrogen fueled SI engine at CR 11:1 and MBT IT. Hence, the NOx emission was increased with increasing engine speed for all ER in between Φ = 0.6 to 0.8. However, for the ER beyond 0.8 (Φ>0.8) the reported NOx emission was decreased with increasing engine speed due to the decreasing amount of oxygen in the charge (Sadiq Al-Baghdadi, 2004). Similarly, it is reported that increase of engine speed contributed to the rise in NO_x emission for gasoline, methane and methane–hydrogen blended fuels in SI engine and became vital beyond 3250 rpm at Φ = 0.8 and 0.7. However, the CO_2 emission reported was remained constant and is not much dependent on the engine speed (Moreno et al., 2012). Jahirul et al. (2010) reported the combustion gas temperature of the CNG fueled engine was increased with increasing engine speed. Further it was reported that CO was oxidized and turned into CO_2at higher combustion temperature. Hence, with increasing engine speed the CO concentration was reduced whereasCO_2emission was increased with higher engine speed and was also attributed due to higher fuel conversion efficiency (Jahirul et al., 2010). Similarly, the effect of speed on the NO_x and HC concentration in the exhaust gas was observed for a LPG fueled SI engine. Due to the increased combustion gas temperature, the rise in engine speed increased the NOx emission. However, the increased engine speed reduced the HC emission irrespective of the stroke length of the engine (Ozcan and Yamin, 2008).

2.5 Summary of Literature

The detailed review of the existing literature published by the researchers in the light of devising the efficient biogas fueled SI engine not only explored the different techniques to efficiently convert the existing commercial SI engines for biogas application but also revealed the effects of various operating parameters on performance, combustion and emission characteristics of the engine. Further, the proposed optimized engine parameters suggested by many scholars are also reviewed for various gaseous alternative fuels along with biogas and are summarized in **Table 2. 1** for some specified operating conditions and engine configurations. The meticulous review of the open literature has drawn the following inferences.

- Researchers have proposed several alternatives to replace the conventional fuels used in the SI engine. However, the gaseous fuels are given the utmost priority because of their ability to emit a lower level of pollutants. Among the listed alternatives, biogas is a promising alternative octane fuel mostly derived through anaerobic digestion of the renewable resources. But, the unavailability of the efficient energy conversion techniques restricted the use of biogas in a limited scale in dual fuel CI/HCCI engines. Further, researchers have also confirmed that biogas cannot be used as a standalone fuel in CI engines. However, the use of biogas as a standalone fuel in SI engines was recommended because of its unique composition and physiochemical characteristic.
- As noticed form the literature, the commercial SI engines available for the conventional fossil fuels do not operate at their best when fueled with biogas. These engines are only suitable for specific applications where constant speed is the prime requirement. However, there is a significant demand for the constant/variable speed, medium and low power single-cylinder engines (3-10 kW) in the rural and remote areas of developing countries for several agriculture applications and decentralized power production. Hence, there is a strong need for an efficient and low-cost biogas powered single cylinder SI engine.
- The methods of conversion from SI into gas/biogas SI mode are quite simple but derate the engine output power approximately by 20%. Hence, to regain the base engine

efficiency, the operating parameters (CR, IT, RAFR/ ER, VT, operating speed, fuel composition, combustion chamber geometry and EGR rate) of the biogas fueled SI engine has to be reconfigured and optimized along with an efficient fuel induction system. However, very few literatures have been spotted in line with proposed method for enhancing the overall efficiency of the biogas fueled engines and are further restricted to specific operating conditions.

- The majority of the experimental findings are based on the synthetically composed biogas. In this manner research identified with crude biogas is still to be investigated. Such examinations would give the useful answer for the performance improvement of a SI engine working with biogas fuel.
- Few researchers have investigated the influence of CO_2 concentration on the performance, combustion and emission characteristics of a constant speed biogas fueled SI engine. The reported literature of this section restricted the upper limit of the CO_2 concentration by 40% for stabilized operation of the biogas engine and recommended the use of scrubbed biogas in SI engine.
- Increased CR is an effective means for enhancing the performance of a biogas fueled SI engine even with the present of CO_2 and N_2 in biogas. However, the maximum operating CR is restricted within the critical limit and defined as the optimum CR for the specified operating condition and fuel composition used in the engine. The optimum CR is not only the function biogas composition but also depends on the various other operating parameters of the engine such as ER, IT and speed of the engine. Hence, a wide spectrum of analysis in multiple dimensions is still being pending with respect to the optimum CR and hardly being attained for variable speed biogas fueled SI engines.
- Ignition timing plays a dominant role to initiate and control the different stages of combustion in SI engine. The optimum IT is primarily governed by the combustion chamber design and engine operating conditions (CR, ER, engine speed, EGR rate and properties of the fuel). As noticed, most of the researchers have investigated the effect of variable IT and recommended the MBT or optimum IT of the SI engines fueled by gasoline, natural gas, hydrogen, producer gas and LPG at some specific operating conditions. However, this investigation has been hardly approached by scholars for

biogas fueled SI engines and is further limited to some specific operating condition of the engine.

- The operating ER or RAFR of the SI engine not only controls the combustion characteristics of the air-fuel mixture, but also regulate the properties of the combustion products and is primarily responsible for the performance and emission of the SI engine. As noticed, most of the researchers have studied the effect operating ER or RAFR on the performance, combustion and emission characteristics of the biogas fueled SI engine but are limited to some specific operating CRs, CO_2 concentration and engine speeds.

2.6 Delineation of Thesis

The motive of the study is not only focused on replacing gasoline with abundantly available renewable gaseous fuel (biogas) but also to devise an efficient standalone biogas fueled variable speed SI engine. After an extensive literature survey, *the theme of this thesis is framed to determine the optimal operating parameters (optimum compression ratio, maximum brake torque timing, throttle position and optimum air-fuel ratio) of a biogas fueled SI engine through a multi fuel, variable compression ratio (VCR), spark ignited research engine setup for effective implementation in a commercial SI engine.* During the course of this investigation three different SI engine setups have been used namely; ***Biogas fueled customized commercial SI engine*** (*ModelPN-1 BG, Make: Prakash Diesels Pvt. Ltd),* ***VCR SI research engine setup****, (Model: 240 PE, Make: Apex Innovation Pvt. Ltd.,) and* ***Gasoline fueled SI engine*** *(Model: GX 200 Make: Honda Siel Power Products Ltd*). The theme of the thesis is being achieved through a predefined sequence of objectives as shown in **Fig. 2.2** and highlights the overview of the thesis.

The preliminary investigation of the study was started with a commercial customized four stroke, water cooled, single cylinder; biogas fueled SI engine (*Make: Prakash Diesels Pvt. Ltd., India; Model: PN-1 BG*) of rated capacity 4.4 kW, which was retrofitted from a CI engine. The commercial biogas engine was tested on site under different loading conditions following standard guideline as specified by the Bureau of Indian Standards (BIS) [IS 10000: Part 6-8]

and the existing complications were identified for the further improvement and design of these kind of engines.

Further, a four-stroke, naturally aspirated, gasoline-fueled, variable compression ratio (VCR), water cooled, single cylinder, variable speed spark ignited research engine setup (*Make: Apex Innovation Pvt. Ltd., Model: 240 PE*) of rated capacity 4.5 kW (at 1800 rpm and CR10) has been retrofitted with a specially designed biogas induction mechanism and developed for biogas mode operation at Energy Efficiency Laboratory, IIT Guwahati. The VCR mechanism of the engine was further redesigned to operate the engine in a wide range of operating CR (CR 8 to CR 14) and retrofitted with an ECU controlled reprogrammable variable ignition timing (VIT) attachment to operate the engine with a wide range of IT.

Additional efforts have been made to focus on the methodologies to enhance the efficiency of the variable speed biogas fueled SI engine by experimentally optimizing the critically operating parameters such as compression ratio (CR), ignition timing (IT), throttle position (TP) and air-fuel ratio (AFR). The optimized operating parameters attained through series of experiments during the investigation with the biogas fueled SI engine are then recommended for the optimized performance of the engine and is the foremost thrust point of the current investigation.

Further, in the process of developing a biogas fueled SI engine, the optimized operating parameters (CR, IT, TP and AFR) attained through series of experiments in the retrofitted spark ignited research engine setup was intended to incorporate in a commercial SI engine (*Make: Honda, Model: GX 200*) commonly used for the stationary power generation application. The particular model (*Honda, GX 200)* is a naturally aspirated, gasoline-fueled, four-stroke, single cylinder, air cooled, variable speed SI engine with a fixed CR (8.5) and rated capacity of 4.1 kW at 3600 rpm. However, due to manufacturing constraints, the operating CR of the commercial SI engine (*Honda, GX 200*) could not be enhanced beyond 9.5 even after the alteration. Hence, The CR and IT of the commercial SI engine has been set to CR 9.5 and 50° CA before top dead center (bTDC).

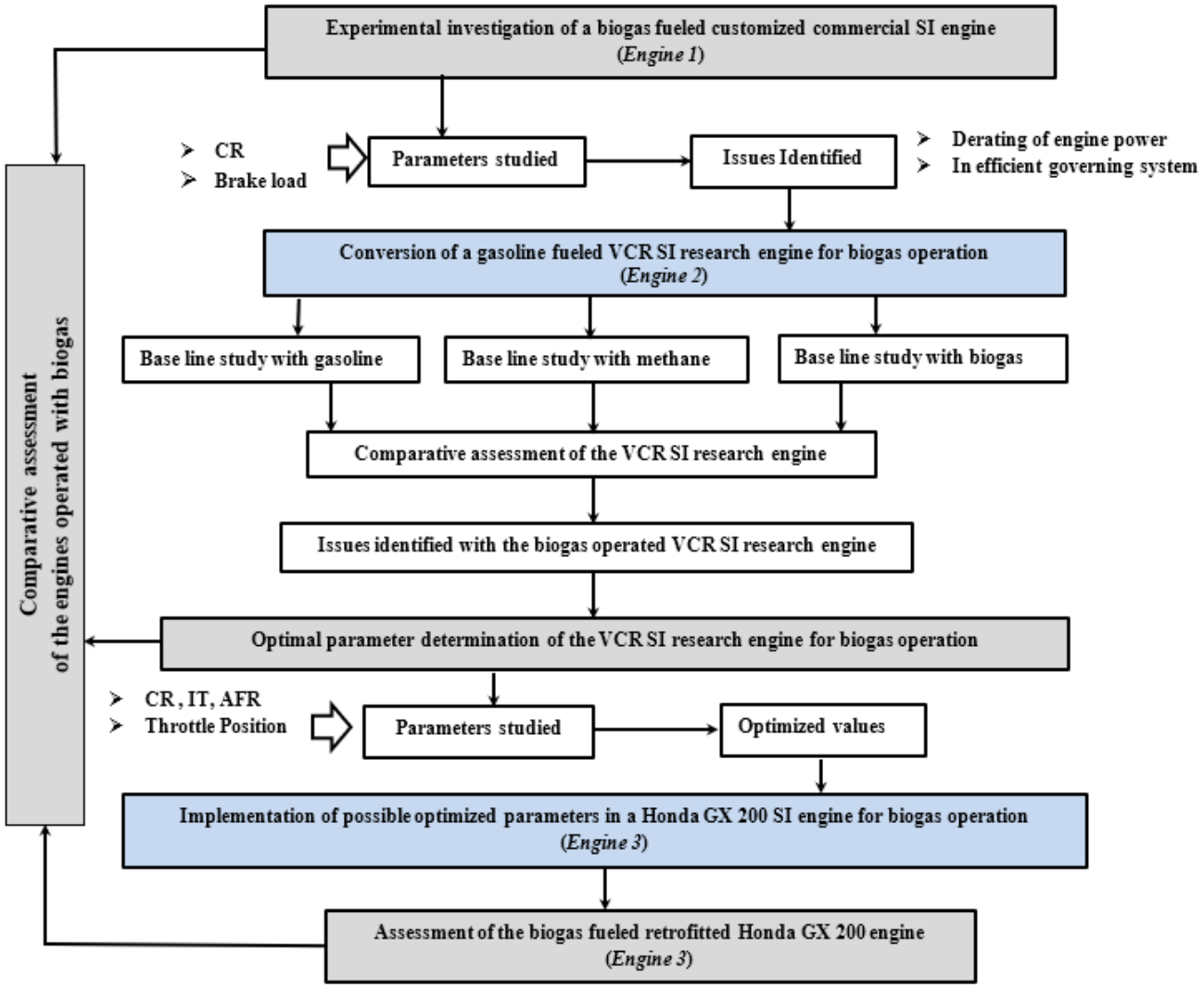

Fig. 2. 2: Overview of the research investigation

The air-fuel intake system of the commercial SI engine was also retrofitted with a biogas induction mechanism and integrated with a venturi type biogas mixture. Further, the retrofitted commercial SI engine (*Honda, GX 200*) was operated and tested with biogas at different operating conditions following standard guideline as specified by the BIS in IS 10000. The performance, combustion and emission study of the developed biogas engine (retrofitted commercial SI engine, *Honda GX 200*) were analyzed and explained in detail in the thesis and the second thrust point of the present work.

The overall objective of the thesis is mainly delineated and highlighted into few sub-categories and are listed as follows:

- Development of a test facility for the preliminary experimental investigation of a commercially customized biogas fueled SI engine (*Make: Prakash Diesels Pvt. Ltd., India; Model: PN-1 BG)*
- Determination of the performance, combustion and emission characteristics of the VCR SI research engine *(Model: 240 PE, Make: Apex Innovation Pvt. Ltd.,)* fueled by gasoline and methane. (Baseline experimental investigation)
- Conversion of the gasoline fueled VCR SI research engine for biogas operation.
- Comparative assessment of the VCR SI research engine fueled with gasoline, methane and raw biogas.
- Optimization of the operating parameters (CR, IA, TP, AFR and engine speed) by investigating its effect on the performance, combustion and emission characteristics of the raw biogas fueled VCR SI research engine.
- Implementation of the optimized operating parameters and conversion of the gasoline fueled *(Honda GX 200)* SI engine for biogas operation.
- Investigation of the performance, combustion and emission characteristics of the raw biogas fueled retrofitted Honda GX 200 SI engine.
- Comparative assessment of the different engines (*Biogas fueled customized commercial SI engine, VCR SI research engine, Honda, GX 200 SI engine)* fueled with raw biogas.

2.7 Organization of The Report

The overall goal of the present work is to devise an efficient biogas fueled SI engine by focusing the concentration towards determining and implementing the optimal operating engine parameters (optimum compression ratio, maximum brake torque timing, throttle position and optimum air-fuel ratio). **Chapter 1** offers the motivation acquired towards the use of renewable gaseous fuels in SI engines. This chapter includes the importance and the application of biogas as a renewable and alternative fuel to gasoline in SI engines. Further, this chapter explicitly discussed the available SI engines for biogas application and highlighted issues and shortfall of those engines followed by the different methods for enhancing the overall performance of biogas fueled SI engines. **Chapter 2** includes the detailed review of the existing literature on the conversion methodologies and performance improvement methods of the conventional SI engines fueled by biogas and other alternative fuel. This chapter also includes the review of the extensive literature on the influence of the operating parameters on the performance, combustion and emission characteristics of the biogas fueled SI engine followed by the summary of the literature, proposed objectives and organization of the dissertation. **Chapter 3** includes the details of the experimental setups (biogas fueled customized commercial SI engine setup, VCR SI research engine setup and retrofitted Honda GX 200 SI engine setup) developed for biogas application along with the methodologies adopted for the engine conversion, engine instrumentation, compression ratio variation control and biogas induction. These chapters also discuss the uncertainties associated with the each experimental setup. **Chapter 4** discusses about the base line experiments conducted in the VCR SI research engine test facility (***Engine 2***) to form the foundation of the dissertation by considering standard gasoline, biogas and methane as the operating fuel for the SI engine. It also includes the experimental matrix, properties of the test fuels, engine operating procedure and assessment of the engine operating characteristics in detail for the respective fuels for specified operating conditions. **Chapter 5** discusses about the experimental matrix, properties of the raw biogas and operating procedures for the biogas fueled VCR SI engine (***Engine 2***) in detail. Further, this chapter also intricately discusses the effects of operating parameters (ignition advance, compression ratio, air-fuel ratio, throttle position, engine speed) on the performance, combustion and emission characteristics of engine and recommend the optimal

operating condition (best possible operating condition) of the biogas fueled VCR SI research engine. The sole objective of the chapter is to identify the optimal operating parameters for improving the performance of the biogas fueled VCR SI engine. **Chapter 6** includes the experimental matrix, operating procedures and in detail experimental investigation of the raw biogas fueled retrofitted Honda GX 200 SI engine (***Engine 3***) with the best possible implemented operating parameters obtained from the investigation of the biogas fueled VCR SI research engine. **Chapter 7** includes the detail investigation of the commercially customized biogas fueled SI engine (***Engine 1;*** Commercially available biogas engine). This chapter explicitly includes the performance, combustion and emission characteristics of the engine under dynamic loading condition at the rated operating CR along with some other predefined operating conditions and report the pro and cons of the engine in the light of further research and development. **Chapter 8** refers to the comparative assessment of the biogas operated VCR SI engine with retrofitted Honda GX 200 SI engine and customized biogas fueled SI engine in terms of the performance, combustion and emission parameters. In the present section, the above-mentioned engines are operated with biogas and the optimal values of the performance, combustion and emission data were compared and discussed in detail. **Chapter 9** summarizes the key findings of the present investigation along with the contribution of the dissertation; thereby, proposing the possible future works.

Table 2. 1: Recommended engine operating condition for different fuels

Author	Fuel	Engine	Parameters studied	Optimum operating conditions/ Recommendations
Huang and Crookes, 1998	Simulated biogas	Ricardo E6 single-cylinder SI engine	CR, RAFR, CO_2fraction at constant N	• Critical CR -13 (At N=2500 rpm, RAFR=0.97, CO_2 fraction=37.5%) • Optimum CR- 13 • Optimum range of RAFR -1.05 to 0.95 • Limiting fraction of CO_2 content - 40%
Porpatham et al., 2008	Biogas	Single cylinder constant speed CI converted SI engine	CH_4 concentration at constant N, CR and TP	• Suitable range of operating CR - 11 to 13 • Optimum range of ER – 0.8 to 0.95 • Acceptable CO_2 content – 20 to 30% • Recommended operating CR – 13:1 (At N=1500 rpm, MBT, WOT, CO2 fraction= 20%, ER= 0.91)
Porpatham et al., 2012	Biogas	Single cylinder constant speed CI converted SI engine	CR and ER at constant N, TP	• Critical CR- 13 • Recommended range of operating conditions at N= 1500 rpm, MBT and WOT ○ CR- 13 to 15, ER- 0.95 to 1.08
Roubaud and Favrat, 2005	Biogas	Six-cylinder turbocharged SI engine	CR and combustion pre- chamber	• The use of un-scavenged pre-chambers is recommended at CR 13.3
Chandra et al., 2011	CNG, Simulated biogas, methane enriched biogas	Single cylinder constant speed CI converted SI engine	Brake load at constant N and CR	• Recommended CR – 12.65 • Optimum IA - 35° CA bTDC at CR 12.65, N = 1500 rpm Methane enriched biogas (95% of CH_4) was recommended • Admissible BL at CR 12.65 ○ 68% for CNG, 66% CH_4 enriched biogas ○ 53.5% for biogas

Montoya et al., 2015	Simulated biogas, methane enriched biogas	Double cylinder constant speed CI converted SI engine	Biogas composition and BL at constant N, CR and ER	• Recommended fuel composition: Mixture of 50% biogas and 50% methane by volume • The optimum operating condition: ○ CR- 15.5, MBT- 12°bTDC, ER- 0.95, N- 1800 rpm • Engine power de-rated by 17.6%
Jaramillo et al., 2018	Simulated biogas	Twin cylinder constant speed CI converted SI	ER, IT and BL at constant N, CR and TP	• Safe operating limit at CR 15.5: ○ Throttle valve opening - 39%, ER- 0.6 to 1, IA - 329º to 358º CA
Kwon et al., 2017	Simulated biogas	Honda GX 200, Single cylinder SI engine	CR and CO_2 concentration at constant N, ER and IT	• Recommended operating condition ○ CR- 9.22, N- 3600 rpm, MBT • Acceptable range of CO_2 content – 0 to 40% by vol
Amorim et al., 2010	CNG, Gasoline	1.3-L 8v Fire Flex variable speed engine	CR	• Optimum operating condition ○ For CNG flexed fueled engine: CR – 15, RAFR (λ) – 0.97, N- 5500 rpm, IA ~ 34º CA bTDC ○ For Gasoline fueled engine: CR – 11:1, N- 5500 rpm, IA ~32º CA bTDC
Zheng et al., 2009	NG	Single cylinder direct injection SI engine	CR	• Optimum operating condition ○ CR – 12, RAFR (λ) – 1.214, N- 1200 rpm, IA - 30º CA bTDC, Injection timing- 180º CA bTDC
Poompipatpong and Cheenkachorn, 2011	NG	Four-cylinder variable speed CI converted SI engine	CR	• Recommended operating condition ○ For best BTE and SFC- CR 9.5, N- 1500 to 2500 rpm. ○ For best BP and BT- CR 10:1
Fleming, 1985	NG	Single cylinder SI engine	CR and ER at constant N, TP	• Optimum operating condition ○ CR – 15.5, ER (Φ) – 0.78, N- 2140 rpm
Ma et al., 2012	Hydrogen enriched CNG	Single cylinder constant speed SI engine	CR and IT at constant N, RAFR and manifold pressure	• Recommended operating condition: ○ CR – 12, RAFR (λ) – 1.6, N- 1200 rpm, IA - 28º CA bTDC, MAP- 50 kpa, at 20% H_2 concentration

CHAPTER 3

Experimental Facilities

Overview

This chapter includes the details of the used test fuels along with its technical specification and methodologies adopted to find out their physicochemical properties. The technical descriptions of the experimental setups developed and used during the current investigation are also highlighted herein this chapter along with their detail operating procedures. The experimental setups involve a biogas fueled commercially customized SI engine test facility (Engine 1), a VCR SI research engine test facility (Engine 2) and a Honda GX 200 SI engine test facility (Engine 3). The engine specifications and the instrumentation techniques adopted for the experimental facilities to record, analyze and post process the recorded experimental data are elaborately explained in the present section. This chapter also explain about the mechanisms and techniques adopted to control the compression ratio and ignition timing for the developed experiential facilities for the present investigation. The developed biogas induction mechanisms for the individual test facilities are also discussed in detail here in this chapter. This chapter also clearly discusses the methodologies adopted to convert the gasoline fueled SI engine for biogas application.

3.1 Test Fuel and their Properties

The overall goal of the present investigation is to device an efficient standalone biogas fueled variable speed SI engine. In this context, three different SI engines have been identified. One is the commercially customized constant speed biogas fueled SI engine (Engine 1), the second one is the variable speed gasoline fueled VCR SI research engine (Engine 2) and the third one is the variable speed gasoline fueled Honda GX 200 SI engine (Engine 3). The VCR SI research engine (Engine 2) and Honda GX 200 SI engine (Engine 3) are originally configured for gasoline operation. However, Engine 2 has been further retrofitted and reconfigured with a methane and biogas induction mechanism followed by the process of operating parameter optimization for biogas application. Similarly, Engine 3 has been further reconfigured with the best possible operating parameters and induction mechanism for biogas operation. Hence, in the current investigation standard gasoline (Grade MG 91), pure methane and raw biogas are considered as the test fuel. Motor gasoline (RON 91) is collected form the Indian Oil Corporation (IOCL), compressed methane cylinders (with 99.99% purity) is obtained from an industrial gas supplier registered as "Om Specialty Gases". Raw biogas was produced by the anaerobic digestion of cow manure and ligno-cellular biomass in a fixed dome type biogas digester of three cubic meter capacity at 'Auniati Satara', North Guwahati, Assam. The composition and most of the physico-chemical properties of motor gasoline and pure methane are stated and certified by the producers and listed in **Table 3.1**. The composition of the biogas generated onsite is monitored in a frequent interval by a GFM406 series portable biogas analyzer (Make: Gas Data, UK). GFM406 is an ATEX multi-channel portable hand-held gas analyzer configured specifically for biogas analysis on site and can analyze the content of CH_4, CO_2, O_2 and H_2S. The detail specification of the instrument and sample reports are given in **Table A- 1** and **Table A- 2** of **Appendix A** respectively. The GFM 406 series biogas analyzer could not analyze the N_2 content. Hence, prior to the use of biogas as a fuel in SI engine, the composition and calorific value of the collected biogas has been re-analyzed each time in a Thermo Scientific Made TRACE 1110 EPC series gas chromatograph and Hardson Co. made Junkers gas calorimeter. The gas chromatograph was equipped with a thermal conductivity detector (TCD) and porapak Q column. Helium was used as the carrier gas for this analysis. Before injecting the biogas sample at the injector port, the column temperature and TCD temperature of the gas chromatograph was set to 45^o C and 180^o C, respectively. The

sample report along with the detail specification of the Thermo Scientific Make TRACE 1110 series gas chromatograph are given in **Table A- 3** of **Appendix A**. The specification, sample report of LHV calculation and the experimental setup of the Junkers gas calorimeter are presented in **Table A- 4, Table A- 5** and **Fig. A- 1** of **Appendix A**, respectively. It has been observed that there was no substantial change in the composition and calorific value of the produced biogas unless until there was a drastic change in environmental operating parameters or change in feed materials to the biogas digester. However, there was a little variation in the composition of the biogas with time according to the activities of the anaerobic bacteria. The average compositions of its constituents and most of its properties were experimentally obtained and mentioned in **Table 3. 1**.

Table 3. 1: Physio-chemical properties of test fuels.

Properties	Gasoline	Methane	Biogas
Molecular formula	$C_nH_{1.87n}$ [$]	CH_4- 99.9%	CH_4- 55.6 ± 2.5 %[#] CO_2- 42.3 ± 3 %[#] N_2- 2.1 ± 0.5 %[#] H_2S- 521± 52 ppm[#]
Density at 15 °C (kg/m^3)	720-775[¥]	0.72	1.11[#]
Lower heating value (MJ/kg)	43.55[#$]	50	17[#]
Heat of vaporization (MJ/kg)	0.33[#$]	0.509	0.5[$$]
Stoichiometric A/F ratio	14.7[*]	17.23	5.51 [*]
Research octane number	91[¥]	120	110 [$$]
Auto ignition temperature(°C)	257[**]	540-600	650 [$$]
Flame Speed (cm/s)	45[**]	38	25 [$$]

[¥] Indian Oil Corporation, * Calculated, [#] Experimental value, [$] (Heywood, 1988), [**](Yüksel and Yüksel, 2004), [$$](Jeong et al., 2009)

3.2 The Commercial Biogas Engine Test Facility (*Engine 1*)

The preliminary investigation of the study was initiated with an extensive literature and field survey at different states of India where, biogas was abundantly generated from different wastes and utilized as a source of energy (by transforming it to electricity for personal or community use). As noticed in most of the cases, dual fuel CI engines or CI converted SI engine are preferred for the purpose of biogas energy conversion. Some of the commercial engine manufactures such as Shanghai Bioenergy Engineering Co. (China), Kirloskar Oil Engines Ltd. (India), Cummins India

Ltd., Montgomery/ Yammer (Brazil), C.A.S./Henkelhause-Deutz (Germany), and Deutz MWM (Germany) have developed 4 stroke LPG/ NG/biogas SI engines of rated capacity in between 20 kW to 2200 kW (Mitzlaff, 1988). The above developed high power multi cylinder gas/ biogas engines are the modified version of the multi-cylinder CI or SI engines. Further, some of the local engine manufactures such as Prakash Diesel Pvt. Ltd. (India), Urja Bio System Ptv. Ltd. (India), Qualitech Engineers Pvt. Ltd. (India), and Enersol Biopower Pvt. Ltd. (India) have claimed to develop standalone biogas fueled SI engine generators in the range of 4.4-58 kW, 2-100 kW, 1.2-100 kW and 5-100 kW, respectively which involves both single and multi-cylinder SI engines.

As of today, most of the commercial gaseous fueled SI engines are multi-cylinder and focused on medium or large-scale applications with specially designed exhaust gas treatment system. However, the small or low powered single cylinder engines are significantly used for decentralized power generation and agricultural activity in the rural or remote areas of the developing countries. Hence a low power biogas fueled commercial SI engine (*Make: Prakash Diesel Pvt. Ltd., Model: PN-1 BG*) of rated capacity 4.4 kW (6 HP) has been chosen for the preliminary investigation of this study. Further, the above-mentioned engine has been customized by the manufacturer as per the test facility requirements for mounting the measuring instruments on the engine head and output shaft.

3.2.1 Engine specification and experimental facility

The pictorial and schematic layout of a single cylinder, 990.6 CC, four stroke, water-cooled, constant speed, biogas fuelled commercially customized SI engine (*Make: Prakash Diesel Pvt. Ltd., Model: PN-1 BG*) setup of rated power and speed of 4.4 kW and 1500 rpm are shown in **Fig. 3. 1** and **Fig. 3. 2**, respectively. The engine is coupled with an electrical braking system through a 3.5 kVA, 230 V, 50 Hz bush type alternator (*Make: Parkash Diesel Pvt Ltd., Model: PS350A*). The detail specification of the engine along with the alternator and all other accessories are listed in **Table B- 1** of **Appendix B**. The rated CR of the engine is 13.94 for biogas mode operation. However, for analysing the effect of CR on the performance, combustion and emission characteristics of the constant speed biogas operated SI engine, the operating CR of the engine was varied in between 10.52 to 15.29. The engine was tested at four different compression ratios (CR 10.52, CR 11.96, CR 13.94 and CR 15.29) by using a suitable CR alternation technique as

mentioned in *section 3.2.3.* The engine is equipped with a mechanical controlled capacitive discharge ignition (CDI) system. The capacitive discharge ignition (CDI) system attached with the engine triggers the sparkplug by a cam operated ignition control system. The engine is also equipped with a mechanical governing system and a T-type gas mixer along with two throttle valves to control the mass flow rate of air and air-biogas mixture at all operating load to maintain the engine speed constant. The biogas and air in flow to the engine is tracked by a biogas flow meter (*Make: Siya Instruments, Model SI-6*) and open U tube manometer. The setup is further equipped with necessary instrumentation for combustion pressure and crank-angle measurements and the details are mentioned in *section 3.2.2*. The pressure and crank angle signals are further interfaced with computer through a piezo-powering unit. The engine is connected to the Labview based software 'Engine soft' to record and analyze the data stored via a NI USB 6210 data logger. The exhaust gas emission of the engine is analyzed by an AVL DIAGAS 444N five gas analyzer as per the method mentioned in *section 3.2. 2.* The detail specification of the AVL DIGAS analyzer is mentioned in **Table B-2** of **Appendix B**. A battery, starter motor and a battery charger are also equipped with the engine setup for smooth electric starting.

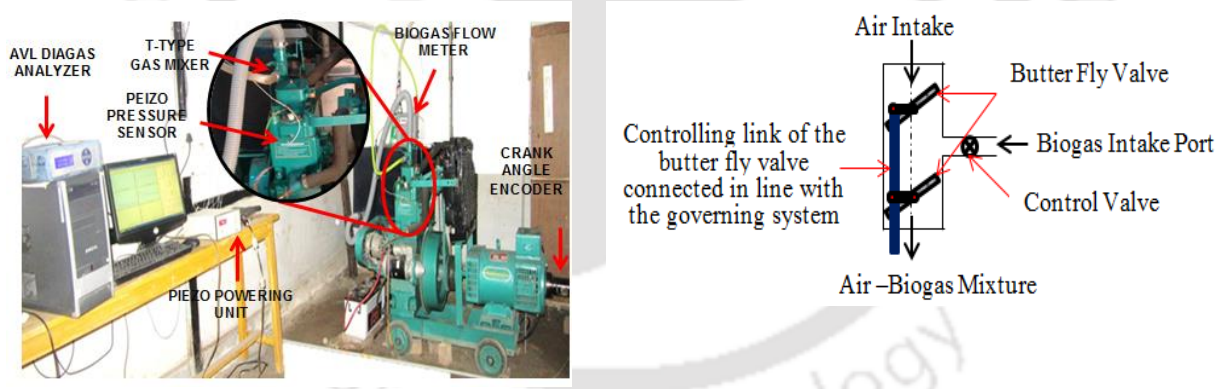

Fig. 3. 1: Commercial biogas engine setup and integrated instrumentation

3.2.2 Engine instrumentation

The engine is well instrumented to track the operating parameters. For measuring the air consumption of the engine, an air box is designed with an orifice of 20 mm diameter and connected to an open U tube manometer. Similarly, the biogas flow rate was tracked down by a biogas flow meter. The engine was loaded electrically to find out the generated BP. To measure the cylinder pressure, a dynamic piezo pressure sensor with built in amplifier and low noise cable are mounted

on the engine head. Similarly, the crank angle rotation is tracked down by an optical crank angle encoder mounted on the crank shaft of the engine. The pressure and crank angle signals are then interfaced to the computer through piezo power unit to observe the pressure and crank angle signals along with the speed of the engine. The detailed description of the engine instrumentation is explained here in this section.

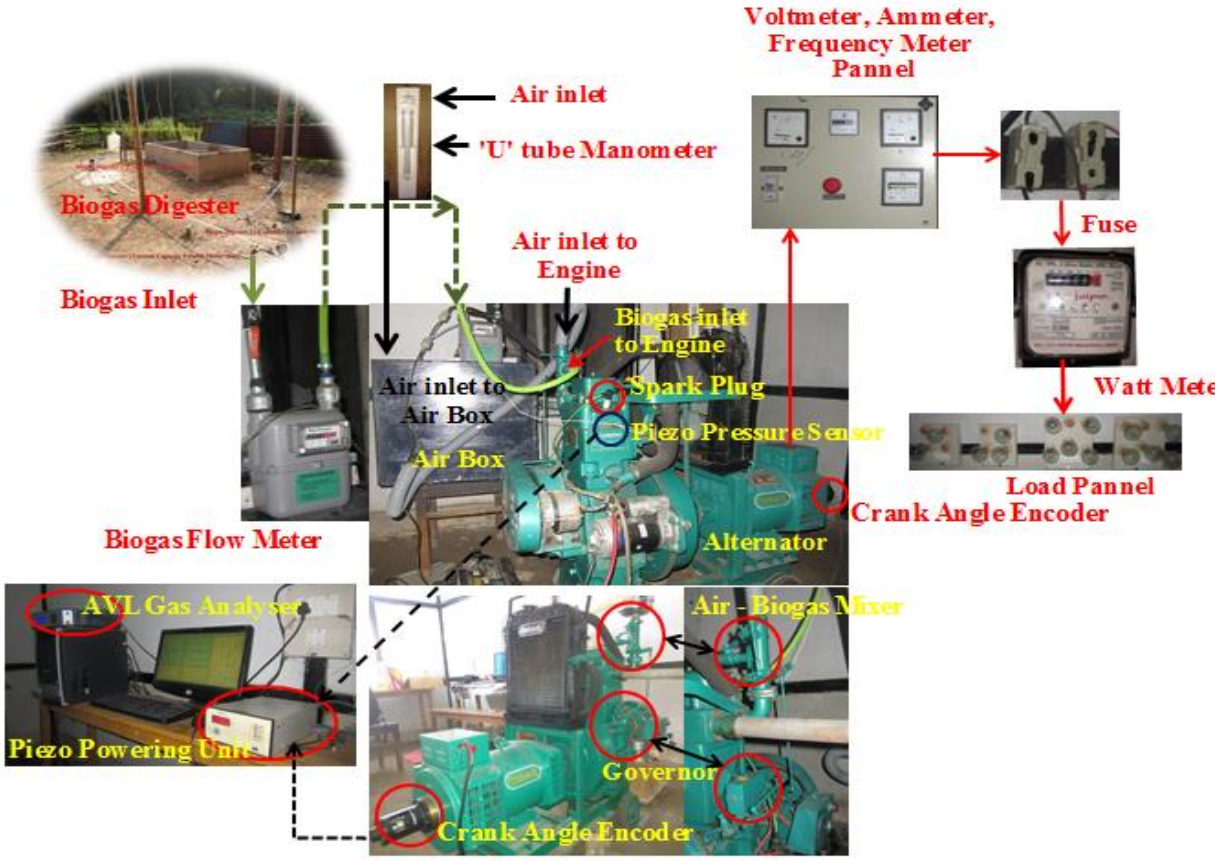

Fig. 3. 2: Schematic layout of the commercial biogas engine test facility

Braking system

The engine is coupled with a single phase, 3.5 kVA alternator (*Make: Parakash Diesel Pvt. Ltd., Model: PS350A*) to generate 230 V and 50 Hz frequency at 1500 rpm. For loading the engine crank shaft, the output of the alternator is connected with a resistive load panel consisting of 15 numbers of 200-Watt bulbs in series. The consumed current and output voltage of the alternator at all loading conditions of the engine are tracked by a voltmeter and an ammeter connected in line with

the load panel. The applied braking load is controlled by varying the voltage and current consumed by the resistive load panel. The average efficiency and power factor of the alternator were 78% and 1, respectively. The output brake power (BP) of the engine is calculated from the data recorded by the designed braking system by using equation 3.1, where 'V' is the voltmeter reading, 'I' is the ammeter reading, cosΦ is the power factor, and 'η_A' is the efficiency of the alternator.

$$BP = \frac{V \times I \times \cos\phi}{1000 \times \eta_A} \qquad 3.1$$

Air intake and fuel mixing system

A T-type air intake and biogas supply system as shown in **Fig. 3. 1** is used in this study. The inlet diameters of the air intake and biogas intake port are 38 mm and 12.7 mm, respectively. The air-biogas mixer is equipped with two throttle valves to control the mass flow rate of air and air-biogas mixture at all operating load to maintain the engine speed constant by supplying an appropriate air-fuel mixture to the engine. The throttle valves are actuated by a unique designed governing system by replacing the fuel injection pump of the base engine and it is directly connected to the installed throttle valves on the gas mixer by joining a link mechanism.

Air consumption measurement

An air box having a suitable volume of 500 times the swept volume of the engine cylinder was fabricated with a sharp edge orifice of 20 mm diameter and attached before the air intake point on its one side. Further, an open U tube manometer is connected to the air box in order to find out the pressure difference across the orifice due to the flow of intake air to the engine. The mass flow rate of the air across the orifice is calculated from the obtained pressure difference by using equation 2.2. Where, C_d is the coefficient of discharge of the orifice and is 0.6; A is the cross-sectional area of the orifice and is 0.000314 m^2; g is the acceleration due to gravity and is 9.81 m/s^2; ρ_w and ρ_a are the density of water and air and are 1000 kg/m^3 and 1.16 kg/m^3, respectively.

$$Mass\ flow\ rate\ of\ air,\ kg/h = C_d \times A \times \sqrt{2gh(\rho_w / \rho_a)} \times \rho_a \times 3600 \qquad 3.2$$

Biogas flow measurement

The mass flow rate of biogas supplied to the engine was calculated by using a biogas flow meter (*Make: Siya Instrument Pvt. Ltd., Model: SI-6*). This biogas flow meter is a positive displacement volume flow meter specially designed and developed for low pressured biogas flow. The flow meter has two chambers formed by moveable diaphragms. With the gas flow directed to the internal valves, the, the chamber alternately fills and expels the biogas and produced a continuous flow through the meter. As the diaphragms expand and contract, levers connected to the crank translates the linear motion of the diaphragm to rotary motion of the crank shaft. To record the flow the crank shaft was connected to a trip odometer to visualize the flow rate. For ensuring the correctness of the reading the biogas flow meter was calibrated with a standardized Coriolis mass flow meter. The biogas flow meter has an accuracy of ±0.4% and the maximum and minimum flow rate of the biogas flow meter was 6 m^3/h and 0.04 m^3/h, respectively. The detail technical specification of the biogas flow meter is given in **Table B- 3** of **Appendix B**.

Load panel

The load panel attached to the setup is an electric resistance load bank which consist of incremental restive load by placing 15 numbers 200-Watt bulbs in series. The loading capacity of the load bank is 0 to 3.0 kW.

P- θ measurement

The PCB Piezotronics made dynamic piezo pressure sensor (*Model M111A22*) with built in amplifier along with low nose cable is fitted on the cylinder head. It is capable to measure pressure of compression, combustion, explosion, pulsation, cavitations, blast, pneumatic, hydraulic, fluidic etc. The maximum operating pressure rage of the pressure sensor is 15000 psi with a resolution and sensitivity of 0.1 psi and 1 mV/psi, respectively. A Kubler make optical crank angle encoder (*Model 8.3700.1321.0360*) is also incorporated and attached to the crank shaft for measuring the speed and each degree rotation of the crank shaft. The resolution and range of the optical encoder was 10 and 5500 rpm with the TDC pulse. The pressure and crank angle signals are then interfaced to the computer through a piezo powering unit and a data accusation system (*NI USB -6210, 16*

bit, 250 kS/s) to record and observe the pressure and crank angle signals as well as to measure the speed of the engine.

Exhaust gas measurement

The AVL made DIGAS 444N gas analyzer is used for measurements of exhaust emissions of liquid and gaseous fuels. The Flue gas analyzer is connected to the AECS software for recording the emission data. The exhaust gas samples are drawn from the tail pipe by using a probe for fixed time duration under the specified set of operating conditions. These gas samples are then analyzed in the flue gas analyzer for direct reading of CO, CO_2, NOx, O_2 and HC concentration in the flue gas.

3.2.3 Compression ratio variation control

The rated CR of the engine is 13.94 for biogas mode operation. But for analyzing the effect of CR on the performance, combustion and emission characteristics of a biogas fueled constant speed SI engine, the CR of the engine is varied manually by altering the clearance volume of the engine. Since the dimensions of the stroke volume (939.69 cc) and the piston cavity (51 cc) are known, the CR of the engine without any clearance slot is calculated and found to be 19.38. Thus by placing correct combination of copper (*C*) and bakelite (*B*) gaskets of thickness 2.65 mm and 1.8 mm, respectively in between the engine head and cylinder block, the CR of the engine is varied for each test. The designated compression ratios of 10.52, 11.96, 13.94 and 15.92 are achieved by maintain the bumping clearance as 5.85 mm (*1B+2C*), 4.25 mm (*1B+1C*), 2.65 mm (*1B*), and 1.8 mm (*1C*), respectively as shown in **Fig. 3. 3**. When the engine head was placed on the cylinder and the bolts were tightened the bakelite gasket was compressed by 0.2 mm and this factor was considered while evaluating the CR for each combination of the gaskets. As mentioned, the above listed bumping clearances are achieved by appropriate combination of copper and bakelite gaskets available in the market. The engine is tested at four different CRs i.e, 10.52, 11.96, 13.94 and 15.92.

Fig. 3. 3: Engine cylinder Block and head with CR variation attachments

3.2.4 Biogas induction mechanism

The biogas fueled commercially customized SI engine (Engine 1) is installed on site where raw biogas was produced by the anaerobic digestion of cow manure and lingo cellular biomass in a Dinabandhu model fixed dome type biogas digester at 'Auniati Satara', North Guwahati, Assam. The integrated capacity of the biogas plant is 12 m^3/ day (four numbers of 3 m^3 biogas digesters). The biogas digesters are further connected to an inverted U shaped (∩) integrated storage unit which is hinged at its both side in a concrete well half filled with water. The accumulated biogas inside the integrated storage unit displaces the water to the outer periphery of the inverted U-shaped unit and build up enough pressure to supply it to the engine room through the H_2S scrubber and moisture trapper (**Fig. 3. 4)**. The gauge pressure of biogas in the integrated storage unit is varied in between 1.6 to 1.8 bar. The H_2S scrubber is made from PVC pipe (Φ=110 mm, L= 500 mm) and packed with annealed compacted steel waste chips of 500 gm. Similarly, the moisture trapper was also made from PVC pipe of 110 mm diameter and 500 mm in length and loosely packed with blue silica gel crystal of mesh size 6-8 mm. The engine was well instrumented and installed in the monitoring room of the onsite laboratory which was approximately 14 m from the integrated storage unit.

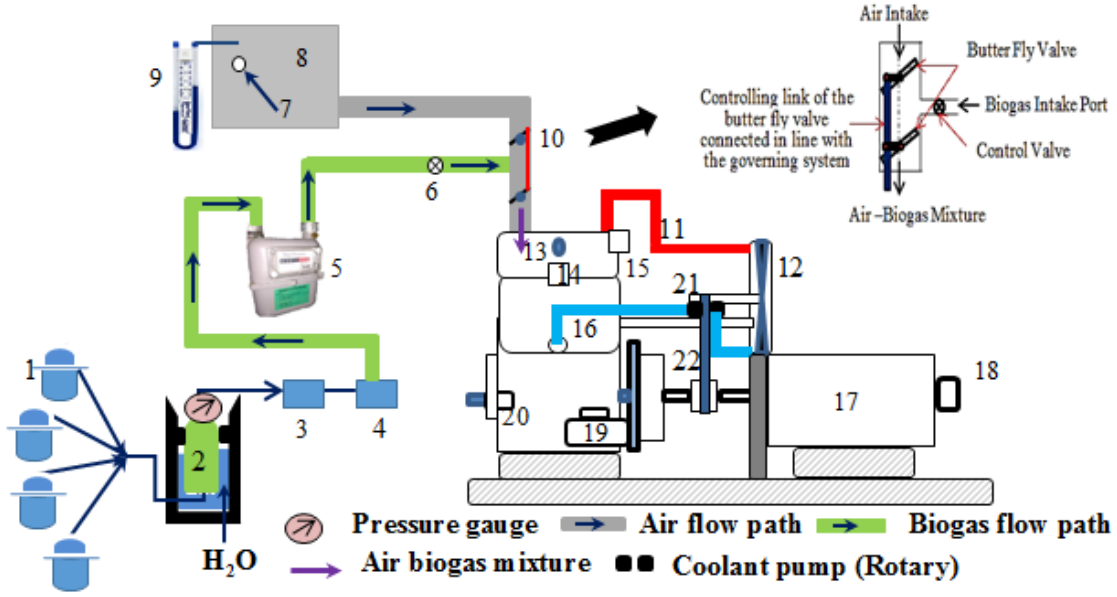

1.Biogas digester 2. Integrated biogas storage unit 3. H_2S Scrubber 4. Moisture Trapper 5. Biogas flowmeter 6. Control valve 7. Orifice 8. Air box 9. Open U tube manometer 10. Air-Biogas mixer 11. Hot coolant flow line to the radiator 12. Radiator 13. Piezo pressure sensor 14. Location of spark plug. 15. Compression lever. 16. Cold coolant flow line to the engine 17. Alternator 18. Crank-angle encoder 19. Stator motor 20. Dynamometer and battery charging unit 21. Coolant pump driven by crank shaft 22. Driver belt connecting the pully and coolant pump

Fig. 3. 4: Biogas induction mechanism attached to the commercially customized SI engine

Fig. 3. 4 shows the schematic of biogas and air induction mechanism to the engine. The biogas passed through the H_2S scrubber and moisture trapper was drawn in to the intake manifold of the engine through the biogas flow meter (*Make: Siya Instrument Pvt. Ltd*.) and air-biogas mixer (T-Type) due to the pressure drop during the intake stroke of the engine. The induced pressure drop in the engine cylinder also draws in a definite quantity of atmospheric air through the air-box and air-biogas mixer. The air–biogas mixer, shown in **Fig. 3. 1** and **Fig. 3. 4** controls the mass flow rate of air and air-biogas mixture through the throttle valves at all operating load to maintain the engine speed constant by supplying an appropriate air-fuel mixture to the engine. The throttle valves are further actuated by an adjustable link mechanism governed by a mechanical governing system.

3.3 VCR-SI Research Engine Test Facility (*Engine 2*)

The issues and inefficiencies pointed out in the commercial customized biogas engine (Engine-1) motivated to explore the possible techniques to efficiently convert the existing gasoline

fueled SI engines into biogas engines. Hence, the gasoline fueled variable compression ratio (VCR) SI research engine test facility (Engine-2) available at Energy Efficiency Laboratory; IIT Guwahati was selected for the further research and development in this regard. The VCR-SI engine is a sophisticated research engine test facility specifically configured for gasoline operation and equipped with a tilting block VCR mechanism. The fuel induction mechanism, fuel injection timing, ignition timing (IT) or ignition advance (IA) corresponding to the operating speed and CR of the VCR SI engine test facility was originally configured for gasoline by the manufacturer. However, the same test facility can also efficiently accommodate gaseous fuels with appropriate modification in the fuel induction mechanism with the incorporation of optimized operating parameters of the engine. Further, these optimized parameters are also dependent on the fuel composition. In the due course of the ongoing investigation, the performance of the test facility was first evaluated for standard gasoline (Grade MG 91) with its original configuration at CR 10 in order to have a baseline for the further reference. Further, the base fuel induction mechanism of the VCR SI engine has been retrofitted with an indigenous gaseous fuel (methane and biogas) induction mechanism followed by optimization of the IT and evaluation of the VCR-SI engine fueled by methane and biogas at CR 10. The comparative assessment of the VCR-SI engine test facility at CR 10, fueled with gasoline, methane and raw biogas identified the limitations of the biogas fueled SI engine. CR is an influential operating parameter which enhances the BTE of the SI engine. Since, biogas has a higher auto ignition temperature; it could even resist knocking at higher CRs. Hence, the range of operating CR of the test facility has also been enhanced by redesigning the customized VCR mechanism as per the method proposed by Larsen (Larsen, 1991). The detail description of the methodologies adopted to redesign the tilting block VCR mechanism is given in *section 3.3.3*. Further in this investigation, the effect of most of the influential operating parameters (CR, IA/IT, engine speed, throttle position, A/F ratio) on the performance of the biogas fueled VCR SI engine has been analyzed and the optimum operating conditions are recommended.

3.3.1 Engine specification

The schematic layout and the pictorial outlook of the gasoline fueled VCR SI research engine test facility are shown in **Fig. 3. 5** and **Fig. 3. 6**, respectively. It is a four stroke, water

cooled, variable speed, manifold injected, single cylinder SI engine (*Make: Apex Innovation Pvt. Ltd., India, Model: 240 PE*) of rated power 4.5 kW at CR 10 and 1800 rpm in gasoline mode operation. The engine is coupled with a water-cooled eddy current dynamometer (*Make: SAJ International Pvt. Ltd, Model AG10*, Sl. no. 21, **Fig. 3. 5**) for loading the engine crankshaft with the induced electro motive force (emf). The engine is equipped with a hemispherical combustion chamber and cooling of the engine is accomplished by circulating water through the jackets of the engine block and cylinder head. The detail technical specifications of the engine along with the mounted accessories and instrumentation are listed in **Table C- 1** of **Appendix C.** The engine is equipped with a tilting block VCR mechanism (Sl. no. 18, **Fig. 3. 5**) by replacing the normal cylinder block. This mechanism is specially implemented to vary the operating CR of the engine. The CR of the VCR-SI engine can be altered in between 6:1 to 10:1 with the manufactures VCR setting. The detailed technical description of the VCR mechanism is explained in *section 3.3.3*. The fuel induction mechanism of the engine in gasoline mode consists of a fuel tank, fuel pump, fuel injector, optical crank angle encoder and a reprogrammable electronic control unit (ECU) to control the gasoline injection timing and duration as shown in **Fig. 3. 5** and **Fig. 3. 6**. Similarly, the ECU controlled direct ignition system (DIS) attached to the engine initiates the ignition process through the ignition coil, spark plug and input signals received from the optical crank angle encoder, and is triggered by the hall effect sensor or trigger sensor. The standalone panel box attached to the engine, consists of an air box, fuel tank, manometer, fuel measuring burette, dynamometer loading unit and the electronic panel along with an ECU and NI USB-6210 data accusation system (DAS). A diaphragm type piezo pressure sensor (*Make: PCB Piezotronics, Model:M111A22*) with built in amplifier and no noise cable is mounted on the engine head (Sl. no. 15, **Fig. 3. 5**) to measure the dynamic response of the cylinder pressure during combustion. The optical crank angle encoder (*Make: Kubler, Model: 8.3700.1321.0360*) attached with the engine (Sl. no. 23, **Fig. 3. 5**) delivers a signal for each degree rotation of the crankshaft. The pressure and crank angle signals are then interfaced to the computer through piezo powering unit (Sl. no. 5, **Fig. 3. 5**). The air flow consumption is measured by an air flow transmitter (*Make: Wika Instruments Ltd., Model: SL1*) attached to the air box, while the rotameters monitor and measure the constant flow rate of cooling water to the engine jacket along with the exhaust gas calorimeter. The liquid fuel (gasoline) consumption is tracked by a differential pressure transmitter (*Make: Yokogawa*

Electrical Corporation, Model:EJA110-EMS-5A-92NN) and a fuel burette attached with the fuel induction system. Similarly, there is a provision to record the gaseous fuel (methane or biogas) consumption by using a specially designed float type variable area rotameters (*Make: Veskler Instruments*). An ECU regulates the triggering, measurements of air and coolant temperatures, throttle positioning, and fuel injection system. The engine is connected to the Labview based software "Enginesoft" to record and analyze the data stored via a NI USB 6210 data logger. The emission analysis is carried out by an AVL DIAGAS 444N gas analyzer.

Further to accommodate the gaseous fuel (methane and biogas) efficiently in the gasoline fueled VCR-SI research engine, suitable techniques and methodologies recommended in the literatures were adopted. The VCR SI research engine is successfully retrofitted for gaseous fuel (methane and biogas) application by redesigning the fuel induction mechanism, setting the IT to MBT, enhancing the operating CR range of the VCR SI engine and setting the IT and CR to the optimum value. The optimum value of IT and operating CR of the SI engine are further dependent on the composition and octane rating of the fuel. Hence, they are different for methane and biogas application for the VCR SI engine. However, the ignition system (DIS), measuring instruments (piezo pressure sensor, optical crank angle encoder, trigger sensor, TPS sensor, idle air sensor, fuel/air flow transmitter) and instrumentation techniques remained almost unaltered (except fuel flow measuring technique). The schematic lay out and photographic outlook of the methane and biogas fueled VCR SI engine test rigs are represented in **Fig. 3. 7** - **Fig. 3. 8** and **Fig. 3. 9** - **Fig. 3. 10,** respectively. The technical specifications of the engines along with the mounted accessories and instrumentation are similar to the gasoline fueled VCR SI engine except the range of operating CR, fuel induction and measuring techniques and are also listed in **Table C- 1**of **Appendix C**. The fuel (methane and biogas) induction technique integrated with the experimental test rig is an in-house developed concept. The conventional fuel injection system (manifold injector) of VCR SI engine is replaced with a T-type air-fuel mixture (Sl no. 16 in **Fig. 3. 9**) along with a positive displacement self-driven diaphragm pump integrated with a heat exchanger for gaseous fuel induction. It not only delivers the required quantity of the fuel to the engine, but also preheats the fuel by capturing the waste heat of the hot water drained from the engine water jacket. *Section 3.3.4*, explains the fuel induction mechanism in detail for methane and biogas fueled VCR SI engine. Similarly, *section 3.3.3* explains the adopted methodology in detail for enhancing the

operating CR range of the VCR mechanism for both methane and biogas fueled VCR SI engine. The operating CR range of the VCR SI engine is enhanced by customizing the tilting block VCR mechanism and is achieved with altering the clearance volume (V_c) of the SI engine. As shown in **Fig. 3. 12**, with the attached VCR mechanism the operating CR of the engine can be varied in between 8:1 to 17.5:1.

3.3.2 Engine instrumentation and measuring techniques

As reported in section 3.3 and 3.3.1, the VCR SI engine test rig is first operated and evaluated with gasoline and later retrofitted for methane and biogas application followed by optimization of operating parameters for biogas mode operation. To evaluate the performance, combustion and emission analysis of this test rig, the engine is well instrumented and the signals are captured with a high-speed data accusation system (NI USB 6210, 16-bit, 250kS/s) for 50 to 80 consecutive engine cycles for each operating condition of the engine. The detailed description of the engine instrumentation and measuring techniques for tracking the operating parameters are highlighted and explained below in the subsections of *3.3.2*. Further, the engine is connected to the Labview based software (Enginesoft) to record and analyze the data online stored via a NI USB 6210 data logger. The Enginesoft environment records the data by configuring it for the fuel density, calorific value, operating CR, specification of the engine cylinder, number of cycles for data collection etc. The parameters evaluated are the BP, BTE, BSFC, air and fuel flow rates, air fuel ratio, power, mean effective pressure, net heat release rate (NHRR), cumulative heat release rate (CHRR), mass fraction burnt (MFB), coefficient of variation (COV) etc. The performance and combustion parameters of the engine in liquid fuel (gasoline) operation are estimated and visualized online during the assessment through the Enginesoft from the recorded data via NI USB 6210 data logger. Similarly for the gaseous fuel (methane and biogas) operation, the data retrieved from the data logger are post processed to evaluate the performance and combustion parameters of the VCR SI engine through an in house developed Microsoft Excel Code. The basic correlations used for estimating the above parameters are included in **Appendix D**. A “PE3” module is used to program the open ECU. This is a reprogrammable ECU and can be reconfigured according to the fuel quality. The detail specification of the PE3 module is given in **Table C- 2** of **Appendix C**.

Braking system

As mentioned in *section 3.3.1*, the crank shaft of the engine is coupled with a water-cooled eddy current dynamometer (Make: SAJ International Pvt. Ltd, Model AG10) for applying variable load on the engine. It consists of a stator and a rotor disc coupled with the engine crank shaft. The stator is mounted with a coil of electromagnets. The supplied DC current to the stator winding activates an electromagnetic field across the air gap in either side of the rotor winding. The motion of the rotor cuts the stator magnetic field by inducing an electromotive force (emf) on the rotor winding. The induced emf opposes the motion of the rotor by creating a breaking effect between the rotor and stator and thus loads the engine. The applied load on the engine is varied manually by regulating the supplied current in the electromagnets through the potentiometer (Sl No. 10, **Fig. 3. 5**) connected to the eddy current dynamometer (Sl No. 21, **Fig. 3. 5**). Since, the rotor is coupled with the engine crank shaft; it gives an angular displacement to the stator casing in spite of the braking effect. A strain gauge type load cell (Sl No 22, **Fig. 3. 5**; Make: Sensotronics Sanmar Ltd., Model 60001) incorporated in the restraining linkage between the rotor casing and dynamometer bed plate measure the exerted load on the engine crank shaft and display on a digital load indicator (Sl No. 4, **Fig. 3. 5**) attached on the engine panel.

Measurement of temperature

It is essential to measure and record the temperature of the working fluid (Air, Fuel, and Coolant) for the thermodynamic analysis of the VCR SI engine test rig at any mode of operation. The PT 100, RTD thermocouple sensors are used to measure the temperature of water flow in and out of the engine jacket and exhaust gas calorimeter. Similarly, the temperatures of the preheated gaseous fuels (methane and biogas) are measured by RTD thermocouples sensors before entering to the inlet manifold of the engine. Further, the temperatures of the exhaust gas flow in and out of the calorimeter are measured by using K-type thermocouples. The installed thermocouples are calibrated properly before using it for the experiments. The outputs of the thermocouples are connected with a multi-channel digital display unit and are further interfaced with the computer through NI USB 6210 data logger for automatic data recording.

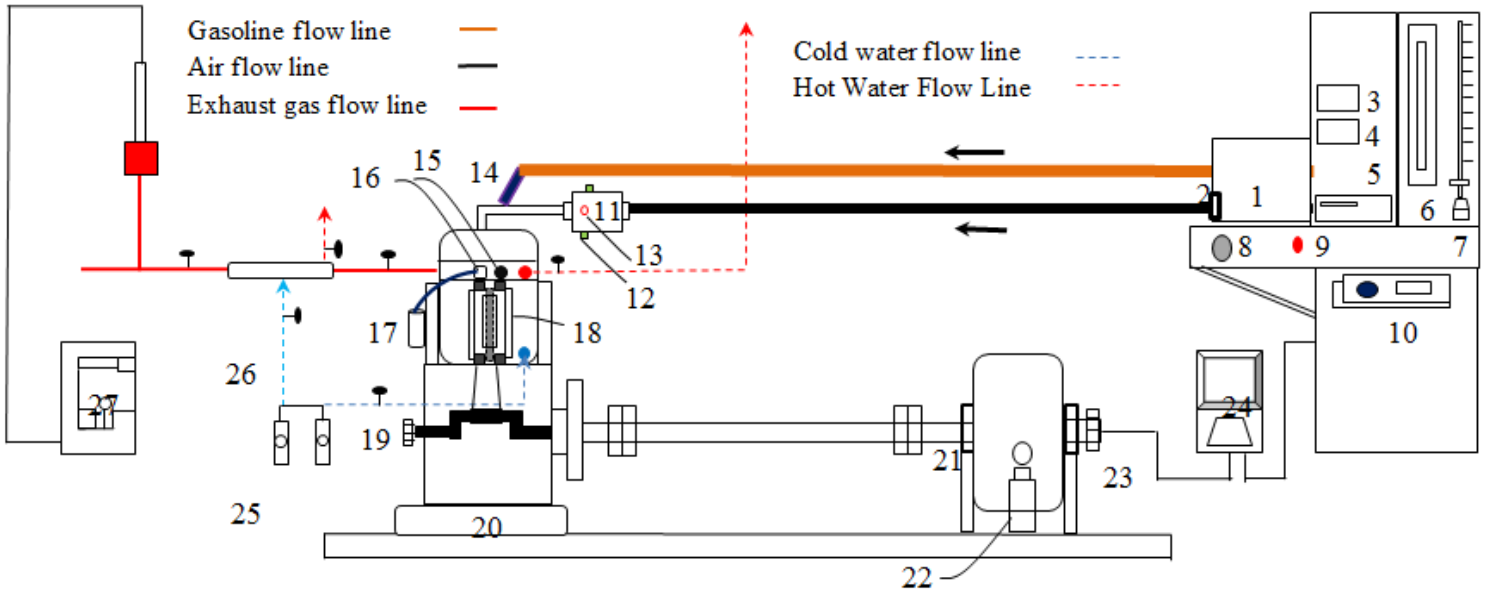

1. Air box, 2. Orifice plate, 3.Temperature indicator, 4. Load Indicator, 5. Piezo powering unit, 6. U- Tube manometer, 7. Fuel measuring tube, 8. Throttle controller, 9. Petrol injector switch, 10. Dynamometer loading unit, 11. Throttling unit, 12. Throttle position sensor, 13. Ideal air sensor, 14. Petrol injector, 15. Pressure sensor, 16. Spark plug, 17. Ignition coil, 18. VCR Mechanism, 19. Hall effect sensor, 20. Crankshaft, 21. Eddy current dynamometer, 22. Load cell, 23. Crank angle encoder, 24. NI- USB data logger connected to PC, 25. Rotameters, 26. Exhaust gas calorimeter, 27. Exhaust gas analyzer.

Fig. 3. 5: Schematic layout of the gasoline fueled VCR SI research engine test facility.

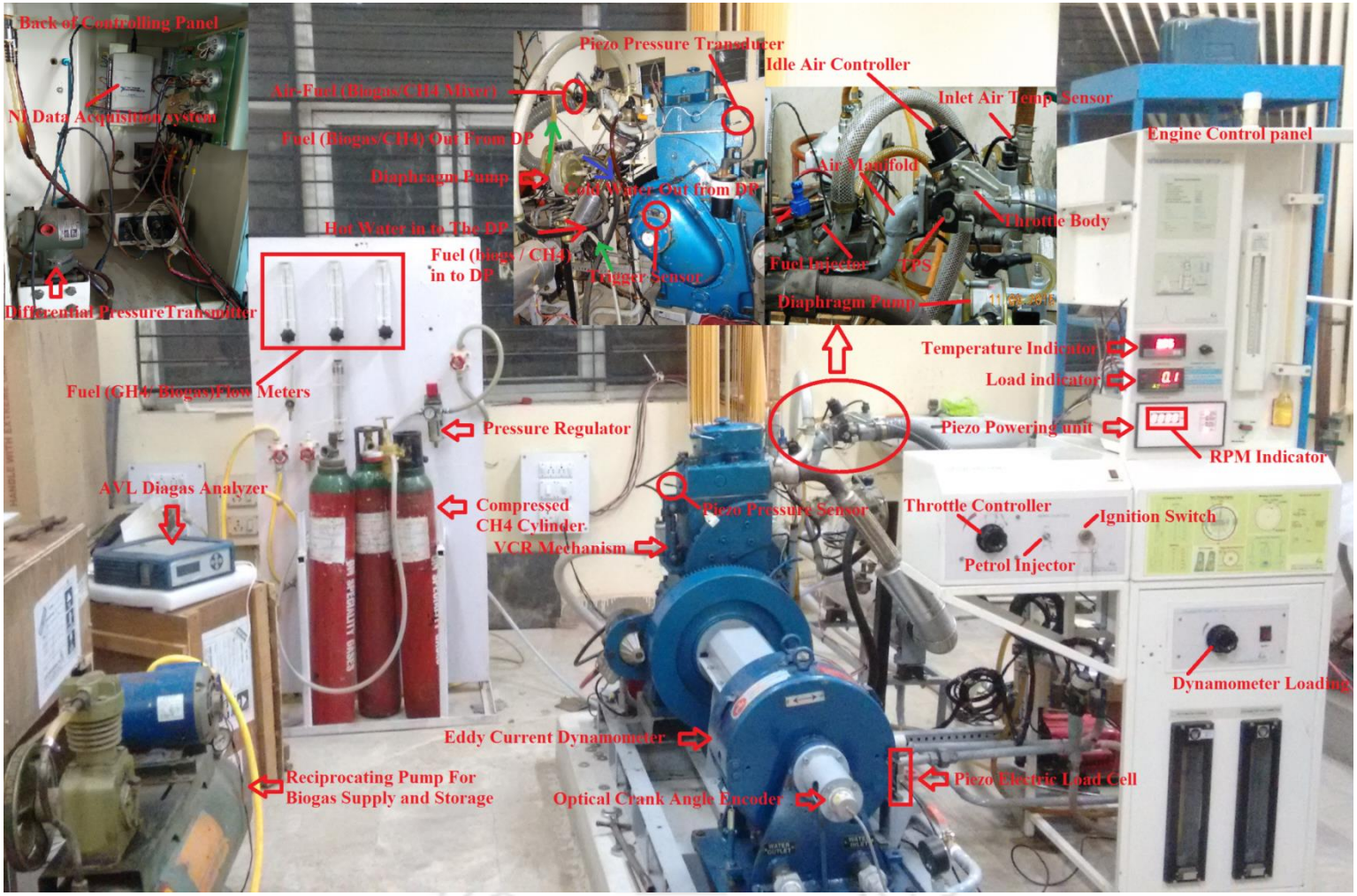

Fig. 3. 6: Pictorial representation of the VCR SI research engine test facility

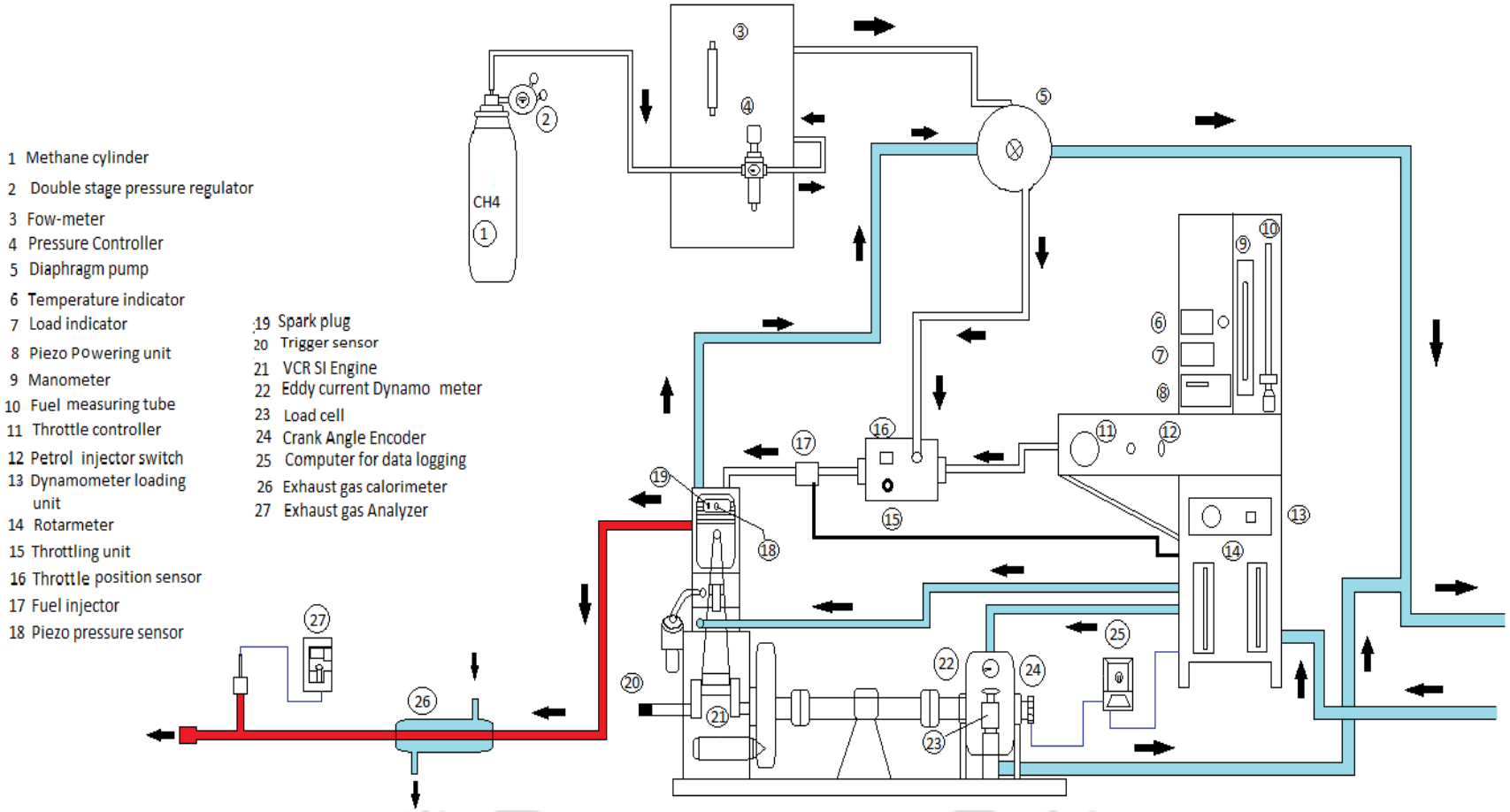

Fig. 3. 7: Schematic layout of the methane fueled VCR SI research engine test facility

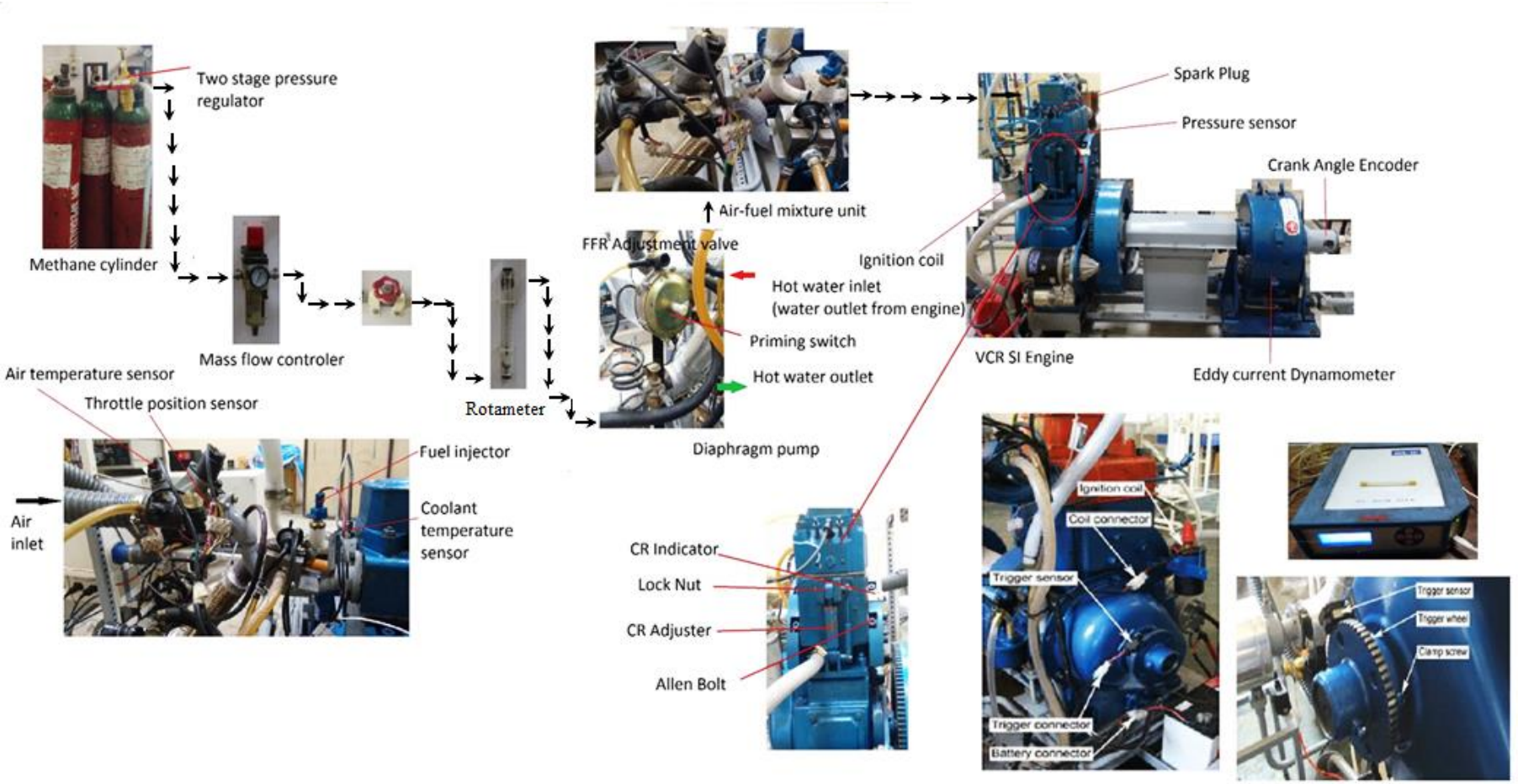

Fig. 3. 8: Photographic presentation of the methane fueled VCR SI research engine test facility

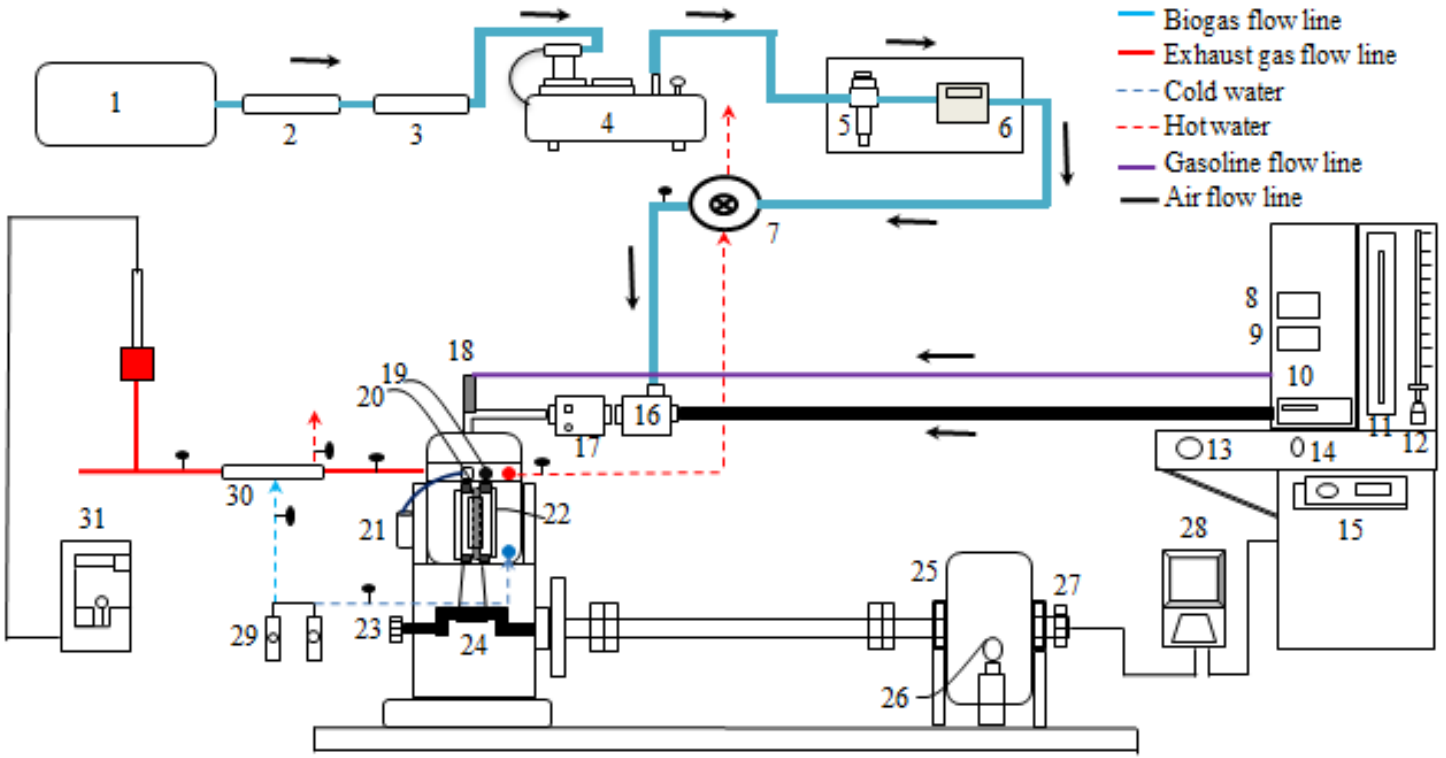

1. Biogas Balloon, 2. H_2S Scrubber, 3. Moisture Trapper, 4. Compressor, 5. Pressure regulator, 6. Biogas flow meter, 7. Diaphragm pump, 8. Temperature indicator, 9. Load Indicator, 10. Piezo powering unit, 11. U- Tube manometer, 12. Fuel measuring tube, 13. Throttle controller, 14. Petrol injector switch, 15. Dynamometer loading unit, 16. T-Type air-fuel mixer, 17. Throttling unit, 18. Petrol injector, 19. Pressure sensor, 20. Spark plug, 21. Ignition coil, 22. VCR Mechanism, 23. Hall effect sensor, 24. Crankshaft, 25. Eddy current dynamometer, 26. Load cell, 27. Crank angle encoder, 28. NI- USB data logger connected to PC, 29. Rotameters, 30. Exhaust gas calorimeter, 31. Exhaust gas analyzer.

Fig. 3. 9: Schematic layout of the biogas fueled VCR SI research engine test facility

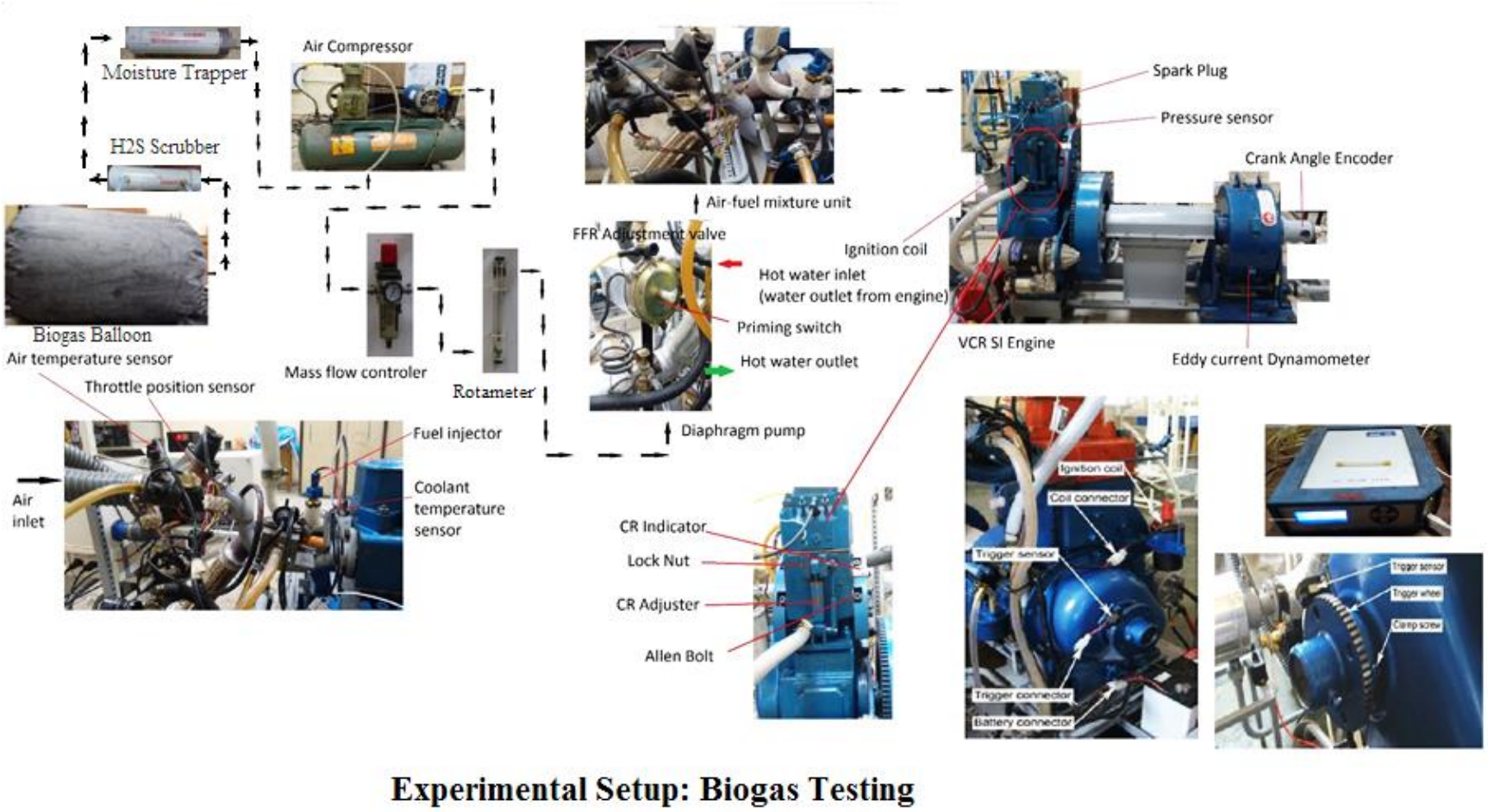

Experimental Setup: Biogas Testing

Fig. 3. 10: Photographic presentation of the biogas fueled VCR SI research engine test facility

Measurements of fuel consumption

In the present investigation, the VCR SI research engine test rig is operated both with liquid and gaseous fuels. Hence, for the measurement of liquid fuel consumption the experimental test rig has the provision of both volumetric method and gravimetric method. Similarly, the gaseous fuel consumption has also been tracked by volumetric method. The methods followed are explained below in detail.

I) *Volumetric method (Liquid fuel):* In this method, the gasoline consumption by the VCR SI engine test rig is measured manually by determining the volume flow rate of the fuel in a specific time interval. A glass burette having graduation in ml is used for the volume flow measurement. Time taken by the engine to consume a particular volume of gasoline is measured by a stop watch.

II) *Gravimetric method:* In this method the time to consume a given weight of the gasoline is measured and recorded automatically. A differential pressure transmitter (Make: Yokogawa Electrical Corporation, Model: EJA110A-DMS5A-92NN) working on the principles of hydrostatic head is used for the fuel consumption measurement. The liquid fuel is supplied to the engine injection pump from the fuel tank under gravity feed through the differential pressure transmitter. The measurement for one minute fuel consumption is performed at a particular engine operating condition on a volumetric basis. This volumetric fuel consumption is further converted to gravimetric basis by measuring fuel density. The DP transmitter is connected with the enginesoft through the NI USB 6210 data logger to record and analyze the data. The detail technical specification of the DP transmitter used for the above purpose is listed in **Table C- 3** of **Appendix C**.

III) *Volumetric method (Gaseous fuel)*: In this method, the gaseous fuel (methane/ biogas) consumption by the VCR SI engine is measured manually by determining the volume flow rate/discharge of the fuel. The measurement of methane and raw biogas consumption is different than that of gasoline. The specific gravity of methane (0.5538) is different than that of raw biogas (0.939) used in this investigation. Further, the raw biogas used in the laboratory is stored in a neoprene coated rubber fabric balloon at

NTP and passed through a H_2S scrubber followed by a moister trapper. Hence in order to accommodate the pressure drop in the biogas supply line the biogas is sucked and discharged through a reciprocating compressor via storage tank. The pressure of the biogas discharged from the storage tank of the compressor is around 1.5 bar which may not sustain by the diaphragm gas flow meter. Because of the above-mentioned reasons, float type variable area rotameter (Make: Veskler Instruments) are used. These acrylic body rotameters are specifically designed for methane (Model: ABR-19-300-A) and biogas (Model: ABR-19-300-B) based on their specific gravity with a flow measuring range and accuracy of 10 to 50 LPM and ± 0.5% FS, respectively. The volumetric fuel consumptions are recorded frequently in liter per min (LPM) for each operating condition of the VCR SI engine. Further, there is a provision for restricting and controlling the mass flow rate of gas to stoichiometric A/F ratio by operating the control valve. The detailed technical specifications of the rotameters used are shown in **Table C- 4** of **Appendix C.**

Measurement of air consumption

The air consumption of the VCR SI research engine test rig is measured with the equipped air box, orifice meter (20 mm diameter) and an open U tube manometer. The flow of intake air to the engine though the air box creates a pressure difference across the attached orifice plate. In order to find out the pressure difference across the orifice plate, one end of the open U tube manometer is connected (at a distance 1.5 times the diameter of orifice plate) to the air box and the other end is kept open to the atmosphere. The difference in height of monomeric fluid (H_2O) is recorded to calculate the pressure difference across the orifice plate. Further, the mass flow rate of the intake air is calculated from the obtained pressure difference by using *Eq. 3.2*. The coefficient of discharge (C_d) of the orifice plate is 0.6. The air flow transmitter (Make: WIKA Instruments Ltd., Model: SL-1) attached on the air box also measures the mass flow rate of intake air to the SI engine and records the data with the connected DAS.

Measurement of pressure and crank angle (P-θ) signals

In order to measure the dynamic variation of the in-cylinder pressure in the combustion chamber a diaphragm type piezoelectric pressure transducers (*Make: PCB Piezotronic; Model: M111A22*) with built in amplifier and noise cancellation cable is attached to the cylinder head. The attached pressure transducer or the pressure sensor is capable of measuring the dynamic pressure variation during compression, combustion, explosion, cavitation, pulsation and blast of pneumatic and hydraulic fluids. The maximum operating pressure rage of the pressure sensor is 15000 psi with a resolution and sensitivity of 0.1 psi and 1 mV/psi, respectively. Similarly, the angular position of the crank shaft during the cyclic process is traced by using an optical crank angle encoder (*Make: Kubler, Model: 8.3700.1321.0360*) mounted coaxially with the engine crankshaft. The angular position of the crankshaft determines the position of the piston in the engine cylinder. The Kubler made, optical crank angle encoder attached to the engine tracks the signal for each degree rotation of the crankshaft and also measures the speed of the engine. The resolution, range and measuring speed of the optical encoder are 1^{o} crank angle (CA), 5500 rpm with TDC pulse and 0-1200 pulse/min, respectively. The pressure and crank angle signals are then interfaced to the computer through a piezo powering unit (*Make: Apex innovation, India, Model:AX-409*) followed by a NI USB 6210 DAS to observe and record the pressure and crank angle signals for 50 to 80 consecutive engine cycles as well as to measure the speed of the engine. The detailed technical specification of the piezo pressure sensor and crank angle encoder are given in **Table C- 5** and **Table C- 6** of **Appendix C**.

Exhaust gas measurement

The AVL made *DIAGAS 444N*gas analyzer is used for the measurement of exhaust emissions of the liquid and gaseous fuels. The Flue gas analyzer is connected to the AECS software for recording the emission data. The exhaust gas samples are drawn from the tail pipe located just after the calorimeter connected to the exhaust manifold of the VCR SI engine using the probe of the analyzer for a fixed time duration for each operating condition of the engine. These gas samples are then analyzed in the flue gas analyzer for direct reading of CO, CO_2, NOx, O_2 and hydrocarbon (HC) emissions. The AVL made DIAGAS 444N gas analyzer uses variety of measuring principles

to determine the concentration of different gases in a gas mixture. A NDIR sensor is used to measure the CO_2 concentration which works on the principle of non-dispersive infrared radiation. Similarly, the catalytic filament method is used for determining HC concentration by using the HC heat effect sensors. A solid-state electrolyte sensor (made of zircon oxide ceramics) coated with layers (electrodes) of porous platinum as catalyst on two surface sides is used for the detection O_2 by following the principle of solid-state conductivity. The electrochemical (potentiometric) sensors working on electrochemical principle of ion selective potentiometry detects the CO, and NO concentration in the exhaust gas. The resolution, accuracy, and range of these parameters are shown in the **Table B-2** of **Appendix B**.

3.3.3 Compression ratio variation control

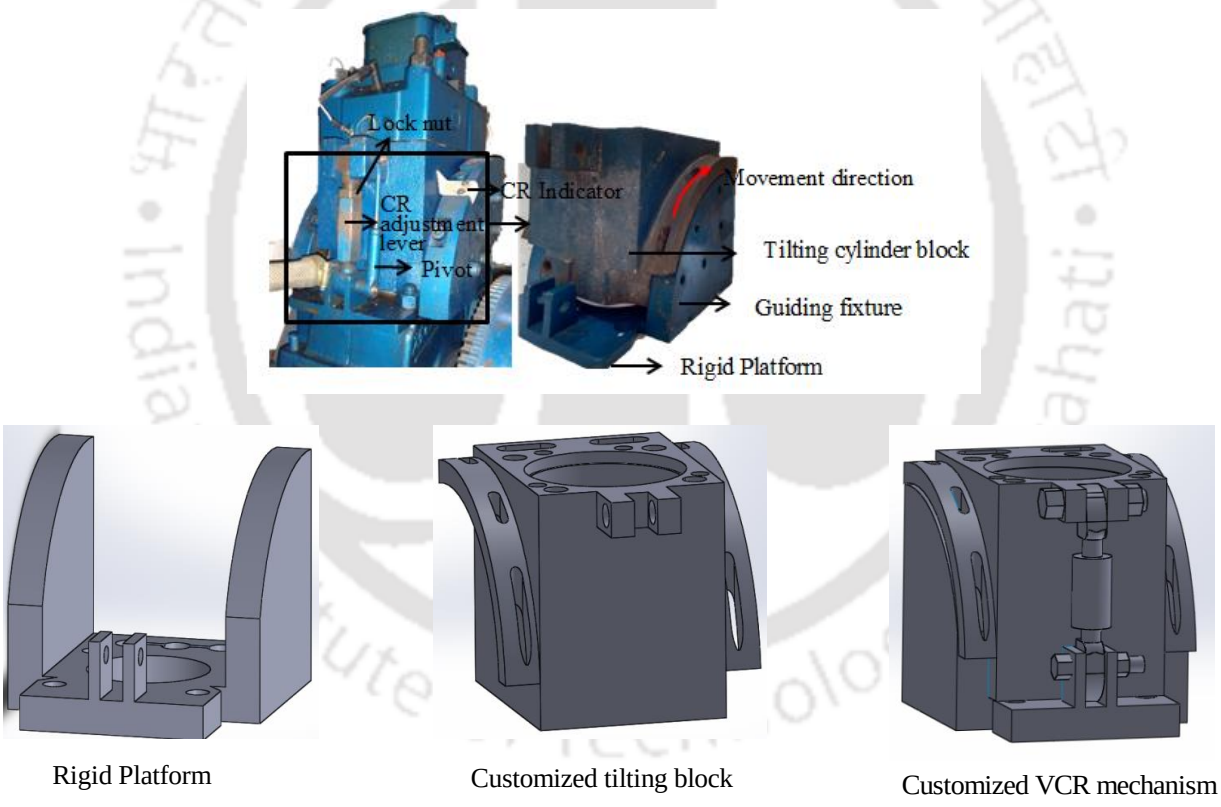

Fig. 3. 11: The tilting block VCR mechanism designed by the manufacturer

The gasoline fuelled VCR SI research engine test rig has a provision for five step CR variations (6 to 10) along with the attached tilting block VCR mechanism as shown in **Fig. 3. 11**. The CR variation of the engine can be achieved by tilting the cylinder block with requisite motion of the

adjustment lever and lock nut. The socket headed allen bolts attached on either side of the tilting blocks need to be loosen for the CR variation. If the CR adjuster turns clockwise, the CR increases and if turns anticlockwise, CR decreases. The CR can be set anytime whether engine is in running or at rest condition. However, the engine starting should be done at the standard CR (10:1) and later on the CR can be changed even if the engine is at running condition

The SI engine used for the current investigation originally had a maximum operating CR of 10:1. Since, both methane and biogas have a higher auto ignition temperature; it could even resist knocking at higher CRs. Meanwhile, the BTE is primarily dependent on the operating CR for a SI engine. Hence, in the current investigation attempt has been made to enhance the thermal efficiency of the biogas fueled SI engine by optimizing the operating CR of the engine. Therefore, the method proposed by Larsen (Larsen, 1991)is implemented to vary the CR of the engine. The tilting block mechanism designed by the manufacturer is replaced by a commercially customized tilting block VCR mechanism as shown in **Fig. 3. 12**. It consists of a rigid platform which was mounted on the crank case, a tilting block mechanism hinged at one end of the platform and guided by two supports, and a CR adjustment lever which connects the rigid platform and the tilting block mechanism. As specified by the research engine manufacturer the designated CR (10:1) of the engine was achieved by placing a spacer plate (5 mm thick) and two head packings (each of 1 mm thick) in between the engine head and cylinder block. With this arrangement, it was observed that, the head packings were compressed by 0.2 mm each while assembling the cylinder block and the engine head. But, for the present purpose the spacer plate and one of the head packings was removed. With the customized tilting block VCR mechanism, engine head, one head packing and without any clearance gap between the piston top and cylinder liner top the achieved CR of the engine was 17.5. Since, the highest achieved CR of the engine is 17.5, the engine was planned to operate within the CR ranging from 8 to 14. Hence, the required clearance gap is maintained between the piston and cylinder liner top at the TDC position to achieve the range of the operating CR by tilting the customized VCR mechanism with the help of the CR adjustment lever. The required clearance gaps are calculated by *Eqs. (3.3-3.5)*, where 'V_s' is the stroke volume, 'V_c' is the clearance volume, t_{hp} is the thickness of head packing and 'v' is the volume on the piston cavity (34 CC). After calculating the clearance gap, the flywheel position is set to TDC and the customized tilting block VCR mechanism is configured for each CR setting by maintaining the

clearance gap only by operating the CR adjustment lever as shown in **Fig. 3. 12**. For each CR setting the obtained clearance gaps were maintained and the corresponding lengths of CR adjustment lever were recoded and presented in **Table 3. 2**.

$$GAP = \left[\frac{\left(\frac{V_s}{CR-1} - v \right)}{\left(\frac{\pi}{4} \times d^2 \right) / 100} \right] \times 10 - t_{hp} \qquad (3.3)$$

$$\text{Where, } V_s = \frac{\pi}{4} \times (d)^2 \times l = 661.45\,cc \qquad (3.4)$$

$$V_c = \frac{V_s}{(CR-1)} \qquad (3.5)$$

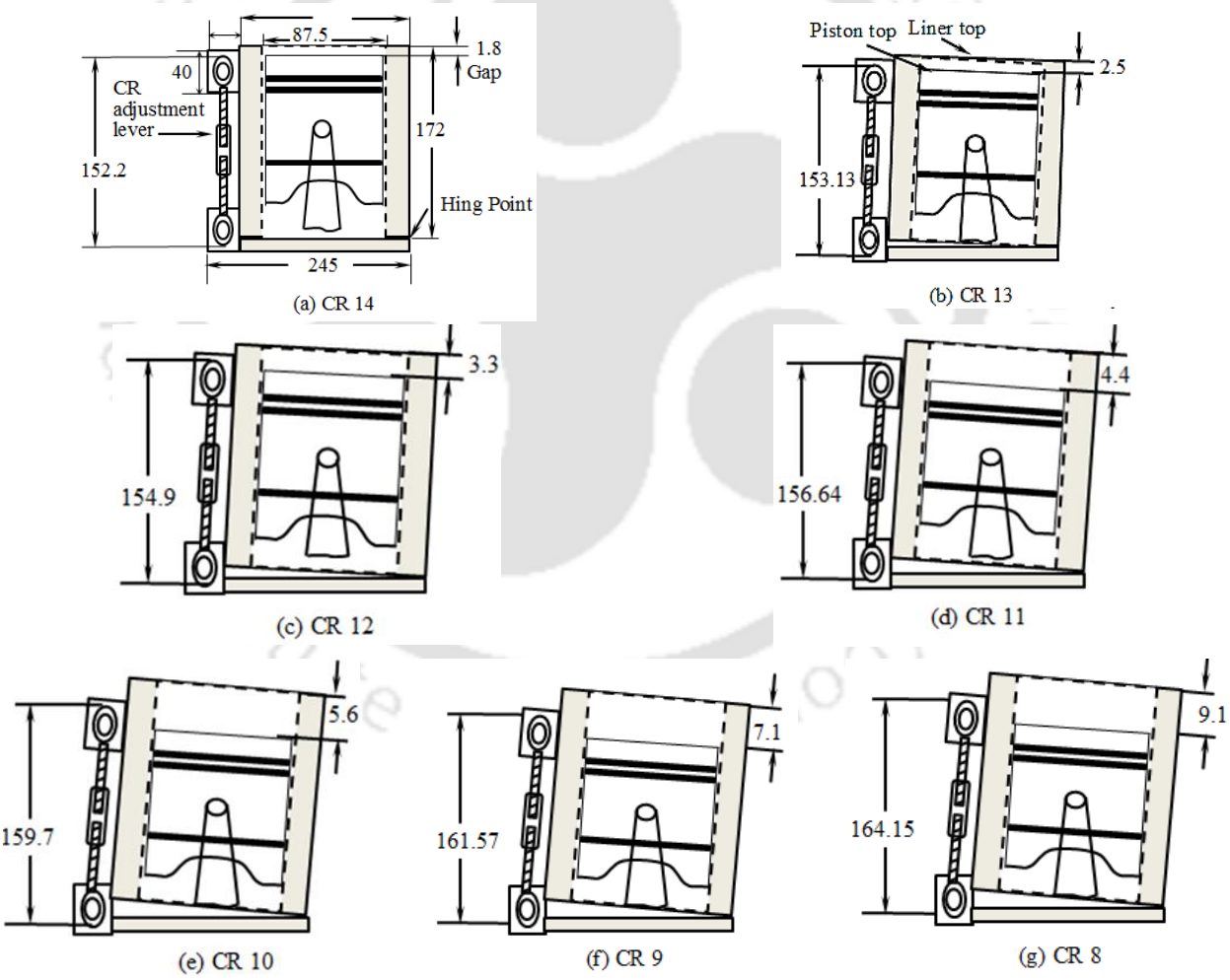

Fig. 3. 12: Schematic diagram of the tilting block mechanism adopted for CR variation

Table 3. 2: Values of calculated gap and length of adjustment lever in VCR mechanism

Compression ratio	GAP bet piston top and cylinder liner (mm)	Length of CR adjustment lever (mm)
8	9.1	164.1
9	7.1	161.5
10	5.6	159.7
11	4.3	156.6
12	3.3	154.9
13	2.5	153.1
14	1.8	152.2
15	1.2	150.9
16	0.7	149.5
17	0.2	148.6
17.5	0	148

3.3.4 Fuel induction mechanism

Gasoline induction mechanism

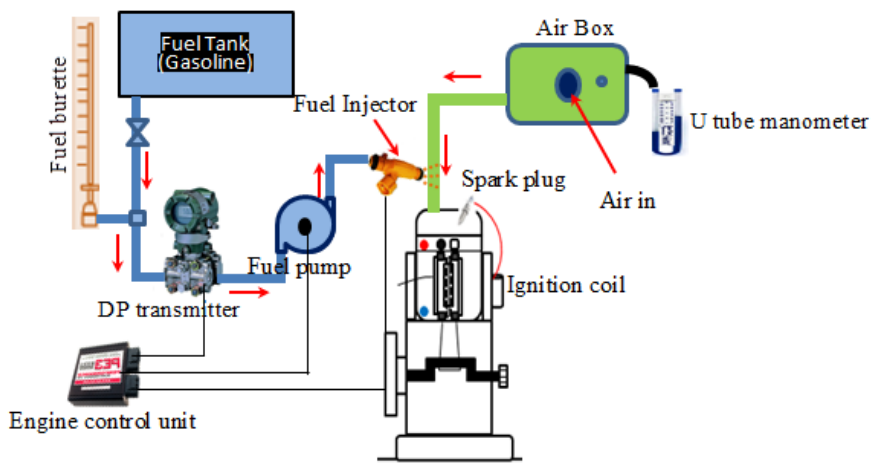

Fig. 3. 13: Fuel induction mechanism for the gasoline fueled VCR SI research engine test rig

The schematic flow path of the gasoline induction mechanism is depicted in **Fig. 3. 13** for the VCR SI engine**.** As mentioned earlier**,** motor gasoline (RON 91) collected from IOCL is used as the fuel for this investigation and is stored in the fuel tank (5 liter) located at the top of the engine panel. Since the test rig is equipped with a manifold fuel injection system (**Fig. 3. 13**), gasoline stored in fuel tank is passed to the fuel pump (*Make Denso, Model: M 800*) through the

fuel metering units (DP fuel transmitter, Fuel burette) by gravity feed method. The fuel pump and the manifold injector (*Make: Denso, Model: M 800*) are controlled by the re-programmable open ECU and can be customized through the 'PE3' module as per the requirement. The injection nozzle has three holes of 0.3 mm diameter with a spray angle of 120°. The fuel injector is a high speed solenoid valve and is allowed to open for few milliseconds during the onset of suction stoke and closes at 210°bTDC. The opening time of the fuel injector has been calibrated and configured by the manufacturer for the gasoline injection throughout the operating speed (0-1800 rpm) and throttle position range (0% -100%) of the engine. The primary fuel table with injector open time (ms) is shown in **Table C- 7, Appendix C**. Further, the induced pressure drops in the engine cylinder draw in the required quantity of fresh air to the manifold and is controlled by the butterfly valve installed on the throttle body. The air drawn into the manifold of the engine mixes homogeneously with the injected fuel before admitting to the inlet valve which opens at 4.5° BTDC during the onset of suction stroke of the engine.

Methane induction mechanism

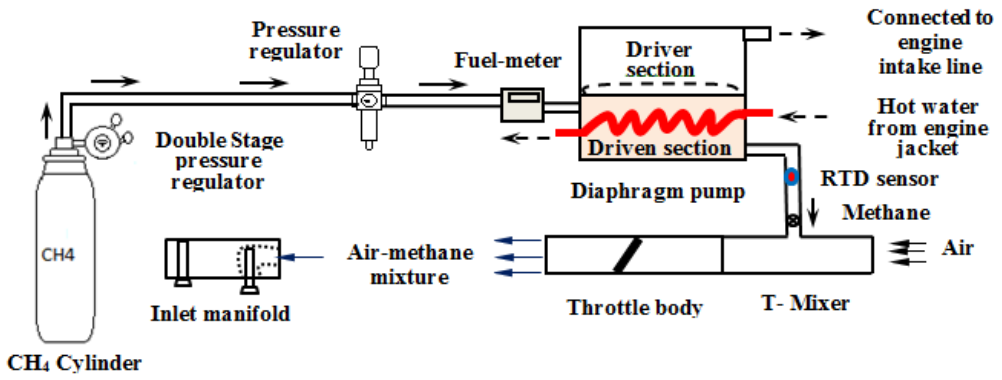

Fig. 3. 14: Fuel induction mechanism for the methane fueled VCR SI research engine test rig

The schematic flow path of methane induction mechanism for the VCR SI research engine is shown in **Fig. 3. 14**. The part of the present investigation is carried out by operating the engine with pure methane as it resembles the purified form of biogas. Compressed methane cylinders with 10 kg of water capacity and 99.99% purity are procured from Om Specialty Gases Pvt. Ltd and attached with a double stage pressure regulator. The outlet pressure of the cylinder was set to 1.5 bar and further connected and controlled by a mass flow controller, where the fuel line pressure

was reduced to 1.2 bar. Methane fuel leaving the mass flow controller is then connected to a fuel metering unit followed by a diaphragm pump driven by the induced pressure drop due to the suction stroke of the engine. The sucked methane gas is also preheated in the diaphragm pump by exchanging heat with the drained hot water from the engine water jacket. The temperature of the hot water drained from the engine jacket is maintained in between 60-63°C due to the constant inflow of cooling water (110 LPH) to the engine at steady state condition. Hence, the temperature of the preheated methane gas leaving the diaphragm pump is maintained in between 45-48°Cat steady state condition. The preheated methane gas leaving the diaphragm pump is further directed to a T-type air-fuel mixer where it mixes with air in the suction stroke and directed to the engine inlet manifold for combustion.

Biogas induction mechanism

The schematic flow path of the biogas and air induction mechanism is shown in **Fig. 3. 15**. The raw biogas collected from the site is stored in a neoprene coated rubber fabric balloon and the same was passed through an in house developed H_2S scrubber followed by a moisture trapper as shown in **Fig. 3. 16** and **Fig. 3. 17**, respectively. The H_2S scrubber is made from a PVC cylindrical pipe (diameter 110 mm and length of 500 mm) and packed with compacted annealed steel waste chips of 500 gm. The annealed steel chips are collected from the waste generated during turning of low carbon steels. The H_2S present in biogas reacts with iron oxide (Fe_2O_3) and the reaction mechanism follows the *Eq. 3.6*. This reaction mechanism is recognized as one of the ways to remove H_2S from biogas by dry desulfurization. The result of this reaction is observed as the precipitation of sulfur in the form of Fe_2S_3 on the surface of the iron oxides, which may reduce the efficiency of desulfurization. Because of this reason after a certain period the used annealed chips were exposed in atmosphere and cleaned by water and then reused further for H_2S capturing.

$$Fe_2O_3 + 3H_2S \rightarrow Fe_2S_3 + 3H_2O \qquad (3.6)$$

The H_2S scrubbed biogas is then passed through a moisture trapper (as shown in **Fig. 3. 17**) fabricated from a cylindrical PVC pipe (110 mm diameter and 500 mm in length) and loosely packed with blue silica gel crystal of mesh size 6-8 mm. Silica gel has a very strong affinity for water and is a highly activated adsorbent. It is also a good adsorbent for CO_2, sulfur and nitrogen

compounds, and many others. The micro porous structure of inter locking cavities in silica gel crystal has a very high surface area ~800 m^2/gm, which makes itself as a high-capacity desiccant. Because of the lower vapour pressure exhibited by the silica gel crystal, water molecules present in the biogas adheres to its surface until and unless the pressure equilibrium condition is reached. The beauty of silica gel is the physical adsorption of water vapour into its internal pores. There is no chemical reaction and no by-products in this process. When saturated with water vapour, the blue silica gel crystal still has the appearance of a dry product but changes its color from blue to pink. Once saturated with water, the gel can be regenerated (dried) by heating it to 150°C.

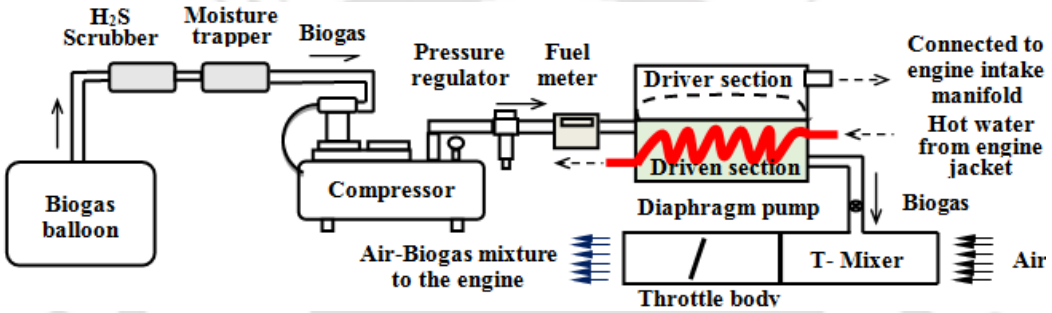

Fig. 3. 15: The biogas induction mechanism

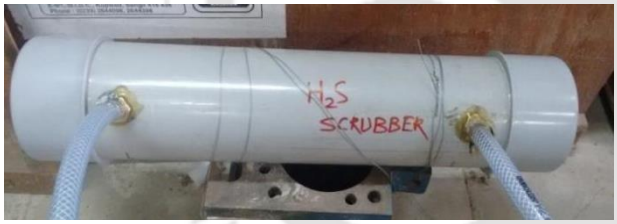

Fig. 3. 16: H_2S Scrubber packed with SS chips

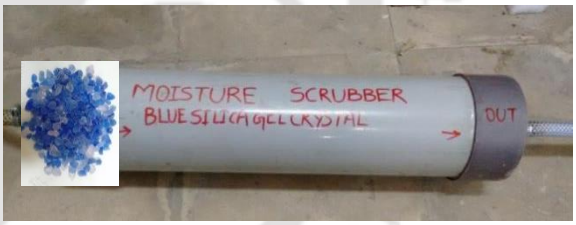

Fig. 3. 17: Moisture scrubber packed with blue silica gel crystal

The raw biogas passes through the H_2S scrubber and moisture trapper is further drawn to the engine cylinder through a single stage reciprocating compressor of 0.37 kW, a pressure regulator, a fuel metering unit, a diaphragm pump followed by a T type air-biogas mixer as shown in the **Fig. 3. 15**. The scrubbed biogas was pressurized and built up to 3 bar and stored in the compressor storage. The pressurized biogas was then redirected through a pressure regulating unit and the pressure is subsequently preset to 1.3 bar. Biogas fuel line leaving from the pressure regulator is passed to a diaphragm pump (*Make: Lovato;* **Fig. 3. 15**) through a fuel metering unit (*Make: Veskler Instruments;* **Fig. 3. 15**). Subsequently, metered quantity of the scrubbed biogas

delivered by the diaphragm pump enters to a T-type air-fuel mixer due to the induced pressure drop created during the suction stroke of the engine at the driver section of the diaphragm pump. The diaphragm pump has a provision of preheating the gaseous fuel in the driven section by exchanging the heat with the outlet hot water from the engine jacket. At, the steady state wide-open throttling (WOT) condition of the engine, the temperature of the hot water coming out from the engine jacket was almost constant and is in the range of 60°C- 63°C. The hot water coming out from the engine jacket was redirected to the diaphragm pump and used to preheat the inducted biogas. Thus, the temperature of the biogas coming out from the diaphragm pump was maintained in between 45-46° C. The T-type air-biogas mixer is installed at the engine intake system before the throttle body unit. Biogas leaving the diaphragm pump is then connected to the in-house fabricated T- type air-biogas mixer where it readily mixes with air in the suction stroke. The T-type biogas mixer is designed based on the average volumetric fuel demand of the engine at stoichiometric operating condition. The diameter of the air inlet, air-biogas mixture out let and length of the mixer are taken as 42 mm and 75 mm because of the dimensional constraint of the connecting parts. Further, the diameter of the biogas pipe is calculated based of the average volumetric fuel demand of the engine so as to maintain the stoichiometric air-fuel ratio. **Fig. 3. 18** describes the detail dimension of the mixer. Finally, the charge (biogas and air mixture) enters to the engine manifold through a throttle body unit (*Make: Tata Motors;* **Fig. 3. 15**).

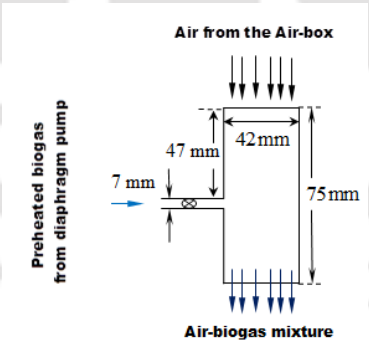

Fig. 3. 18: T-type air-biogas mixer

Ignition timing variation control

The IT is a crucial operating parameter in the engine control and diagnostics system. The time from ignition of charge to the development of maximum combustion pressure is not only

dependent on the fuel composition but also affected by the CR, engine speed, throttle position, temperature of the combustion chamber and manifold pressure. The ignition must initiate earlier if the engine speed is higher and the operating CR of the engine is lower. Further, for complex operating conditions the engine must operate with optimum ITs. Hence, the VCR SI research engine test rig is equipped with a direct ignition system (DIS) and is governed by a microcontroller based reprogrammable ECU (Make: Performance Electronics Ltd., Model: PE3). **Fig. 3. 19** shows the overall circuit diagram of the ECU controlled direct ignition system. The crankshaft position sensor (Optical Crank Angle Encoder, CAE) and trigger sensor (Hall Effect Sensor, HES) mounted on the crank and cam shaft generate the NE and G signals respectively. The ECU identifies the position of crank shaft and TDC along with the engine speed from the generated NE and G signals. Similarly, few auxiliary sensors such as throttle position sensor (TPS), idle air sensor (IAS), temperature sensor (TS), piezo pressure sensor (PS), and emission sensors (ES) are mounted on the engine in the respective positions to observe the throttle opening, air flow rate, in-cylinder temperature, pressure and emission levels and feed it back to the ECU for effective control of the IT. Further, the ECU contains an array of user defined optimum data set consisting of the optimum ITs for various operating conditions (speed, fuel composition, air-fuel ratio, load, in cylinder temperature and pressure, throttle position, and emission level) of the engine. The ECU determines the optimum IT based on the input signals from these sensors by retarding or advancing the IT from the idle ignition timing and triggers the spark plug through the igniter and ignition coil.

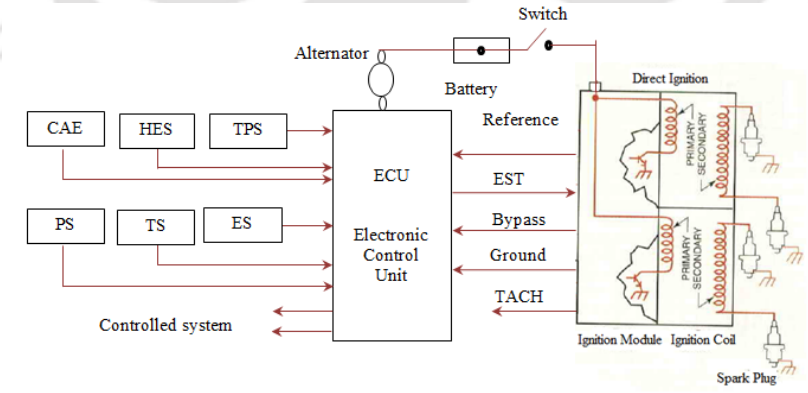

Fig. 3. 19: The ECU controlled direct ignition system (DIS) mounted on the VCR SI engine

The ECU is configured by the manufacturer for the gasoline operation of the VCR SI engine. However, with the PE3 software interface, the ECU can be configured for any fuel composition and operating condition of the engine by reprogramming the IT with respect to the throttle position (0 to 100%) and operating speed (900 to 2000 rpm). The ECU is reprogrammed by setting the IT to MBT timing for part throttle (PT) and wide-open throttle (WOT) condition of the engine running with methane or biogas. Further, to find out the optimum IT, the IT of the engine is initially fixed at an arbitrary crank angle bTDC by maintaining the other operating parameters (CR, engine speed, ER, TP) constant followed by recording the performance parameters of the engine. The above-mentioned process is further repeated by either advancing or retarding the IT bTDC and the recorded performance, combustion and emission parameters are compared to find out the optimum IT for the particular operating condition of the engine. This method is versatile in the sense of varying the ignition timing for optimizing MBT for the fuels under study. The safe operating range of ITs for the VCR SI research engine operating with $CH_4$was observed in between 24° to 42° bTDC without any trace of misfire and knocking but are limiting values. Similarly, with the biogas operated VCR SI research engine, the limiting ITs are in the range of 23° to 55° bTDC. The process for IT optimization and its effects are discussed in detail in the **Chapter 4** and **Chapter 5**.

3.4 The Honda GX 200 SI Engine Test Facility (*Engine 3*)

The development of the dedicated biogas engine (*Engine 3*) at energy efficiency laboratory, IIT Guwahati was initiated with the laboratory scale experimentation and optimization of operating parameters in a biogas fueled VCR SI research engine test rig of rated capacity 4.5 kW (*Engine 2*). From the experimental observation it is found that, for converting a commercial single cylinder SI engine for biogas application, the best possible CR and IA has to be maintained at CR 10 and 45° CA bTDC, respectively. However, the best performance of the engine can be achievable in between CR 12 to13 along with the corresponding ignition advances. Hence, in the present stage of investigation, the optimized operating parameters are incorporated in a popular commercial SI engine (Honda GX- 200) mostly used for decentralized power generation (as a Generator Set) in Indian market. The rated power of the selected engine (Honda GX- 200) is close to that of the Engine 1 and Engine 2, which will be further useful for comparative analysis. But, because of the

manufacturing constraints, the CR of the Honda GX- 200 SI engine could not be enhanced beyond 9.5. Hence, the CR and IA of the commercial SI engine are set at CR 9.5 and 50° CA bTDC, respectively. The (air-fuel) intake system of the commercial SI engine is also retrofitted with a biogas induction mechanism and is explained in detail in *section 3.4.2* and **Appendix D**. **Fig. 3.20** shows the photographic representation of the retrofitted Honda GX 200 SI engine setup turned in dedicatedly for biogas application. Similarly, **Fig. 3. 21** shows the schematic layout of the biogas fueled retrofitted Honda GX 200 SI engine test rig.

(a) Mounted instruments on biogas fueled retrofitted Honda GX 200 SI engine test rig

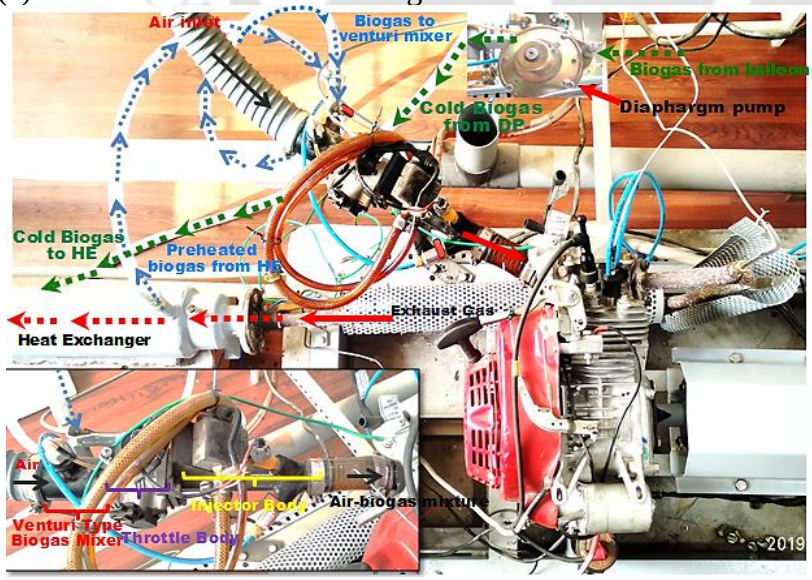

(b) Air and biogas induction mechanism attached to the retrofitted Honda GX 200 SI engine test rig

(C) Honda GX 200 SI engine test rig

Fig. 3. 20: Photographic layout of the biogas fueled retrofitted Honda GX 200 SI engine test rig

3.4.1 Engine specification and instrumentation

As shown in **Fig. 3. 21**, the experimental setup consists of a natural aspirated, single cylinder, four stroke, air-cooled, manifold injection variable speed SI engine (Make: Honda, GX 200) of rated IP and BP of 4.1 kW (5.5 HP) and 3.6 kW, respectively at 3600 rpm. It is a gasoline fueled, fixed CR (8.5) engine configured in SI mode with maximum speed of 3600 rpm. The detailed technical specification of the engine (Honda, GX 200) is given in **Table C- 8** of **Appendix C**. For enabling the engine to operate with biogas, the inbuilt carburetor of the GX 200 engine has been replaced by a biogas induction mechanism followed by a venturi-type air-biogas mixer. The biogas induction mechanism and the in house developed venturi type air-biogas mixer attached to the engine are explained in detail in the forthcoming *section 3.4.2* and **Appendix E**, respectively. Similarly, the inbuilt magneto coil ignition system of the GX 200 engine is replaced by an ECU controlled direct ignition system (DIS) as explained in *section 3.3.5*. Further, to avoid the initial starting difficulty with the raw biogas, the engine is equipped with an ECU controlled gasoline fuel injection system (*Make: Denso, Model: M 800*). The operating CR of Honda: GX 200 SI engine is further enhanced by replacing the original engine head with machined head of Honda: GX 160. The outcome of the engine head replacement resulted in increased operating CR from 8.5 to 9.5. The detailed method of CR variation is explained in *section 3.4.3*. The instrumentation and measuring techniques followed for the performance evaluation of the biogas fueled retrofitted Honda GX 200 SI engine are similar to that of the VCR SI research engine test rig as mentioned in *section 3.3.2*.

As shown in **Fig. 3. 21**, the standalone panel box attached to the engine consists of an air box, fuel tank, fuel pump, manometer, fuel measuring burette, air and fuel flow transmitters, TP controlling unit, ignition switch, fuel pump relay, injector relay, ignition coil relay, ECU relay, piezo powering unit, multi-channel temperature display, dynamometer loading unit and the electronic panel along with a NI USB-6210 data accusation system (DAS). The applied load on the engine is controlled by the induced emf of a water-cooled eddy current dynamometer (Sl. no. 24, **Fig. 3. 21**) coupled with the engine crankshaft. The magnitude of the applied load is further sensed by a pre-calibrated strain gauge type load cell (Sl. no. 25, **Fig. 3. 21**) and displayed on the digital load indicator attached to the engine panel. The fluctuation of the in-cylinder pressure and the instantaneous

crank angle are traced by a diaphragm type piezo pressure sensor with built in amplifier (Sl. no. 19, **Fig. 3. 21**) and optical crank angle encoder (Sl. no. 26, **Fig. 3. 21**). The signal generated by the piezo pressure sensor and crank angle encoder are interfaced to the 'PE3' software through a piezo powering unit (Sl. no. 10, **Fig. 3. 21**) and DAS (NI USB-6210) mounted on the engine panel. The air and biogas consumptions are measured by an air flow transmitter (Make: Wika Instruments Ltd.) and a float type biogas rotameter (Make: Veskler Instruments) installed on the engine panel and fuel induction mechanism, respectively. The temperature of the inducted air and biogas along with the exhaust gas are measured by using RTD sensors and K-Type thermocouples at different location in the test rig. The HES (Sl. no. 22, **Fig. 3. 21**) and TPS (Sl. no.17, **Fig. 3. 21**) mounted on the camshaft and inlet manifold record the cylinder and throttle position, respectively during the engine operation. The ECU (*Make: Performance Electronics*) integrated with the engine control panel regulates the triggering of ignition coil and fuel injection system though the respective relays based on the input signals from HES, TPS, and CAE. The ECU attached is reprogrammable based on the fuel type through the 'PE3' software. The engine control system is further connected to Labview based software 'Enginesoft' to record and analyze the data stored via a NI USB 6210 data logger. The exhaust of the engine is passed through a concentric tube counter flow heat exchanger (Sl. no. 28, **Fig. 3. 21**) which preheats the inducted biogas to the engine. The exhaust gas composition of the biogas fueled retrofitted Honda GX 200 engine is analyzed online and recorded by an AVL DIAGAS 444N gas analyzer (Sl. no. 29, **Fig. 3. 21**) and AECS software.

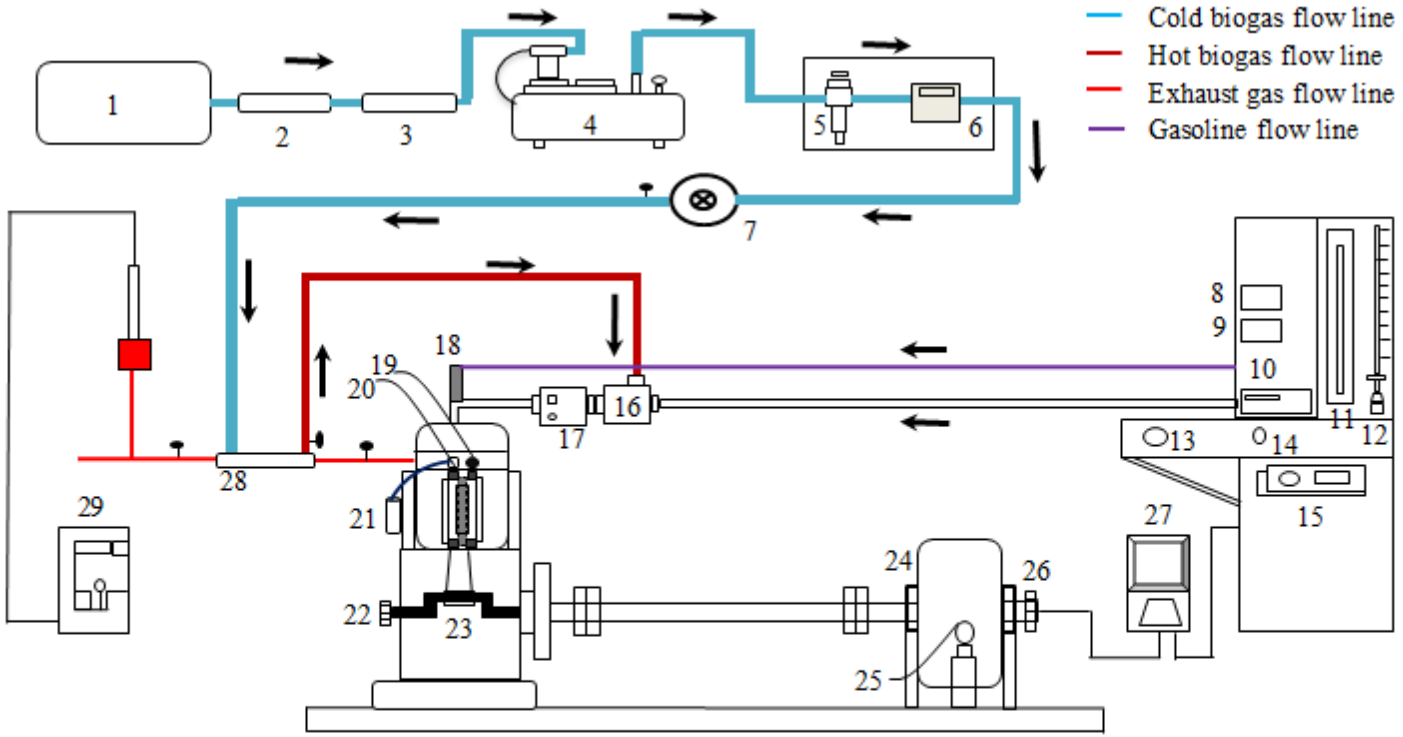

1. Biogas Balloon 2. H_2S Scrubber, 3. Moisture Trapper, 4. Compressor, 5. Pressure regulator, 6. Biogas flow meter, 7. Diaphragm pump, 8. Temperature indicator, 9. Load Indicator, 10. Piezo powering unit, 11. U- Tube manometer, 12. Fuel measuring tube, 13. Throttle controller, 14. Petrol injector switch, 15. Dynamometer loading unit, 16. Air-fuel mixer, 17. Throttling unit, 18. Petrol injector, 19. Pressure sensor, 20. Spark plug, 21. Ignition coil, 22. Hall effect sensor, 23. Crankshaft, 24. Eddy current dynamometer, 25. Load cell, 26. Crank angle encoder, 27. NI- USB data logger connected to PC, 28. Heat exchanger, 29. Exhaust gas analyzer.

Fig. 3. 21: Schematic layout of the biogas fueled retrofitted Honda GX 200 SI engine test rig

3.4.2 Biogas induction mechanism for the HONDA GX 200 SI engine

The gaseous fuel induction technique integrated with experimental setup is developed in-house as shown in **Fig. 3. 22**. The schematic flow path of biogas and air intake mechanisms is shown in **Fig. 3. 20b** and **Fig. 3. 21**. The raw biogas stored in a neoprene coated rubber fabric balloon (2 m^3 capacity) is drawn to the engine by a 0.37 kW single stage reciprocating compressor through an in house developed H_2S scrubber and moisture trapper. The pressure is initially built up to 2 bar in the compressor storage and subsequently preset to 1 bar in a pressure regulator before entering to the biogas metering unit. Biogas leaving the pressure regulator is then passed to a diaphragm pump (*Make: Lovato*) through a fuel-metering unit (*Make: Veskler Instruments*) followed by a concentric tube counter flow heat exchanger which exchanges heat in between the hot exhaust gas and the cold biogas drawn by the venture type air-biogas mixer. Subsequently, it entered the biogas mixer due to the induced pressure drop during the suction stroke of the engine at the diaphragm pump and throat of the venturi type air-biogas mixer. At, the steady state wide-open throttling condition, the temperature of the exhaust gas coming out from the engine (at 100 mm from exhaust manifold) is in the range of 550°C- 590°C. The exhaust gas coming out from the engine is redirected to the heat exchanger and thus preheats the inducted biogas. Further, the heat exchanger is intensely uninsulated to avoid excess heating of the inducted biogas.

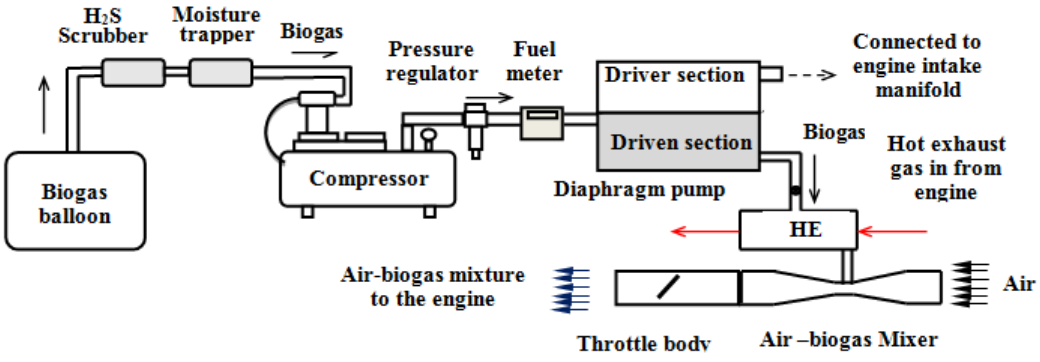

Fig. 3. 22: Schematic layout of the biogas induction mechanism for the Honda GX 200 engine setup

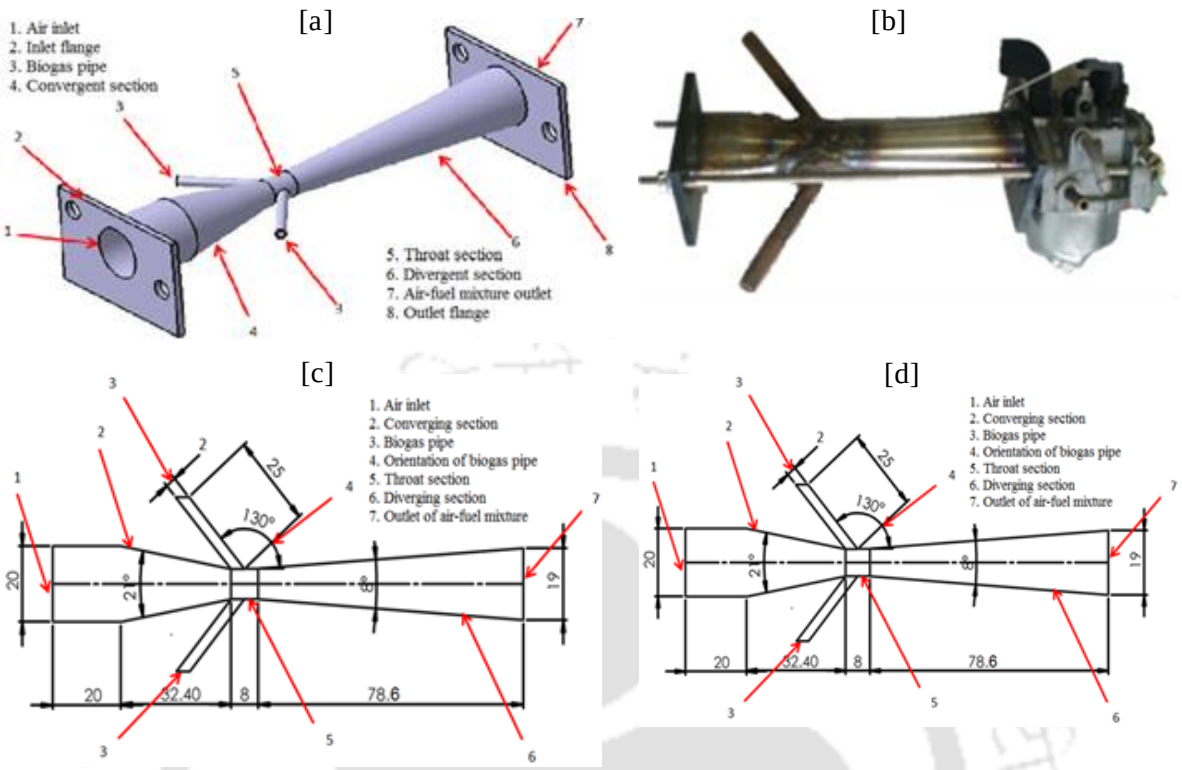

Fig. 3. 23: (a) 3D- model and (b) Fabricated sample of the of the venturi type biogas mixer (c) Detailed specification along with the front and (d) Side sketch of the venturi mixer.

In this way, the temperature of the inducted biogas coming out of the heat exchanger is maintained in between 50- 60^{o} C. Finally, the charge (biogas and air mixture) enters to the engine manifold through a venture type biogas mixer followed by a throttle body unit (Make: Tata Motors). The venturi-type biogas mixer shown in **Fig. 3. 23 (a, b)** is specifically designed for the Honda GX 200 SI engine for biogas application. The details specifications of the biogas mixer are obtained through an analytical method followed by a rigorous computational analysis and depicted in **Fig. 3. 23 (c, d).** The analytical method and the computational investigation followed for optimizing the dimensions of the venture type biogas mixer are explained in detail in **'Appendix E'**. The diameter of the throat, diameter of the biogas pipes, converging and diverging angle of the venture mixer are obtained through the analytical method and found 8 mm, 2 mm, ~21° and 8° respectively. Similarly, the recommended position and orientation of the biogas supply pipes are confirmed through a series of computational investigation. The induced effect of position (at the inlet and middle of the throat) and orientation (30° to 150° from the converging angle) of the biogas supply pipes on the pressure, velocity and mass

fraction distribution along the length of the biogas mixer are investigated in this analysis. The inclination angle of the biogas pipe is proposed to be 50^{o} and the middle position of the throat is suggested to utilize for superior mixing of air and biogas.

3.4.3 Compression ratio variation technique in Honda GX 200 engine

The auto ignition temperature and octane rating of biogas is very high. Hence, biogas fueled SI engine can resist and operate efficiently at higher CR than the gasoline fueled SI engines. In the present case the standard CR of the Honda GX 200 SI engine is 8.5. As mentioned in *Section 3.4*, the optimum CR of biogas fueled SI engine is 12. Hence, in order to enhance the efficiency and enable the engine to run efficiently with biogas, the CR of the engine has to be enhanced. However, due to the associated manufacturing constraints, it was quite difficult to enhance the CR of the engine beyond 9.5 without any major modification in the engine design. Hence, the CR of the engine is increased from 8.5 to 9.53 by following the below mentioned steps. The CR of the engine is defined as the ratio of total volume to the clearance volume as mentioned in *Eq. 3.7*.

$$CR = \frac{V_C + V_S}{V_C} = 1 + \frac{V_S}{V_C} \tag{3.7}$$

Here '*Vc*' is the total clearance volume and '*Vs*' is the swept volume of the engine. Total clearance volume is defined as the volume between the cylinder head and piston top along with the volume of combustion chamber when the piston is at the TDC of the engine as shown in **Fig. 3. 24**. By measuring the combustion chamber volume (V_{CC}), deck clearance, thickness of head gasket, volume of piston cavity and bore diameter of the cylinder, the total clearance volume is calculated from *Eq. 3.8*. But, in the present case the CR of the Honda GX 200 engine is defined by the manufacturer. Hence, the clearance volume can be calculated by using *Eqs. 3.9* and *3.10*.

$$V_C = V_{CC} + \frac{\pi}{4} \times \left(\text{Cylinder bore}\right)^2 \times \left\{\left(\text{Deck clearance}\right) + \left(\text{Gasket thickness}\right)\right\} + \left(V_{\text{Piston cavity}}\right) \tag{3.8}$$

$$V_{C\,GX200} = \frac{V_{S\,GX200}}{(CR_{GX200} - 1)} \tag{3.9}$$

$$V_{S\,GX200} = \frac{\pi}{4} \times \left(Cylinder\,bore\right)^2 \times l_{GX\,200} \tag{3.10}$$

As mentioned by the manufacturer, the stroke length (l) of the GX 200 engine is 54 mm. Hence, the stroke volume '$V_{s\,GX200}$' is 196.1 CC and the clearance volume of the engine '$V_{C\,GX200}$' is 26.148 CC. Further, in order to verify the calculated value, the Honda GX 200 engine is disassembled and volume of combustion chamber (V_{CC}), deck clearance, gasket thickness and piston cavity are measured with different techniques. The deck clearance is the clearance between the cylinder head and piston top when the piston is at the TDC as shown in **Fig. 3. 24** and **Fig. 3. 25**. The deck clearance and the gasket thickness are 1 mm and 0.3 mm, respectively. Further, the piston used in GX 200 is not exactly a flat top piston; rather it has a small cavity on the piston top as shown in **Fig. 3. 25** and **Fig. 3. 26**. The diameter and depth of the piston cavity are measured and found to be 54 mm and 1.4 mm, respectively.

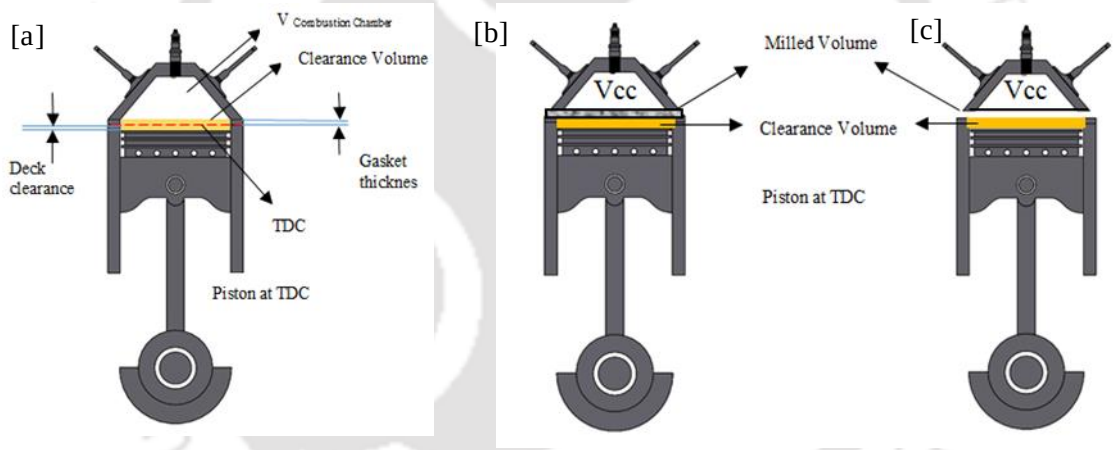

Fig. 3. 24: Lay out of the engine cylinder and head assembly (a) Honda GX 200 engine with CR 8.5; (b) Honda GX 200 with milled GX 160 engine head; (c) Retrofitted GX 200 engine witch CR 9.53

Further, the volume of the combustion chamber is measured by filling equivalent volume of IS1448, 20W-40 lubricant oil, having a density of 0.8877 $g.ml^{-1}$. The weight of the filled lubricating oil is measured in a digital weight balance as shown in **Fig. 3. 26** and found to be approximately 15.8 g. From the above obtained data, the volume of the combustion chamber (V_{CC}) is evaluated and found 17.798 CC. The total clearance volume (V_C) of GX 200 engine was determined from *Eq. 3.8* and found to be 25.726 CC. The measured value was quite close to the calculated value (26.148 CC) from the manufacturer's specification.

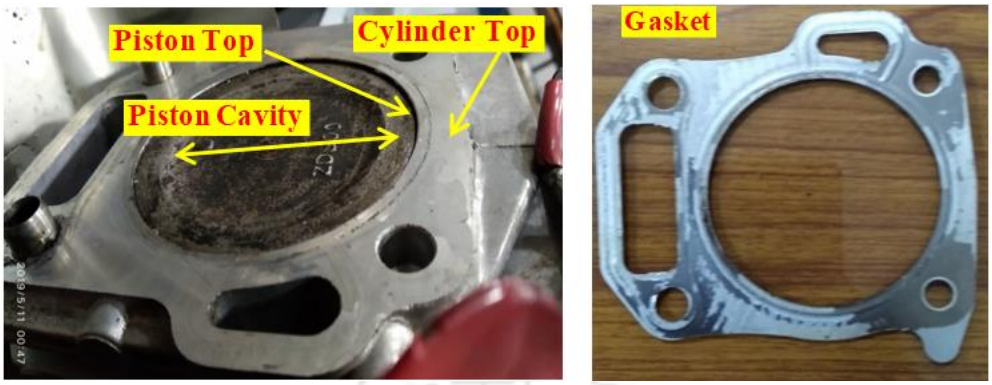

Fig. 3. 25: Deck clearance, piston cavity and gasket thickness of Honda GX 200 engine

Fig. 3. 26: Measuring technique of piston cavity and combustion chamber volume: Honda GX 200

In order to increase the CR of the engine the total clearance volume (V_C) has to be decreased. This can be only achieved by reducing the volume of the combustion chamber (V_{CC}) or by using a flat top piston, since the other clearances are almost constant and cannot be altered. Hence, in the present case a suitable engine head of the same manufacturer has been chosen which is comparable to the rest of the assembly of GX 200 model. The engine head of Honda GX 160 is compatible with GX 200 engine assembly and can be further milled to remove extra material form the surface of the engine head as per requirement. However, the profile of 'Vcc' of GX 160 is technically differing from GX 200. Further, the 'Vcc' of GX 160 engine head is measured as shown in **Fig. 3.27** by following the same technique as mentioned earlier in case of GX 200. The volume of the 'V_{CC}' of GX 160 engine head is found 18.249 CC and was attached to the GX 200 assembly. Since, rest of the clearances other than 'Vcc' was remained unchanged; the CR of the retrofitted engine assembly almost remained constant (8.49). Further, to increase the operating CR of the setup it is proposed to reduce the 'V_{CC}' by

milling the cylinder head of GX 160. Hence, 0.8 mm of material from the GX 160-cylinder head is milled and assembled with the GX 200-cylinder block without altering any other clearance volume as shown in **Fig. 3. 24**. Finally, the CR of the retrofitted Honda GX 200 assembly with GX 160 engine head is calculated by using *Eq 3.7*. The calculated value presented, the Honda GX 200 engine with a 0.8 mm milled GX 160-cylinder head along with a piston cavity of 3.206 CC has a CR of 9.53.

Fig. 3.27: Measuring technique of combustion chamber vol.: Honda GX 160 engine head

3.5 Uncertainty Analysis

The resolution of the employed instruments directly affects the accuracy of the measured parameters. The uncertainty associated with these instrumental resolution leads to systematic uncertainty. Similarly, the operating condition and surrounding experimental environment are the key parameters that accounts for the random uncertainty. In combination of both the systematic and random uncertainties, overall uncertainties of the desired parameters are quantified. The detailed information regarding the associated uncertainties of aforementioned instruments used for all the experiments is elaborated in **Appendix F.**

CHAPTER 4

The Baseline Experiments in the VCR SI Engine Test Facility

Overview

This chapter includes the baseline investigations carried out in the VCR SI research engine test facility (Engine 2) with gasoline (MG 91), methane (purity 99.99 %) and biogas (CH_4:55.6 %, CO_2:42.3%, N_2:2.1%) as the test fuels. The motive behind attempting this investigation is to characterize the engine's performance, combustion and emission parameters with the test fuels at the highest operating CR (10) of the engine designated by the manufacturer. The present study also set a baseline for the further investigation of the commercially customized biogas engine (Engine 1), biogas fueled VCR SI research engine (Engine 2) at its optimized configuration and biogas fueled retrofitted Honda GX 200 SI engine (Engine 3). As the operating parameters (IT, ER and operating CR) of the VCR SI research engine were preconfigured for gasoline operation by the manufacturer, the baseline investigation was carried out towards assessing the optimized IT at CR 10 for methane and biogas operation over its operating speed limits. Further herein this section, the performance, combustion and emission characteristics of the gasoline operated SI engine (Engine 2) is also compared with the methane and biogas fueled engine (Engine 2) for the optimum IT setting obtained at CR 10 over the operating speed range. The detailed experimental matrix and the operating procedure of these engines are also elaborated in this chapter. Optimization of IT of methane and biogas operated SI engine at CR 10 and comparative assessment of the gasoline, methane and biogas operated VCR SI engine at the obtained optimized IA setting at CR 10 are the main objectives of this chapter.

4.1 Experimental Matrix and Operating Procedure

The baseline experimental investigation is conducted in an open ECU controlled gasoline fueled VCR SI engine (*Engine 2*) of rated IP 4.5 kW at CR 10. The research engine is successfully retrofitted for the application of gaseous fuel (methane and biogas) by replacing the liquid fuel induction mechanism. The conventional fuel injection system of the VCR SI engine is replaced with a T-type air-fuel mixture along with a positive displacement self-driven diaphragm pump integrated with a heat exchanger for gaseous fuel induction. The CR of the VCR engine is set to the maximum operating CR designated by the manufacturer for gasoline operation. Hence, the operating CR of the engine was set to 10 for this investigation. The detailed technical specification of the VCR SI engine and the gaseous fuel induction mechanism is explained in *Sections 3.3.1and 3.3.4 of Chapter 3.* Standard gasoline (Grade: MG 91), methane (purity 99.99 %) and biogas (CH_4:55.6 %, CO_2:42.3%, N_2:2.1%) are used as the test fuel for this investigation. Biogas is composed of 2/3rd of methane (the only combustible substance in biogas), and the VCR SI engine is preconfigured for gasoline operation by the manufacturer. Hence, standard gasoline and methane with a purity of 99.99% are used as the reference fuel for this investigation. The physicochemical properties of the test fuels are mentioned in **Table 3. 1** of *Chapter 3*. Further, this investigation is initiated to characterize the performance, combustion and emission characteristics of the VCR SI research engine with the respective test fuels at the maximum operating CR (10) of the engine designated by the manufacturer.

4.1.1 Experimental matrix for the baseline investigation

The baseline investigation is carried out in three different phases. At the 1st stage of the investigation, the retrofitted VCR SI engine is operated with methane at wide open throttle (WOT) and part throttle (PT) conditions to optimize the IT at CR 10. Here WOT refers to 100% throttle opening, and PT refers to 50% of the throttle opening. Similarly, in the 2nd stage of the investigation, the retrofitted VCR SI engine is operated with biogas at WOT and PT condition to optimize the IT at CR 10. The IT is progressively advanced through the reprogrammable ECU and varied in between 24^o to 42^o bTDC and 33^o to 47^{o}bTDC for the

methane and biogas operation of the engine, respectively. The speed of the engine and the equivalence ratio (ER) of the air-fuel mixture are maintained constant while optimizing the IT at any throttle position for both methane and biogas mode operation. The experimental matrix for optimizing the IT for methane and biogas fueled VCR SI engine at CR 10 is depicted in **Table 4. 1**.The effect of ignition advance (IA) on the performance, combustion, and emission parameters has been studied for the methane and biogas operation of the VCR SI engine. The analyses are presented in *Sections 4.3.1 and 4.3.2,* respectively. The manufacturer defined the optimum IT (MBT) for the gasoline fueled VCR SI engine is verified as 28^{o} bTDC for the speed range of 1450 to 1700 rpm at CR 10. A similar, conclusion regarding the MBT of gasoline fueled SI engine is also present in the open literature. Hence, the analysis of MBT for gasoline fueled VCR SI engine is not included here in this investigation. At the 3rd stage of the investigation, the VCR SI engine is operated with gasoline, methane and biogas with the corresponding MBT's at CR 10 over the speed range of 1450 to 1700 rpm. The engine is operated both in WOT and PT conditions for the comparative assessment and the associated experimental matrix is presented in **Table 4. 1**.

Table 4. 1: Experimental matrix for the baseline investigation

<table>
<tr><td colspan="2" rowspan="2">Base line investigation</td><td colspan="6">Operating condition</td></tr>
<tr><td>CR</td><td>Engine Speed (rpm)</td><td>Throttle position</td><td colspan="3">Ignition timing (^{o} CA bTDC)</td></tr>
<tr><td rowspan="4">IT optimization</td><td rowspan="2">Methane fueled VCR SI Engine</td><td rowspan="2">10</td><td rowspan="2">1650</td><td>WOT</td><td colspan="3" rowspan="2">24 to 42^{o} bTDC , Progressive advance interval in each 2^{o}</td></tr>
<tr><td>PT</td></tr>
<tr><td rowspan="2">Biogas fueled VCR SI Engine</td><td rowspan="2">10</td><td rowspan="2">1650</td><td>WOT</td><td colspan="3" rowspan="2">33 to 47, ^{o}bTDC , Progressive advance interval in each 2^{o}</td></tr>
<tr><td>PT</td></tr>
<tr><td rowspan="4">Comparative assessment</td><td rowspan="4">Gasoline, methane and biogas fueled VCR SI engine</td><td rowspan="4">10</td><td rowspan="4">1450 to 1700</td><td rowspan="2">WOT</td><td>For gasoline</td><td rowspan="4">MBT</td><td>28^{o} bTDC</td></tr>
<tr><td rowspan="2">For methane</td><td rowspan="2">40^{o} bTDC</td></tr>
<tr><td rowspan="2">PT</td></tr>
<tr><td>For biogas</td><td>45^{o} bTDC</td></tr>
</table>

4.1.2 Operating procedure of the methane fueled VCR SI engine

The retrofitted VCR SI research engine facility shown in **Fig. 3. 7 and Fig. 3. 8** is operated with pure methane to find out the optimum IT (MBT) and explore its overall performance over the speed range of 1400 to 1700 rpm at CR 10. Preheated methane gas with a purity of 99.99% is supplied to the engine intake manifold through the fuel induction mechanism, as explained in *Section 3.3.4.2* of *Chapter 3*. The intake fuel temperature is maintained in between 45-48°C at steady state operating condition of the engine. Further to explore the effect of IA or to find out the optimum IT, the SI engine is initially started by gasoline and set to WOT condition with a small amount of brake load and allowed to achieve the steady-state condition. Here steady-state condition refers to the stable operating state of the engine, which is identified as the point where the water jacket temperature reaches 60^{o} C. Once the steady-state condition is achieved, the engine speed is set to 1650 rpm by controlling the applied load through the potentiometer and the IT is set to 24^{o} bTDC by following the process of ignition timing variation controlled mentioned in *3.3.5 of Chapter 3*. At that exact moment, the methane fuel line valve is opened and the gasoline injector is turned off. Subsequently, the speed of the VCR engine operating on methane is stabilized to 1650 rpm by adjusting the applied brake load. Once the speed is stabilized, the Enginesoft (Labview based data monitoring and recording interface) was configured to acquire the dynamic pressure, crank angle, brake load, engine speed, throttle position, and temperature at various sections for 50 engine cycles. However, the fuel consumption, volume flow of water to the engine, and calorimeter are recorded manually. Afterward, the exhaust gas compositions are recorded by the flue gas analyzer. Further, the IT is progressively advanced from 24^{o} to 42^{o} bTDC through the PE3 software interface in an interval of 2^{o} CA without altering the operating conditions (WOT, CR, N, ϕ) of the engine. The corresponding performance, combustion and emission data are recoded for each operating IT of the engine by following the procedures mentioned above. The steps for data recording are also repeated for the IT optimization in PT operating condition of the engine. Further, to evaluate the overall performance of the methane fueled VCR SI engine operating with CR 10 and MBT, the speed of the engine is varied from 1400 to 1700 rpm in an interval of 50 rpm both in WOT and PT conditions. Further, the aforementioned steps for data recording are repeated for each operating speed of the engine.

4.1.3 Operating procedure for the biogas fueled VCR SI engine

The retrofitted VCR SI research engine shown in **Fig. 3.9** and **3.10** is operated with biogas to find the optimum IT (MBT) and explore its overall performance over the speed range of 1400 to 1700 rpm at CR 10. The aforementioned operating procedure of the engine in *Section 4.1.2* remained invariant of the test fuel (biogas) except the biogas induction mechanism explained in *Section 3.3.4.3* of *Chapter 3*. The SI engine is primarily started with gasoline and set to WOT at an IA of 28^{o} bTDC and allowed to achieve the steady state condition at 1650 rpm. Once the engine is stabilized, the ECU is reconfigured through the PE3 interface and the IT is customized to 33^{o} bTDC. At the same instance, the biogas fuel line valve is opened and the preheated biogas leaving the diaphragm pump at 45^{o}-46^{o} C is allowed to enter the T-type air biogas mixer. Soon after supplying the preheated biogas to the engine, the petrol injector is turned off and the air-fuel (air-biogas) adjustment knob on the diaphragm pump is tuned to stabilize the engine speed. Once the speed of the engine is stabilized, it is set to 1650 rpm only by controlling the load on the engine. It was also ensured that for a particular throttle position the mass flow rate of the biogas should remain constant. Now the engine solely runs with biogas and after retaining steady state operation, the test data (performance, combustion and emission) are recorded though the Enginesoft interface for 50 engine cycles. Further, in line with the proposed baseline experiment, the IT is progressively advanced from 33^{o} to 47^{o} bTDC in an interval of 2^{o} CA without altering the operating conditions (WOT, CR, N, ϕ). The steps of data logging are repeated for each operating IT of the engine. Similarly, the steps for data logging are also repeated for the IT optimization in PT operating condition of the engine. Further, to evaluate the overall performance of the biogas fueled VCR SI engine operating at CR 10 and MBT, the speed of the engine is varied from 1400 to 1700 rpm in an interval of 50 rpm both in WOT and PT conditions. The aforementioned steps for data recording are repeated for each operating speed of the engine.

4.1.4 Operating procedure for the gasoline fueled VCR SI engine

The VCR SI research engine test facility shown in **Fig. 3. 6** is preconfigured by the manufacturer for gasoline operation with established MBTs over the speed range of 1450 to 1700 rpm at CR 10. Thereby experiments are only performed to evaluate the overall

performance of the gasoline fueled engine at WOT and PT conditions over the speed range of 1450 to 1700 rpm at CR 10. The MBT of the engine for gasoline operation is maintained at 28^{o} bTDC irrespective of the throttle position and operating speed range. The operating procedure and data logging for the present set of experiment are similar to the method mentioned earlier in *Section 4.1.2*.

4.2 Experimental Uncertainty

The measuring instruments used in the current investigation are made by different manufacturers and follow different methodologies to measure several unlike parameters. Moreover, the accuracy of those measuring devices is instrument-specific and dependent on the operating conditions as well as the surrounding experimental environment. Hence, both the systematic and random errors are taken care while evaluating the overall uncertainty of the measured parameters. The root mean square technique proposed by Kline and Mc. Clintock and Moffat (Kline and McClintock, 1953; Moffat, 1982) are followed to evaluate the systematic, random and overall uncertainty of the experimental data by using *Eq. F1, F2 and F3* of ***Appendix F***, respectively. The uncertainty analysis and the sample calculations are explained in detail in *Appendix F*. The systematic, random and overall uncertainties associated with the gasoline, methane and biogas mode operation of the VCR SI research engine test rig at CR 10 and WOT condition is presented in **Table 4. 2**.

4.3 Assessment of the Optimized IT for the VCR SI Engine

The combustion in the SI engine is divided into four phases: spark ignition, early flame development, flame propagation, and flame termination. Ignition timing plays a crucial role in regulating these stages of combustion in the SI engine irrespective of the operating conditions (Hallgren, 2005; Heywood, 1988). If the combustion event is gradually advanced before the TDC, the work transfer during the compression stroke increases. Similarly, the progressive retirement of IT resulted in delayed combustion processes, where the peak cylinder pressure appears later in the expansion stroke and is reduced in magnitude. These changes reduce the extent of the work transfer in expansion stroke (Stone et al., 1993; Stone, 2012). To effectively utilize the expansion work, the ignition timing has to be correctly configured and must locate

in advance by a certain crank angle before the completion of the compression stroke. Hence, optimization of the IT becomes an essential part of this investigation before operating the engine with methane and biogas at the operating CR. Moreover, the combustion chemistry of methane and biogas is different from the base operating fuel (Gasoline) for the engine. Further, the slower flame front propagation rate and higher auto-ignition temperature of methane (38 $cm.s^{-1}$, 540-600^{o}C) and biogas (25 $cm.s^{-1}$, 650^{o}C) lead to delay in initiation, development and propagation of the flame front after the spark ignition. Hence, the IT set for gasoline operation could not operate the VCR SI engine effectively for methane and biogas at CR 10. In light of the above-mentioned contextual, the IT has been primarily optimized for methane and biogas operation before the comparative evaluation of the engine with gasoline over the engine's operating speed.

Table 4. 2: Overall uncertainties corresponding to the performance parameters

Derived parameters		Systematic uncertainty (%)			Random uncertainty (%)			Overall uncertainty (%)		
		Gasoline	Methane	Biogas	Gasoline	Methane	Biogas	Gasoline	Methane	Biogas
Performance Parameter	A/F	± 0.70	± 0.70	± 0.70	± 1.60	± 2.59	± 1.80	± 1.76	± 2.68	± 1.94
	BT	± 0.25	± 0.25	± 0.25	± 0.10	± 0.12	± 0.13	± 0.27	± 0.27	± 0.28
	BP	± 0.39	± 0.39	± 0.39	± 1.55	± 1.72	± 1.19	± 1.60	± 1.76	± 1.25
	BTE	± 0.64	± 0.80	± 0.80	± 1.57	± 1.72	± 1.2	± 1.68	± 1.90	± 1.44
	BSFC	± 0.40	± 0.63	± 0.63	± 2.12	± 3.02	± 2.03	± 2.18	± 3.1	± 2.15
	VE	± 0.58	± 0.58	± 0.58	± 1.00	± 1.04	± 0.87	± 1.15	± 1.18	± 1.04
Combustion parameter	NHRR	± 0.28	± 0.28	± 0.29	± 0.41	± 0.32	± 0.35	± 0.50	± 0.43	± 0.46
	MGT	± 0.57	± 0.57	± 0.58	± 0.70	± 0.70	± 0.73	± 0.91	± 0.90	± 0.93
	MFB	± 0.29	± 0.28	± 0.28	± 0.31	± 0.17	± 0.23	± 0.42	± 0.33	± 0.37
Emission parameter	CO	± 3	± 3	± 3	± 5.55	± 5.43	± 5.88	± 6.31	± 6.20	± 6.6
	CO_2	± 3	± 3	± 3	± 2.66	± 1.42	± 2.73	± 4.01	± 3.32	± 3.76
	HC	± 3	± 3	± 3	± 3.96	± 4.05	± 2.99	± 4.96	± 5.04	± 4.23
	NO_X	± 1	± 1	± 1	± 2.48	± 1.65	± 2.96	± 2.68	± 1.93	± 3.12

4.3.1 Assessment of the optimum IT for the methane fueled VCR SI engine

At the present stage of the investigation, the VCR SI engine is fueled with pure methane and operated at CR 10 and 1650 rpm. The ER (ϕ) is maintained approximately constant in between 0.710 - 0.718 (~0.715) and 0.718 - 0.722 (~0.719), respectively for the WOT and PT throttle operating condition of the engine. The IT is progressively advanced from 24^o to 44^o bTDC in an interval of 2^o CA without altering the operating condition of the engine. However, for the PT operating condition, advancing the IT beyond 42^o bTDC resulted in the unstable operating state of the engine. Hence, the higher range of IA for the present investigation is restricted to 42^o CA bTDC for WOT and PT operating conditions. The corresponding performance (BT, BP, BSFC, BTE, VE, ER), combustion (P-Θ, NHRR, MFB, MGT), and emission (CO, CO_2, HC, NOx) characteristics of the engine are assessed both for WOT and PT condition of the engine by following the standard guidelines as specified by the Bureau of Indian Standards (BIS) in IS 10000: Part 6, 7 and 8. Each set of experiments is repeated thrice to ensure the correctness of the capture data. The average of these values is considered for the evaluation of different engine parameters. The performance and combustion parameters of the engine are evaluated from *Eqs. D1-D11* and *D12-D25* as described in ***Appendix D***. Further, the exhaust gas analyzer (AVL Diagas 444N) is used to quantify the exhaust emissions from the engine.

Performance analysis

This section assesses the effect of IA on the BT, BP, BSFC, BTE and VE of the methane fueled VCR SI engine by following the *Eqs. D1, D2, D3, D5* and *D6* of ***Appendix D,*** respectively. **Figure 4.1** shows the effect of IA on the BT and BP of the methane fueled VCR SI engine for the WOT and PT operating conditions at CR 10 and 1650 rpm. As the IT is progressively advanced from the TDC (360^o CA), the induced BT and BP of the engine are consistently improved up to 40^o CA bTDC both for WOT and PT conditions. Further advancement of the IT beyond 40^o CA bTDC reduced the BT and BP of the engine at CR 10. This may be due to the faster flame propagation speed with respect to the progressive IA, which decelerates beyond 40^o CA bTDC. The faster flame propagation speed at 40^o CA bTDC reduced the combustion duration (rapid burn angle), which enhanced the peak pressure and net heat

release to produce maximum work during the expansion stroke compared to other cases of IA (Sadiq Al-Baghdadi, 2004). On the other hand, the over advancement of IT increases the compression work transfer to the cylinder gases and thereby reduces the network transfer (Zareei and Kakaee, 2013). Hence, this may be considered the key reason for the drop-off of the BT and BP beyond 40° CA bTDC. The optimum IT (MBT), which developed the maximum BT and BP for the engine's present configuration, is observed at 40° CA bTDC. Similar observations are also reported in the open literature for the optimum IT of gasoline (Kakaee et al., 2011), CNG (Chandra et al., 2011), and methane enriched biogas (Montoya et al., 2015) operated SI engines at CR 10.5, 12.65 and 15.5, respectively.

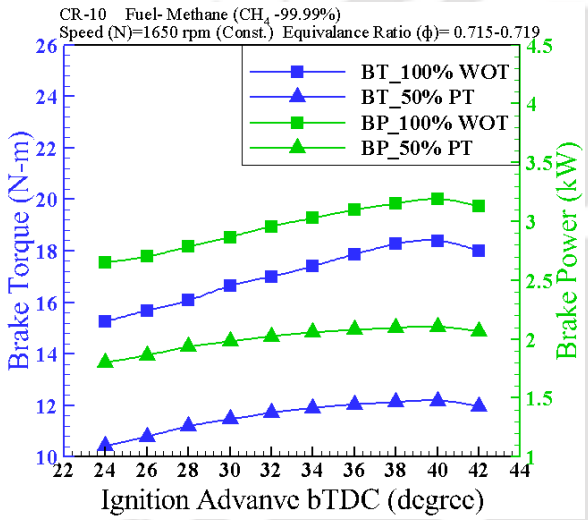

Fig. 4. 1: Effect of IA on the BT and BP of the methane fueled VCR SI engine at CR 10

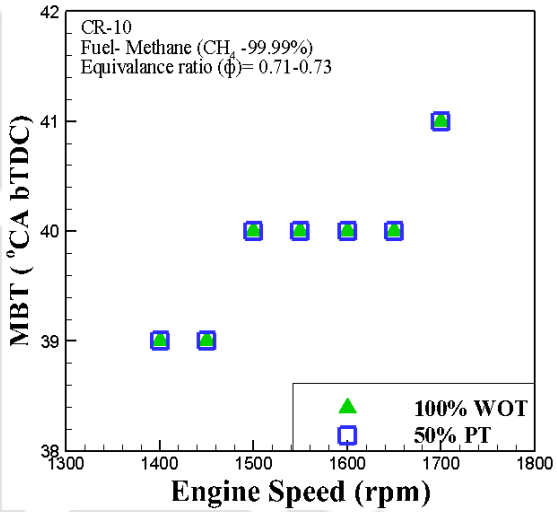

Fig. 4. 2: Effect of engine speed on the MBT of the methane fueled VCR SI engine at CR 10

As depicted in **Fig. 4. 1**, the maximum BT of the engine for the WOT and PT operating conditions are 18.4 N-m and 12.2 N-m, respectively at 40° CA bTDC. Similarly, the maximum BP of the engine running with WOT and PT conditions are found to be 3.19 and 2.1 kW, respectively at 40° CA bTDC. The engine speed also plays a crucial role while optimization of the IT at any operating CR. **Fig. 4. 2** shows the effect of engine speed on the optimum IT (MBT) both at WOT and PT operating conditions. As the engine speed is increased, the optimum IT is advanced due to the shorter time interval of combustion duration (Sadiq Al-Baghdadi, 2004). However, due to the shorter span of operating speed, the observed fluctuation

of MBT is not so significant for the present case. Hence for the current operating speed range (1400-1700 rpm), 40° CA bTDC is considered as the optimum IT for both WOT and PT conditions.

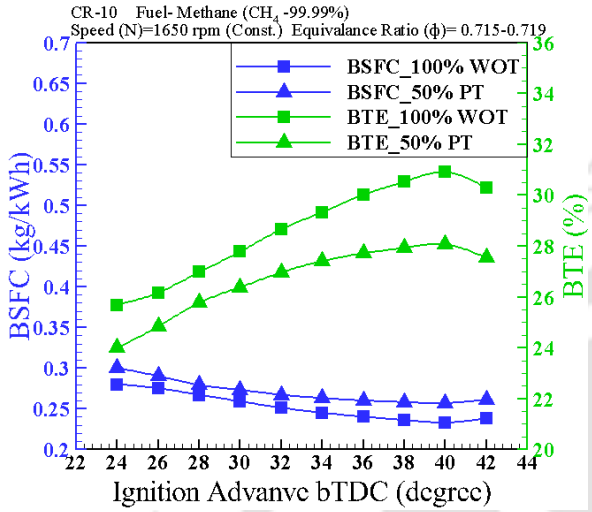

Fig. 4. 3: Effect of IA on the BSFC and BTE of the methane fueled VCR SI engine at CR 10

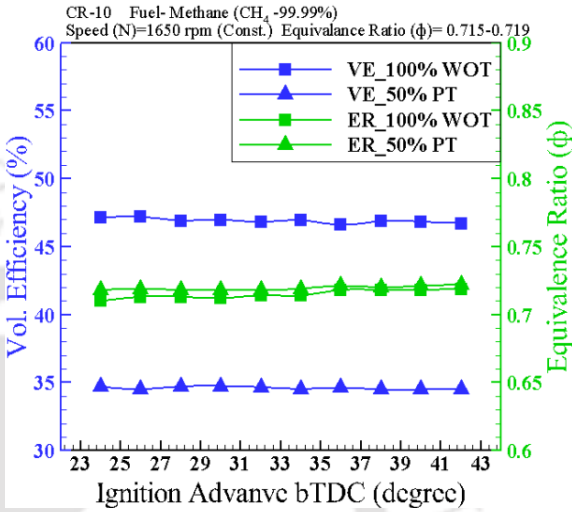

Fig. 4. 4: Effect of IA on the VE and ER of the methane fueled VCR SI engine at CR 10

The effect IA on the BSFC and BTE of the methane fueled SI engine is depicted in **Fig. 4. 3** for the WOT and PT conditions. The minimum BSFC and maximum BTE of the methane fueled VCR SI engine is observed at 40° CA bTDC for WOT and PT conditions. The BSFC of the engine drops down consistently for the progressive IA up to 40° CA bTDC and ascends with further IA. This happening may be the consequence of the developed BP with the increasing IA of the engine. The mass flow rate of fuel for the WOT and PT conditions of the engine is maintained (0.743 kg/h and 0.54 kg/h) constant irrespective of the IA of the engine. However, the developed BP followed an increasing trend and found maximum at 40° CA bTDC for WOT and PT conditions. Hence, the BSFC is observed minimum at 40° CA bTDC. The minimum BSFCs at WOT and PT conditions are 0.233 kg/kW-h and 0.257 kg/kW-h, respectively. Whereas, BTE portrayed an opposite trend and is unlike BSFC of the engine. The BTE increases with progressive IA up to 40° CA bTDC and drops off further. The maximum BTEs at WOT and PT conditions are found to be 30.89% and 28.05%, respectively. It may be due to the minimum specific fuel consumption at MBT, both in WOT and PT conditions. Since the IT is optimized in the present investigation, the remaining operating parameters (CR, N, ϕ

and throttle opening) are maintained constant during each working condition. As depicted in **Fig. 4. 4**, 'ϕ' is held almost constant for WOT and PT conditions. It may be noted that the operating ER is retained in between 0.71-0.724 and 0.718-0.722 for WOT and PT conditions, respectively. However, the average maintained ERs are 0.715 and 0.719 for the WOT and PT conditions, respectively. Similarly, no significant variation in the recorded VEs of the engine is observed with respect to the operating IA. The recorded VE is found to fluctuate between 46.5%-47.5% and 34.2%- 34.7% for the WOT and PT conditions, respectively.

Combustion analysis

Methane as a fuel has a higher volumetric energy density and wider flammability limit compared to gasoline. The combustion chemistry of methane in the SI engine depends on the flame propagation rate which further depends on the flame speed and auto ignition temperature in the turbulent environment (Ma et al., 2012). Because of these reasons, the IT of the gasoline fueled VCR SI engine needs to be advanced for gaseous fuels like methane. However, the excess advancement of IT may increase the compression work due to the possibility of peak cylinder pressure before TDC. Similarly, the delayed combustion may also reduce the expansion work due to the probability of peak cylinder pressure much later in the expansion stroke (Mehrnoosh et al., 2012). Hence, before identifying the MBT for the fuel, the aspects mentioned above have been thoroughly investigated. The cylinder pressure (p) and crank angle (θ) data are captured for 50 consecutive cycles for each experiment. The combustion parameters viz. *P-θ, P-V*, net heat release rate (NHRR), mass fraction burnt (MFB) and mean gas temperature (MGT) are evaluated from the *Eqs. D12-D25* of ***APPENDIX D*** as referred from the literature (Heywood, 1988; Stone, 2012). The average values of the data points are considered for the discussion.

The effect of IA on the average cylinder pressure of the methane fueled VCR SI engine is portrayed in **Fig. 4. 5** and **Fig. 4. 6** respectively for the WOT and PT operating conditions. The CR (10), engine speed (1650 rpm) and ER (0.715 at WOT and 0.719 at PT) are maintained constant while operating the engine at different IT. A noticeable rise in the peak cylinder pressure (PCP) is observed with the progressive advance of the IT from the TDC both in WOT and PT conditions. The above occurrence may be due to the accelerated combustion process,

which increased the cylinder gas temperature and led to a higher energy release rate, resulting in the rise in in-cylinder pressure with progressive IA (Papagiannakis and Zannis, 2013). Irrespective of the operating conditions, the progressive advancement of the IT shifts the location of the peak pressure (LPP) closer to the TDC. As shown in **Table 4. 3**, the average PCP at WOT is increased from 22.3 bar to 31.2 bar due to the progressive IA from 24^o bTDC to 38^o bTDC, respectively. Further advancing the IT increased the PCP to 31.6 bar and 31.9 bar respectively at 40^o bTDC and 42^o bTDC. It is evident from **Fig. 4. 5** that the slopes of the pressure gradients before the TDC gradually increased with the IA and are observed almost constant for the IAs of 40^o bTDC to 42^o bTDC. However, the area under the *P-V* curve gradually increases with the IA up to 40^o bTDC and declines with further IT advancement. The maximum area under the P-V curve is observed at 40^o bTDC and found 3264.9, as shown in **Fig. 4. 7**. The above happening may be due to faster flame propagation (shorter combustion duration), resulting in improved thermal efficiency and power output at 40^o bTDC. Hence, 40^o bTDC is considered the optimum IT for the WOT condition and justifies the proposed MBT in the performance analysis section. A similar observation is also noticed from the P-θ plot (**Fig. 4. 6**) at the PT condition.

Table 4. 3: Effect of IT on the PCP and LPP of the methane fueled SI engine at CR 10

IT (^{o} CA bTDC)	WOT		PT	
	PCP (bar)	LPP (^{o} CA)	PCP (bar)	LPP (^{o} CA)
24	22.3	380	14.0	387
26	24.8	377	16.2	382
28	26.9	375	18.2	379
30	27.2	375	18.8	378
32	27.9	374	19.3	378
34	29.1	372	19.4	377
36	30.2	371	19.5	377
38	31.2	370	19.6	376
40	31.6	369	20.5	376
42	31.9	368	20.4	374

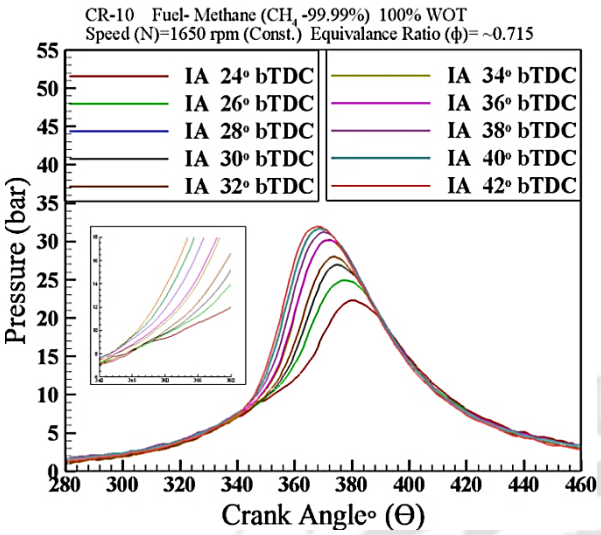

Fig. 4. 5: Effect of IA on the average cylinder pressure at CR 10 and WOT condition

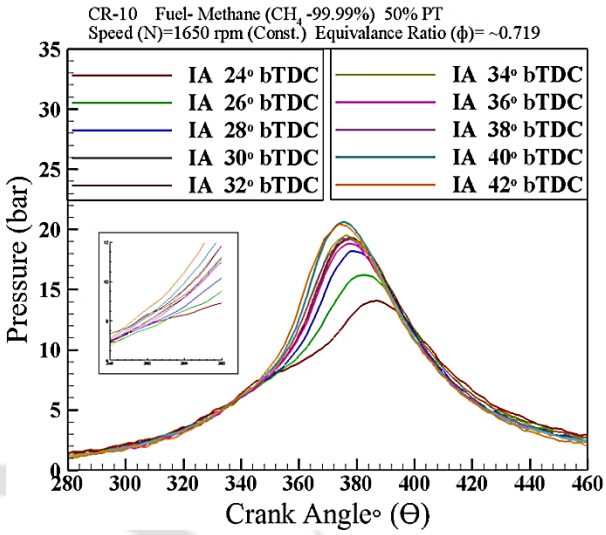

Fig. 4. 6: Effect of IA on the average cylinder pressure at CR 10 and PT condition

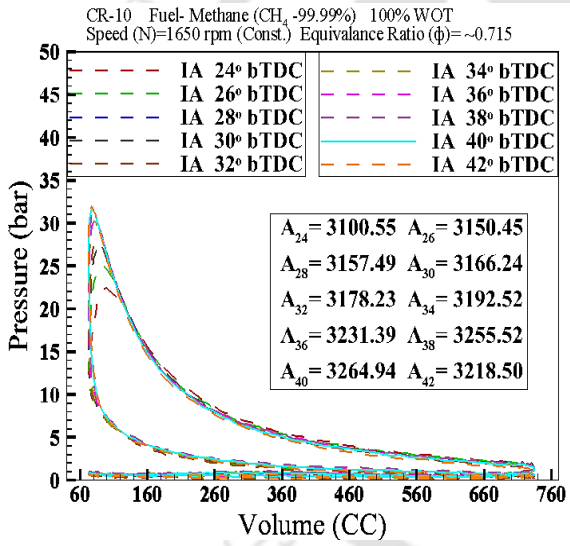

Fig. 4. 7: Effect of IA on the P-V curve at CR 10 and WOT condition

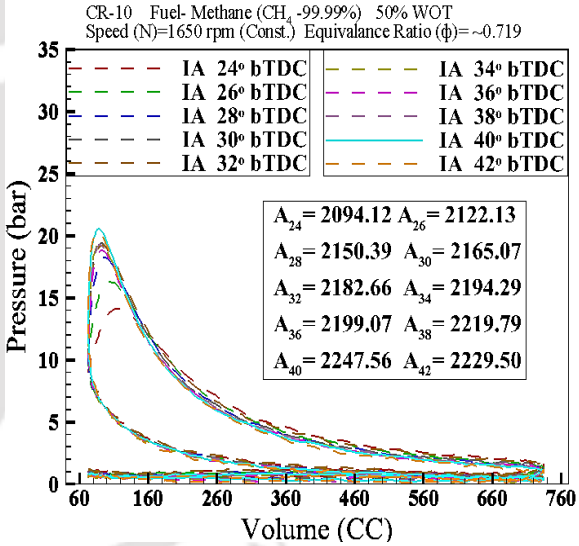

Fig. 4. 8: Effect of IA on the P-V curve at CR 10 and PT condition

As shown in **Table 4. 3**, the average PCP at PT condition is increased from 14 bar to 20.5 bar due to the progressive IA from 24° bTDC to 40° bTDC, respectively. Further advancing the IT reduced the PCP to 20.4 bar at 42° bTDC. The above occurrence may be due to the over-advanced IT, which increased the compression work transfer and decreased PCP and cylinder gas temperature at this condition (Jaramillo et al., 2018). The area under the P-V

curve shown in **Fig. 4. 8** also exhibits a similar tendency at PT condition. However, the maximum area under the P-V curve is observed at 40° bTDC. Hence, 40° bTDC is also considered as the MBT for the PT condition. It was also observed that irrespective of the throttle opening (WOT or PT), the MBT remains invariant for the current operating speed range of the methane fueled SI engine at CR 10.

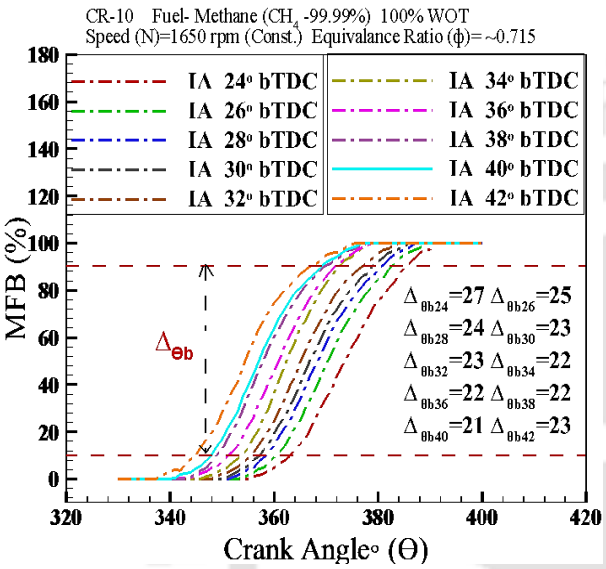

Fig. 4. 9: Effect of IA on the MFB at CR 10 and WOT condition

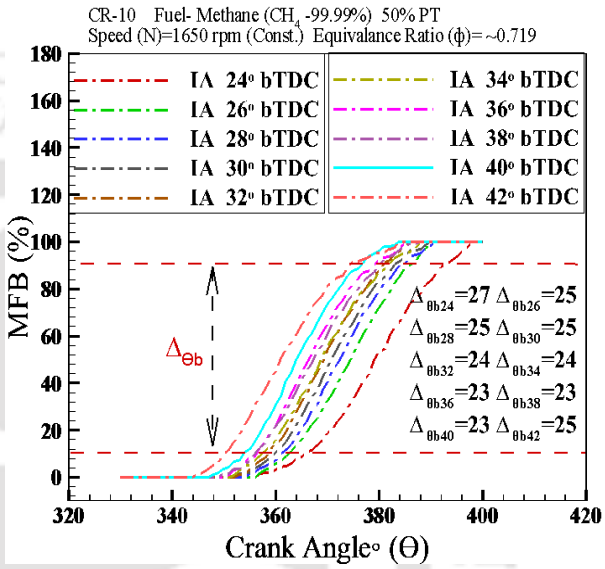

Fig. 4. 10: Effect of IA on the MFB at CR 10 and PT condition

Fig. 4. 9 and **Fig. 4. 10** describe the effect of IA on the mass fraction burnt (MFB) for the methane fueled SI engine operating at WOT and PT conditions at CR 10, respectively. The MFB is calculated by following the method shown in *Eqs*. D17-D19 of ***APPENDIX D*** and proposed by Rassweiler and Withrow (Rassweiler and Withrow, 1938). For the present case, the rapid burn angle (RBA) '$\Delta\theta_b$' is considered as the crank angle interval between the end of flame development stage (mass fraction burnt of 10%) and the end of flame propagation (mass fraction burnt of 90%) (Heywood, 1988). The rapid burn angles (RBA) for the IAs of 24° bTDC, 26° bTDC, 28° bTDC, 30° bTDC, 32° bTDC, 34° bTDC, 36° bTDC, 38° bTDC, 40° bTDC and 42° bTDC are referred as $\Delta\theta_{bIA24}$, $\Delta\theta_{bIA26}$, $\Delta\theta_{bIA28}$, $\Delta\theta_{bIA30}$ $\Delta\theta_{bIA32}$, $\Delta\theta_{bIA34}$, $\Delta\theta_{bIA36}$, $\Delta\theta_{bIA38}$, $\Delta\theta_{bIA40}$ and $\Delta\theta_{bIA42}$ respectively in the present section. As observed from **Fig. 4. 9** and **Fig. 4. 10,** the combustion event and the flame development

(mass burn fraction 0-10%) are initiated earlier during the end of the compression stroke and advanced progressively before the TDC due to the advancement of IT bTDC. However, as the combustion is initiated before the piston reaches the TDC, the fresh air-fuel mixtures are being pushed towards the developing flame front. As a result, the flame propagation rate increases and reduces the combustion duration with progressive IA bTDC. Alongwith the further advanced IT, the in-cylinder pressure and temperature drop, resulting in higher cyclic variation in flame development and propagation stage during the combustion process. Hence beyond the optimum IA, the flame propagation rate is decreased by extending the combustion duration. Researchers also noticed similar observations (Ma et al., 2012; Jaramillo et al., 2018) for biogas and hydrogen operated SI engines at different operating conditions. **Table 4. 4** listed the recorded crank angles at the end of flame development and propagation stage along with the RBA at the respective operating IT both for WOT and PT condition of the engine. $\Delta\theta_{bIA24}$, $\Delta\theta_{bIA26}$, $\Delta\theta_{bIA28}$, $\Delta\theta_{bIA30}$ $\Delta\theta_{bIA32}$, $\Delta\theta_{bIA34}$, $\Delta\theta_{bIA36}$, $\Delta\theta_{bIA38}$, $\Delta\theta_{bIA40}$ and $\Delta\theta_{bIA42}$ are repoted 27°CA, 25°CA, 24°CA, 23°CA, 23°CA, 22°CA, 22°CA, 22°CA, 21°CA and 23°CA, respectively. Similar observation is also noticed for PT operating condition. As, the RBA was found minimum at an IT of 40° CA bTDC, the flame propagation speed is considered faster at this IT for both WOT and PT condition of the methane fueled engine.

Table 4. 4: Effect of IT on the RBA of the of the methane fueled SI engine at CR 10

IT (° CA bTDC)	WOT			PT		
	°CA@ MFB 10%	°CA@ MFB 90%	RBA'$\Delta\theta_b$' (°CA)	°CA@ MFB 10%	°CA@ MFB 90%	RBA'$\Delta\theta_b$' (°CA)
24	368	395	27	369	396	27
26	360	385	25	369	390	25
28	358	382	24	364	389	25
30	357	380	23	363	388	25
32	355	378	23	363	387	24
34	354	376	22	361	385	24
36	351	373	22	360	383	23
38	349	371	22	359	382	23
40	348	369	21	358	381	23
42	345	368	23	359	384	25

The net heat release rate (NHRR) is evaluated by applying the 1st law analysis to the combustion chamber and considering the content of the combustion chamber as a single zone that behaves like a semi-perfect gas. It is assumed that the combustion products and reactants are thoroughly mixed in the combustion chamber, and there is no mass transfer across the control volume. The NHRR is calculated by using *Eq. D16* of ***APPENDIX D***. The variation of NHRRs with progressive IA of the methane operated SI engine is shown in **Fig. 4. 11** and **Fig. 4. 12** for the WOT and PT conditions, respectively. The NHRR for the intermediate ITs is not included herein these figures to clearly distinguish the difference in the NHRRs. Irrespective of the throttle position, there is an appreciable improvement in the NHRR with progressive IA up to 40° bTDC. The above phenomenon is because of the early flame propagation rate where the energy conversion efficiency is maximum (Kemal and Sayin, 2014). However, with further advanced IT (beyond 40° bTDC), the NHRR is dropped due to the increased compression work and rapid conversion of the heat energy to accommodate the negative work done before the TDC. The peak neat heat release rate (PNHRR) and the location of the peak net heat release rate (LPNHRR) are listed in **Table 4. 5** for both WOT and PT conditions of the engine. As observed from **Table 4. 5** the LPNHRR shifts closer to thre TDC with the progressive advance of IT bTDC both at WOT and PT conditions. Moreover, the maximum NHRRs are observed at 40° bTDC (MBT) and found 27.9 J/ °CA and 18.9 J/ °CA at 361 °CA and 366 °CA, respectively for the WOT and PT operating conditions of the engine. The above happenings may be attributed to the reducing combustion duration with the progressive IA and is minimum at 40° bTDC.

Table 4. 5: Effect of IT on the PNHRR and LPNHRR of the methane fueled SI engine at CR 10

IT (° CA bTDC)	WOT		PT	
	PNHRR (J/°CA)	LPNHRR (° CA)	PNHRR (J/°CA)	LPNHRR (° CA)
24	24.7	374	17.4	380
28	26.2	366	18.6	376
32	26.5	366	18.6	370
36	26.8	363	17.9	371
40	27.9	361	18.9	366
42	26.1	356	16.9	367

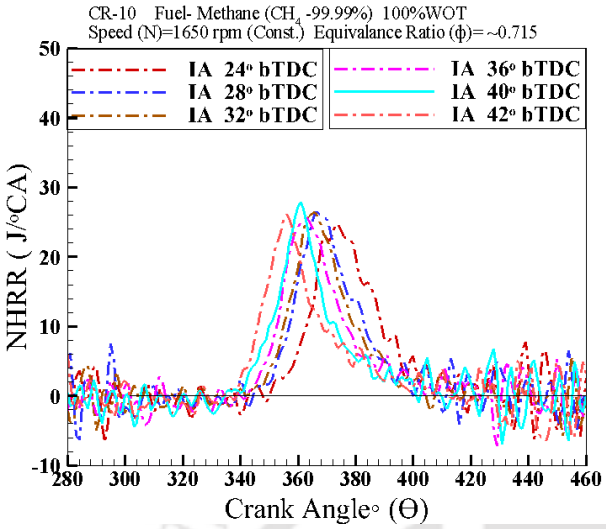

Fig. 4. 11: Effect of IA on the NHRR at CR 10 and WOT condition

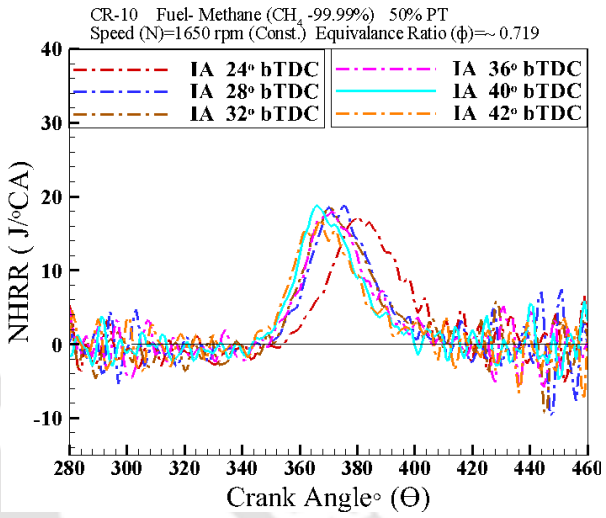

Fig. 4. 12: Effect of IA on the NHRR at CR 10 and PT condition

The mean gas temperature (MGT) is evaluated from *Eq. D20* of ***APPENDIX D***. Here, it assumes a single zone for combustion, which implies the product and reactant are fully mixed during combustion. Hence the molecular weights of the burned and unburned gases are considered identical (Heywood, 1988). Since the pressure and volume at each crank angle are known, the gas mass is assumed constant for a particular IT of the engine. The characteristics gas constant 'R' is evaluated using the correlation R= 0.287+(0.020 × Φ) (Stone, 2012; Kriger and Borman 1986). **Fig. 4. 13** and **Fig. 4. 14** illustrate the effect of IA on the MGT of the methane fueled SI engine at WOT and PT conditions, respectively. Irrespective of the operating throttle, the MGT and its slope are constantly increasing between 340° CA to 390° CA with the progressive IA. However, the peak MGT (PMGT) is dropped at 42° bTDC. The PMGTs and their locations (LPMGT) at different IAs are shown in **Table 4. 6** Further, it is interpreted that the LPMGT shifts towards the TDC with the IA up to 40° bTDC and shift away at 42° bTDC. Moreover, the LPMGT appears consequently after LPCP and LPNHRR for both WOT and PT conditions. The PMGT at WOT and PT conditions are 1019 K at 376° CA and 823 K at 384° CA, respectively. The above happening is attributed to the trend of PCP and NHHR, which progressively improved the MGT up to the IA of 40° bTDC.

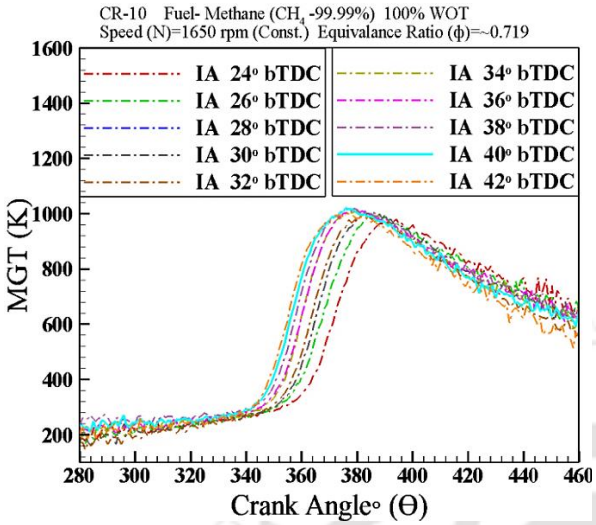

Fig. 4. 13: Effect of IA on the MGT at CR 10 and WOT condition

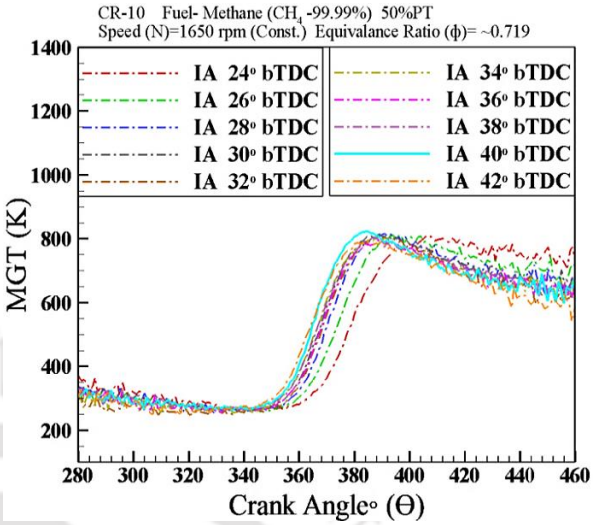

Fig. 4. 14: Effect of IA on the MGT at CR 10 and PT condition

Table 4. 6: Effect of IT on the PMGTs and LPMGTs of the methane fueled SI engine at CR10

IT (^{o} CA bTDC)	WOT		PT	
	PMGT (K)	LPMGT (^{o} CA)	PMGT (K)	LPMGT (^{o} CA)
24	980.6	394	802.6	406
26	992.9	388	804.9	394
28	998.5	386	806.3	391
30	1005.5	386	808.5	389
32	1006.9	383	810.9	387
34	1010.7	381	812.9	388
36	1014.0	380	813.7	392
38	1016.9	379	815.3	387
40	1018.9	376	822.9	384
42	1001.1	377	793.4	390

Emission analysis

In the present case, the exhaust emission concentrations are recorded with an AVL DIAGAS analyzer by following the method described in *section 3.3.2.6* of ***Chapter 3***. The CO,

CO_2 and HC, NO_X concentrations are reported in volume percent (vol %) and parts per million (ppm), respectively, in **Fig. 4. 15** and **Fig. 4. 16**. However, the emission concentrations are converted in brake-specific basic (g/kWh) and compared with the established emission standards (BS-VI and Euro 6) (The Gazette of India, 2016) and reported in **Table 4. 7**. The general relation *(Eq. 4.1)* reported in the literature (Heseding and Daskalopoulos, 2006; Pilusa et al., 2012; Ağbulut et al., 2019) is used to convert the emission level from vol %, ppm to brake specific basis (g/kWh). *Eqs. 4.2- 4.5* are used to estimate the CO, CO_2 HC and NO_X emission, respectively, on brake specific basis. Where, 'EP_i' is the pollutant mass with respect to 'P_{eff}', '$EV_{i,d}$' is the reported exhaust emission on dry basis (ppm), '$EV_{i,w}$' is the reported exhaust emission on wet basis (ppm), 'M_i' is the molecular mass of the component (g/mol), '$M_{Exh,d}$' is the molecular mass of the exhaust gases on dry basis (g/mol), '$M_{Exh,w}$' is the molecular mass of the exhaust gases on wet basis (g/mol), '$m_{Exh,d}$' is the mass flow rate of exhaust gas (kg/h) and 'P_{eff}' is the power output (kW). The molecular mass of the exhaust gas ($M_{Exh,d}$ and $M_{Exh,w}$) is mainly influenced due the concentration of O_2 and N_2 in the exhaust emission. However, the overserved variations are limited to 0.21- 0.46 g/mol with in the operating IA and throttle condition of the engine. Hence the average values of $M_{Exh,d}$ and $M_{Exh,w}$ are taken in account and assumed constant for the defined operating condition of the engine.

$$EP_i = EV_{i,d} \times \left(\frac{M_i}{M_{Exh,d}} \times \frac{m_{Exh,d}}{P_{eff}} \right) = EV_{i,w} \times \left(\frac{M_i}{M_{Exh,w}} \times \frac{m_{Exh,w}}{P_{eff}} \right) \quad 4.1$$

$$EP_{CO} = \left(\frac{EV_{CO}}{1 \times 10^6} \right) \times \left(\frac{M_{CO}}{M_{Exh,d}} \times \frac{m_{Exh,d}}{P_{eff}} \right)$$
$$= \left(EV_{CO} \times 10^{-6} \right) \times \left(\frac{28.01}{30.21} \times \frac{m_{Exh,d}}{P_{eff}} \right) = \left(\frac{EV_{CO} \times m_{Exh,d}}{P_{eff}} \right) \times 0.927 \times 10^{-6} \quad 4.2$$

$$EP_{CO_2} = \left(\frac{EV_{CO_2}}{1 \times 10^6} \right) \times \left(\frac{M_{CO_2}}{M_{Exh,w}} \times \frac{m_{Exh,w}}{P_{eff}} \right)$$
$$= \left(EV_{CO_2} \times 10^{-6} \right) \times \left(\frac{44.01}{28.84} \times \frac{m_{Exh,d}}{P_{eff}} \right) = \left(\frac{EV_{CO_2} \times m_{Exh,d}}{P_{eff}} \right) \times 1.526 \times 10^{-6} \quad 4.3$$

$$EP_{HC} = \left(\frac{EV_{HC}}{1\times10^{6}}\right)\times\left(\frac{M_{HC}}{M_{Exh,w}}\times\frac{m_{Exh,w}}{P_{eff}}\right)$$
$$= \left(EV_{HC}\times10^{-6}\right)\times\left(\frac{13.02}{28.84}\times\frac{m_{Exh,d}}{P_{eff}}\right) = \left(\frac{EV_{HC}\times m_{Exh,d}}{P_{eff}}\right)\times0.451\times10^{-6} \quad 4.4$$

$$EP_{NO_X} = \left(\frac{EV_{NO_X}}{1\times10^{6}}\right)\times\left(\frac{M_{NO_X}}{M_{Exh,w}}\times\frac{m_{Exh,w}}{P_{eff}}\right)$$
$$= \left(EV_{NO_X}\times10^{-6}\right)\times\left(\frac{46.01}{28.84}\times\frac{m_{Exh,d}}{P_{eff}}\right) = \left(\frac{EV_{NO_X}\times m_{Exh,d}}{P_{eff}}\right)\times1.595\times10^{-6} \quad 4.5$$

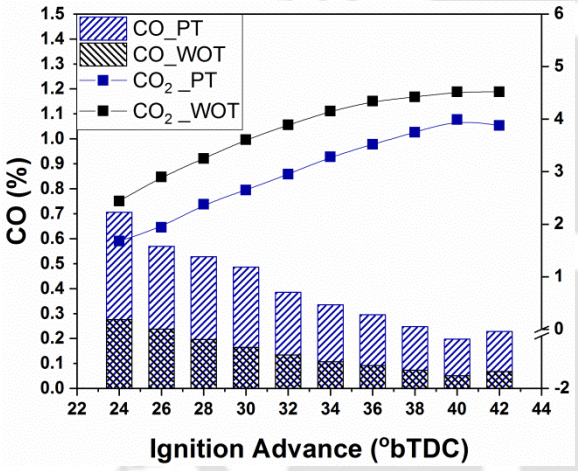

Fig. 4. 15: Effect of IA on the MGT at CR 10 and WOT condition

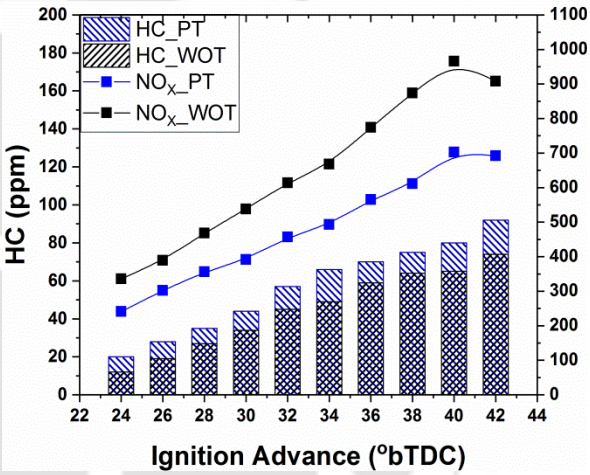

Fig. 4. 16: Effect of IA on the MGT at CR 10 and WOT condition

Fig. 4. 15 depicts the effect of IA on the CO and CO_2 emission of the methane fueled VCR SI engine at CR 10 both at WOT and PT condition. Irrespective of the throttle operating condition, the concentration of CO in the exhaust emission followed a decreasing trend with the progressive IA and deviates after the point of MBT. The least CO emission is observed at 40° bTDC and found as 0.05% (1.8 g/kWh) and 0.19% (7.1 g/kWh) at WOT and PT operating condition, respectively. Whereas the maximum CO concentration is detected at 24° bTDC and found 0.28% (9.9 g/kWh) and 0.71% (25.4 g/kWh) respectively for the WOT and PT operating condition of the engine. In general, local reach regions, poor mixing of air and fuel mixture and incomplete combustion are the typical casus of CO emission (Pulkrabek, 1997). However, the cylinder charge temperature is also equally responsible for the formation and control the

rate of oxidization of CO (Stone, 2012). In the present case, the engine is operated with a lean equivalence ratio at CR 10 both at WOT and PT conditions. Advancing the IT initiates the combustion earlier relative to the TDC (**Fig. 4. 9 - Fig. 4. 10**). This results in an increase in maximum cylinder temperature up to the point of MBT (**Fig. 4. 13 - Fig. 4. 14**) and favors the CO formation mechanism. However, at the same time, the progressive IA results in an increased time interval during the expansion phase for which the high temperature (> 800 K at WOT and 700 K at PT) persists in the engine cylinder. Hence it positively affects the CO oxidization rate, which reduced the CO level and increased the CO_2 level at advanced ITs (Papagiannakis and Zannis, 2013). Hence, the above mentioned justifies the CO and CO_2 emission pattern with respect to the advanced IT. The CO_2 concentration in the exhaust emission followed an increasing trend and found maximum at the point of MBT (40^o bTDC) irrespective of the throttle operating condition. The maximum CO_2 emission is found 4.5% (286 g/kWh) and 4% (253.3 g/kWh) at WOT and PT operating conditions, respectively. The minimum CO_2 concentration is detected at 24^o bTDC and found 2.44% (155 g/kWh) and 1.7% (106.6 g/kWh) respectively for the WOT and PT operating condition of the engine. The minimum CO emission at 40^o bTDC signifies an enhanced combustion process, but is gained with maximum CO_2 emission at this condition.

Similarly, the effect of progressive IA on the HC and NO_X emission of the methane fueled SI engine at WOT and PT conditions is depicted in **Fig. 4. 16**. Rich air-fuel ratio with insufficient oxygen promotes the incomplete combustion of fuel as a misfire produces the unburnt HC emission (Heywood, 1988). The progressive IA increased the cylinder pressure and leads to a greater mass fraction of HC trapped in the piston crevices. However, the drop in-cylinder pressure during the expansion phase draws in the trapped unburnt HC from the crevice volume and creates a reverse blow followed by flame quenching. This process leaves the unreacted fuel particles in the exhaust and the mass fraction of these particles is greater with progressive advanced IT (Türköz et al., 2014). Further, the lower exhaust gas temperature at advanced ITs does not oxidase the unburnt HC from the crevices. Hence, with the progressive advance of IT, the HC concentration is increased in exhaust emission. The HC concentration in the exhaust emission is increased from 12 to 74 ppm (0.02 to 0.15 g/kWh) with progressive IA at WOT and found 65 ppm (0.13 g/kWh) at 40^o bTDC. Whereas, at PT

operating condition, the HC concentration is increased from 20 to 92 ppm (0.04 to 0.18 g/kWh) with progressive IA and found 80 ppm (0.16 g/kWh) at 40° bTDC. The lower HC concentration at WOT is because of the enhanced volumetric efficiency which triggered a superior combustion process compared to the PT condition. Similarly, the NOx emission is strongly related to lean fuel mixture with high charge cylinder temperature. NO_X is mainly formed due to higher MGT through the oxidation of nitrogen present in the inducted air-fuel mixture and is mainly composed of NO and a small amount of NO_2. The MGT in the present case is enhanced with the progressive IA up to 40° bTDC and dropped at further advanced ITs. Hence, the maximum NO_X concentration in the exhaust emission is found 966 ppm (6.41 g/kWh) and 703 ppm (4.67 g/kWh, respectively for the WOT and PT condition of the engine at the MBT IT. The concentration of logged pollutants is presented in **Table 4. 7** and found within the limited range for the MBT IT as specified in BS-VI.

Table 4. 7: CO, HC and NOx concentration in brake specific basis at different IT

IT (° CA bTDC)	CO (g/kWh)			HC (g/kWh)		NO_x (g/kWh)		HC+ NO_x
	WOT	PT	*Std.	WOT	PT	WOT	PT	*Std.
24	9.91	25.35		0.02	0.04	2.23	1.60	
26	8.91	20.43		0.04	0.06	2.58	2.00	
28	7.04	18.96		0.05	0.07	3.11	2.36	
30	5.93	17.45		0.07	0.09	3.57	2.60	
32	4.81	13.83	≤ 250#	0.09	0.11	4.07	3.03	≤ 12#
34	3.84	12.03	≤ 3.5$	0.10	0.13	4.43	3.27	≤ 7.5$
36	3.30	10.59		0.12	0.14	5.14	3.75	
38	2.62	8.91		0.13	0.15	5.80	4.05	
40	**1.83**	**7.11**		**0.13**	**0.16**	**6.41**	**4.67**	
42	2.44	8.19		0.15	0.18	6.03	4.59	

*Emission standard set by the Govt. of India for the #genset run on petrol and natural gas (NG) or petrol and liquid petroleum gas (LPG) and $ genset run on dedicated natural gas (NG) or liquid petroleum gas (LPG) as mentioned in GSR 281(E) (The Gazette of India, 2016)

4.3.2 Assessment of the Optimum IT for the Biogas Fueled VCR SI Engine

The raw biogas (CH_4:55.6%, CO_2:42.3%, N_2:2.1%) having physicochemical properties mentioned in **Table 3.1** of ***Chapter 3*** is used as the test fuel for the present investigation. The VCR SI engine is fueled with raw biogas and operated with WOT and PT conditions at CR 10 and 1650 rpm. Operating ERs (ϕ) are almost maintained constant at ~0.81 and ~0.83, respectively for the WOT and PT operating conditions of the engine. The procedure of optimum IT assessment recommends maintaining the rest operating parameters of the engine constant during the evaluation process. Hence, the fuel composition, operating CR, ER, and engine speed are maintained constant. The IT is progressively advanced from 33^o to 47^o bTDC in an interval of 2^o CA both in WOT and PT operating conditions of the engine. The corresponding performance, combustion and emission characteristics of the engine are assessed both for WOT and PT conditions by following the standard guidelines as specified by the BIS in IS 10000: Part 6, 7 and 8. Based on the engine performance the optimum IT of the engine is evaluated. However, the accessed IT may not be optimum for the operating speed range (1400 -1700 rpm) of the engine. Hence, the process of optimum IT assessment is also repeated for the operating speed range of the engine. Each set of experiments is repeated thrice and averages of these values are considered for the evaluation of different engine parameters. The performance and combustion parameters of the engine are evaluated from *Eqs. D1-D11* and *D12-D2* respectively, as described in ***Appendix D***. Further, the exhaust gas analyzer (AVL Diagas 444N) is used to quantify the exhaust emissions from the engine. The MBTs of the biogas fueled engine for the operating speed range at CR 10 are recommended below based on the detailed analysis of performance, combustion and emission characteristics of the engine for both WOT and PT conditions.

Performance analysis

This section evaluates the effect of IT on the performance of the biogas operated SI engine both for the WOT and PT operating conditions at CR 10. The performance parameters, such as BT, BP, BSFC, BTE and VE of the biogas fueled engine are evaluated respectively from the *Eqs. D1, D2, D3, D5* and *D6* of ***Appendix D.*** At the preliminary stage of investigation, the experiments are conducted for a constant engine speed of 1650 rpm and an equivalence

ratio (ϕ) of ~0.81 and ~0.83, respectively at WOT and PT conditions. Whereas, in the later stage of the investigation, the effect on engine speed on the optimum IT (MBT) of the biogas fueled engine is also taken in to consideration. At CR 10 and 1650 rpm, the biogas fueled engine is found operative in the limiting IA range of 23^o to 55^o CA bTDC. Beyond these limits, there is onset on knocking and misfire resulting in unstable engine operation. However, the present analysis only discusses the effect of IT within the range of 33^o to 47^o CA bTDC. The overall uncertainties associated performance parameter of the biogas fueled SI engine at CR 10 is mentioned in **Table 4. 2**.

Fig. 4. 17 shows the effect of IA on the BT and BP of the biogas fueled SI engine at CR 10 and 1650 rpm for both WOT and PT conditions. As the IT is progressively advanced from the TDC (360^o CA), the induced BT and BP of the engine followed an increasing trend up to 45^o CA bTDC for both WOT and PT conditions. Further advancement of IT beyond 45^o CA bTDC declined the induced BT and BP of the engine at CR 10. This happening may be attributed due to the increasing flame propagation speed of biogas with progressive IA which declined beyond 45^o CA bTDC. The faster flame propagation speed reduced the combustion duration which enhance the peak pressure and net heat release rate to produce maximum expansion work compared to the cases of IA (Sadiq Al-Baghdadi, 2004). On the other hand, the over advanced IT increases the network transfer during the compression stroke. Hence both the BT and BP are dropped off at the IA beyond 45^o CA bTDC. The optimum timing, which gives the maximum BT, is the MBT timing and is 45^o bTDC for both throttling cases. This is the MBT timing both in WOT and PT condition. At this optimum condition, the maximum BT and BP at WOT are 15.4 N-m and 2.6 kW, respectively. The corresponding values for PT condition are 9.2 N-m and 1.6 kW, respectively. Similar observations are also reported by researchers (Huang and Crookes, 1998a; Crookes, 2006; Jatana et al., 2014) towards the range of optimal IT of biogas engines operating at CR in between 8:1 to 15:1. The engine speed also plays a vital role towards the optimization of IT at any operating CR of the biogas fueled SI engine. The effect of engine speed on the MBT of the biogas fueled engine is depicted in **Fig. 4. 18** both at WOT and PT condition. As noticed, the optimum IT is advanced with increasing engine speed both at WOT and PT condition at CR 10. This happening may be attributed due reduced time interval for complete combustion followed by unstable combustion at higher

engine speed. Hence to extend the reaction time in during the combustion process of the air-biogas mixture, the IT is advanced optimally. Similar observations are also noticed in open literature (Sadiq Al-Baghdadi, 2004) for fuels like CNG and hydrogen. However, the observed fluctuation of MBT is not much significant in the present case due to shorter span of engine speed. The MBT is varied in between 43° to 46° CA bTDC over the speed range of 1400 to 1700 rpm. Hence for the current operating speed range (1400-1700 rpm), 45° CA bTDC is assumed as the optimum IT for both WOT and PT conditions.

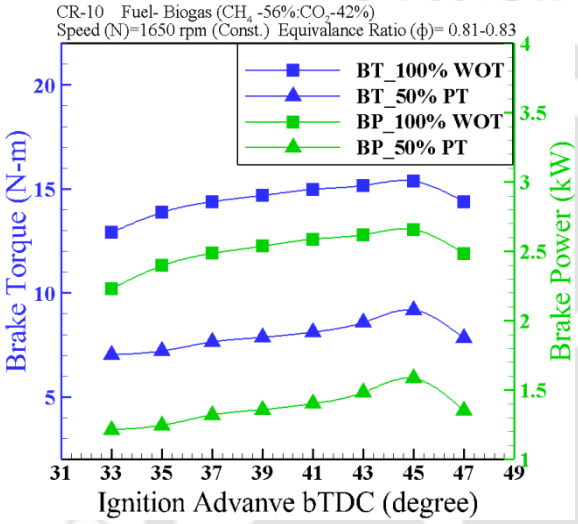

Fig. 4. 17: Effect of IA on the BT and BP of the biogas fueled VCR SI engine at CR 10

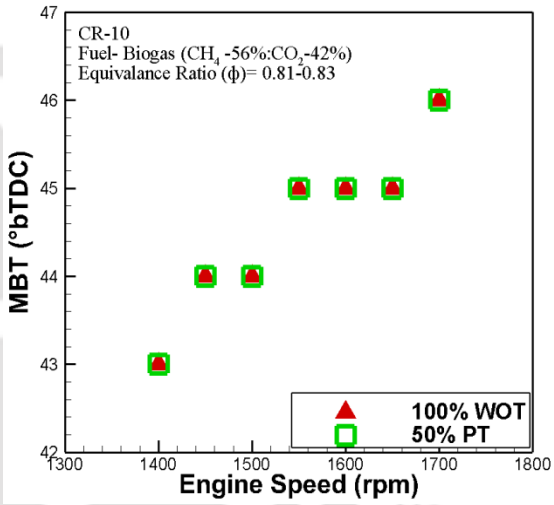

Fig. 4. 18: Effect of engine speed on the MBTs of the biogas fueled VCR SI engine at CR 10

The effect of IA on the BSFC and BTE of the biogas operated SI engine are shown in **Fig. 4. 19** and **Fig. 4. 20**, respectively at CR 10 for both WOT and PT conditions. In line with the fact that the maximum BT and BP are observed at 45° CA bTDC for the biogas operated engine at CR 10, the minimum BSFC and maximum BTE are also observed at the same IA for both WOT and PT operating condition. The BSFC of the engine falls consistently with progressive IA up to 45° CA bTDC and rises with further advance in IA. Whereas, the BTE increases with progressive IA up to 45° CA bTDC and drops off with further advance IT. The minimum BSFC are noticed 0.814 and 0.909 kg/kW-h, respectively at WOT and PT conditions while the maximum BTE at same throttle conditions, are observed 26% and 23.2%, respectively. BSFC and BTE are functions of mass flow rate of the fuel consumed and BP. For a particular throttle

operating condition, the mass flow rate of fuel consumed is almost constant (2.16 kg/h and 1.44 kg/h at WOT and PT condition, respectively) even for different IA. Because of which, the BSFC and BTE are the only function of BP. At the point of optimum IA (45° CA bTDC), the MBT, BP and BTE are found maximum with minimum BSFC. Since the conventional SI engine is operated with raw biogas as a replacement to gasoline, it is desired to study the effect of IA on the volumetric efficiency and equivalence ratio. It is evident from **Fig. 4. 20** that, the volumetric efficiency of the engine at WOT (39 %) and PT (25 %) conditions are almost remained constant irrespective of the operating IT. It must be noted that the operating ER is retained in between 0.81-0.82 and 0.83-0.84 at WOT and PT condition of the engine. However, the average maintained ERs at WOT and PT conditions are 0.82 and 0.83, respectively at the optimized IA (45° CA bTDC).

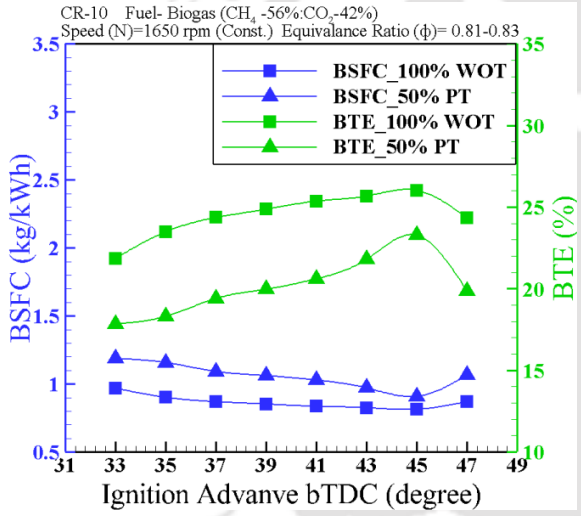

Fig. 4. 19: Effect of IA on the BSFC and BTE of the biogas fueled VCR SI engine at CR 10

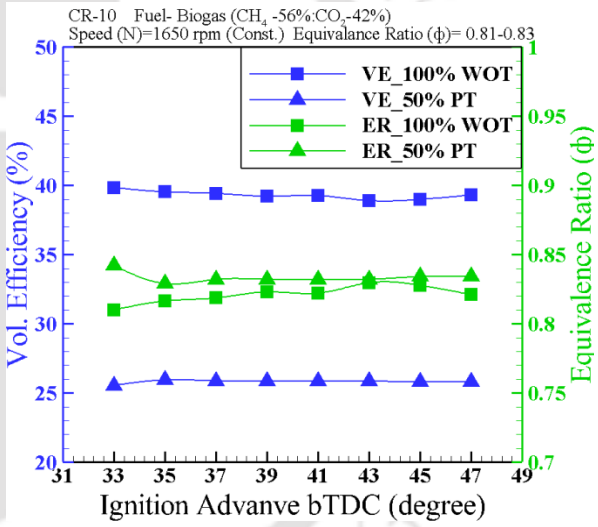

Fig. 4. 20: Effect of IA on the VE and ER of the biogas fueled VCR SI engine at CR 10

Combustion analysis

Biogas as a fuel has extremely low energy density on the volume basis on account of its higher CO_2 content. The CO_2 content reduces the calorific value, flame velocity and flammability limit of biogas but enables the engine to operate with higher CR. The combustion process is completely dependent on the flame propagation, which ultimately depends on the

flame speed (0.25 m/s) and auto ignition temperature (650^{o}C). Because of these reasons the IT of a gasoline fueled SI engine needs to be advanced when fueled with biogas. If the ignition is too early, the peak pressure may arise before the TDC and the compression work transfer increases. If the ignition is too late the peak pressure will arise much later in the expansion stroke, which may reduce the expansion work due to incomplete combustion (Mehrnoosh et al., 2012). Hence, before identifying the MBT for the fuel, the aspects mentioned above have been thoroughly investigated. The cylinder pressure (P) and crank angle (θ) data are captured for 50 consecutive cycles for each experiment. The combustion parameters viz. P-V, NHRR, MFB and MGT are evaluated from the average P-θ data by following the *Eqs. D12-D25* of ***Appendix D*** as referred in the open literature (Heywood, 1988; Stone, 2012). The overall uncertainties associated combustion parameter of the biogas fueled SI engine at CR 10 is mentioned in **Table 4. 2**.

Fig. 4. 21 and **Fig. 4. 22** describes the effect of IA on the average cylinder pressure of the biogas fueled SI engine respectively for the WOT and PT operating conditions at CR 10. The operating CR (10), engine speed (1650) and ER (~0.82 at WOT and ~0.83 at PT condition) are maintained almost constant while operating the engine at different ITs. A noticeable rise in the PCPs are observed with progressive advance of the ITs before the TDC both in WOT and PT conditions. As the IA is progressed bTDC, the PCP increases significantly and shifts the LPP close to the TDC until 45^{o} CA bTDC irrespective of the operating condition. Whereas, the observed PCP is dropped and shifted away from the TDC at 47^{o} CA bTDC irrespective of the throttle position. The above happenings may be attributed due to the accelerated combustion process which enhanced the in cylinder gas temperature and led to higher energy release rate followed by rise in in-cylinder pressure with progressive IA (Papagiannakis and Zannis, 2013). As noticed, the PCP is increased from 17.2 to 23.2 bar and the LPP is shifted from 382^{o} to 376^{o} CA, as the IT is advanced from 33^{o} to 45^{o} CA bTDC at WOT condition. Whereas the PCP is suddenly dropped to 22.2 bar and the LPP is shifted to 377^{o} CA when the IT is advanced further to 47^{o} CA bTDC. Similar happenings are also noticed at PT operating condition of the engine and depicted in **Table 4. 8**.

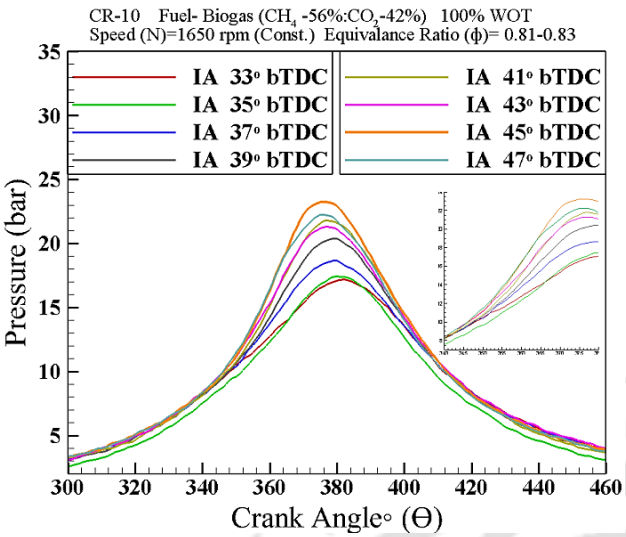

Fig. 4. 21: Effect of IA on the average cylinder pressure of the biogas fueled engine at CR 10 and WOT

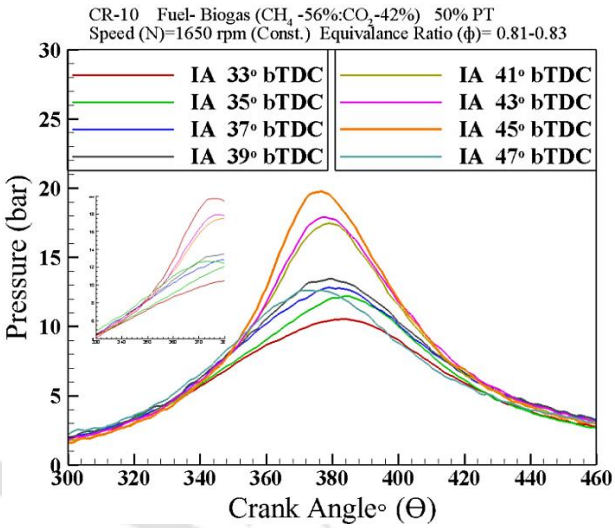

Fig. 4. 22: Effect of IA on the average cylinder pressure of the biogas fueled engine at CR 10 and PT

Table 4. 8: Effect of IT on the PCP and LPP of the biogas fueled SI engine at CR 10

IT (^{o} CA bTDC)	WOT		PT	
	PCP (bar)	LPP (^{o} CA)	PCP (bar)	LPP (^{o} CA)
33	17.2	382	10. 6	384
35	17.4	380	12.2	384
37	18.6	379	12.8	380
39	20.4	379	13.4	379
41	21.3	377	17.4	379
43	21.8	377	17.9	377
45	23.2	376	19.7	376
47	22.2	377	12.6	377

The above occurrence may be due to the over advanced IT, which increased the compression work transfer and decreased PCP and cylinder gas temperature at this condition (Jaramillo et al., 2018). It is also observed that, irrespective of the throttle position (**Fig. 4. 21 - Fig. 4. 22**), the slope of the pressure gradients slowly rises with progressive IA up to 45^o CA bTDC and declines at 47^o CA bTDC. The above observation of pressure gradients, PCPs and

LPPs clearly justifies the MBT proposed in the performance analysis section. The P-V curve analysis also gives the clear picture of maximum work output at different IA and helps to identify the optimum IT for both WOT and PT conditions. As shown in **Fig. 4. 23** and **Fig. 4. 24**, the area under the *P-V* curve gradually increases with progressive IA up to 45^{o} CA bTDC and declines with further advancement of IT. The maximum area under the *P-V* curve is observed at 45^{o} CA bTDC and found 2777.2 and 2600.4 respectively for the WOT and PT operating condition of the engine. The above happening may be due to the faster flame propagation (shorter combustion duration), resulting in improved thermal efficiency and power output at 45^{o}CA bTDC. Hence, 45^{o}CA bTDC is considered as the optimum IT for both WOT and PT conditions and justifies the proposed MBT in the performance analysis section.

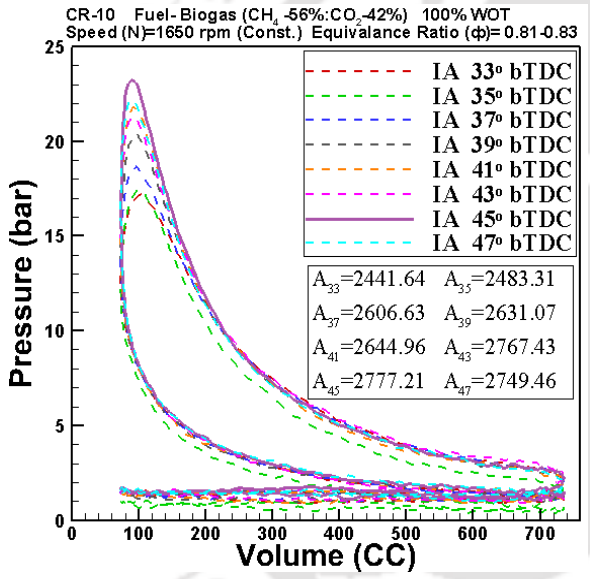

Fig. 4. 23: Effect of IA on the area under *P-V* curve at CR 10 and WOT

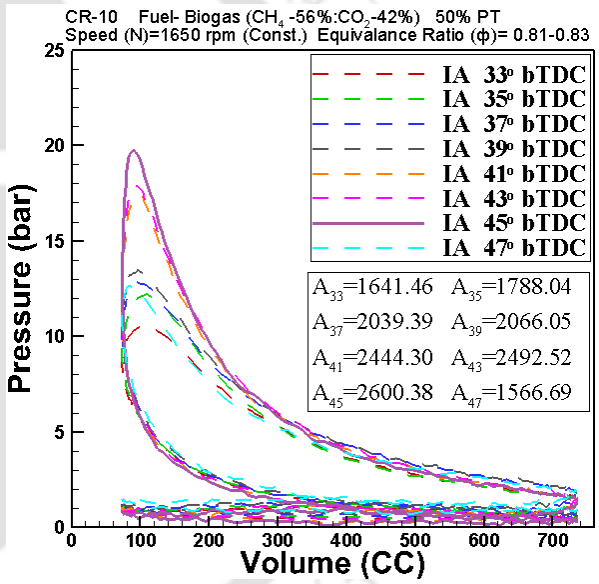

Fig. 4. 24: Effect of IA on the area under *P-V* curve at CR 10 and WOT

The MFB for the biogas fueled SI engine is evaluated from the average pressure data by following method proposed for the burn rate analysis by Rassweiler and Withrow (Rassweiler and Withrow, 1938) as mentioned in *Eqs. D17-D19* of ***Appendix D*. Fig. 4. 25** and **Fig. 4. 26** describes the effect of IA on the MFB of the biogas fueled engine at CR 10 for both WOT and PT operating conditions. The RBA is designated as '$\Delta\theta_b$' for the present analysis and defined as the crank angle interval between the end of flame development (MFB 10%) and end of flame

propagation (90% MFB). As observed form the **Fig. 4. 25** and **Fig. 4. 26**, the flame development

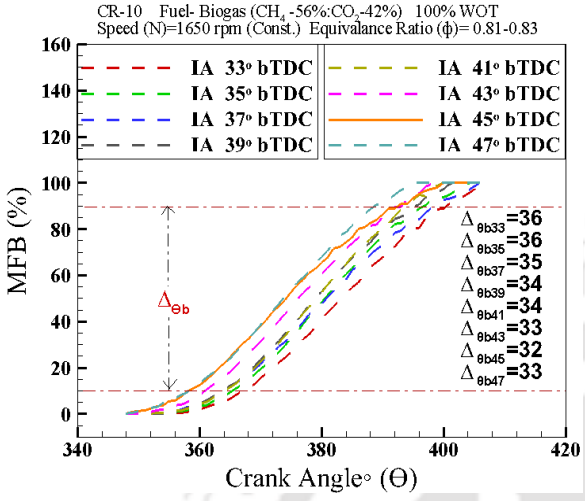

Fig. 4. 25: Effect of IA on the MFB of the biogas fueled engine at CR 10 and WOT

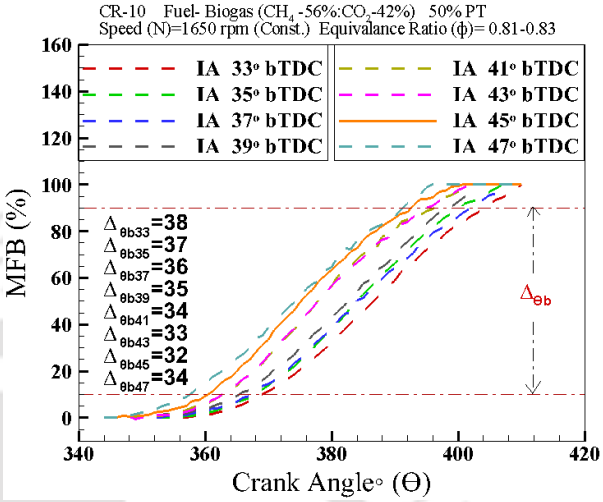

Fig. 4. 26: Effect of IA on the MFB of the biogas fueled engine at CR 10 and PT

and the combustion event are advanced progressively with the advancement of the IT bTDC for both throttle conditions. Since the complete flame development (MFB 10%) at the proposed MBT (45° CA bTDC) is observed before the piston reaches to TDC, the compressed fresh fuel-air charges are pushed towards the developed flame front. As a result, the flame front propagation rate is increased and reduced the combustion duration. However, with further advanced IT, the in-cylinder pressure and temperature drops, resulting in higher cyclic variation in flame development and propagation stage during the combustion process. Hence beyond the proposed MBT, the flame propagation rate is decreased by extending the combustion duration. The magnitude of RBA is also dropped with progressive advancement of the IT bTDC and observed minimum at an IT of 45° CA bTDC for both throttle operating conditions of the biogas fueled engine at CR 10. However, further advancement of IT bTDC (47° CA bTDC) extended the RBA for both throttle condition of the engine. Similar observations are also documented by researcher (Ma et al., 2012; Jaramillo et al., 2018) for biogas and hydrogen operated SI engines. The RBAs ($\Delta_{\theta b}$) at the IA of 45° CA bTDC are reported 32° CA for both WOT and PT throttle operating condition of the biogas engine at CR 10 and 1650 rpm. Since the reported RBA is found minimum at 45° CA bTDC irrespective of

the operating throttle condition, it clearly validate the claim of optimum IT made in the performance analysis section and justifies the maximum BTE obtained by the engine at this condition.

Fig. 4. 27 and **Fig. 4. 28** describe the effect of IA on the NHRRs of the biogas fueled SI engine. The NHRR is evaluated from the 1st law analysis of combustion chamber (CC) by assuming a single zone model where the product and reactants are thoroughly mixed and there is no mass transfer across the CV. The heat release analysis evaluated the data on differential basis from *Eq. D16* of ***Appendix D.*** This leads to fluctuation in the computed results at the lower pressure zones where the discretization is the larger proportion of the signal.

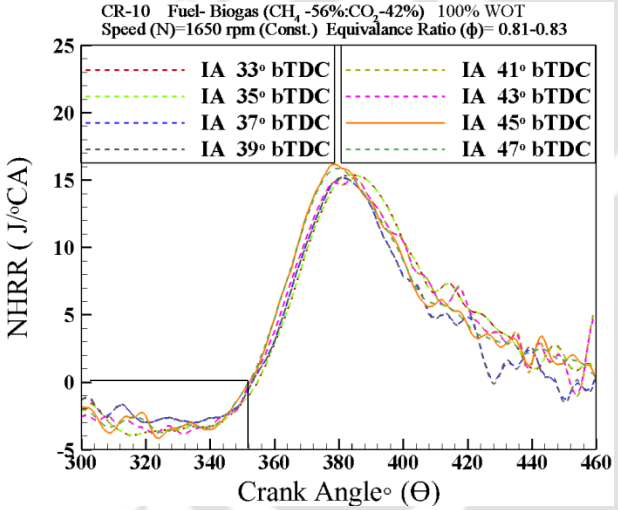

Fig. 4. 27: Effect of IA on the NHRR of the biogas fueled engine at CR 10 and WOT condition

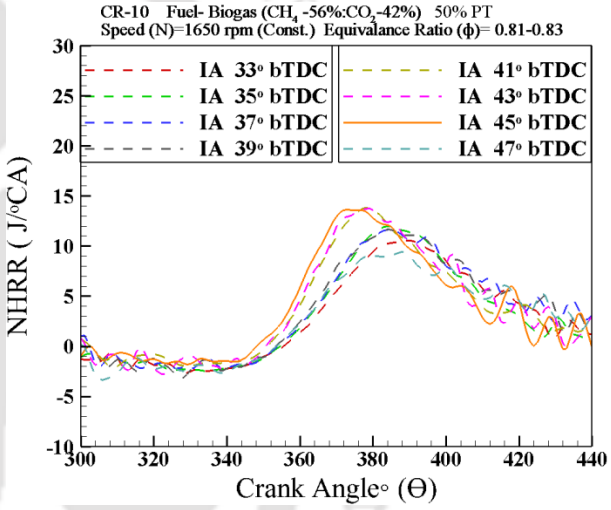

Fig. 4. 28: Effect of IA on the NHRR of the biogas fueled engine at CR 10 and PT condition

The negative NHRR shown in **Fig. 4. 27** and **Fig. 4. 28** indicates the heat transfer to the cylinder wall and the ignition should be close to the minimum NHRR. This may be due to the lower initial rate of combustion (lower MFB) and addition of negative value of heat transfer after the completion of combustion process. The NHRR is found improving with progressive advance of IT up to the MBT timing and drops off with further IA. The PNHRR at 45°CA bTDC is found 16.9 and 13.6 J/°CA, respectively for both WOT and PT condition of the engine and observed maximum over the reported range of IT in **Table 4. 9**. This happening may be

attributed due to the early flame development, propagation rate and maximum energy conversion efficiency at 45°CA bTDC MBT timing (Kemal and Sayin, 2014). However, with advanced IT (beyond 45°CA bTDC), the NHRR is dropped due to the increased compression work and rapid conversion of the heat energy to accommodate the negative work done before the TDC. The PNHRRs and the LPNHRRs are listed for different operating ITs for both WOT and PT conditions of the engine in **Table 4. 9**. As observed the LPNHRR shifts closer to the TDC with the progressive advance of IT bTDC at both WOT and PT conditions. Moreover, the maximum NHRRs are observed at 45° bTDC and found 16.9 and 13.6 J/ °CA at 378 and 374 °CA, respectively for the WOT and PT operating conditions of the engine.

Table 4. 9: Effect of IT on the PNHRR and LPNHRR of the biogas fueled SI engine at CR 10

IT (° CA bTDC)	WOT		PT	
	PNHRR (J/°CA)	LPNHRR (° CA)	PNHRR(J/°CA)	LPNHRR (° CA)
33	15.4	388	10.8	390
35	15.6	386	11.5	385
37	15.8	383	11.6	383
39	16.1	381	11.8	383
41	16.4	379	13.4	379
43	16.8	379	13.5	376
45	16.9	378	13.6	374
47	15.6	383	9.5	384

Fig. 4. 29 and **Fig. 4. 30** illustrate the effect of IA on the MGT of the biogas fueled SI engine, respectively at WOT and PT conditions. The MGT is evaluated from ***Eq. D20*** of ***Appendix D*** assuming a single zone combustion model. The characteristic gas constant 'R' is evaluated from the correlation R= 0.287+(0.020 Φ (Stone, 2012; Kriger and Borman 1986). The MGTs and its slopes are constantly increasing with the progressive advance of IT up to 45°CA bTDC. However, the peak MGT and the slope of the MGT curve are dropped at the IA of 47° bTDC. The PMGTs and LPMGTs at different operating IA are depicted in **Table 4. 10**. Further, it is observed that the LPMGT shifts towards the TDC with the IA up to 45° CA bTDC

and shift away at 47º bTDC. Moreover, the LPMGT appears consequently after LPCP and LPNHRR for both WOT and PT conditions. The PMGT at WOT and PT conditions are 941 K at 394º CA and 656 K at 409ºCA, respectively. The above happening is attributed due to the trend of PCP and NHHR, which progressively improved the MGT up to the IA of 45º CA bTDC.

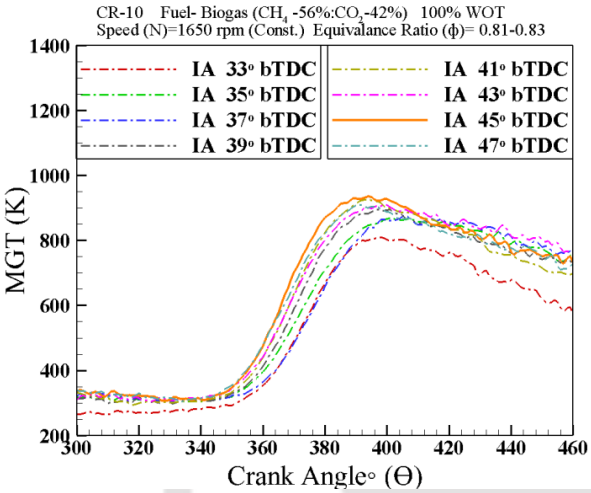

Fig. 4. 29: Effect of IA on the MGT of the biogas fueled engine at CR 10 and WOT condition

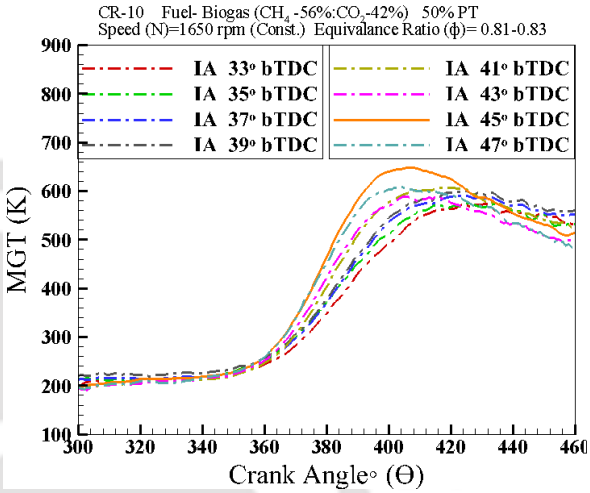

Fig. 4. 30: Effect of IA on the MGT of the biogas fueled engine at CR 10 and PT condition

Table 4. 10: Effect of IT on the PMGTs and LPMGTs at CR 10

IT (º bTDC)	WOT		PT	
	PMGT (K)	LPMGT (º CA)	PMGT (K)	LPMGT (º CA)
33	812.6	398	579.5	434
35	875	409	583.5	433
37	886.3	406	591.3	429
39	899.8	399	598.6	421
41	913.6	397	605.4	426
43	931.4	394	617.1	413
45	941.8	394	656.1	409
47	912.7	392	610.7	404

Emission analysis

The concentrations of the CO, CO_2, HC and NO_x in the exhaust emission from the biogas operated SI engine are recoded with an AVL DIAGAS 444N gas analyzer. The operating procedure and specification of the gas analyzer are described respectively in *section 3.3.2.6* of *Chapter 3 and* **Table B2** of ***Appendix B.*** The CO and CO_2 concentrations are recorded in percentage of volume (vol %) on dry basis, whereas the HC and NO_x concentrations are recoded in PPM on dry basis. The recoded concentrations are converted to brake-specific basis (g/kW-h) following *Eq. 4.1* (Heseding and Daskalopoulos, 2006; Pilusa et al., 2012; Ağbulut et al., 2019) and compared with the established emission standard standards (BS-VI and Euro 6) (The Gazette of India, 2016) and reported in **Table 4. 11**. The sample conversion procedure of vol %, and ppm to brake-specific basis (g/kWh) is explained in detailed in ***Appendix F*****. Fig. 4. 31** depicts the effect of IA on the CO and CO_2 emission of the methane fueled VCR SI engine at CR 10 both at WOT and PT condition. Irrespective of the operating throttle, the CO concentration in the exhaust emission is decreasing with progressive IA but, the trend deviates after the point of MBT timing.

The least CO emission is observed at 45^o bTDC and recoded 0.035% (1.3 g/kWh) and 0.039% (1.4 g/kWh) respectively at WOT and PT operating conditions of the engine. Whereas the maximum CO emission is reported at 33^o bTDC and found 0.08% (2.87 g/kWh) and 0.09% (3.26 g/kWh), respectively at the WOT and PT operating conditions of the engine. Incomplete combustion resulted either due to poor mixing or fuel rich mixture is the typical origin of CO emission. However, the in cylinder temperature is also equally responsible for the formation and control the rate of oxidization of CO (Stone, 2012). In the present case, the engine is operating with lean equivalence ratio in the range of 0.82 to 0.83 for both WOT and PT condition. Hence, the in-cylinder temperature is only responsible for the formation of CO in the present investigation. Advanced IT initiated the combustion earlier relative to the TDC and reduced the combustion duration due to the faster flame propagation rate. As a result, the MGT followed an increasing trend with progressive IA up to the MBT timing and favors the CO formation mechanism. Whereas, at the same moment, the progressive IA also increased the time interval of expansion phase for which highest temperature (average at WOT $\geq$ 730 K and

average at PT ≥520 K) persists in the engine cylinder. Hence it positively affects the CO oxidization rate, which reduced the CO level and increased the CO_2 level at advanced ITs (Papagiannakis and Zannis, 2013). Hence, the above mentioned justifies the CO and CO_2 emission pattern with respect to the advanced IT. Irrespective of the operating throttle, the CO_2 content in exhaust emission is found increasing with progressive IA and reported maximum at CA 45^o bTDC. This also signifies complete combustion at this point of IA. The maximum CO_2 emission reported at WOT and PT operating conditions are 6.3 % (398 g/kWh) and 4.9 % (314 g/kWh), respectively. However, the minimum CO_2 concentration is detected at 33^o bTDC and found 3.5 % (220 g/kWh) and 1.9% (119 g/kWh) respectively for the WOT and PT operating condition of the engine. The minimum CO emission at 45^o bTDC signifies an enhanced combustion process, but is gained with maximum CO_2 emission at this condition.

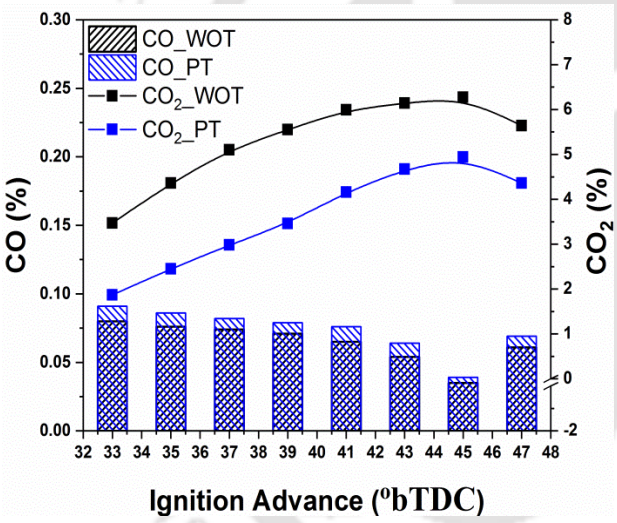

Fig. 4. 31: Effect of IA on the CO and CO2 emission of the biogas fueled engine at CR 10 and WOT condition

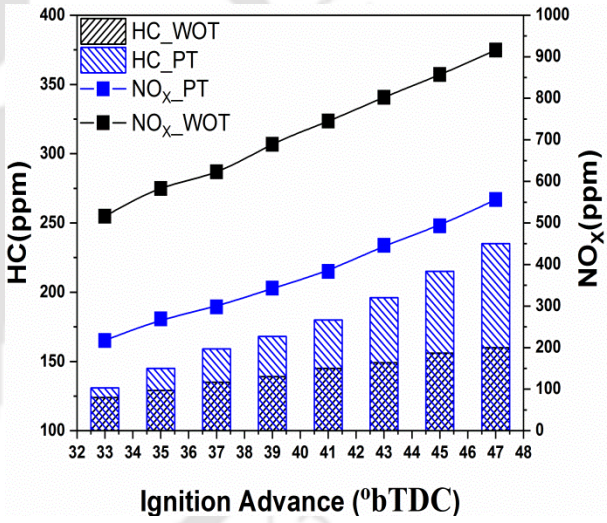

Fig. 4. 32: Effect of IA on the HC and NOx emission of the biogas fueled engine at CR 10 and PT condition

Similarly, the effect of IA on the HC and NO_x concentration of the biogas fueled SI engine at WOT and PT operating conditions is depicted in **Fig. 4. 32**. As observed, irrespective of the operating throttle, the concentration HC in the exhaust emission of the biogas fueled SI engine increases constantly with progressive IA and found maximum at 47^o bTDC. The concentration HC in exhaust emission is increased from 124 ppm (0.25 g/kWh) to 160 ppm (0.32 g/kWh) with progressive IA at WOT. Whereas in PT operating condition, the

concentration of HC is increased from 131 ppm (0.26 g/kWh) to 235ppm (0.47 g/kWh) with progressive advance of IT from 33 to 47^{o} bTDC. Generally, the advanced IT leads to reduced THC and increased NOx emission for high energy density fuels such as NG and gasoline (Min et al., 2002; Park et al., 2011). However, in the present case the HC content in the exhaust emission is increasing with progressive advance of IT from 33 to 47^{o} bTDC. This happening may be attributed because of the grater mass of HC trapped in piston crevices due to increased cylinder pressure at advanced ITs. The trapped HC are drawn to the combustion space during the later stage of expansion phase and creates a reverse blow followed by flame quenching. The above happening leaves the unreacted HC particles in the exhaust. However, the mass fraction of these particles increases with progressive advance of IT. Further, the lower exhaust gas temperature at advanced ITs does not oxidase the unburnt HC from the crevices. Hence, with the progressive advance of IT, the HC concentration is increased in exhaust emission. Similar observation are also reported in open literatures with other alternative fuels (Etahnol, E-85) under variable ignition timing (Türköz et al., 2014). However, The HC emission at MBT timing is found 156 ppm (0.31 g/kWh) at WOT and 215 ppm (0.43 g/kWh) at PT operating condition of the engine and observed within the acceptable limit of the established emission standard standards. Further, the lower HC concentration at WOT is because of the enhanced volumetric efficiency which triggered a superior combustion process compared to the PT condition.

The NOx emission is strongly related to lean fuel mixture with high charge cylinder temperature. NO_X is mainly formed due to higher MGT through the oxidation of nitrogen present in the inducted air-fuel mixture and is mainly composed of NO and a small amount of NO_2. The NOx emission in the present case is increasing with progressive advance of IT and found 875 ppm (5.7 g/kWh) and 493 ppm (3.3 g/kWh), respectively for WOT and PT operating condition of the engine at the MBT timing. Similar observations are also reported in (Midkiff et al., 2001; Porpatham et al., 2012; Türköz et al., 2014; Ravi et al., 2017) open literature and is also verified with the data published by (Midkiff et al., 2001; Porpatham et al., 2012; Ravi et al., 2017). The concentration of logged pollutants is presented in **Table 4. 11** and found within the limited range for the MBT IT as specified in BS-VI.

Table 4. 11: CO, HC and NOx concentration in brake specific basis at different IT

IT (^{o} bTDC)	CO (g/kWh)			HC (g/kWh)		NO_x (g/kWh)		HC+ NO_x
	WOT	PT	*Std.	WOT	PT	WOT	PT	*Std.
33	2.87	3.27		0.25	0.26	3.42	1.44	
35	2.73	3.09		0.26	0.29	3.87	1.79	
37	2.66	2.94		0.27	0.32	4.13	1.98	
39	2.55	2.84	$\leq 250^{\#}$	0.28	0.34	4.57	2.28	
41	2.33	2.73	$\leq 3.5^{\$}$	0.29	0.36	4.94	2.48	$\leq 12^{\#}$
43	1.94	2.30		0.30	0.39	5.32	2.96	$\leq 7.5^{\$}$
45	1.26	1.40		0.31	0.43	5.69	3.27	
47	2.19	2.48		0.32	0.47	6.08	3.69	

*Emission standard set by the Govt. of India for the $^{\#}$genset run on petrol and natural gas (NG) or petrol and liquid petroleum gas (LPG) and $^{\$}$ genset run on dedicated natural gas (NG) or liquid petroleum gas (LPG) as mentioned in GSR 281(E) (The Gazette of India, 2016)

4.4 Comparative Assessment of the VCR SI Engine (*Engine 2*)

The motive behind this investigation is to explore the short fall of the VCR SI research engine (*Engine 2*) for biogas operation at its original configuration (CR 10). The original configuration of the engine refers to the technical specification (**Table C1** of ***Appendix C***) and maximum achievable operating CR (10:1) designed by the manufacturer for gasoline operation. As described in *Section 4 and, Sections 3.3.1 and 3.3.4 of* ***Chapter 3***, the VCR SI research engine is successfully retrofitted for the gaseous fuel application by replacing the liquid fuel induction mechanism. Hence, in the present investigation, the ECU controlled, single cylinder, SI engine is operated at WOT and PT conditions with the test fuels (gasoline, methane and biogas) at CR 10 over the speed range of 1450-1700 rpm. The operating ITs are set to the MBT conditions (optimum IT) for each operating fuels as recommended in *Section 4.2 and 4.3*. The operating ITs are set to 28^o CA bTDC, 40^o CA bTDC and 45^o CA bTDC,

respectively for the gasoline, methane and biogas operation of the SI engine. The baseline investigation is performed with gasoline and the subsequent analyses are carried with methane and biogas respectively. The basic objective of the investigation is to highlight the de-rating of engine power, deterioration in the fuel conversion efficiency and emission quality of the biogas fueled SI engine at CR 10 through a comparative assessment with gasoline and methane operated SI engine at the same operating CR. The corresponding performance (BT, BP, BSFC, BTE, VE), combustion (P-Θ, NHRR, MFB, MGT, COV) and emission (CO, CO_2, HC, NO_x) characteristics of the engine are assessed for both WOT and PT condition with the respective test fuels. The associated experimental matrix and uncertainty analysis are presented in **Table 4. 1** and **Table 4. 2**, respectively. Each set of experiments is repeated thrice to ensure the correctness of the capture data. The average of these data is considered for the evaluation of different engine parameters. The performance and combustion parameters of the engine are evaluated from *Eqs. D1-D11* and *D12-D25* as described in ***Appendix D***. Further, the exhaust gas analyzer (AVL Diagas 444N) is used to quantify the exhaust emissions from the engine.

4.4.1 Performance analysis

Fig. 4. 33 and **Fig. 4. 34**, depict the comparative assessment on the BT and BP output of the VCR SI research engine fueled with gasoline, methane and biogas at CR 10 for WOT and PT conditions, respectively. The effect of operating speed on the produced BT and BP of the engine is also explained here in **Fig. 4. 33** and **Fig. 4. 34** for the test fuels taken into consideration. As observed, the induced BT and BP followed a decreasing trend along with the progressive advancement of the engine speed. The maximum BT for the gasoline, methane and biogas operated SI engine are recorded 22.3, 19.5 and 19.1 N-m, respectively at 1650 rpm and WOT condition. The corresponding values in PT condition at the same speed are noticed 16.5, 12 and 11.7 N-m, respectively for the gasoline, methane and biogas operated SI engine. Similarly, the maximum BP output at WOT and PT condition are observed at 1450 rpm and recoded 3.4 and 2.5 kW for gasoline operation, 3.0 and 1.8 kW for methane operation and 2.8 and 1.7 kW for biogas operation. The average BP output of the methane fueled engine is dropped by 13.5% and 29% respectively at WOT and PT condition in comparison to the gasoline operation. Similarly, the average reduction in the BP of the biogas operated SI engine

in comparison to the gasoline operation are noticed 17.5 % and 37.5 % respectively, at the WOT and PT operations. The difference in BP among the throttle positions are due to the lower volumetric efficiency and higher fuel–air equivalence ratio maintained in PT operating condition of the engine. It is also observed that, irrespective of the operating fuel, there is reduction in the BT and BP at higher operating speed of the engine. The higher engine speed is the result of reduced dynamometer load applied on the crank shaft, the BT and BP followed and increasing trend with the decreasing speed of the engine. The BT and BP of the biogas fueled SI engine are observed lower than that of methane and gasoline operated engine at same operating CR throughout the operating speed range at any throttle position. This may be

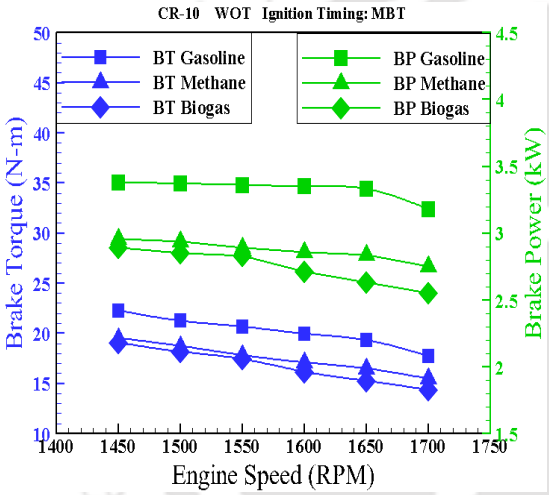

Fig. 4. 33: BT and BP variation with engine speed at WOT condition

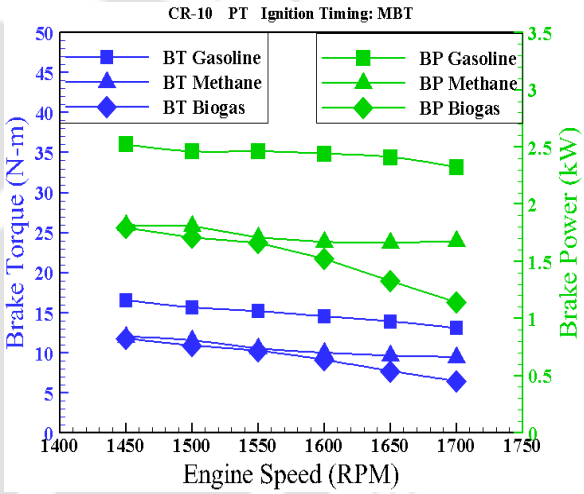

Fig. 4. 34: BT and BP variation with engine speed at PT condition

attributed due to the lower heating value and lower energy density of the biogas. As a result, the net heat release during the combustion phase of raw biogas is much lower than that of methane and gasoline. Additionally, displacement of air by the raw biogas and the slower flame velocity are the key element for producing lesser BT and BP as compared to the methane and gasoline operated engine. Further, in case of liquid fuels, it is considered that the fuel does not reduce the amount of air sucked into the engine cylinder. Hence, a gasoline-fueled engine converted for biogas operation could produce lower power output at the same operating CR. From the above presented observation, it may be noted that, the methane and biogas fueled SI

engine are de-rated respectively, by 13.5% and 17.5% in comparison with the gasoline fueled engine operating at the same CR at WOT condition.

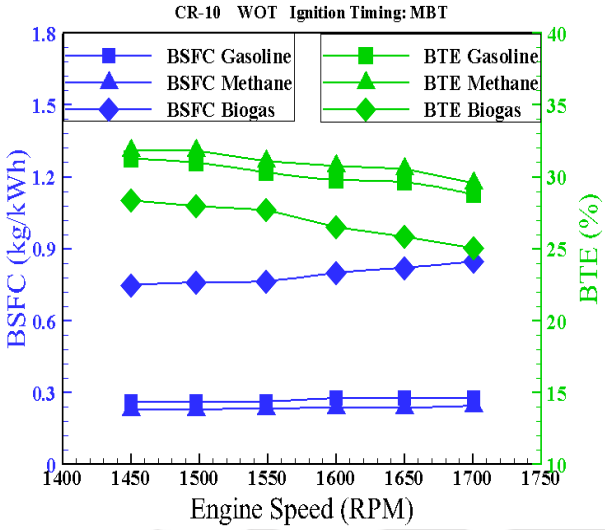

Fig. 4. 35: BSFC and BTE variation with engine speed at WOT condition

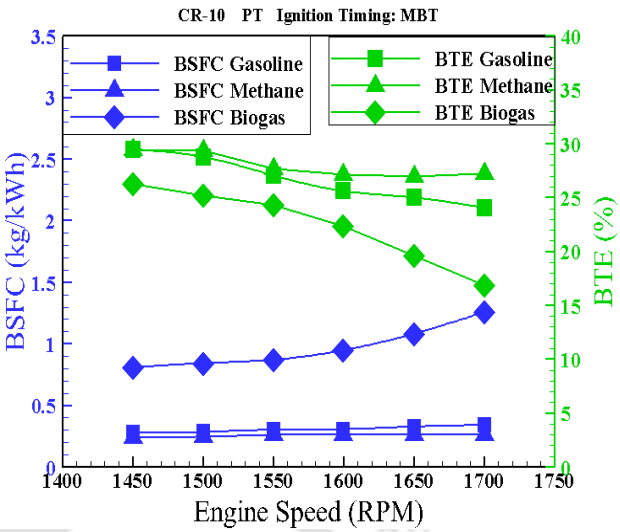

Fig. 4. 36: BSFC and BTE variation with engine speed at PT condition

Fig. 4. 35 and **Fig. 4. 36** reveals, the comparative investigation of the BSFC and BTE of the gasoline, methane and biogas operated SI engine over the speed range of 1450-1700 rpm at WOT and PT conditions, respectively. Irrespective of the throttle position, the BSFC of the biogas fueled engine is higher than that of gasoline and methane fueled SI engine throughout its speed range. However, in the order of BSFC, the methane operated SI engine recorded the lowest specific fuel consumption rate followed by gasoline and biogas operation. It is also observed that the BTE of the methane fueled SI engine is always higher than that of the gasoline and biogas fueled SI engine throughout the speed range both in WOT and PT condition. This is due to the fact that, the LHV of the methane (50 MJ/kg) is higher than that of gasoline (44.5 MJ/kg) and biogas (17 MJ/kg). Additionally, the average amount of fuel consumed in case of methane fueled SI engine is 0.67 kg/h and 0.44 kg/h at WOT and PT conditions, which is lower than that of the gasoline (0.89 kg/h at WOT and 0.75 kg/h at PT) and biogas (2.16 kg/h at WOT and 1.44 kg/h at PT) operated SI engine. Hence, the BTE of the methane fueled engine is found higher over the operating engine speed. However, the recoded BTE of the biogas fueled engine is found much lower than that of methane and gasoline operated engine over the operating speed range. This happening is mainly attributed due to the lower LHV, and the higher fuel

consumption rate observed at WOT and PT condition. At WOT and PT condition the BTE for the test fuels decreases along with the increasing speed of the engine. This could be due to the reduced of volumetric efficiency as shown in **Fig. 4. 37** and **Fig. 4. 38**. As the BSFC is the inverse of BTE, their values at WOT and PT condition for test fuels follows an increasing trend along with the progressive advancement of the engine speed. The minimum and maximum BSFC at WOT condition are recoded 0.227 and 0.243 kg/kWh for methane operation, 0.26 and 0.28 kg/kWh for gasoline operation, 0.747 and 0.846 kg/kWh for biogas operation. Similarly, the minimum and maximum BSFC at PT condition are recoded 0.224 and 0.264 kg/kWh for methane operation and 0.278 and 0.340 kg/kWh for gasoline operation and 0.81 and 1.26 kg/kWh for biogas operation. The average BSFC for biogas fueled SI engine is increased by 66 % and 67.9 % at WOT and PT condition, respectively. The maximum BTE at WOT condition of the engine is found 31.8%, 31.6% and 28.4 % for the methane, gasoline and biogas operation of the engine, respectively at 1450 rpm. Similarly, the maximum BTE at PT condition of the engine is found to be 29.5%, 29.4 % and 27.5% for the methane, gasoline and biogas operated engine, respectively at 1450 rpm. With reference to gasoline operation, the average BTE of the biogas fueled SI engine is reduced by 12 % and 17 % at WOT and PT condition, respectively.

Fig. 4. 37 and **Fig. 4. 38** describes the effect of engine speed on VE of the methane, gasoline and biogas fueled SI engine, respectively at WOT and PT condition. Irrespective of the operating throttle and engine speed, the VE of the methane fueled SI engine is greater than that of gasoline and biogas operation. Further, it is noticed that the volumetric efficiency of the gasoline fueled SI engine is greater than that of the biogas operation both at WOT and PT condition. This is because of the fact that, when the engine is fueled with biogas, part of air sucked into the cylinder is displaced by the biogas. But, in case of liquid fuels (gasoline), the fuel did not reduce the amount of air sucked into the engine cylinder. Hence, gasoline fueled SI engine exhibits higher volumetric efficiency than the biogas fueled SI engine. At WOT condition, the average volumetric efficiency of the engine fueled with methane, gasoline and biogas are found 48.7%, 43.4 % and 41.5 %. However, at PT condition, the average volumetric efficiency is calculated 39.5%, 29 % and 26.2 % when fueled with methane, gasoline and raw biogas, respectively. As compared with gasoline fueled SI engine, the volumetric efficiency of

the biogas fueled SI engine is reduced by 4.5 % and 9.3 % at WOT and PT condition, respectively.

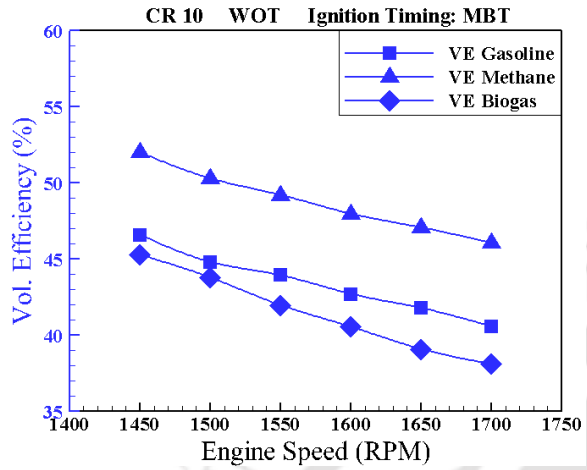

Fig. 4. 37: Effect of engine speed on VE of the engine at WOT condition

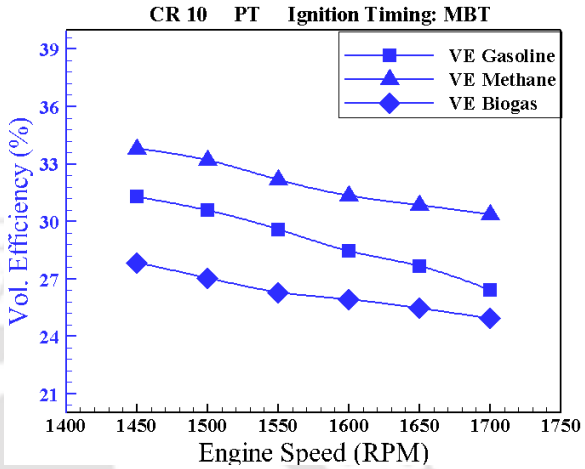

Fig. 4. 38: Effect of engine speed on VE of the engine at PT condition

4.4.2 Combustion analysis

The variation of the average cylinder pressure of the methane, gasoline and raw biogas fueled SI engine at WOT and PT operating condition are shown in **Fig. 4. 39** and **Fig. 4. 40**, respectively for 1650 rpm. Irrespective of the operating throttle, the average peak cylinder pressure (PCP) of the gasoline fueled engine is found higher than that of methane and biogas operated SI engine at CR 10. At WOT, the average PCPs are found 32.1 bar at 368^{o} CA, 34.4 bar at 375^{o} CA and 23.6 bar at 379^{o} CA, respectively for the methane, gasoline and biogas operated SI engine. Thus, at WOT, the PCPs of the methane and biogas fueled SI engine are dropped respectively by 6.6 % and 31.4% as compared with the gasoline operated engine. In PT condition, the corresponding PCP are noted as, 20.7 bar at 374^{o} CA, 24.8 bar at 376^{o} CA and 13.58 bar at 382^{o} CA respectively for the methane, gasoline and biogas operated SI engine. Thus, the PCPs of the methane and biogas fueled engine are dropped by 16.5% and 55.4 % with reference to the gasoline fueled engine. This happening is mainly governed by the input chemical energy/cycle and the energy conversion efficiency for the considered test fuels for the engine operation. Since the input chemical energy for the gasoline operation (0.83 kJ/cycle) is higher than that of methane (0.69 kJ/cycle) and biogas (0.76 kJ/cycle), it may be possible to

have lower BP and PCPs for methane and biogas operated engine. However, it also depends on the energy conversion efficiency.

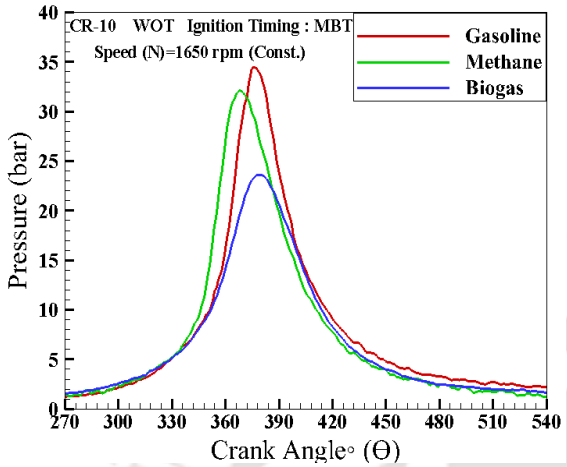

Fig. 4. 39: Variation of the average cylinder pressure with respect to crank angle at WOT for different test fuels

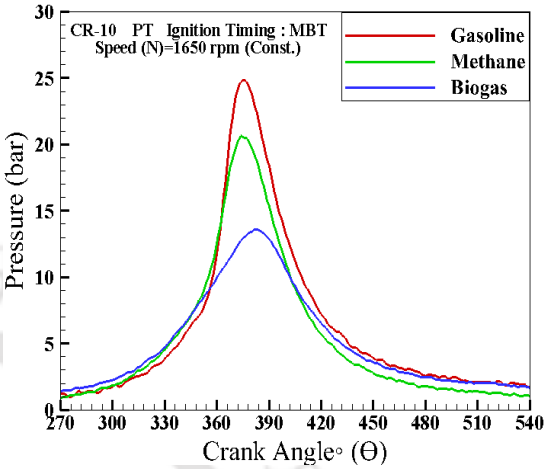

Fig. 4. 40: Variation of the average cylinder pressure with respect to crank angle at PT for different test fuels

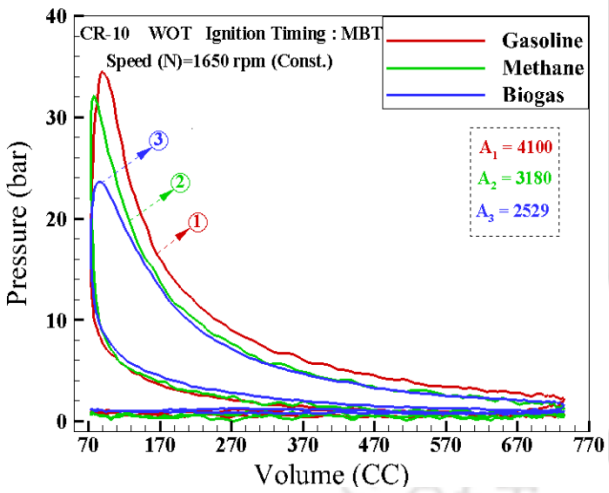

Fig. 4. 41: Area under the P-V curve for different test fuel at WOT

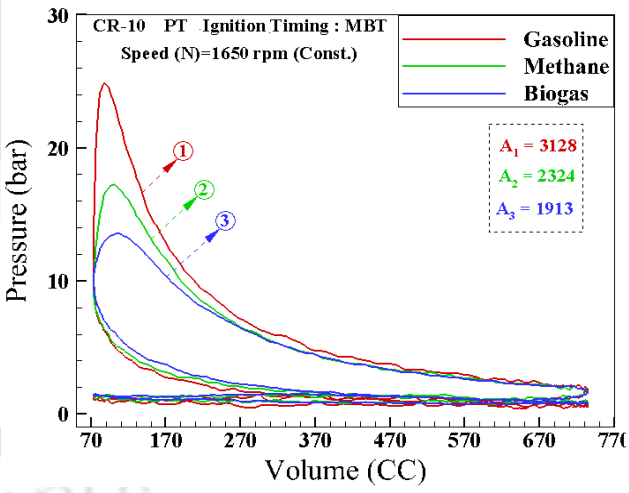

Fig. 4. 42: Area under the P-V curve for different test fuel at PT

The lower peak pressure is attributed to comparatively lesser indicated and brake power in case of biogas fueled SI engine. The area under P-V curve, shown in **Fig. 4. 41** and **Fig. 4. 42** gives a clear understanding of the IP output at WOT and PT operating condition of the

engine for the selected test fuel. As noticed, irrespective of the throttle condition, the area under the P-V curve is found maximum for gasoline operation followed by methane and biogas operation. Hence, the BP of the methane and biogas fueled engine are dropped by 13.5% and 17.5 %, respectively at WOT. Further, irrespective of the throttle position, the location of average PCP of methane operated engine is found 4 to 7° CA in advance from the location of PCP of gasoline engine. However, the location of average PCP of the biogas engine is shifted by 2° to 6° CA from the PCP of gasoline fueled engine. The MBT timing and flame propagation rate of methane and biogas are the key reasons for the above happening.

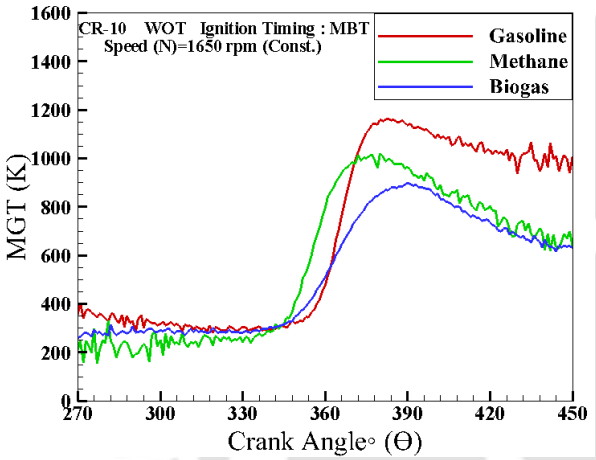

Fig. 4. 43: Variation of the MGT with respect to crank angle at WOT for different test fuels

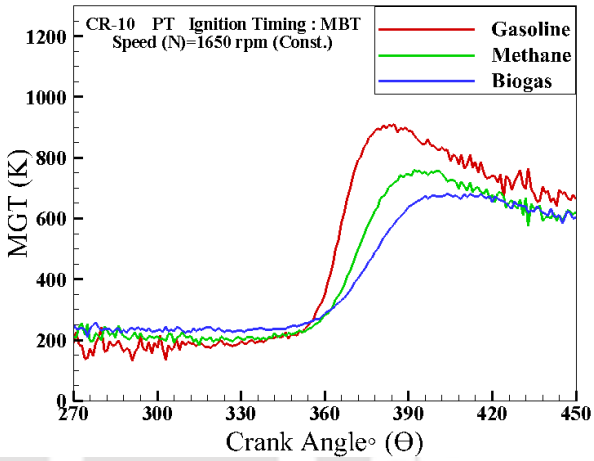

Fig. 4. 44: Variation of the MGT with respect to crank angle at PT for different test fuels

The variation of MGT of the methane, gasoline and biogas fueled SI engine are shown in **Fig. 4. 43** and **Fig. 4. 44**, respectively at WOT and PT condition. The MGT is evaluated from *Eq. D20* of ***Appendix D*** assuming a single zone combustion model. The characteristic gas constant 'R' is evaluated from the correlation R= 0.287+0.020 * Φ (Stone, 2012; Kriger and Borman 1986). Irrespective of the operating fuel and throttle conditions, the MGT followed an increasing trend just after the point of respective MBT but certainly with an ignition delay. However, the location of peak MGT (LPMGT) appeared after the location of PCP and PNHRR in the expansion stroke. At WOT, the PMGTs are found 1163 K at 383° CA, 1019 K at 380° CA and 897 K at 391° CA, respectively for the gasoline, methane and biogas operated engines. Similarly, at PT condition, the PMGTs are recoded 908 K at 385° CA, 760

K at 392° CA and 680 K at 412° CA for the gasoline, methane and biogas operated engines. As noticed, the MGT of the biogas operated engine always found lower than the gasoline and methane fueled engine in the expansion stroke. This happening is mainly attributed due to the lower heating value of biogas and its effect is also reflected in the PCP and NHRR curve of the biogas operated engine.

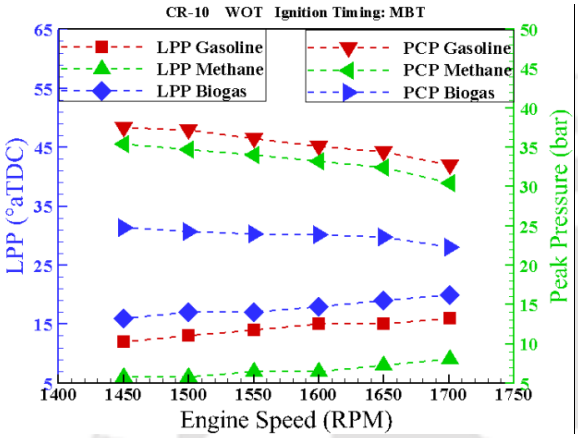

Fig. 4. 45: Variation of LPP and PCP with respect to the engine speed for the Test fuels at WOT

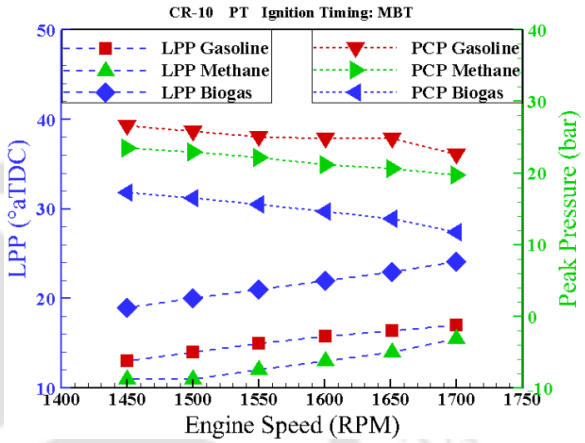

Fig. 4. 46: Variation of LPP and PCP with respect to the engine speed for the Test fuels at PT

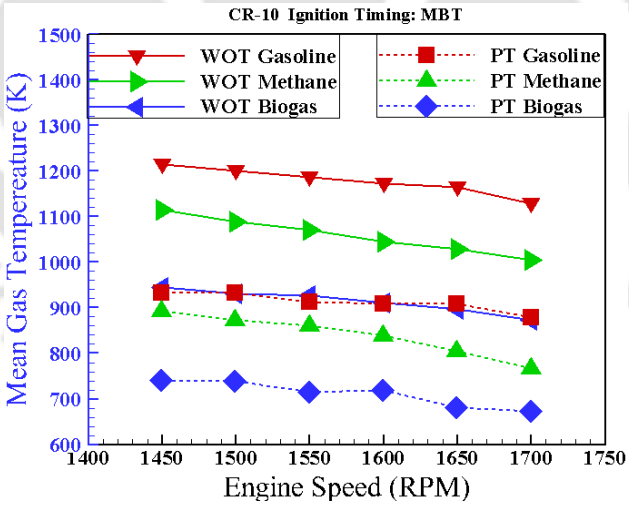

Fig. 4. 47: Variation of peak MGT for the Test fuels at WOT and PT condition

The effect of engine speed on the PCP and location of peak pressure (LPP) of the gasoline, methane and biogas operated SI engine are portrayed in **Fig. 4. 45** and **Fig. 4. 46,** respectively for WOT and PT condition. Irrespective of the operating fuel and throttle

condition, the PCP drops constantly along with the engine speed. Whereas, the LPP shifts away progressively from the TDC. Similar observations are also reported by researchers (Chaudhari, 2017; Chaudhari et al., 2014) .The effect of drop in PCP is also clearly reflected in **Fig. 4. 33** and **Fig. 4. 34**, which further validate the reason behind reduced BT and BP at higher engine speed. The shifting of PCP away from TDC, certainly reduced the expansion work output from the engine, which could have been optimized. The reason behind this happening may be the fixed MBT timing that has been maintained constant for the operating speed range of the engine irrespective of the test fuels. The combustion of any fuel takes a definite time interval for the reaction to took place and is also influenced by the combustion environment. However, with progressive engine speed, the time interval of the expansion stroke is reduced and resulted in incomplete combustion. The drop in PCP at higher operating speed is also supported and explained by the trend of peak MGT as depicted in **Fig. 4. 47**.

As noticed, the peak MGT follows a decreasing trend with increasing speed of the engine. This signifies an abnormal and uneven combustion at higher speed of the engine, which is not letting the in-cylinder temperature to rise at higher speed. This may be because of the lower volumetric efficiency at higher speed of the engine. Irrespective of the throttle position and throughout the speed range, the PCP and LPP of the biogas fueled SI engine is much lower and appears later in the expansion phase as compare to the methane and gasoline operation. The drop of PCP may be due to the lower heating value (17 MJ/kg) and density (1.11 kg/ m^3) of biogas. The lower flame speed (0.25 m/s) and ignition advance (45^o bTDC) are the key reasons for shifting the PCP in the expansion stroke for the biogas fueled SI engine. At WOT and PT operating condition and within the operating speed range (1450 to 1700 rpm), the PCP of biogas fueled engine is dropped by 34 to 31% and 34 to 48%, respectively in comparison with the gasoline engine. The LPP of the biogas operated engine in comparison with the gasoline operation is shifted by 3-4^o CA and 6-7^o CA, respectively at WOT and PT condition. Similarly with reference to the methane fueled engine, the PCP of the biogas operated engine is dropped by 26-30%, shifted by 10^o CA.at WOT and 26-40%, shifted by 8^o CA at PT condition, respectively.

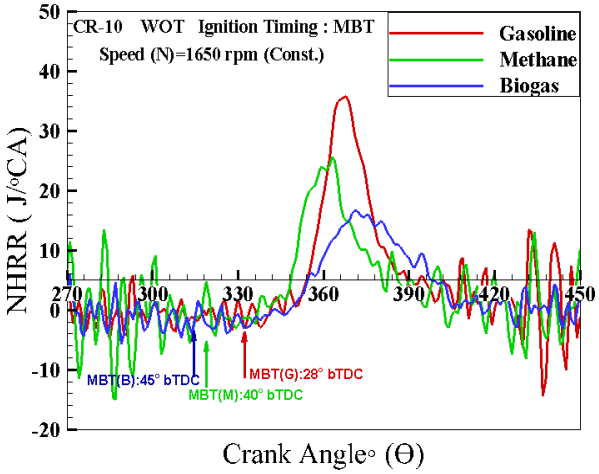

Fig. 4. 48: Variation of NHRR for the test fuels at WOT condition

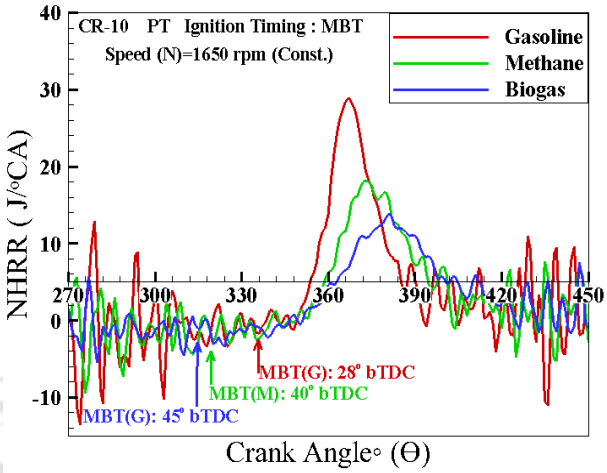

Fig. 4. 49: Variation of NHRR for the test fuels at PT condition

The variation of NHRR with progressive advance of engine speed of the gasoline, methane and biogas fueled SI engine at WOT and PT operating conditions are shown in **Fig. 4. 48** and **Fig. 4. 49**, respectively. The NHRR is evaluated by assuming a single zone combustion model where the product and reactants are thoroughly mixed and there is no mass transfer across the CV. The heat release analysis evaluated the data on differential basis from *Eq. D16* of ***Appendix D*** and this leads to noise in the computed data specially in the lower pressure regions. The negative NHRR implies that there is heat transfer to the cylinder wall and ignition should be close to the minimum NHRR. This may be due to the lower initial rate of combustion (lower MFB) and addition of negative value of heat transfer after the completion of combustion process. It has been noticed, irrespective of the throttle position, the peak NHRR of the biogas fueled SI engine, compared with the methane and gasoline operation is much lower and appears later in the expansion stroke. This may be due to the moderate flame propagation rate of the biogas, where the conversion efficiency is minimum. At WOT conditions, the peak NHRR of gasoline, methane and biogas fueled SI engine are recoded 35.8 J/^{o}CA, 25.6 J/^{o}CA and 16.7 J/^{o}CA at 368 ^{o}CA, 365^{o} CA and 372^{o}CA, respectively. Whereas, at PT condition, the peak NHRRs are 28.9 J/^{o} CA, 18.2 J/^{o} CA and 13.9 J/^{o}CA at 367 ^{o}CA, 373^{o}CA, 381 ^{o}CA, respectively. AT WOT, the peak NHRR of the biogas fueled SI engine is dropped by 39.1 % and 25 %, respectively in comparison with the gasoline and methane fueled engine.

Fig. 4. 50 and **Fig. 4. 51**, describe the variation of the MFB for the gasoline, methane and biogas operated SI engine at WOT and PT operating condition, respectively. The MFB is evaluated using the technique proposed in the open literature (Rassweiler and Withrow, 1938). The rapid burn angle (RBA, $\Delta\theta_b$), for the present case is considered as the CA interval between the end of flame development (MFB of 10%) and the end of flame propagation process (MFB of 90%). The ignition delay (ID, $\Delta\theta_d$) is considered as the CA interval between the spark timing and flame initiation point. It was noticed that, at WOT and PT operating conditions, the combustion of gasoline was initiated at 351^{o}CA and 356^{o}CA, and terminated at 398^{o}CA and 401^{o}CA, receptively. Similarly, methane combustion is initiated at 347^{o}CA and 352^{o}CA and terminated at 379^{o}CA and 395^{o}CA, respectively at WOT and PT condition. However, for biogas, the flame is initiated at 341^{o}CA and 350^{o}CA, and terminated at 391^{o}CA and 400^{o}CA, receptively for WOT and PT operating conditions. The end of flame development stage, for the gasoline, methane and biogas operated SI engine at WOT and PT conditions are observed at 358°CA and 368^{o}CA, 352°CA and 365°CA, and 352°CA and 362^{o}CA, respectively.

As witnessed from **Fig. 4. 50** and **Fig. 4. 51**, the ID ($\Delta\theta_d$) is found maximum for biogas and subsequently followed by methane and gasoline, respectively irrespective of the operating throttle. The respective ignition delays are depicted in **Table 4. 12**. Similarly, the duration of RBA ($\Delta\theta_b$) is also found maximum for the biogas combustion irrespective of the operating throttle condition. From the above observations, it can be inferred that, although the combustion event (flame development) for the biogas fueled engine is initiated earlier, it takes more time to propagate the flame due to the lower energy density and weaker flame front propagation rate. Irrespective of the test fuel the ID ($\Delta\theta_b$) is found maximum for PT condition. Similarly, the RBA is also found maximum at PT condition for methane and biogas combustion. However, the higher ER and lower volumetric efficiency observed at this condition (MBT: 28^{o}CA bTDC, 1650 rpm) could be the reason for extended RBA at PT condition for the gasoline combustion.

Table 4. 12: Summary of RBA and ID for the test fuels at WOT and PT condition

Operating Throttle	Gasoline		Methane		Biogas	
	RBA ($\Delta\theta_{bG}$)	ID ($\Delta\theta_{dG}$)	RBA ($\Delta\theta_{bM}$)	ID ($\Delta\theta_{dM}$)	RBA ($\Delta\theta_{bB}$)	ID ($\Delta\theta_{dB}$)
PT	27	24	26	32	34	35
WOT	31	19	23	27	32	28

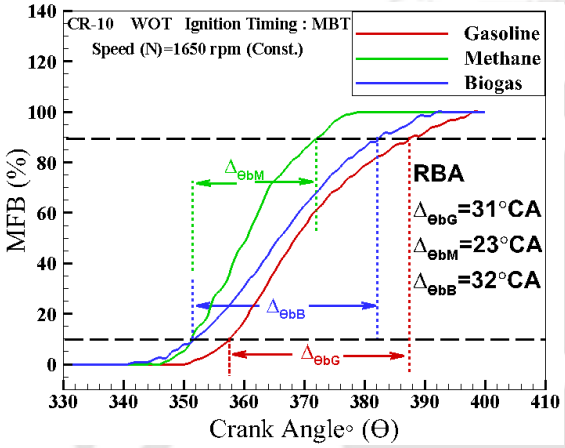

Fig. 4. 50: Variation of MFB for the test fuels at WOT condition

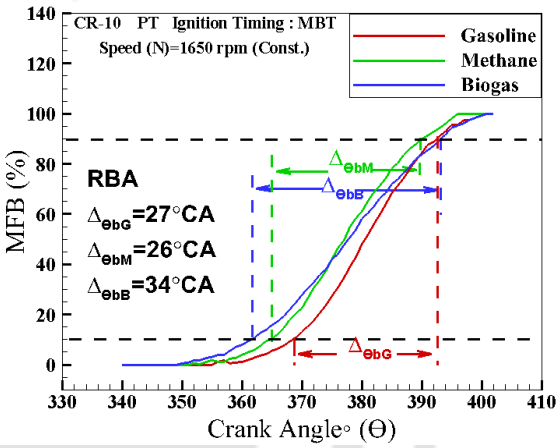

Fig. 4. 51: Variation of MFB for the test fuels at PT condition

The study of cyclic-by-cyclic variations delivers an elaborative understanding of the stability of the combustion process in SI engines. Hence, in the present case, 50 conjunctive cyclic data points of pressure at each crank angle has been recorded for each test fuels over the operating speed of the engine. The coefficient of variance of IMEP (COV_{IMEP}) and peak cylinder pressure (COV_{pp}) are evaluated from *Eq. D21 and D22* of ***Appendix D***. The variation in the COV_{IMEP} and COV_{pp} of the gasoline, methane and biogas operated SI engine at WOT and PT condition are shown in **Fig. 4. 52** and **Fig. 4. 53**, respectively over the operating speed range. The COV_{pp} and COV_{IMEP} are the relative measures to compare the cycle-by-cycle variation of PCP and IMEP of the SI engine. The COV_{pp} and COV_{IMEP} follow the same trend and the scale increase with increasing speed of the engine. This signifies, the fluctuation of PCP and IMEP becomes more intense with increasing speed of the engine. This may be due to

the cycle-by-cycle variations (CCV) on the amount of the air and fuel supplied to the engine as well as the CCV in the residual gas left from the previous cycle.

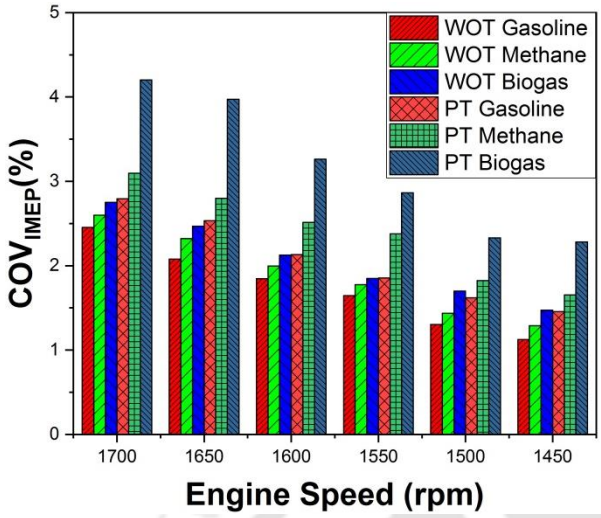

Fig. 4. 52: Variation of COV_{IMEP} for the test fuels

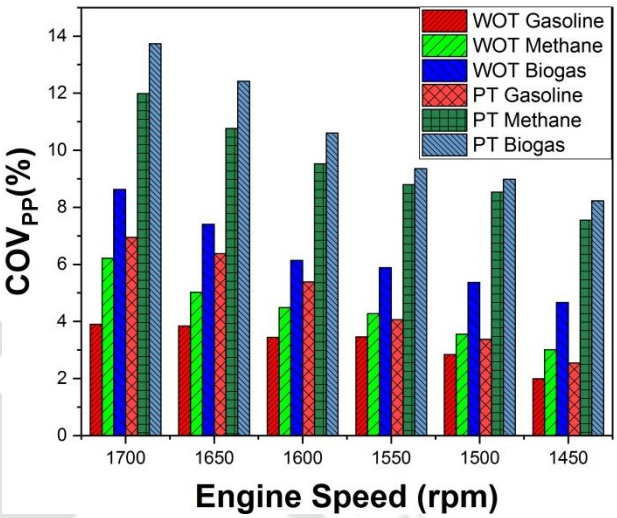

Fig. 4. 53: Variation of COV_{PP} for the test fuels

The COV_{pp} at WOT condition varies between 2 to 4%, 3 to 6%, and 4.7 to 8.6%, respectively for the gasoline, methane and biogas fueled SI engine over the operating speed range. Similarly, at PT operating condition the COV_{pp} varied between 2.5 to 7%, 7.5 to 12%, and 8.2 % to 13.7% respectively for the gasoline, methane and biogas fueled SI engine. As observed, the COV_{pp} became intensive for the biogas fueled engine at PT condition. Whereas the recoded data is within the acceptable limit at WOT condition. The COV_{IMEP} for the biogas fueled SI engine at WOT and PT condition is found to very between 1.4 to 2.7 % and 2.3 to 4.2%, respectively throughout the speed range of the engine whereas, for the gasoline fueled engine, the COV_{IMEP} is varied between 1.1 % to 2.4 % and 1.4 % to 2.7% at WOT and PT condition respectively. Whereas the COV_{IMEP} is found to very between 1.3 to 2.5% and 1.5 to 2.8%, respectively at WOT and PT condition. It is noticed that, irrespective of the operating condition, the COV_{pp} and COV_{IMEP} of the biogas fueled SI engine is higher than the gasoline fueled SI engine. This may be because of the non-uniformity in the amount of supplied air and fuel ratio to the engine in each cycle due to the presence of biogas mixer at the inlet manifold.

4.4.3 Emission analysis

The concentrations of CO and CO_2 in the exhaust emission of the gasoline, methane and biogas fueled SI engine at WOT and PT condition have been explained in **Fig. 4. 54** and **Fig. 4. 55**, respectively. Irrespective of the throttle position and test fuels, the CO concentration in the exhaust emission followed an increasing trend with progressive rise in the engine speed. However, the recorded CO_2 concentration declines with rise in speed of the engine irrespective of the test fuel and throttle position. The pattern of CO and CO_2 concentration in the exhaust emission perceived opposite to each other. The observed pattern may be explained with the understanding of MGT of the engine cylinder.

As observed from **Fig. 4. 47**, the MGT of the engine decreases with increasing engine speed irrespective of the throttle condition and test fuels. CO oxidizes and turned into CO_2 at higher combustion temperature (Jahirul et al., 2010). Hence, the rate of oxidization of CO and formation of CO_2 reduces with lower combustion temperature or with increasing speed of the engine. Similar observation on the CO and CO_2 emission of the gasoline, CNG and LPG fueled engine are reported in open literature (Jahirul et al., 2010; Mehrnoosh et al., 2012; Usman et al., 2020). It is also observed that, irrespective of the operating throttle and speed range, the CO emission of the gasoline fueled engine is higher than methane and biogas operation. However, the lowest CO emission is observed for methane fueled engine.

Similarly, the recorded average CO_2 emission is found maximum for biogas operated engine followed by methane and biogas operation. In general, poor mixing of air and fuel, local rich regions, incomplete combustion are typical causes of CO emission (Pulkrabek, 1997). The drop in CO concentration in the exhaust emission of methane and biogas operated engine signifies enhanced combustion as compared to that of gasoline engine. Further, with the lean mixture CO is always present owing to dissociation, but the concentration reduces with decrease in combustion temperature (Stone, 2012). The lower C/H ratio and MGT in case of methane and biogas combustion may be the key reason for lesser CO and higher CO_2 emission compared to gasoline (Usman et al., 2020). The average CO emission of the methane and biogas operated engine are dropped by 52% and 49% at WOT, and 97% and 96% at PT condition of the engine, respectively with reference to the gasoline operation. Whereas, the

average CO_2 emission of the methane and biogas fueled engine are increased by 8% and 37% at WOT and, and 21% and 61% at PT condition, respectively with reference to the gasoline engine. The higher CO_2 emission of biogas fueled engine may be attributed to the inherent presence of CO_2 (about 42 %) in raw biogas which is incombustible in nature.

The concentration of HC and NO_x emission of the gasoline, methane and biogas operated SI engine are shown in **Fig. 4. 56** and **Fig. 4. 57** respectively at WOT and PT operating condition. As observed, irrespective of the operating throttle and test fuel, the concentration of HC in the exhaust emission increases with increasing engine speed. This happening may be the consequence of VE shown in **Fig. 4. 37** and **Fig. 4. 38**. At lower operating speeds, the air-fuel mixture has enough oxygen to promote complete combustion because of the higher VE and produces lesser unburnt HC in the exhaust emission. But, at higher operating speed, the lower VE resulted in incomplete combustion and leads to greater unburnt HC.

However, irrespective of the operating throttle, the HC emission is found maximum for gasoline operation followed by biogas and methane operated engines, respectively. The least HC emission is recoded for the methane operated engine both at WOT and PT condition. The unburnt HC emission in SI engine is high mostly due to incomplete combustion (Mehrnoosh et al., 2012). Methane and biogas form better mixture with the incoming air, whereas gasoline first atomizes and then vaporizes to form homogeneous mixture with the intake air which takes comparatively more time. Hence, the better mixer formation may initiate superior combustion and produces less HC for methane and biogas fueled engine. Further, methane and biogas has lower molecular weight compared to gasoline. Hence, the gaseous fuel engine is expected to produce lesser HC compared to the gasoline engine (Usman et al., 2020). As reported, the average HC emission for methane and biogas operated engine are dropped by 65% and 27% at WOT and 64% and 14% at PT condition with reference to the gasoline fueled engine.

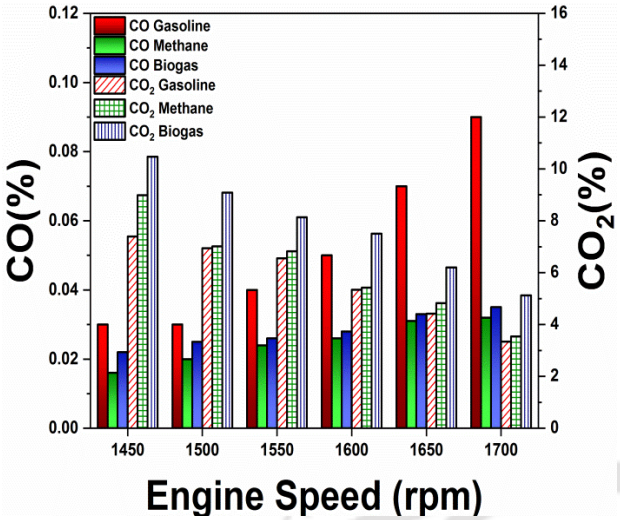

Fig. 4. 54: CO and CO2 emission of the engine for the test fuels at WOT condition

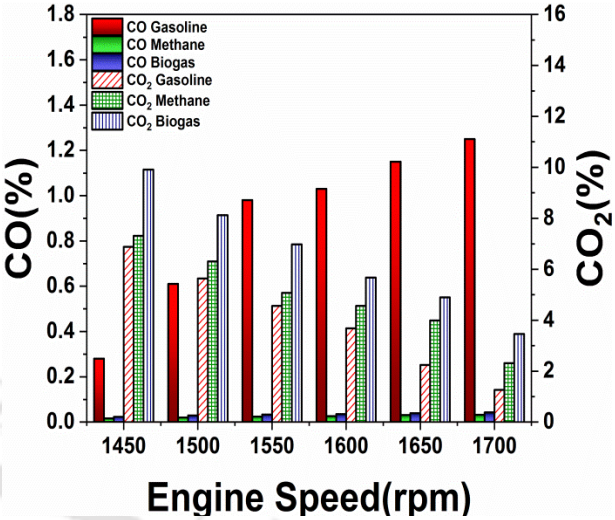

Fig. 4. 55: CO and CO2 emission of the engine for the test fuels at PT condition

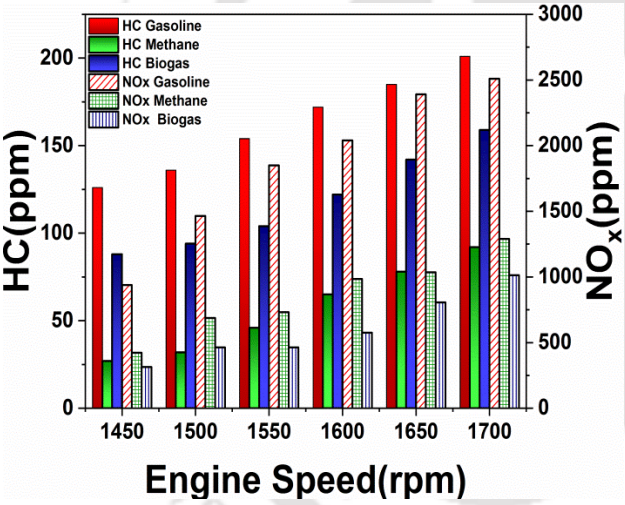

Fig. 4. 56: HC and NOx emission of the engine for the test fuels at WOT condition

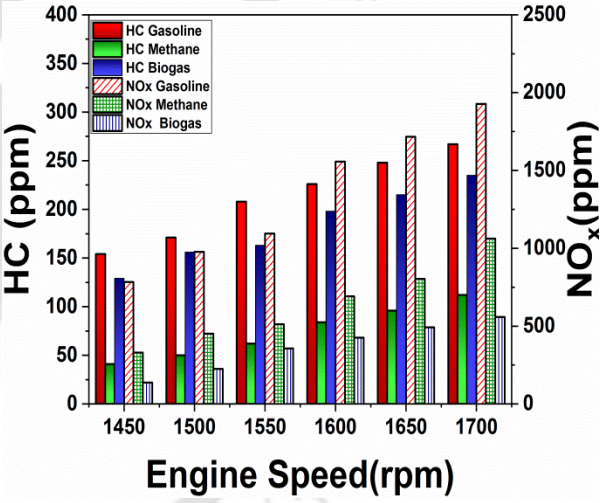

Fig. 4. 57: HC and NOx emission of the engine for the test fuels at PT condition

The NO_x emission is strongly related to the lean fuel with high cylinder temperature or high peak combustion temperature. As shown in **Fig. 4. 56** and **Fig. 4. 57**, irrespective of the operating fuel and throttle condition, the NO_x concentration in exhaust emission increases with the increasing engine speed. The MGT in case of gasoline fuelled SI engine is much higher than that of methane and biogas. Hence, the NO_x emission of the methane and biogas fuelled engine are found lower than that of the gasoline throughout the operating speed range. The average NO_x emission is reduced by 54 % and 68 % at WOT and 52% and 73% at PT condition,

respectively for the methane and biogas fuelled SI engine. The reported experimental data in **Fig. 4. 54** to **Fig. 4. 57** are converted to specific emissions based on energy produced (by using *Eq. 4.1*) and reported in **Table 4.13**. As identified in the open literature (Jeong et al., 2009; Jahirul et al., 2010; Mehrnoosh et al., 2012), the obtained values of CO, CO_2, HC and NO_x concentrations are in the permissible ranges for the gasoline, methane and biogas operated engines

Table 4. 13: Summary of pollutant emission from the test fuel based on the energy produced

↓Engine Speed	CO (g/kWh)				HC (g/kWh)			NO_x (g/kWh)			HC+ NO_x
Fuel	**G**	**M**	**B**	***Std**	**G**	**M**	**B**	**G**	**M**	**B**	***Std**
Throttle	**WOT**				**WOT**			**WOT**			
1450	1.08	0.57	0.79		0.25	0.05	0.18	6.22	2.80	2.09	
1500	1.08	0.72	0.90		0.27	0.06	0.19	9.72	4.57	3.07	
1550	1.44	0.86	0.93		0.31	0.09	0.21	12.28	4.86	3.07	
1600	1.80	0.93	1.01		0.34	0.13	0.24	13.54	6.53	3.82	
1650	2.51	1.11	1.19		0.37	0.16	0.28	15.87	6.87	5.36	
1700	3.23	1.15	1.26	≤ 250[#]	0.40	0.18	0.32	16.66	8.56	6.72	≤ 12[#]
Fuel	**G**	**M**	**B**		**G**	**M**	**B**	**G**	**M**	**B**	
Throttle	**PT**				**PT**			**PT**			
1450	10.05	0.72	0.83		0.31	0.08	0.26	5.20	2.19	0.92	
1500	11.13	0.93	1.04		0.34	0.10	0.31	6.48	2.99	1.49	
1550	35.19	1.11	1.19		0.42	0.12	0.33	7.27	3.40	2.36	
1600	36.99	1.22	1.26		0.45	0.17	0.40	10.33	4.59	2.83	
1650	53.87	1.33	1.40		0.50	0.19	0.43	11.39	5.33	3.27	
1700	44.89	1.44	1.51	≤ 3.5[$]	0.53	0.22	0.47	12.79	7.05	3.71	≤ 7.5[$]

*Emission standard set by the Govt. of India for the [#]genset run on petrol and natural gas (NG) or petrol and liquid petroleum gas (LPG) and [$] genset run on dedicated natural gas (NG) or liquid petroleum gas (LPG) as mentioned in GSR 281(E) (The Gazette of India, 2016)

**G-Gasoline, M-Methane, B-Biogas

4.5 Summary

In the current experimental investigation, the optimum IT of the methane and biogas fuelled SI engines are determined over the operating speed range at CR 10 under WOT and PT conditions. Further to explore the shortfall of biogas fuelled SI engine over the operating speed range at CR 10, a comparative assessment is carried out by operating SI engine with gasoline, methane and biogas with their respective optimum IT. The characteristics feature of the test fueled engines are studied experimentally and summarized here based on the experimental evidence of performance, combustion and emission analysis.

4.5.1 Optimum IT of the methane fuelled SI engine:

- Irrespective of the operating throttle and engine speed, the methane fueled SI engine is found operative in the IA range of 24^o to 42^o CA bTDC at CR 10. However, the maximum BT and BP of the engine are developed at 40^o CA bTDC and reported 18.4 N-m and 3.19 kW at WOT, and 12.2 Nm and 2.1 kW at PT operating condition at 1650 rpm. Further, with increasing engine speed, the MBT timing is advanced. However, the observed fluctuation of MBT is found insignificant over the short-range of engine speed (1400-1700 rpm). The BSFC and BTE of the engine are also reported optimum and found 0.233 kg/kWh and 30.9% at WOT, 0.257 kg/kWh and 28% at PT condition.
- The area under the P-V curve is observed maximum at MBT timing and therefore justifies the development of maximum BP at this condition. The duration of RBA is detected minimum (21^o CA at WOT and 23^o CA at PT) and indicates the higher flame front propagation rate at the MBT timing. The NHRR and MGT are also observed maximum at this condition.
- The CO emission at the MBT timing is observed minimum and reported 1.8 g/kWh and 7.1 g/kWh, respectively at WOT and PT condition. However, the CO_2, HC and NO_x emission at the MBT timing are found maximum and reported 286 g/kWh, 0.13 g/kWh and 6.41 g/kWh, at WOT condition. Although, the CO_2, HC and NO_x emission are found maximum at the MBT timing, the concentrations are within the acceptable emission standards. Hence for the current operating speed range and experimental

condition 40^{o} CA bTDC is recommended as the optimum IT for both WOT and PT conditions of the methane fueled SI engine.

4.5.2 Optimum IT of the biogas fuelled SI engine:

- The biogas fueled SI engine is found operative within the IA ranges of 23^{o} to 55^{o} CA bTDC at CR 10 both at WOT and PT condition. However, the maximum BT and BP of the engine are found at 45^{o} CA bTDC for both throttle conditions and recorded 15.4 Nm and 2.6 kW at WOT and, 9.2 Nm and 1.6 kW at PT operating condition at 1650 rpm. The rise in engine speed resulted in advanced the MBT timing. However, the observed fluctuations of MBT timings are found insignificant over the operating speed range (1400 to 1700 rpm) of the engine. Hence, 45^{o} CA bTDC is considered as the MBT timing for the current speed range of the engine at CR 10. The BSFC and BTE are also reported optimum at this condition and recorded 0.814 kg/kW-h and 26% at WOT and 0.909 kg/kW-h and 23% at PT condition.
- The area under the P-V curve is also observed maximum at 45^{o} CA bTDC and justifies the claim of MBT IT for the biogas fueled engine. The reported RBA is also found optimum at 45^{o} CA bTDC irrespective of the operating throttle. The early flame development and propagation rate resulted in maximum energy conversion efficiency at 45^{o} CA bTDC.
- The minimum CO and maximum CO_2 emissions are observed at 45^{o} CA bTDC and recorded 1.3 g/kWh and 398 g/kWh at WOT and 1.4 g/kWh and 314 g/kWh at PT operating conditions. The HC concentration is increased with progressive IA and found 0.31 g/kWh and 0.43 g/kWh at 45^{o} CA bTDC, respectively at WOT and PT conditions. The NO_X concentration at MBT timing are observed 5.7 g/kWh and 3.3 g/kWh, respectively for the WOT and PT conditions of the engine. Although, the CO_2, HC and NO_x emission are found maximum at the MBT timing, the concentrations are within the acceptable emission standards. Hence for the current operating speed range and experimental condition 45^{o} CA bTDC is recommended as the optimum IT for both WOT and PT conditions of the biogas fueled SI engine.

4.5.3 Comparative analysis of the SI engine fueled with the test fuels:

- In comparison with the gasoline fueled engine, the BP of the methane and biogas operated engines are dropped by 13.5% and 17.5% at WOT, and 29% and 37.5% at PT operating condition. The methane and biogas fueled SI engine are de-rated respectively by 13.5% and 17.5% in comparison with the gasoline fueled engine operating at the same CR at WOT condition.
- Irrespective of operating condition, the BSFC of the biogas fueled engine is always higher than the methane and gasoline operation. With reference to the gasoline engine, the average BSFC of biogas fueled engine is increased by 66 % and 68 %, respectively.at WOT and PT condition. However, the BSFC of the methane operated engine is dropped by 13% at WOT and 16% at PT condition.
- The BTE of the biogas fueled SI engine is dropped by 12% and 14.3% with reference to the gasoline engine, respectively at WOT and PT condition. However, a minor improvement in BTE of the methane fueled engine has been noticed both at WOT and PT condition. The maximum BTE of the gasoline, methane and biogas operated engine are found 31.6 %, 31.8 % and 28.4 %, respectively at WOT and 29.4 %, 29.5% and 26.3%, respectively at PT condition
- At WOT and PT conditions, the PCPs and LPPs of the biogas fueled SI engine are dropped by 31 to 34%, 34 to 49% and shifted by 3-4^{o}, 6-7^{o} CA, respectively with reference to the gasoline fueled engine. Similarly, inference to the methane operated engine, the PCPs of the biogas fueled engine are dropped by 27 to 30% at WOT and 26 to 48% at PT condition.
- The average CO emission of the biogas fueled SI engine is reduced by 45.5 % and 96 %, respectively at WOT and PT condition with reference to the gasoline engine. However, the average CO_2 emission is increased by 37% and 61% at WOT and PT condition. Similarly, with reference to the gasoline engine, the average CO_2 emission of methane fuelled engine is increased by 8% and 22% respectively at WOT and PT condition. With reference to the gasoline engine, the average unburnt HC and NO_x emission of the biogas fuelled engine is dropped by 27% and 67.5% at WOT and 14% and 73% at PT operating condition. Similarly, the average unburnt HC and NO_x

emission of the methane fuelled engine is dropped by 65% and 54% at WOT and 65% and 52.5% at PT operating condition.

- The BP and BTE of the biogas engine operating at PT condition are dropped by 36% and 4.2%, respectively in comparison with the WOT condition. Although, the CO, HC and NOX emission at PT operating condition of the biogas fueled engine are reduced, the reported CO_2 emission is much higher and the engine is derated by 36% at PT condition. Hence, the biogas operated SI engine must be operated at WOT condition.

CHAPTER 5

Influence of Operating Parameters on the Overall Performance of the Biogas Fueled VCR-SI Engine

Overview

The VCR SI research engine (Engine 2) is primarily configured for gasoline application with a limiting CR of 10:1. Hence, it could not be possible for the biogas operated engine to achieve the BT and BTE of the gasoline engine at the same operating CR. The inefficiency and the associated drawbacks identified during the baseline investigation of the biogas fueled VCR SI engine (Engine 2) is addressed here in this chapter by accessing the influence of operating parameters. Therefore, to achieve the maximum possible work output and fuel conversion efficiency, the influence of critical operating parameters on the overall performance of the biogas fueled SI engine is investigated. The implementation of a customized VCR mechanism, ECU controlled DIS system and biogas induction mechanism enabled the engine to operate in a wide range of operating CR, IT and ER. The investigation started with the experimental optimization of the IT by exploring it's influence on the overall performance of the biogas fueled engine over a wide range operating CR and engine speed. Further, the operating CR of the engine is also optimized for the biogas application over the speed range. Finally, the effect of operating equivalence ratio of the engine is investigated for the optimized CR and IT setting of the biogas engine. The outcome of these experiments are the optimum operating CR, IT, ER and speed combination for the biogas fueled variable speed SI engine operation. The detailed experimental matrix and the operating procedure associated with the optimization of IT, CR and ER of the biogas operated VCR SI engine are also included here in this chapter.

5.1 Experimental Matrix and Operating Procedure

The baseline investigation of the biogas operated VCR SI research engine (Engine 2) highlighted certain issues at CR 10. As summarized in *Chapter 4*, the biogas fueled engine is de-rated by 17.5% at WOT and 37.5% at PT condition. Similarly, the BTE of the biogas engine is dropped by 12% and 14.3%, respectively at WOT and PT condition. Further, the average CO_2 emission of the engine is increased by 37% and 61% at WOT and PT condition for biogas operation. Although, there are certain positive aspects of lower CO, HC and NO_x emission, the de-rated engine power and BTE along with increased level CO_2 emission cannot be ignored at CR 10. Further, it has also noticed that the engine does not performs well in PT operating condition. Hence, to resolve the highlighted issues and attain the best fuel conversion efficiency with biogas mode operation, the influence of operating parameters of the engine has been explored only at WOT condition. Techniques, such as CR and IT optimization, preheating, pre-chamber ignition are few recommended methods to enhance the performance, combustion and emission characteristics of the biogas fueled SI engine (Porpatham et al., 2013a, 2012; Carrera et al., 2013; Corti et al., 2014; Alagumalai, 2014). Thus, the present attempt blends few of the recommended techniques and optimizes the critical operational parameters to enhance the efficiency of the biogas fueled SI engine. In order to find out the precise setting of this critical operating parameter over the operating speed range, the influence of each parameter on the performance, combustion and emission characteristics of the engine has been studied individually.

5.1.1 Experimental matrix for optimizing the critical operating parameters

Biogas produced from the anaerobic digestion of cow dung and lignocellulos biomass is used as the fuel for the current investigation. The average composition of the produced biogas (CH_4:55.6 %, CO_2:42.3%, N_2:2.1%) and most of its properties are experimentally attained and listed in **Table 3. 1** of ***Chapter 3***. The single cylinder, VCR SI research engine (*Engine 2*) mounted with a commercially customized tilting block VCR mechanism, a specially developed biogas induction mechanism and an ECU controlled direct ignition system (DIS) shown in **Fig. 3. 9** and **Fig. 3. 10** of ***Chapter 3*** are used as the experimental setup for this

investigation. The detail technical specifications of the engine along with the mounted accessories and its functioning are listed respectively in **Table C- 1** of ***Appendix C***, *sections 3.3.3, 3.3.4* and *3.3.5*.

Table 5. 1: Experimental matrix for investigating the influence IT

Operating parameters				**Performance Parameters**		
IT (^{o} CA bTDC)	Throttle position (%)	CR	Engine speed (rpm)	Performance analysis	Combustion analysis	Emission analysis
23 25 27 29 31 33 35 37 39 41 43 45 47 49 51 53	WOT 90%	8 9 10 11 12 13 14	1400 1450 1500 1550 1600 1650 1700	BT BP BTE BSFC ER VE	Variation P-θ Variation P-V COV_{PP} COV_{IMEP} NHRR MFB MGT	CO CO_2 NO_X HC

The ongoing experimental investigation is carried out in three steps at WOT condition for the biogas fueled SI engine. At the 1st stage, the influence of operating ITs are inspected at different operative CR and speed range of the engine. The IT is progressively advanced from 23^o to 55^o CA bTDC for each operating CR and engine speed configuration while the operating ER is maintained almost constant (ϕ =0.79~0.80). The CR and engine speed are progressively varied from CR 8 to 14 and 1400 to 1700 rpm, respectively. Based on the overall performance of the biogas fueled engine, the optimum ITs are identified for each operative CR and speed range of the engine. **Table 5. 1** depicts the experimental matrix to investigate the influence of IT towards improving the performance of the biogas fueled SI engine over the operating CR and speed range. Similarly, at the 2nd stage of investigation, the influence of the operating CR over the speed range of the engine is analyzed with the respective MBTs.

Table 5. 2: Experimental matrix for investigating the influence of CR and engine speed

Operating parameters				Performance Parameters		
CR	Throttle position (%)	IT (°CA bTDC)	Engine speed (rpm)	Performance Analysis	Combustion analysis	Emission analysis
8	WOT 90%	MBT (23°- 55°)*	1400	BT, BP, BTE, BSFC, ER, VE	Variation of P-θ, Variation of P-V, COV_{PP}, COV_{IMEP}, NHRR, MFB, MGT	CO, CO_2, NO_X, HC
9			1450			
10			1500			
11			1550			
12			1600			
13			1650			
14			1700			
*** Operating ignition timing range**						

Table 5. 3: Experimental matrix for investigating the influence of operating ER

Operating parameters					Performance Parameters		
ER (ϕ)	Throttle position (%)	CR	IT (°CA bTDC)	Engine speed (rpm)	Performance Analysis	Combustion analysis	Emission analysis
0.744	WOT 90%	12	MBT*	1650	BT, BP, BTE, BSFC, ER, VE	Variation of P-θ, Variation of P-V, NHRR, MFB, MGT	CO, NO_X, HC
0.780							
0.833							
0.874							
0.926							
0.972							
1.002							
1.052							
1.109							
***MBT obtained for CR 12**							

The CR is progressively advanced from CR 8 to 14 for each operating speed of the engine by retaining the ER almost constant (ϕ = 0.80~0.83). The optimum CR is identified over the operating speed range of the engine based on the overall performance of the engine. The experimental matrix for the optimization of the CR over the operating speed range of the engine is shown in **Table 5. 2**. Further, at the 3rd stage of the investigation, the influence of

operating ER (ϕ) over the operating speed range of the engine is identified for the optimum CR and IT setting of the engine. The ER is progressively varied from 0.744 to 1.109 (A/F ratio: 5.11 to 7.16) over the operating speed range for the optimum CR and IT configuration. Based on the overall performance, the optimum ER is identified over the operating speed range of the engine. **Table 5. 3** depicts the experimental matrix to investigate the influence of operating ER over the speed range and at the optimum CR and IT setting of the biogas fueled engine.

5.1.2 Experimental procedures

The retrofitted VCR SI engine (Engine 2) test rig shown in **Fig. 3. 9** and **Fig. 3. 10** is operated with biogas for the current investigation. The engine is mounted with a customized VCR mechanism, specially designed biogas induction mechanism and a reprogrammable ECU controlled DIS. The biogas induction mechanism supplies a metered quantity of H_2S scrubbed, preheated biogas to the engine intake system just at the upstream of the throttle body unit through a T-type air-fuel mixture. The customized VCR mechanism and the ECU controlled DIS enables the engine to operate with a CR ranging from 8 to 17.5 and IT ranging from 1 to 55^o CA bTDC, respectively. The speed of the engine is varied by controlling the applied load and is maintained in between 1400 rpm to 1700 rpm for each operating CR of the engine. Present choice of the speed range is based on the maximum rated speed of the engine and limitations on its idling speed due to possibility of engine operation with multiple fuels. Subsequently, the engine is only operated at WOT condition in each set of experiment. The throttle position is maintained 90% of total throttle opening at WOT condition.

To initiate the investigation, the VCR SI engine is started by gasoline at a desired CR and throttle setting. Subsequently, the throttle position is slowly increased to attain the WOT condition. The engine speed is controlled simultaneously by applying adequate amount of load through the eddy current dynamometer. In this process the outlet water temperature from the engine jacket is closely monitored till the engine attains the steady state condition. For the current investigation, the steady sate condition corresponds to 60° C engine jacket water outlet temperature. Once the engine is stabilized, the ECU is reconfigured through the PE3 interface and the IT is customized to 23^o CA bTDC. At the same instance, the biogas fuel line valve is

opened to mix with the inducted air before entering the engine manifold. The preheated biogas leaving the diaphragm pump at 1.3 bar and 45-46^{o} C is allowed to enter the T-type air biogas mixer. Soon after supplying the preheated biogas to the engine, the applied load on the engine is lowered without altering the TP followed by disengagement of petrol injector. Further, the air-fuel (air-biogas) adjustment knob on the diaphragm pump is tuned to stabilize the engine speed. Once the speed of the engine is stabilized, desired engine speed is set by controlling the load on the engine. Now the engine solely runs with biogas and after retaining steady state condition, the test data (performance, combustion and emission) are recorded in a NI USB 6210 DAS through the "Enginesoft" interface for 50 engine cycles (18000 data points) for each combination of IT, CR and engine speed.

For investigating the influence of IT at any operating CR, the ER and engine speed are kept constant. The IT is progressively advance from 23-53^{o} CA bTDC over the operating CR range of CR 8 to 14, while the engine speed and ER are maintained constant at 1650 rpm and 0.79~0.80 respectively. Further, the influence of IT over the variable speed range of the engine (1400 to 1700 rpm) is also analysed for each operating CR of the engine. Similarly, to investigate the influence of CR at any operating speed, the CR is progressively advanced form CR 8 to 14 with the respective optimized IT and over the operating speed range of engine. The operating ER is almost kept constant and maintained at 0.80~0.83 during this investigation. Further to investigate the influence of operating ER with the optimized CR and IT configuration of the engine, the operating ER is progressively advanced from 0.744 to 1.11 at 1650 rpm. The concentrations of the CO, CO_2, HC and NO_x in the exhaust emission of the biogas operated VCR SI engine are recoded with an AVL DIAGAS 444N gas analyzer. The operating procedure and specification of the gas analyzer are described respectively in *section 3.3.2 and* ***Table B-2*** of ***Appendix B.*** Each set of experiments is repeated thrice to ensure the correctness of the capture data. The average of these data is considered for the evaluation of different engine parameters. The uncertainties associated with the different parameters of the biogas fueled VCR SI engine test rig at CR 12 and WOT are evaluated following the root mean square technique (Kline and McClintock, 1953; Moffat, 1982) and presented in **Table 5. 4**.

Table 5. 4: Uncertainties associated with the performance parameters

Derived Parameters		Systematic Uncertainty (%)	Random Uncertainty (%)	Overall Uncertainty (%)
Performance Parameter	A/F	± 0.70	± 1.46	± 1.64
	BT	± 0.25	± 0.11	± 0.27
	BP	± 0.39	± 1.26	± 1.34
	BTE	± 0.80	± 1.48	± 1.70
	BSFC	± 0.63	± 1.91	± 2.02
	VE	± 0.58	± 0.77	± 0.96
Combustion parameter	NHRR	± 0.28	± 0.38	± 0.48
	MGT	± 0.57	± 0.48	± 0.75
	MFB	± 0.28	± 0.28	± 0.40
Emission parameter	CO	± 3	± 3.87	± 4.9
	CO_2	± 3	± 1.88	± 3.5
	HC	± 3	± 4.37	± 5.30
	NO_X	± 1	± 3.63	± 3.7

5.2 Influence of the IT Over the Operating CR and Speed Range of the Biogas Fueled SI Engine

The present investigation plays a vital role to enhance the performance of the biogas fueled SI engine by exploring the influence of IT over a range of operating CR and engine speed. Therefore, to accomplish the above cited objective, experiments are outlined to arrive at an optimum IT or MBT timing at each operating CR of the biogas fueled SI engine. The influence of operating ITs (23 to 53ºCA bTDC) are observed through the performance, combustion and emission characteristics of the biogas fueled engine for each operating CR (8 to 14) while the ER (0.79~0.80) and engine speed are maintained constant at WOT. The observed characteristics of engine at different ITs over the operating CR range is only summarized here for engine speed of 1650 rpm. Further, to evaluate the influence of IT over the operating speed range, the engine is operated over 1400-1700 rpm at each IT and CR configuration by maintaining the ER (0.79~0.80) constant at WOT condition. Based on the experimental evidence, the influence of IT over the operating CR and speed range of the engine is summarized here in this section.

5.2.1 Performance analysis

The present section evaluates the influence of operating IT on the performance characteristics of the biogas fueled SI engine at different CRs. The performance characteristics, such as BT, BP, BSFC, BTE, VE and ER are evaluated from *Eqs. D1-D11of* **Appendix *D***. **Fig. 5. 1** and **Fig. 5. 2** explains the influence of IT on the developed BT and BP of the engine over the operating CR at WOT and 1650 rpm. As observed from **Fig. 5. 1**, the IT of the engine is progressively advanced from 23 to 55^{o} CA bTDC for each operating CR by maintaining the ER approximately constant (0.79 ~0.80) at 1650 rpm. Irrespective of the operating CR, the progressive advance of IT recorded a satisfactory development of the induced BT and archives the MBT followed by the declined BT at the over advanced ITs. The development of BT may be attributed due to the faster flame propagation rate and increased expansion work at advanced ITs up to the point of MBT. The faster flame propagation speed reduced the combustion duration which enhance the peak pressure and NHRR to produce maximum expansion work compared to the other cases of IA (Sadiq Al-Baghdadi, 2004). However, the declined BT at the over advanced ITs may be endorsed due to the enhanced compression work caused by the increased pressure and temperature before the TDC (360^{o} CA). Further, the CA at which the obtained BT and BP are found maximum are different for each operating CR and designated as the MBT timing or MBT IT for the respective operating CR (Chaudhari et al., 2019).

The MBT timings are found retarding (shift closer to TDC) with progressive rise in the operating CR. Increasing the operating CR, from CR 8 to CR 9, CR 10, CR 11, CR 12, CR 13 and CR 14 has enhanced the MBT by 10%, 14.5%, 33.6%, 49.7%, 42.9% and 39.6%, and retarded the MBT timing by 4°CA, 8°CA, 14°CA, 20°CA, 24°CA and 28°CA respectively. The magnitude of the MBT over the operting compression ratios are repoted 13.3 N-m, 14.6 N-m, 15.2 N-m, 17.8 N-m, 19.9 N-m, 19 N-m and 18.6 N-m at 53°CA, 49°CA, 45°CA, 39°CA, 33°CA, 29°CA and 25°CA bTDC, respectively for CR 8, CR 09, CR 10, CR 11, CR 12, CR 13 and CR 14. Thus, it is evident that the MBT timing is retarding (shift towards TDC) as the operating CR increases (Sadiq Al-Baghdadi, 2004; Porpatham et al., 2012). This may be due to the increased pressure and temperature at the end of compression stroke along with reduced fraction of residual gas at higher CR. This phenomenon creates a favorable condition for reduction of ignition lag and enhances the flame speed. It is also noticed that, the BT obtained

with CR 12 is 19.9 N-m and found maximum among all the operating CRs. The same trend is also followed by the BP curve over the operating range of IT and CR of the engine at 1650 rpm and reflected in **Fig. 5. 2**. The enhancement in the maximum BP of the engine is recorded 10%, 14.5%, 33.6%, 49.7%, 42.9% and 39.6% respectively for CR 9, CR 10, CR 11, CR 12, CR 13 and CR 14and observed respectively at 53°CA, 49°CA, 45°CA, 39°CA, 33°CA, 29°CA and 25°CA bTDC. The BP obtained at CR 12 and MBT timing of 33°CA bTDC is 3.08 kW and reported maximum among all the operating CRs.The summary of MBT timing, MBT and maximum BP with respect to the ratio of engine volumes are shown in **Table 5. 5** for different CRs at 1650 rpm of the biogas operated SI engine.

It has been observed that the obtained MBT timings for the operating CR range of the engine are only acceptable at 1650 rpm. Whereas, the engine speed also plays a key role to identify the MBT timing over the operating CR range of the engine. Hence, the influence IT over the operating speed range of the engine is investigated for each operating CR of the engine. However, the findings are concise here and the obtained MBT timings for the operating speed range of the engine are presented at each CR in **Fig. 5. 3**. It can be observed that, the obtained MBT timings are progressively advanced by certain CA with increasing engine speed irrespective of the operating CR. It has relevance with the shorter time interval of combustion process with increment in engine speed due to turbulence (Sadiq Al-Baghdadi, 2004). As the engine speed increases, the turbulence inside the engine cylinder increases and leads to increase the flame speed. However, in the present case, the effect of engine speed on the MBT timing of the biogas fueled SI engine at any operating CR is seen to have less dependence on the operating speed of the engine. For example, as shown in **Fig. 5. 3**, the MBT timing increases from 31 to 35 °CA bTDC when the engine speed was increased from 1400 to 1700 rpm at CR 12. Similarly, for the present speed variation, the MBT timing is found to fluctuate in a narrow range over the operating CRs of the engine. Hence, the MBT timings obtained for respective CRs at 1650 rpm are considered for the further discussion.

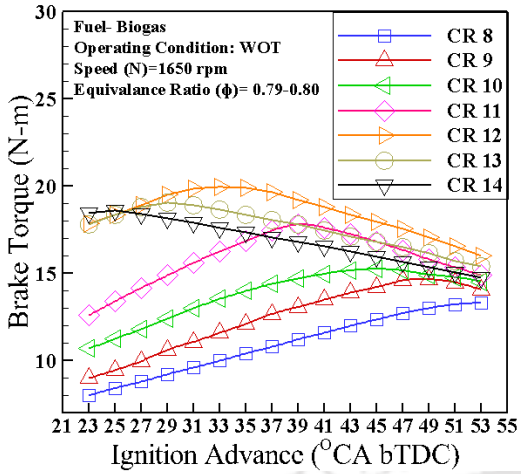

Fig. 5. 1: Effect of IA on the BT over the operating CR range of biogas fueled SI engine

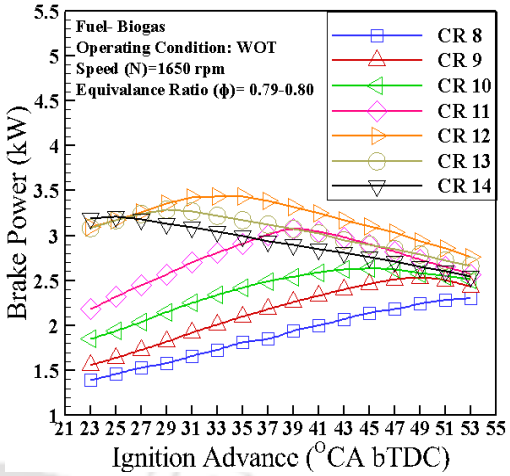

Fig. 5. 2: Effect of IA on the BP over the operating CR range of biogas fueled SI engine

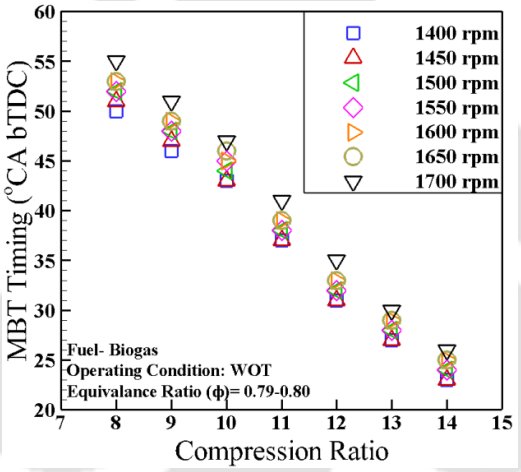

Fig. 5. 3: Effect of engine speed on the MBT over the operating CR range of the engine

Table 5. 5: Summary of MBT timing, MBT, BP, BSFC and BTE at different operating CR

CR	Bore/ Stroke	Engine speed	MBT timing	Maximum BT MBT	Maximum BP	Minimum BSFC	Maximum BTE
	(D_b/L_s)	(rpm)	(°CA bTDC)	(N-m)/ CC	(kW)/ CC	(kg/kW-h)	(%)
8	0.795	1650	53°	0.020	0.0034	0.94	22.5
9			49°	0.022	0.0038	0.85	24.8
10			45°	0.023	0.0040	0.82	25.8
11			39°	0.026	0.0044	0.76	27.9
12			33°	0.028	0.0047	0.71	29.8
13			29°	0.027	0.0046	0.71	29.7
14			25°	0.027	0.0046	0.73	29.1
Engine Swept Volume (V_S) = 661.453 CC							

The effect of IA on the BSFC and BTE of the biogas fueled SI engine is depicted in **Fig. 5.** 4 and **Fig. 5.** 5 respectively over the operating CR range of the engine. Irrespective of the operating CR, the BSFC of the engine drops down consistently with the progressive advance of IA up to the MBT timing and ascends further with the over advanced IT.

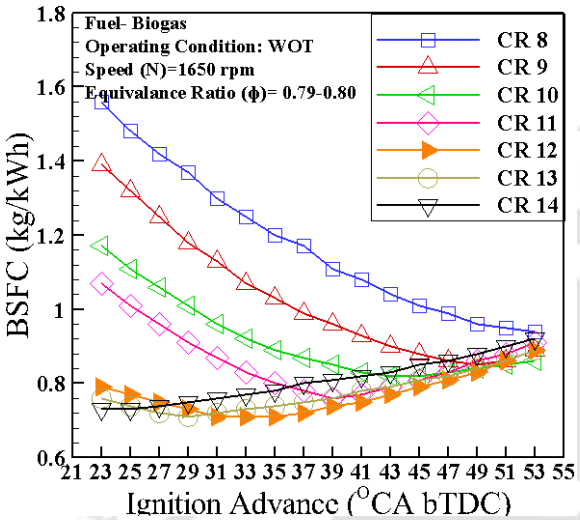

Fig. 5. 4: Effect of IA on the BSFC over the operating CR range of biogas fueled SI engine

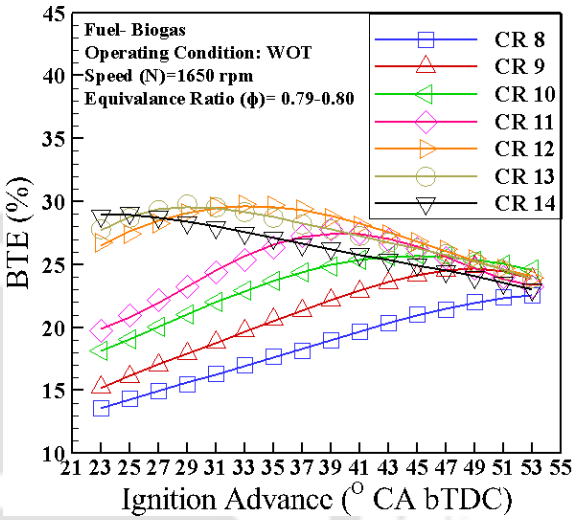

Fig. 5. 5: Effect of IA on the BTE over the operating CR range of biogas fueled SI engine

Similarly, the progressive rise in operating CR reduced the BSFC up to CR 12 and increased with further rise in operating CR. The minimum BSFC is observed at the respective MBT timing for the operating CR. The IT at which minimum BSFC is observed retires with the increased CR. The BSFC is mostly influenced by the mass of the fuel consumed and the developed BP. As the mass flow rate of the biogas is almost kept constant (2.16 to 2.24 kg/h), the developed BP only influences the pattern of BSFC. The least BSFC observed is 0.71 kg/kW-h with CR 12 at 33°CA bTDC. The rise in operating CR reduced the BSFCs by 9.2 %, 12.7 %, 18.9 %, 24.3%, 24.2% and 22.4%, respectively at CR 9, CR 10, CR 11, CR 12, CR 13 and CR 14 with reference to CR 08. Similarly, irrespective of the operating CR, the progressive advance of IT enhanced the BTE of the engine up to the MBT timing and declined further with the over advanced IT. The rise in operating CR enhanced the BTE up to CR 12 and declined with further increased CR. The rise in operating CR shifts the points of maximum BTE to the respective MBT timing. The rise in operating CR enhanced the BTE by 10.1 %, 14.5%, 23.3

%, 32.1 %, 31.9% and 28.9%, respectively at CR 9, CR 10, CR 11, CR 12, CR 13 and CR 14 with reference to CR 08. The maximum BTE of the biogas fueled SI engine is reported 29.8% with CR 12 at the IA of 33°CA bTDC. *Table 5.5* also listed the minimum BSFCs and the maximum BTEs of the biogas fueled SI engine over the operating CR and IA range.

5.2.2 Combustion analysis

The higher CO_2 content and the auto ignition temperature of biogas enabled the SI engines to operate at higher CR. However, the combustion process of biogas is completely dependent on the flame front propagation and auto ignition temperature. Hence, it is essential to identify the limiting CR and optimum IT configuration for the biogas fueled SI engine. If the charge is ignited too early, the peak pressure may arise before the TDC and increases the compression work. Achieving the peak pressure before the TDC may also auto ignite the air-biogas mixture. Further, if the ignition is too late the peak pressure will arise much later in the expansion stroke, which may reduce the expansion work due to incomplete combustion. Hence, before identifying the optimum IT for the present configuration of the engine, the aspects mentioned above have been thoroughly investigated over the operating CR range. The cylinder pressure (P) and crank angle (θ) data are captured for 50 consecutive cycles for each experiment. The combustion parameters viz. P-V, NHRR, MFB and MGT are evaluated from the average P-θ data by following the *Eqs. D12-D25* of ***Appendix D*** as referred in the open literature (Heywood, 1988; Stone, 2012). The overall uncertainties associated combustion parameters of the biogas fueled SI engine (*Engine 2*) are mentioned in ***Appendix F***.

Fig. 5. 6 and **Fig. 5. 7** depict the effect of IA on the PCP and LPP over the operating CR range of the biogas fueled engine at WOT condition. To investigate the effect of IA, the engine speed (1650 rpm) and ER (0.79~0.8) are maintained constant for each operating CR of the engine. The PCP and LPP at the operating CR against each operating IA is represented **Table 5. 6**. As the IA is progressed bTDC, the PCP increases significantly (**Fig. 5. 6**) and shifts the LPP close to the TDC (**Fig. 5. 7**) irrespective of the operating CR. The above happenings may be attributed due to the accelerated combustion process which enhanced the in cylinder gas temperature and led to rise in cylinder pressure with progressive IA (Papagiannakis and Zannis,

2013). Further, with progressive rise in operating CR there is a considerable growth in PCP (**Fig. 5. 6**) and shift of LPP close to the TDC (**Fig. 5. 7**) irrespective of the operating IT.

Table 5. 6: PCP and LPP at different operating IA and CR combination

IA	CR 08		CR 09		CR 10		CR 11		CR 12		CR 13		CR 14	
	PCP	LPP	PCP	LPP	PCP	LPP	PCP	LPP	PCP	LPP	PCP	LPP	PCP	LPP
23	8.5	33	10.7	26	13.2	23	18.3	18	21.8	17	24.3	17	27.2	16.0
25	8.9	32	11.3	26	13.8	23	19.0	18	23.1	17	25.3	15	**27.9**	**15.0**
27	9.7	31	12.7	25	15.4	22	20.8	17	25.6	16	27.7	15	30.0	14.0
29	9.8	31	13.0	24	15.9	20	21.2	17	25.9	16	**29.5**	**14**	31.4	12.0
31	10.2	29	13.7	23	16.8	20	22.9	16	27.3	14	30.5	12	32.4	11.0
33	11.6	28	14.9	22	17.2	19	24.0	14	**28.1**	**13**	31.2	11	33.2	10.0
35	12.2	28	15.2	22	18.7	19	24.5	14	28.7	13	31.2	10	33.9	9.0
37	12.5	27	15.8	21	19.4	17	26.5	13	29.4	12	32.5	10	34.1	9.0
39	13.0	27	16.3	20	20.8	17	**28.4**	**13**	30.9	11	32.9	9	34.6	8.0
41	13.6	26	16.6	19	21.3	15	28.9	11	31.0	10	33.1	9	35.2	8.0
43	14.4	24	17.9	19	22.9	**14**	29.2	10	31.7	10	33.1	8	35.9	7.0
45	15.1	24	18.0	18	**23.2**	14	31.2	9	32.9	9	36.1	7	38.1	6.0
47	15.5	23	18.7	17	23.8	12	31.1	9	33.5	9	36.7	7	38.4	6.0
49	16.2	22	**19.0**	**17**	24.7	11	31.5	8	34.9	7	37.2	6	38.6	5.0
51	16.1	21	19.2	15	25.9	10	32.3	7	35.1	6	37.5	5	39.2	4.0
53	**16.9**	**21**	21.1	14	26.6	9	32.8	6	35.3	6	38.6	5	39.4	4.0

IA – Ignition advance (^{o} CA bTDC); PCP- Peak cylinder pressure (bar); LPP- Location of peak cylinder pressure (^{o} CA aTDC)

The LPPs are observed very close to TDC (within 10-12^{o} CA aTDC) at CR 11, CR 12, CR 13 and CR 14 beyond the progressive IA of 35^{o} CA bTDC. Hence, the engine may experience increased compression work when operated beyond 35^{o} CA bTDC at CR 11, CR 12, CR 13 and CR 14. Although, the rise in PCP and shifting of PCP close to TDC are the positive indications of improved combustion process, the state of cylinder pressure and temperature of the gas mixture just before the TDC contribute a crucial role to identify the optimum IT for the engine (Sadiq Al-Baghdadi, 2004). Further to identify the optimum IT and verify the claimed MBT in **Table 5. 5** for each operating CR of the engine at *section 5.2.1*, the average pressure, *P-V*, MGT, NHRR and MFB curves are analyzed carefully. However, it is not possible here in this section to represent the data of all these curves for the mentioned CR range of the engine. Since, the nature and pattern of these data are exactly similar for all

operating CRs of the engine; the data of CR 12 is only represented here over the operating IA range of the engine and carefully analyzed.

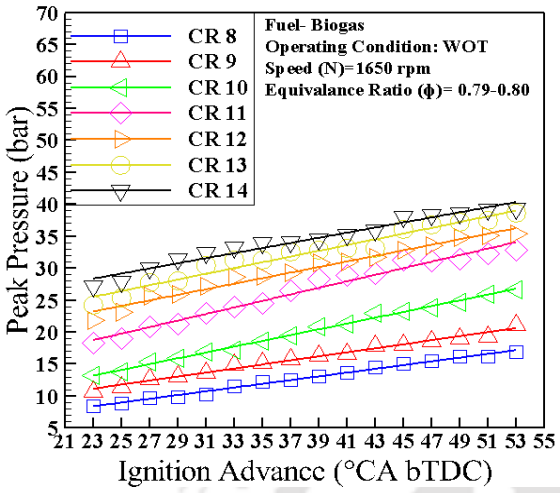

Fig. 5. 6: Effect of IA on the PCP over the operating range of CR at 1650 rpm

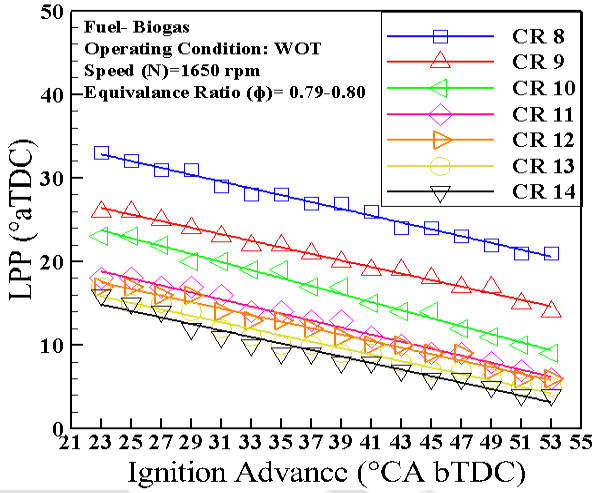

Fig. 5. 7: Effect of IA on the LPP over the operating range of CR at 1650 rpm

Table 5. 7: Summary of ACP and MGT just bTDC, PMGT, LPMGT, PNHRR, and LPNHRR over the operating IA range at CR 12

IA (°CA bTDC)	CR	ACP just bTDC (bar)	MGT just bTDC (K)	PMGT (K)	LPMGT (° CA)	PNHRR (J/°CA)	LPNHRR (° CA)
23	12	15.2	371.7	850.6	392	19.7	372
25		15.3	376.2	877.6	390	20.5	371
27		15.5	377.7	883.2	391	20.7	371
29		16.1	378.8	894.7	389	21.0	370
31		16.5	406.7	895.3	388	21.2	369
33		17.4	428.5	905.1	387	21.4	368
35		18.4	455.5	904.3	386	20.6	365
37		19.2	476.3	898.4	385	20.9	365
39		21.6	539.9	904.6	384	16.0	361
41		22.5	560.2	903.6	383	15.8	361
43		23.9	593.3	904.8	382	15.1	359
45		26.1	647.6	904.4	379	15.0	358
47		25.9	666.3	904.2	380	14.3	358

Fig. 5. 8 and **Fig. 5. 9,** illustrates the effect of IA on the average cylinder pressure (ACP) and MGT of the wide-open throttled biogas fueled SI engine at CR 12 and 1650 rpm. As

observed, with the progressive IA, the slope of the pressure and temperature gradients are constantly increasing just before the TDC. The average cylinder pressures (ACP) and MGT recoded just before the TDC (359° CA) are listed in **Table 5. 7** for the IA range of 23° to 47° CA bTDC. The PMGTs are found increasing with progressive IA up to 33° CA bTDC and reported 905 K and found maximum at 387° CA. As claimed in *section 5.2.1*, the MBT timing for CR 12 is 33° CA bTDC. Whereas, the ACP and MGT profiles depicted in **Fig. 5. 8** and **Fig. 5. 9** are found lower at the point of ignition with over advanced ITs beyond 33° CA bTDC. Further, the profile of ACP and MGT of the over advanced ITs (beyond 33°CA bTDC) are overriding the ACP and MGT profiles of the former ITs at 339° CA. The overriding profile of ACPs and MGTs at the over advanced ITs are the consequence of greater proportion of combustion event exhibited during the compression stroke and resulted in higher pressure and temperature before the TDC. Hence, it may increase the compression work transfer and reduced the network output at the over advanced ITs beyond the claimed MBT timing of 33°CA bTDC. Similar observation are also reported in open literature for 39% throttled biogas fueled SI engine operating at CR 15.5:1 and reported knock intensity close to 2.5 (Jaramillo et al., 2018).

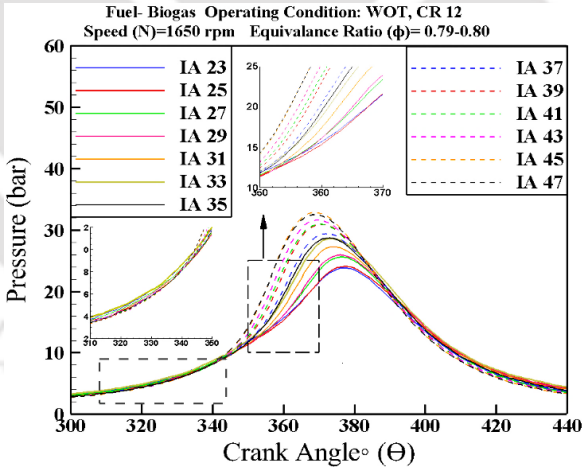

Fig. 5. 8: Effect of IA on the average cylinder pressure at CR 12

The claimed MBT timing at CR 12 is also justified by the P-V plot in **Fig. 5. 10**. It can be observed that, although PCPs are constantly increasing with progressive IA, the area under the *P-V* curve is found maximum at 33°CA bTDC. The area under the P-V curve which

represents the network output during the cycle found improving up to the MBT timing. The above happening may be attributed due to the faster flame propagation (shorter combustion duration), resulting in improved thermal efficiency and power output at 33^{o} CA bTDC. Hence from the above cited experimental evidences, the MBT claimed at CR 12 may be considered as the optimum IT. Similar observations are also recorded from the PCP, LPP, P-θ, MGT and P-V plots over the operating CR range of the engines. The claimed MBT timings at the above cited CRs can also be justified through the similar combustion analysis. Hence, the claimed MBT timings are considered as the optimum IT and recoded 53 ^{o} CA,49 ^{o} CA,45 ^{o} CA,39 ^{o} CA,33 ^{o} CA,29 ^{o} CA and 25 ^{o} CA bTDC, respectively at CR 8, CR 9, CR 10, CR 11, CR 12 CR 13 and CR 14. The open literature suggests very close recommendation. 25^{o} CA bTDC is the best IT configuration to have improved combustion process and better stability for the lean fueled (ER: 0.6) biogas combustion at CR 15.5 and 3000 rpm (Jaramillo et al., 2018) .

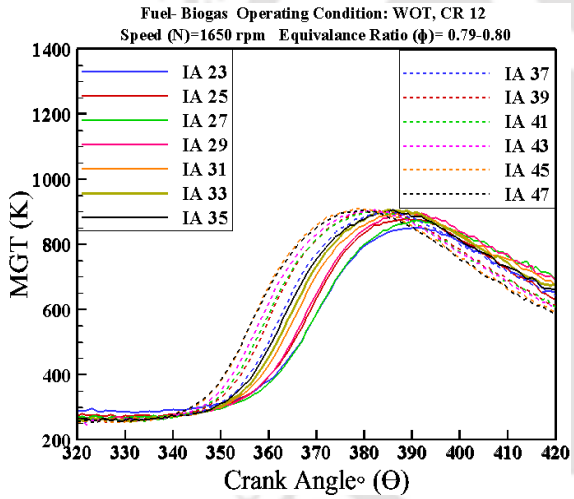

Fig. 5. 9: Effect of IA on the MGT of the biogas fueled engine at CR 12

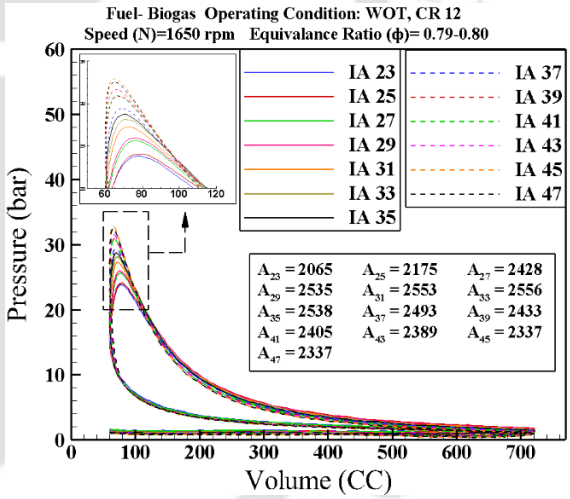

Fig. 5. 10: Effect of IA on the area under the P-V curve at CR 12

The NHRR at CR 12 is evaluated by applying the 1st law analysis to the combustion chamber and considering the content of the combustion chamber as a single zone model. It is assumed that the combustion products and reactants are thoroughly mixed in the combustion chamber, and there is no mass transfer across the control volume. The variation of NHRR with progressive IA of the biogas operated SI engine operating at CR 12 is shown in **Fig. 5. 11**. The NHRR is found improving with progressive IA up to 33^{o} CA bTDC and observed maximum at this IT. The above phenomenon is attributed due to the faster flame propagation rate of

biogas where the energy conversion efficiency is maximum (Kemal and Sayin, 2014). However, with progressive IA beyond 33ºCA bTDC, the PNHRRs is dropped due to the increased compression work and rapid conversion of the heat energy to accommodate the negative work done before the TDC. Further, it is also noticed that, with over advanced IT beyond 35º CA, the peak neat heat release rates (PNHRR) are observed before TDC. Hence, it could be concluded that almost 40-60% of the inducted charge is combusted by the end of compression stroke in case of over advanced ITs beyond 35º CA bTDC. The state of ACPs and MGTs developed just before TDC at the over advanced ITs are because of the profile of PNHRRs and are the key factors to increasing the compression work. The peak neat heat release rate (PNHRR) and the location of the peak net heat release rate (LPNHRR) are listed in **Table 5. 7**. As observed, the LPNHRR shifts closer to the TDC with the progressive advance of IT bTDC. The maximum NHRR is observed at 33º CA bTDC (at the MBT timing) and reported 21.4 J/ ºCA at 368 ºCA for the wide-open throttled biogas engine. The above happenings may be attributed due to the reduced combustion duration (minimum rapid burn angle) at 33º CA bTDC.

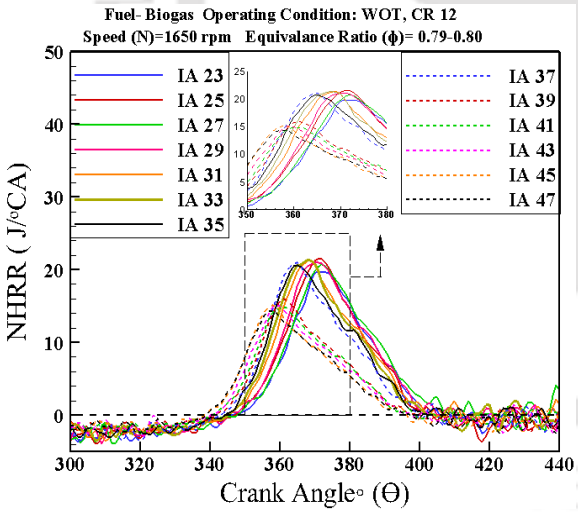

Fig. 5. 11: Effect of IA on the NHRR of the biogas fueled engine at CR 12

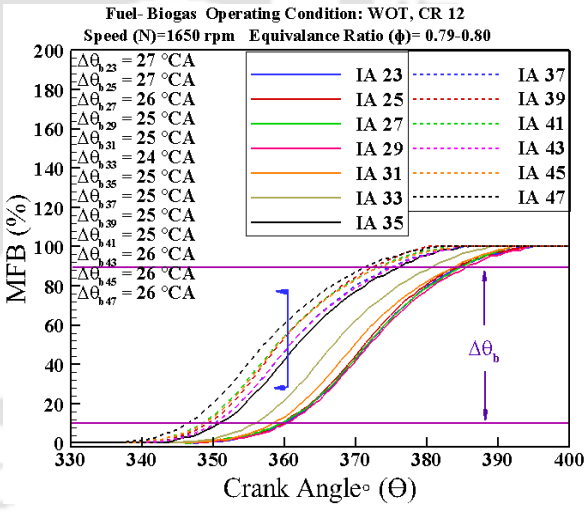

Fig. 5. 12: Effect of IA on the MFB of the biogas fueled engine at CR 12

Fig. 5. 12 describes the effect of IA on the mass fraction burnt (MFB) for the biogas fueled SI engine operating at WOT at CR 12. The MFB is evaluated following the method proposed by Rassweiler and Withrow (Rassweiler and Withrow, 1938). The rapid burn angle (RBA) '$\Delta\theta_b$' is consider as the crank angle interval between the end of flame development

(mass fraction burnt of 10%) and the end of flame propagation (mass fraction burnt of 90%)stage (Heywood, 1988). As observed**,** the flame development is progressively advanced before TDC with advanced IT. With advanced ITs, the combustion events are progressively initiated just before the TDC towards the end of compression stroke. However, the flame initiation is noticeably delayed with advanced IT. As recoded, the ignition delay, the combustion event and the flame development (mass burn fraction 0-10%) are initiated earlier during the end of the compression stroke and advanced progressively before the TDC due to the advancement of IT bTDC. However, as the combustion is initiated before the piston reaches the TDC, the fresh air-fuel mixtures are being pushed towards the developing flame front. As a result, the flame propagation rate increases and reduces the combustion duration with progressive IA bTDC. Along with the further advanced IT, the in-cylinder pressure and temperature drop, resulting in higher cyclic variation in flame development and propagation stage during the combustion process. Hence beyond the optimum IA, the flame propagation rate is decreased by extending the combustion duration. Researchers also noticed similar observations (Ma et al., 2012; Jaramillo et al., 2018) for biogas and hydrogen operated SI engines at different operating conditions.

5.2.3 Emission analysis

The effect of CR and IA on the carbon monoxide (CO) emission of the biogas fueled engine at running a constant speed (1650 rpm) is shown in **Fig. 5. 13** for WOT condition. It can be seen that; the CO emission is decreasing with progressive advance of IA irrespective of the CR. Furthermore, at a constant IA, the percentage of CO in the exhaust gas increases up to CR 12 and afterwards follows a declining trend. However, from **Fig. 5. 14**, a contrary trend is seen with CO_2 emission being minimum at CR 12 at a fixed IA. Also, almost an increasing trend of CO_2 emission is observed with advanced IA irrespective of the CR. The CO formation is rate is primarily dependent on the rich equivalence ratios due to incomplete combustion. However, the unburnt gaseous fuel in the engine cylinder and the cylinder charge temperature are also equally responsible for the formation of CO as well as control the rate of fuel decomposition and oxidization (Papagiannakis and Zannis, 2013). In the present case, with lean equivalence ratio (0.79-0.80), CO can be present to owing to dissociation of CO_2 and its

concentration reduces with reducing combustion temperature. Although the peak MGT is increasing with the advanced IT, the average combustion temperature is found decreasing with progressive advance of IT. The average combustion temperature at CR 12 was reported 642°C, 606°C, 586°C, 542 °C, 517°C, 488°C and 467°C respectively, at the IA of 25 °CA bTDC, 29 °CA bTDC, 33 °CA bTDC, 39 °CA bTDC, 45 °CA bTDC, 49 °CA bTDC and 53 °CA bTDC. Hence, it can be justified that, the higher CO_2 content and chemical kinetics of biogas combustion with lean mixture leads to increased CO and decreased CO_2 emission with progressive advance of IT (Fisher et. al., 2015). The equivalent CO, HC and NOx emissions are presented in g/kWh scale and compared with BS-VI standard in **Table 5. 8**. For the optimum CR and IT configuration of the engine (CR:12, IT: 33 °CA bTDC), the CO, HC and NOx concentration are reported 3.20 g/kWh, 0.22 g/kWh and 11 g/kWh, respectively.

Table 5. 8: Summary of CO, HC and NOx emission at different IA and CR setting

IA	CR	CO			HC		NO_x		HC+ NO_x
		(vol %)	(g/kWh)	*Std	(ppm)	(g/kWh)	(ppm)	(g/kWh)	*Std
25	10	0.09	3.23		106	0.21	1774	12	
	12	0.112	4.02		86	0.17	2001	13	
	14	0.078	2.80		104	0.21	1485	10	
29	10	0.079	2.84		112	0.22	1598	11	
	12	0.096	3.45		98	0.20	1833	12	
	14	0.064	2.30		117	0.23	1286	9	
33	10	0.07	2.51		124	0.25	1369	9	
	12	0.089	3.20	≤ 250[#]	110	0.22	1609	11	≤ 12[#]
	14	0.052	1.87	≤ 3.5[$]	127	0.25	1182	8	≤ 7.5[$]
39	10	0.049	1.76		139	0.28	955	7	
	12	0.07	2.51	*Std.(The Gazette of India, 2016) (g/kWh)	126	0.25	1139	9	*Std.(The Gazette of India, 2016) (g/kWh)
	14	0.038	1.36		140	0.28	918	6	
45	10	0.035	1.26		156	0.31	807	5	
	12	0.062	2.23		141	0.28	1043	7	
	14	0.03	1.08		158	0.32	696	5	
49	10	0.032	1.15		168	0.34	682	5	
	12	0.056	2.01		153	0.31	884	6	
	14	0.024	0.86		167	0.33	594	4	
53	10	0.03	1.08		177	0.35	496	3	
	12	0.048	1.72		164	0.33	596	4	
	14	0.018	0.65		175	0.35	451	3	

*Emission standard set by the Govt. of India for the [#]genset run on petrol and natural gas (NG) or petrol and liquid petroleum gas (LPG) and [$] genset run on dedicated natural gas (NG) or liquid petroleum gas (LPG) as mentioned in GSR 281(E) dated 7th March 2016.

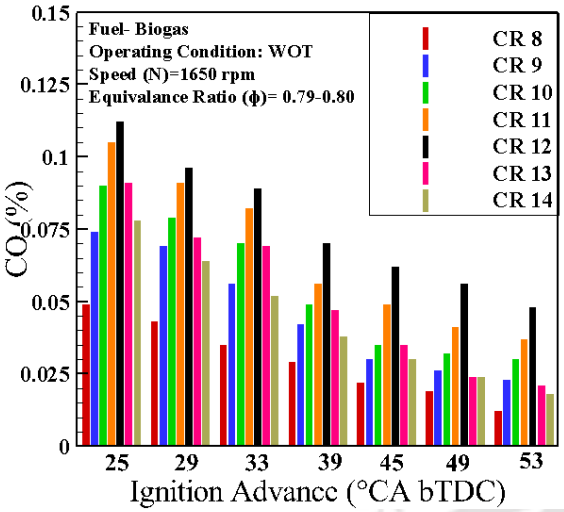

Fig. 5. 13:CO emission level at different IA and CR.

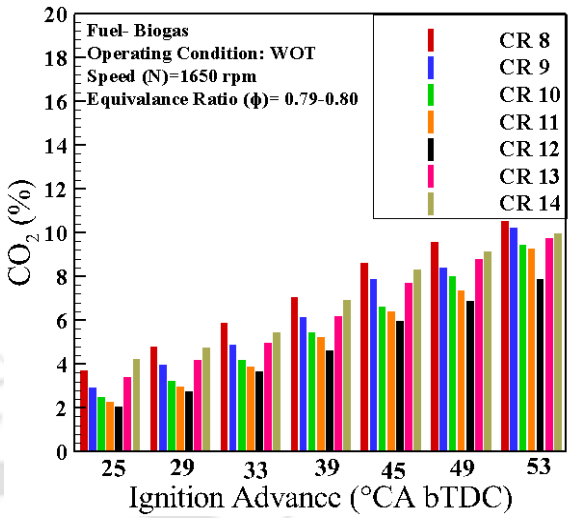

Fig. 5. 14: Percentage of CO_2 in the exhaust at varying CR and IA.

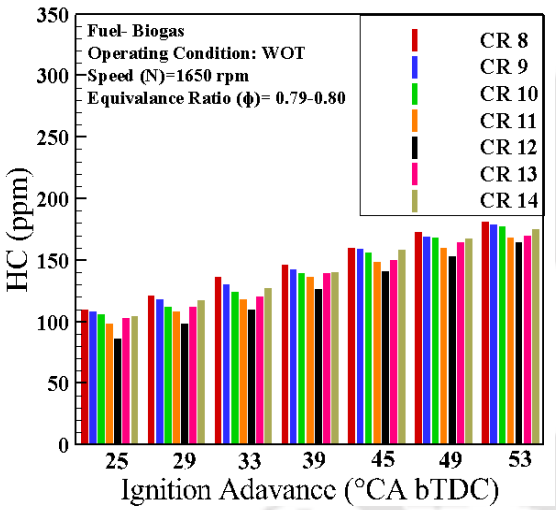

Fig. 5. 15: Emission level of HC with variation in IA and CR.

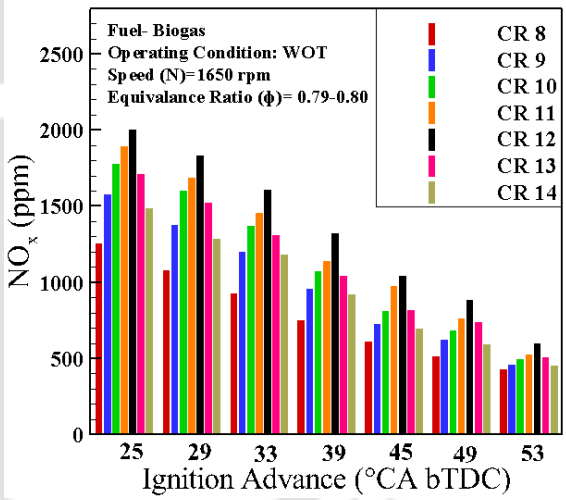

Fig. 5. 16: Effect of variation in CR and IA on NO_x level in exhaust gas.

Fig. 5. 15 and **Fig. 5. 16**, depict the effect of IA on the HC emission of the biogas fueled SI engine for different operating CR of the engine at 1650 rpm. HC emission seems to be identical for the extreme cases of the CR for a fixed IA with percentage of HC being the lowest for CR 12. Moreover, around 10-12% increase in HC level is evident with increase in IA for a constant CR. The maximum and the minimum HC emission was recoded with CR 14 and CR 08, respectively. Irrespective of operating CR, the maximum HC emission was recoded with advanced ITs. **Fig. 5. 16** signifies the effect on NO_x emission due to the considered variations

in CR and IA. The trend of variation in NO_x level in the exhaust is similar to that of the emission observed in the case of CO with NO_x level being maximum for CR 12. The NO_x formation mechanism is mostly influenced by the temperature profile of engine cylinder. In the present case, as the average MGT of the engine cylinder follows an increasing decreasing trend with advance IT. Hence resulted in reduced NO_x concentration with advanced IT. However, the maximum NO_x concentration was recoded with CR 12, irrespective of the operating IT. The recoded HC and NO_x concentration are found within the limiting emission level of BS VI.

5.3 Influence of CR and Engine Speed on the Overall Performance of the Biogas Fueled SI Engine

The present study plays a vital role to enhance the performance of the biogas fueled SI engine by exploring the influence of CR over the operating speed range of the engine at their obtained MBT timings. The outcome of the above cited objective are the critical or optimum operating CR and the engine speed combination that leads to the maximum output power and thermal efficiency for the given operating condition of the engine. To investigate the influence of CR and operating speed, the biogas fueled SI engine is operated with the obtained MBT timing for each operating CR of the engine by maintaining the ER almost constant (0.80~0.83). The CR of the engine is progressively varied from CR 08 to CR 14 at each operating speed of the engine and for each operating CR the speed of the engine is varied from 1400 to 1700 rpm. Further, the performance, combustion and emission analyses are carried out to find out the optimized CR and the speed range suitable for operating the biogas fueled SI engine. Based on the experimental evidence, the influence of CR over the operating speed range of the engine is summarized here in this section.

5.3.1 Performance analysis

The performance parameters like BT, BP, BSFC, BTE, VE and operating equivalence ratio are evaluated from the *Eqs.D1-D8* of ***Appendix D*** as referred in the literatures (Heywood, 1988; Stone, 2012). The average values of the data points obtained are considered for further analysis.

The influence of CR and the engine speed on the BT and BP of the biogas fueled SI engine operated with the corresponding MBT timing at WOT condition are shown in **Fig. 5. 17** and **Fig. 5. 18 .** It is observed that, with increasing CR, the BT and BP of the engine increase up to CR 12 and then decline further irrespective of the operating speed of the engine. Increment in CR beyond CR 12 has not resulted in any improvement either on BT or BP of the engine. This may be due to the pre-ignition conditions, wherein the auto ignition temperature attains much earlier in the compression stroke when operated beyond CR 12. The in-cylinder pressure and temperature, before the spark initiation, are higher at higher CRs and are mainly responsible for the deteriorated BT and BP. It may also be noted that, though the combustion pressure (peak cylinder pressure) in the expansion stroke increases at CR greater than CR 12, the benefit of additional indicated power does not compensate the mechanical losses from friction (Huang and Crookes, 1998a). Upon increasing the operating CR from CR10 to CR 11, the maximum BT and BP increase by 9.6 %. Similarly, further rise in operating CR enhances the maximum BT and BP by 20.5%, 19.5%, and 18.3% at CR 12, CR 13 and CR 14, respectively with reference to CR 10. The maximum BT and BP of the engine are observed at CR 12 and found 24 N-m and 3.52 kW, respectively at 1400 rpm. It is also noted that irrespective of the operating CR, the BT and BP followed an increasing trend with the decreasing speed of the engine.

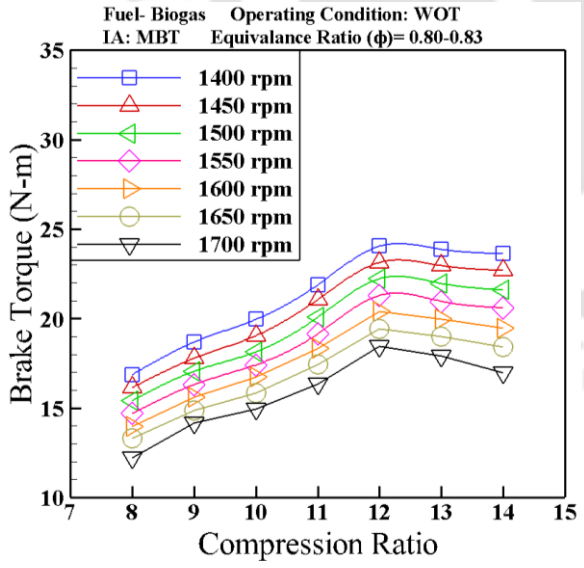

Fig. 5. 17: Effect of CR and engine speed on the BT of the biogas fueled SI engine

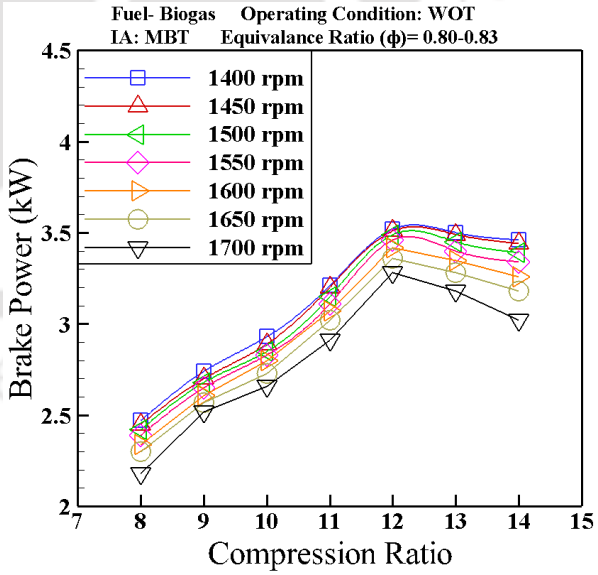

Fig. 5. 18: Effect of CR and engine speed on the BP of the biogas fueled SI engine

This has relevance with the fact that the rise in BT is directly related to the brake load and the brake load increases with decreasing engine speed for the variable speed of the engine since the TP was maintained at WOT condition. Additionally, the BP increases with increasing BT, but decreases with increasing speed of the engine. Irrespective of the operating CR, the maximum BT and BP of the engine are noticed at 1400 rpm. Moreover, at this engine speed (1400 rpm) the maximum BT and BP are only observed at CR 12 and reported be 24 N-m and 3.52 kW, respectively.

Fig. 5. 4 and **Fig. 5. 5** reveal the influence of CR and engine speed on the BSFC and BTE of the biogas fueled SI engine. Increase in CR brings an advantage of fuel economy attributing to the improved thermal efficiency. As shown in **Fig. 5. 19**, the BSFC of the biogas fueled SI engine decreases steadily with the rise in CR up to a critical point of CR 12. Enhancing the CR further deviates the trend and starts increasing the BSFC. This is because, with increasing CR up to CR 12, the mass of fuel consumed is lesser than the rise in BP and the mass of fuel consumed to generate unit BP is comparatively lesser at higher CRs. Beyond this critical CR, the mass of fuel consumed is higher than the rise in BP. Upon raising the CR from CR 10 to CR 11, the BSFC is seen to be reduced by 5.9% at 1400 rpm. Similarly, upon further raising the operating CR, the minimum BSFC gets reduced by 10.1%, 9.4% and 8.5% at CR 12, CR 13 and CR 14, respectively with reference to CR 10. Irrespective of the engine speed, the minimum BSFC is observed at CR 12 and found to be 0.66 kg/kW-h at 1400 rpm. It must also note that irrespective of the operating CR, the BSFC followed an increasing trend with increasing speed of the engine and the minimum and maximum values of BSFCs are observed at 1400 rpm and 1700 rpm, respectively. As shown in **Fig. 5. 20**, the BTE of the biogas fueled SI engine increases steadily with the rise in CR up to CR 12 and above this limiting CR, the BTE starts decreasing for higher CRs. The BTE of the engine gets enhanced by 4.2% at 1400 rpm for increment in CR from CR 10 to CR 11. Similarly, further rise in operating CR brings the improvement in peak BTE by 11.2%, 10.3%, and 9.26% at CR 12, CR 13, and CR 14, respectively with reference to CR 10. Irrespective of the engine speed, the maximum BTE is observed only at CR 12 which further has the maxima of 31.8% at 1400 rpm. Moreover, irrespective of the operating CR, the BTE followed a decreasing trend with increasing speed of the engine where it is found to be maximum at 1400 rpm.

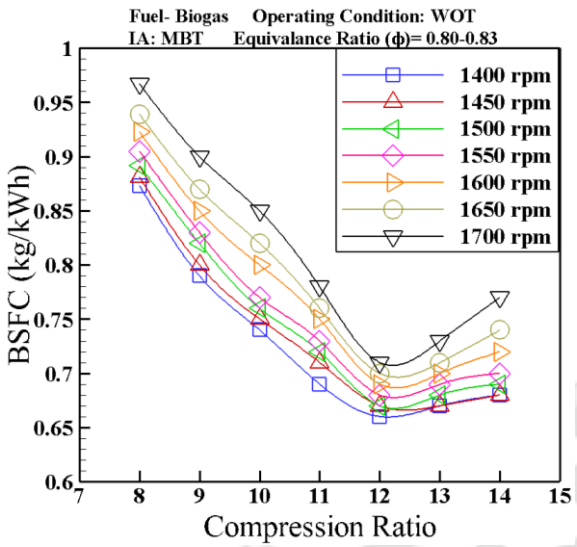

Fig. 5. 19: Effect of CR and engine speed on the BSFC of the biogas fueled SI engine

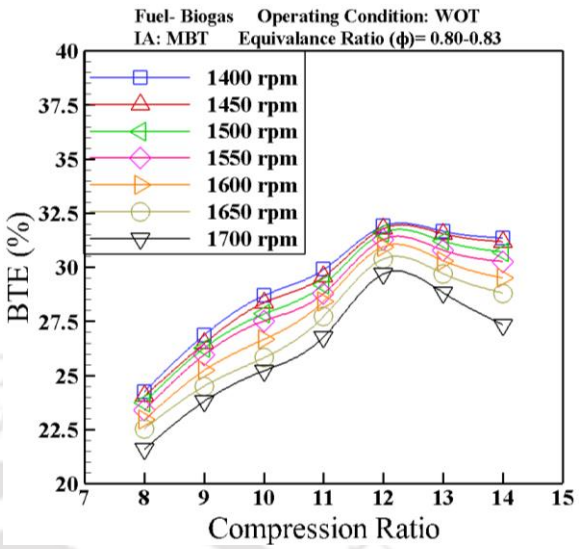

Fig. 5. 20: Effect of CR and engine speed on the BTE of the biogas fueled SI engine

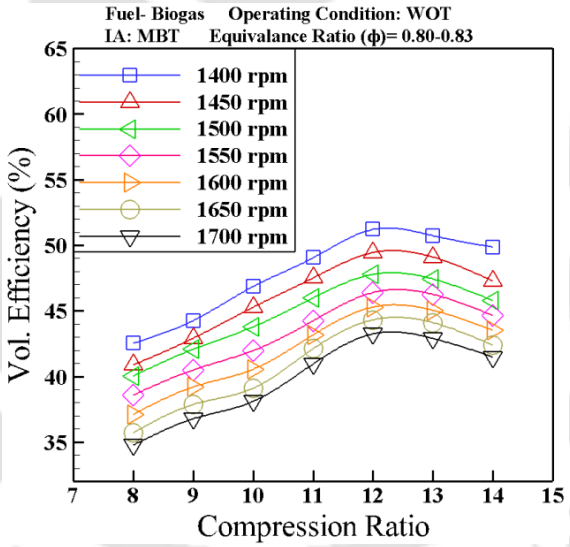

Fig. 5. 21: Effect of CR and engine speed on the VE of the biogas fueled SI engine

The influence of CR and the engine speed on the VE of the biogas fueled SI engine operated at WOT condition is shown in **Fig. 5. 21**. It is noticed that; the VE of the engine follows an increasing trend with increased operating CR of the engine. Increasing the CR from CR 10 to CR 11 enhances the VE by 4.66%. Similarly, the further rise in CR enhances the VE by 9.3%, 8.2%, and 6.4% at CR 12, CR 13 and CR 14, respectively with reference to CR 10. The maximum VE is marked at CR 12 and it is 51.2% at 1400 rpm. It is also observed that,

irrespective of the CR, the rise in engine speed reduces the VE of the engine and the maximum VE of the engine is always seen at 1400 rpm. Further, the summary of maximum BT, BP, BTE, VE and minimum BSFC with respect to the ratio of engine volume are shown in **Table 5. 9** for different opertaing CRs of the biogas operated SI engine.

Table 5. 9: Summary of maximum BT, BP, BTE, VE and minimum BSFC at different CR

CR	Bore/ Stroke	Engine speed	Maximum BT	Maximum BP	Maximum BTE	Maximum VE	Minimum BSFC
	(D_b/L_s)	(rpm)	(N-m/CC)	(kW/CC)	(%)	(%)	(kg/kWh)
08	0.795	1400	0.026	0.0037	24.25	42.53	0.87
09			0.028	0.0041	26.86	44.26	0.79
10			0.030	0.0044	28.69	46.86	0.74
11			0.033	0.0049	29.61	49.05	0.69
12			0.036	0.0053	30.32	51.20	0.66
13			0.036	0.0053	29.01	50.72	0.67
14			0.036	0.0052	28.89	49.85	0.68

5.3.2 Combustion analysis

The combustion parameters viz. P-θ, P-V, net heat release rate (NHRR), mass fraction burnt (MFB) and mean gas temperature (MGT) are evaluated using the *Eqs.D12-D20* of ***Appendix D***. The average values of the data points are considered for discussion.

The cylinder pressure (P) and crank angle (θ) data are measured for 50 consecutive cycles during each experiment with the help of a piezo pressure sensor and optical crank angle encoder. The effect of CR and engine speed on the average cylinder pressure is shown in **Fig. 5. 22**. As observed, the average peak cylinder pressure (PCP) increases and shifts towards TDC with increasing CR and at constant operating speed of 1650 rpm. As the CR is increased from CR 08 to CR 09, the PCP is increased by 28.6% and the position of PCP shifted by 2°CA towards the TDC. The PCP is increased by 12% and the position of PCP shifted by 5°CA when the CR is raised from CR 09 to CR 10. Similarly, further rise in CR from CR 10 to CR 11, increased the PCP by 15.5 % and shifted the position of the PCP by 1°CA towards the TDC.

For further increment in CR, the PCP increases by 28.5%, 23.1%, and 16.1% and shifts by 2°CA, 1°CA, and -2°CA towards TDC at CR 12, CR 13 and CR 14, respectively with reference to CR 10 at 1650 rpm. It is evident here that biogas could withstand the higher CR without knocking since biogas has higher antiknock index. Shifting of peak pressure towards TDC is a positive indication of better combustion. This is mainly due to the faster flame front propagation, which also results in improved thermal efficiency and power output at this condition.

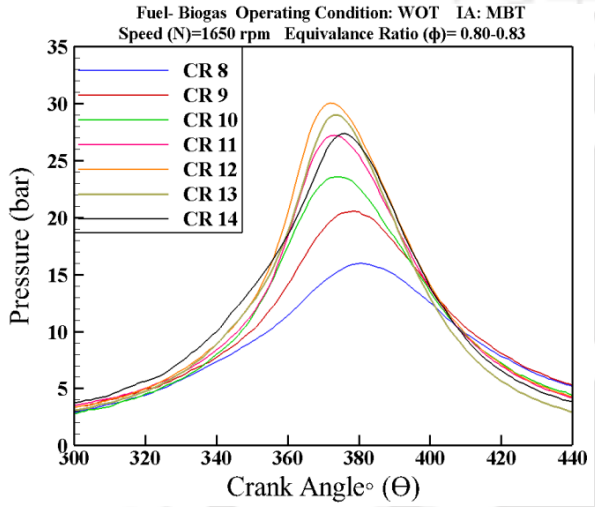

Fig. 5. 22: Effect of CR and on the average cylinder pressure of the biogas fueled SI engine

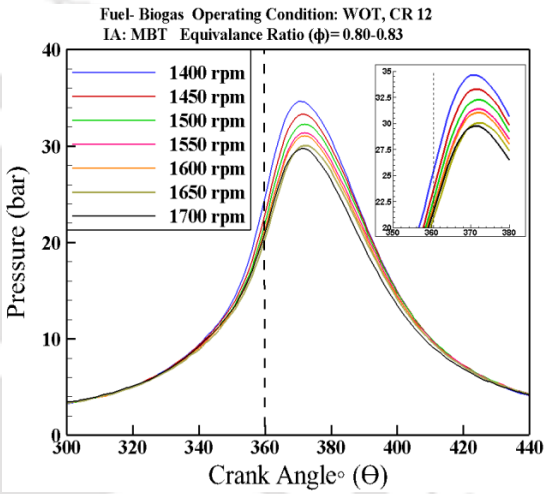

Fig. 5. 23: Effect of engine speed on the average cylinder pressure of the biogas fueled SI engine

The effect of engine speed on the average cylinder pressure at CR 12 is shown in **Fig. 5. 23.** It is observed that the average PCP increases with decrease in speed of the engine, and attains the maximum at 1400 rpm. The PCP is found to be maximum at the lower speed of the engine because decrement in speed results in higher brake load and BT on the engine. The average PCPs at 1400 rpm, 1450 rpm, 1500 rpm, 1550 rpm, 1600 rpm, 1650 rpm and 1700 rpm are noted to be 34.65 bar ,33.29 bar, 32.23bar, 31.40 bar, 31.1 bar, 30.05 bar and 29.73 bar at 371°CA, 372°CA, 372°CA, 372°CA, 372°CA, 372°CA and 372°CA, respectively. It is also observed that, with decreasing engine speed the average peak cylinder pressure slightly shifts towards TDC.

The instantaneous volume (V_θ) at each crank angle during the cyclic operation of the engine is evaluated from *Eq.5.1* (Stone, 2012). The instantenous volume and the corresponding

pressure are then used to plot the *P-V* diagram. The indicated power (IP) for each cycle is thus calculated from the area under the *P-V* plot by using *Eq.5.2* (Heywood, 1988). The net indicated power includes the pumping work as well. The averages of 50 conjunctive cyclic data under variable operating CR and speed of the engine are plotted in the subsequent figures. The effect of CR and the engine speed on the area under P-V diagram are shown in **Fig. 5. 24** and **Fig. 5. 25,** respectively. Further, **Table 5. 10** and **Table 5. 11** explicitly quantify the effect of CR and engine speed on the area under P-V diagram in **Fig. 5. 24** and **Fig. 5. 25** respectively.

$$V_\theta = V_c + A\left[r\left(1-\cos\theta\right) + l - \sqrt{\left(l^2 - r^2\sin^2\theta\right)} \right] \tag{5.1}$$

$$IP = \frac{W_{c,in} \times N}{\eta_R} = \frac{Area\,under\,the\,P-V\,curve \times N \times 10^{-4}}{\eta_R \times 60} \tag{5.2}$$

As depicted in **Fig. 5. 24** and **Table 5. 10**, it can be understood that, with increasing CR the area under P-V curve increases but it becomes almost identical for CR 12 and 13. Further enhancing the CR reduces the area under the P-V curve even though CR 14 corresponds to the maximum peak pressure. Since the engine speed is maintained constant for investigating the effect of CR, the net IP also follows the same trend as that of the area under the P-V curve. As a result of this the maximum net IP is seen to be 3.75 kW at CR 12. The maximum BP and BTE of the engine are also observed at CR 12 irrespective of the operating speed of the engine as shown and explained in **Fig. 5. 18** and **Fig. 5. 20**, respectively. One of the major reasons to justify the fact of optimum CR to be 12 might be the trend of mean gas temperature (MGT) and in-cylinder pressure just before the completion of compression stroke (355°CA) as well as the pressure at TDC position (360°CA) as shown in **Fig. 5. 26**. It is clearly marked that the MGTs and in-cylinder pressures just before the completion of compression stroke, are 419°C, 459°C, 464°C, 487°C, 443°C and 14 bar, 16.5 bar, 18.2 bar, 21 bar, 22.4 bar, respectively at CR 10, CR 11, CR 12, CR 13, and CR 14. Similarly, the MGTs and in cylinder pressures at the TDC (360°CA) are 512°C, 610°C, 626 °C, 627°C, 568°C and 17.5 bar, 22.6 bar, 25.4 bar, 28.2 bar, 29.8 bar, respectively for CR 10, CR 11, CR 12, CR 13, and CR 14. As a result of this, the pressure rise before the completion of compression stroke is higher in case of CR 13 and CR 14. Hence, the increase in work input during compression stroke is greater than the increase in work done on the piston during expansion stroke at CR

13 and CR14. Therefore, CR 12 is considered as the optimum CR for the present engine under the specified operating conditions.

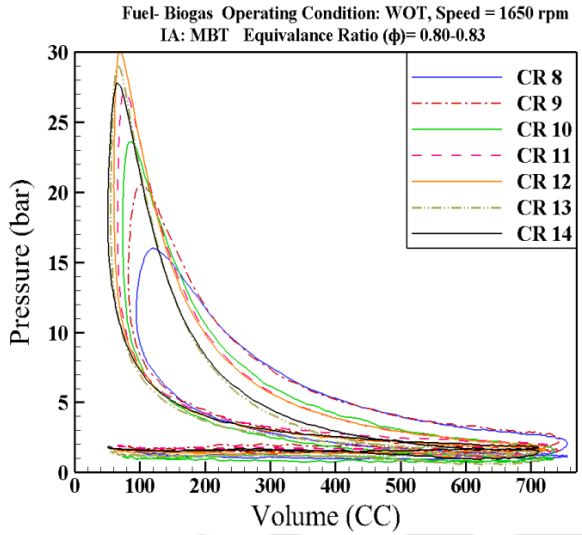

Fig. 5. 24: Effect CR on the P-V plot area of the biogas fueled SI engine

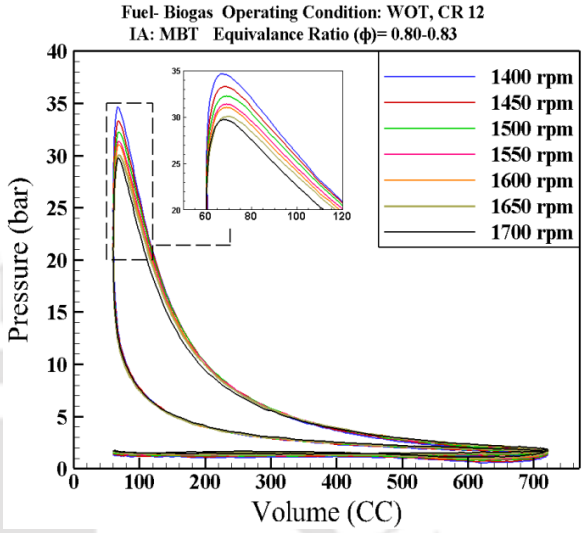

Fig. 5. 25: Effect of engine speed on the P-V plot area of the biogas fueled SI engine

Table 5. 10: Summary of the P-V Plot at 1650 rpm (Fig. 5. 24)

CR	P-V Plot	IP(kW)	BP (kW)
CR 08	2369.57	3.26	2.299
CR 09	2410.97	3.32	2.571
CR 10	2529.66	3.48	2.634
CR 11	2657.32	3.65	3.016
CR 12	2725.72	3.75	3.358
CR 13	2591.25	3.56	3.282
CR 14	2497.84	3.42	3.182

On the other hand, from **Fig. 5. 25** and **Table 5. 11**, it is also seen that the area under the P-V curve decreases almost linearly with increasing speed of the engine under constant operating CR and throttle position. As noticed, the maximum and minimum areas under the P-V curve are 3150.64 and 2656.8 at 1400 rpm and 1700 rpm, respectively. Since, the engine speed is varied from 1400 to 1700 rpm at CR 12; the net IP follows the exact opposite trend as that of area under the P-V curve. The maximum and minimum net IPs are 3.763 kW and 3.685

kW at 1700 and 1400 rpm, respectively because the net IP is the function of engine speed and area under the P-V curve. Additionally, the rate of increase in engine speed is comparatively greater than the rate of decrease in the area under the P-V curve. Hence, the net IP increases with increasing speed of the engine. However, the maximum BP and BTE are observed at 1400 rpm which decrease with increasing speed of the engine irrespective of the operating CR as shown and explained in **Fig. 5. 17** and **Fig. 5. 18** respectively. One of the major reasons to justify the fact of obtaining maximum BP at 1400 rpm is the trend of MGT and in cylinder pressure while operating the biogas engine with optimum CR as shown in **Fig. 5. 26**. As noticed from **Fig. 5. 27**, the maximum MGTs at 1400 rpm, 1450 rpm, 1500 rpm, 1550 rpm, 1600 rpm, 1650 rpm and 1700 rpm are found to be 1017°C, 1001°C, 980°C, 957°C, 943°C, 924°C and 884°C at 384°CA, 385°CA, 384°CA, 385°CA, 386°CA, 381°CA and 381°CA, respectively. These numbers clearly indicate that, the MGT follows an increasing trend with the decreasing speed of the engine and is maximum at 1400 rpm. Additionally, with decreasing speed of the engine, the locations of the peak MGT shift slightly away from the TDC and extend the combustion duration. Similarly, the peak cylinder pressure at 1400 rpm, 1450 rpm, 1500 rpm, 1550 rpm, 1600 rpm, 1650 rpm and 1700 rpm are found to be 34.64 bar ,33.29 bar, 32.25bar, 31.40 bar, 31.05 bar, 30.05 bar and 29.73 bar at 371°CA, 372°CA, 372°CA, 372°CA, 372°CA, 372°CA and 372°CA, respectively. This also indicates that, the peak cylinder pressure increases and shifts towards TDC and ensures better combustion at reduced engine speed.

Table 5. 11: Summary of the P-V Plot at CR 12 (Fig. 5. **24**25)

Engine	P-V Plot area	IP (kW)	BP (kW)
1400	3150.64	3.685	3.52
1450	3058.17	3.695	3.51
1500	2963.06	3.703	3.49
1550	2878.34	3.718	3.46
1600	2797.86	3.73	3.42
1650	2725.72	3.747	3.36
1700	2656.86	3.763	3.28

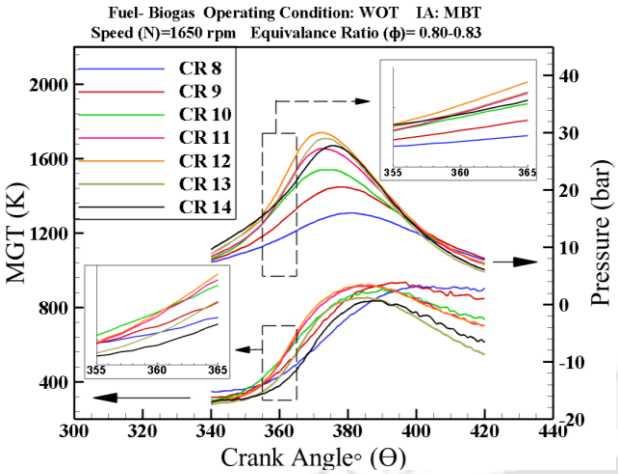

Fig. 5. 26: Effect of CR on the MGT and cylinder pressure of the biogas fueled SI engine

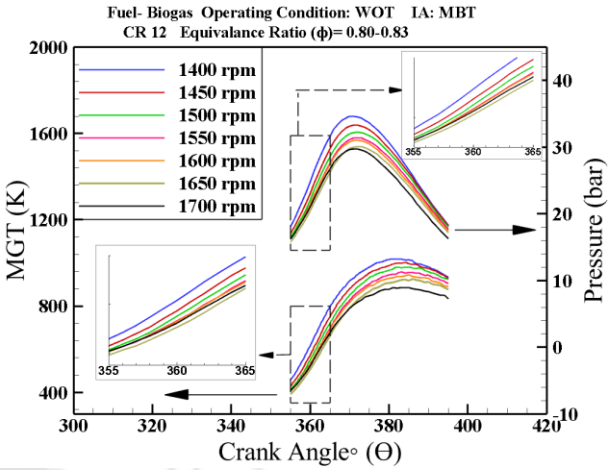

Fig. 5. 27: Effect of engine speed on the MGT and cylinder pressure of the biogas fueled SI engine

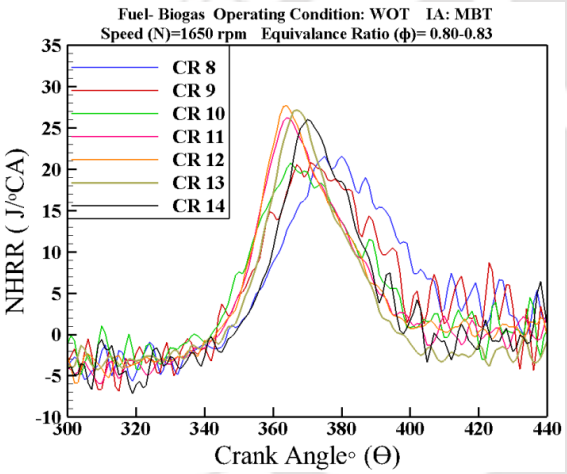

Fig. 5. 28: Effect CR on the NHRR of the biogas fueled SI engine

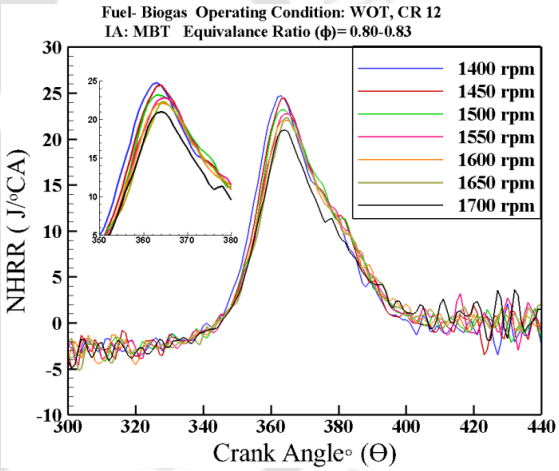

Fig. 5. 29: Effect of engine speed on the NHRR of the biogas fueled SI engine

The net heat release rate (NHRR), evaluated from *Eq. D16* of ***Appendix-D*** for different CR, speed and WOT condition, is shown in **Fig. 5. 28** and **Fig. 5. 29**, respectively. Consider specific case of 1650 rpm, it is observed here that, there is an improvement of NHRR with progressive advancement of CR up to the critical CR (CR 12), beyond which the NHRR starts declining and the maximum NHRR is found to be 22.3 J/°CA at 365°CA. Upon increasing the CR from CR 10 to CR 11, CR 12, CR 13 and CR 14, the maximum NHRR increases by 20.7%, 33.5%, 30.1%, 25.25% and shifts by 2°CA, 3°CA, 4°CA and 5°CA towards TDC, respectively.

This is due to the faster flame propagation at CR 12 where the energy conversion efficiency is maximum(Kemal and Sayin, 2014). Furthermore, the effect of engine speed on the NHRR of the biogas fueled SI engine operating at CR 12 and WOT condition, is shown in **Fig. 5. 29**. It is evident that, there is an improvement of NHRR with progressive decrement of the engine speed and NHRR is maximum at 1400 rpm when operated at CR 12. The peak NHRR of engine operating with CR 12 and 1400 rpm is 23.6 J/°CA, at 360°CA. Hence, CR 12 and 1400 rpm with WOT is proposed to be the best operational combination for the present engine.

Fig. 5. 30 and **Fig. 5. 31**describe the effect of CR and engine speed on the mass fraction burnt (MFB) for the biogas fueled SI engine operating at WOT condition. The MFB is calculated by following the method shown in *Eqs. D17-D19* and proposed by Rassweiler and Withrow (Rassweiler and Withrow, 1938). For the present case, the rapid burn angle (RBA) '$\Delta\theta_b$' is considered as the crank angle interval between the end of flame development stage (mass fraction burnt of 10%) and the end of flame propagation (mass fraction burnt of 90%) (Heywood, 1988). The rapid burn angle (RBA) for CR 10, CR 11, CR 12, CR 13 and CR 14 is mentioned in the present section as $\Delta\theta_{bCR10}$, $\Delta\theta_{bCR11}$, $\Delta\theta_{bCR12}$, $\Delta\theta_{bCR13}$ and $\Delta\theta_{bCR14}$, respectively.

As noticed from **Fig. 5. 30**, the end of flame development stage for biogas combustion is observed at 361°CA, 358°CA, 355°CA, 355°CA, 353°CA, 356°CA and 358°CA and the end of flame propagation process is observed at 394°CA, 389°CA 385°CA, 380°CA, 377°CA, 379°CA, 381°CA, respectively for CR08, CR 09, CR 10, CR 11, CR 12, CR 13 and CR 14. Hence, $\Delta\theta_{bCR10}$, $\Delta\theta_{bCR11}$, $\Delta\theta_{bCR12}$, $\Delta\theta_{bCR13}$ and $\Delta\theta_{bCR14}$ are found to be 33°CA, 31°CA, 30°CA, 25°CA, 23°CA 23°CA and 23°CA, respectively. From the above observations, it can be inferred that, with increased CR the combustion event and flame development are initiated progressively before the TDC up to CR 12 and thus, the RBA (actual burn duration) reduces due to faster flame propagation. The burn durations in case of CR 13 and CR 14 is lower compared to CR 12 and it signifies fastest flame propagation. It is the state of in-cylinder pressure and MGT which reduce the network transfer as explained in **Fig. 5. 26**.

Similarly, **Fig. 5. 31** explains the effect of engine speed on the MFB of a biogas fueled SI engine operated at CR 12 and WOT condition. As shown, the rapid burn angles are found to be 27°CA, 27°CA, 26°CA, 25°CA, 25°CA, 24°CA, and 25°CA, respectively at 1400 rpm, 1450 rpm, 1500 rpm, 1550 rpm, 1600 rpm, 1650rpm and 1700 rpm of the engine. From **Fig. 5. 31**, it can be inferred that, with decrease in engine speed the combustion process and flame development initiates progressively before the TDC and terminates earlier in the expansion stroke after TDC. but the rapid burn angle remains almost same throughout the operating speed of the engine.

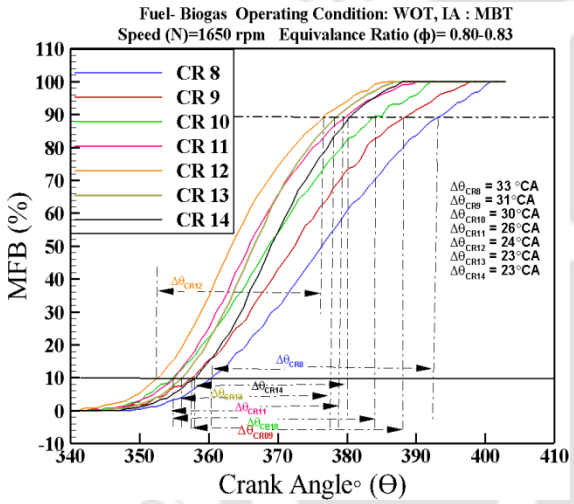

Fig. 5. 30: Effect of CR on the MFB of the biogas fueled SI engine

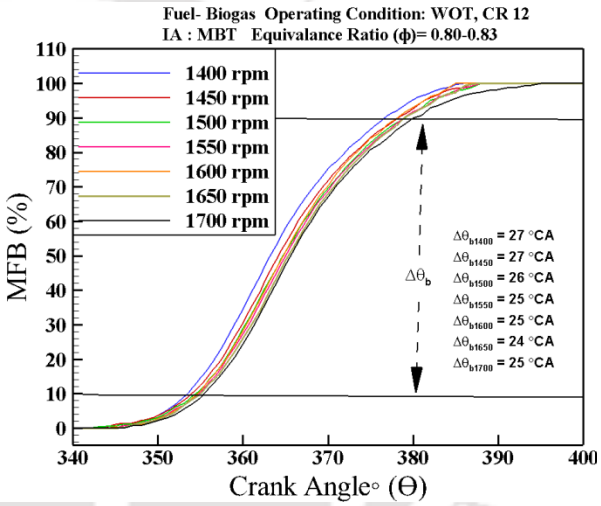

Fig. 5. 31: Effect of engine speed on the MFB of the biogas fueled SI engine

5.3.3 Emission analysis

The effect of CR and engine speed on the carbon monoxide (CO) emission at WOT condition is shown in **Fig. 5. 32** and **Table 5. 12**. It can be seen that, irrespective of the operating speed of the engine, the CO concentration in the exhaust emission of the biogas fueled engine follows an increasing trend with rise in CR. It is found maximum at CR 12 and gradually drops for further higher operating CRs. In general, CO emission has relevance with fuel rich equivalence ratios due to incomplete combustion (Pulkrabek, 1997), but with lean equivalence ratios also, CO can be present owing to dissociation of CO_2 and its concentration reduces with reducing combustion temperature (Stone, 2012). In the present case, the engine

is operated with fuel lean equivalence ratios (Φ) ranging from 0.808 to 0.835, at different CRs and speed range of the experimental matrix. Additionally, the initial concentration of CO_2 in biogas is very high and the average combustion temperatures at CR 10, CR 11, CR 12, CR 13 and CR 14 are 658.23°C, 659.24°C, 670.83°C, 567.83°C and 519.30°C, respectively. Hhigher CO_2 content in biogas and the chemical kinetics of biogas combustion with lean and stoichiometric mixture leads to lower NO_x and higher CO production at higher temperatures (Fischer and Jiang, 2015). Hence, the maximum CO concentration in the exhaust emission of the biogas fueled SI engine is only observed at CR 12, irrespective of the operating speed of the engine. It has also been noted that, for all the operating CRs, the CO concentration in the exhaust emission follows a decreasing trend with progressive increment in the engine speed and it is found to be maximum at 1400 rpm. The maximum CO concentration at CR 12 and 1400 rpm of the engine is marked to be 0.258%. This observation is in line with the reported literature. The maximum and minimum CO concentrations for all operating CRs of the engine are at 1400 rpm and 1700 rpm, respectively.

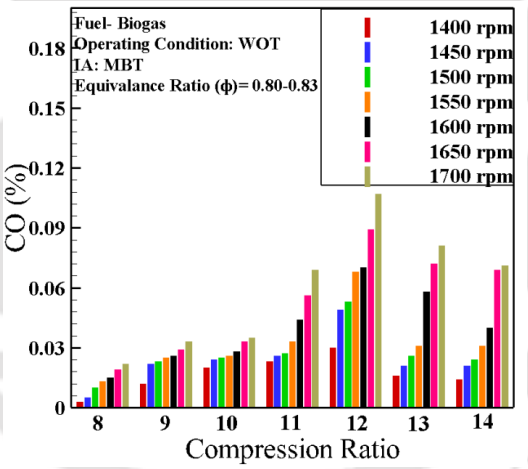

Fig. 5. 32: Effect of CR and engine speed on the CO emission of the biogas fueled SI engine

Fig. 5. 33 and **Table 5. 12** illustrate the effect of CR and engine speed on the unburnt HC emission. The unburnt HC emission in SI engine is high due to flame quenching, crevices, valve leakage, oil layers, liquid fuels and more importantly due to incomplete combustion (Mehrnoosh et al., 2012). In the present investigation, it has been noticed that, the unburnt HC emission for all speeds follows an increasing trend with progressive increment of the operating CR. With increasing CR, the surface to volume ratio of the combustion chamber increases and

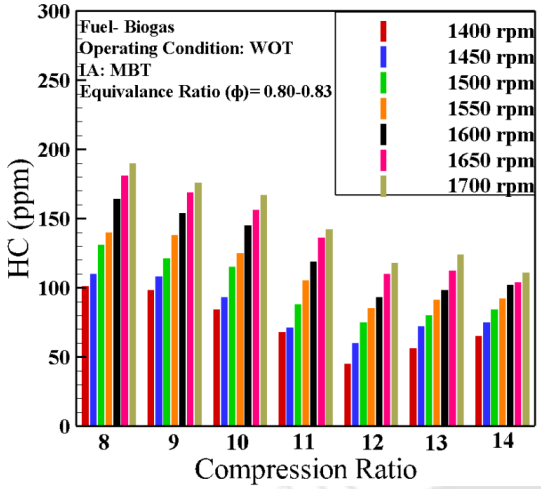

Fig. 5. 33: Effect of CR and engine speed on the HC emission of the biogas fueled SI engine

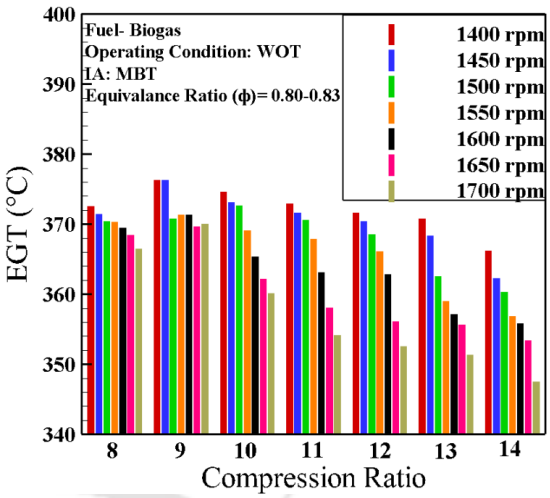

Fig. 5. 34: Effect of CR and engine speed on the EGT of the biogas fueled SI engine

enhances the mass of unburnt fuel in the crevices (Corti et al., 2014). During expansion stroke, drop in cylinder pressure draws the compressed unburnt fuel from the crevice volume and creates a reverse blow which is then followed by flame quenching. This process leaves in the unreacted fuel particles in the exhaust (Porpatham et al., 2013a). In addition, the rise in CR reduces the post oxidation of HC molecules in the exhaust since the exhaust gas temperature (EGT) is lower due to increasing CR and speed of the engine as shown in **Fig. 5. 34**.Therefore, the unburnt HC emission is found higher at higher operating CR of the engine. This fact has also been reported in the literature (R. J. Crookes, 2006; Huang and Crookes, 1998a; Porpatham et al., 2012).

Hence, the maximum unburnt HC emission is traced at CR 14, irrespective of operating speed of the engine. The maximum and minimum unburnt HC concentration at CR 14 are 165 ppm and 74 ppm, respectively at 1700 rpm and 1400 rpm of the engine. Moreover, it can be concluded from the above observation that, increasing the CR from CR 10 to CR 12 limits the intensification of unburnt HC emission only by 6.2%. It is also observed that, irrespective of the CR, the unburnt HC emission follows an increasing trend with increasing speed of the engine. This may be due to the trend of volumetric efficiency as shown in **Fig. 5. 21**. At lower operating speeds, the air-fuel mixture has enough oxygen to promote complete combustion because of the higher volumetric efficiency and produces lesser unburnt HC in the exhaust

emission. But, at higher operating speed, the air fuel mixture with insufficient oxygen experiences the incomplete combustion of fuel and leads to greater unburnt HC because of lower volumetric efficiency. Enhancing the engine speed from 1400 rpm to 1700 rpm increases the unburnt HC emission by 101.5%, 95.5%, 85.13%, 75.9% and 122.9%, respectively at CR 10, CR 11, CR 12, CR 13 and CR 14.

Table 5. 12: Summary of CO, HC and NOx concentration at different CR

CR	Engine Speed (rpm)	CO (vol %)	CO (g/kWh)	CO *Std.	HC (ppm)	HC (g/kWh)	NO_x (ppm)	NO_x (g/kWh)	HC+NO_x *Std.
10	1400	0.034	1.22	≤ 250# ≤ 3.5$ (The Gazette of India, 2016) (g/kWh)	64	0.13	295	1.95	≤ 12# ≤ 7.5$ (The Gazette of India, 2016) (g/kWh)
	1700	0.010	0.36		129	0.26	1013	6.72	
11	1400	0.095	3.41		68	0.14	289	1.91	
	1700	0.037	1.32		133	0.26	1286	8.53	
12	1400	0.258	9.26		74	0.15	325	2.15	
	1700	0.038	1.36		137	0.27	1928	12.79	
13	1400	0.096	3.44		79	0.16	250	1.65	
	1700	0.030	1.07		139	0.28	1860	12.34	
14	1400	0.097	3.48		74	0.15	210	1.39	
	1700	0.036	1.39		165	0.33	1368	9.07	

*Emission standard set by the Govt. of India for the #genset run on petrol and natural gas (NG) or petrol and liquid petroleum gas (LPG) and $ genset run on dedicated natural gas (NG) or liquid petroleum gas (LPG) as mentioned in GSR 281(E) dated 7th March 2016.

Fig. 5. 35 explains the effect of CR and engine speed on the nitrogen oxide (NO_X) emission. The NO_X emission is strongly related to the lean fuel with high cylinder temperature or high peak combustion temperature. With the higher temperature of combustion gases inside the engine cylinder, NO_X is mainly formed through oxidation of nitrogen present in the inducted air fuel mixture and is mainly composed of NO and small amount of NO_2. It is observed that, irrespective of the engine speed, the increase in CR results in increased level of NO_X concentration up to a point where CR is 12:1. Further increment in CR, beyond CR 12 reduces the NO_X level in the emission. This might be due to the trend of inside cylinder temperature or the MGT and the average combustion temperature which initially increase with increasing CR and attain the maxima at CR 12 but later on decrease with increasing CR (Corti et al., 2014). The higher combustion temperature with abundance of oxygen in addition to the

reduction of the time required for dissociating NO to N_2 and O_2 is the major reason for getting higher NOx concentration at CR 12 (Sadiq Al-Baghdadi, 2004). The maximum NO_X concentration at 1700 rpm of the engine at different operating CR of the engine is reported in **Table 5. 12**. Increasing the CR from CR 10 to CR 12 increases the NO_X concentration by 90.3 % at 1700 rpm. It is also marked that the NO_X emission increases with increasing engine speed at any CR and it is found to be maximum at higher speed of the engine at 1700 rpm. This also follows the findings reported in the open literature (Sadiq Al-Baghdadi, 2004). The notable point from Table 9 is that though the emission remains high for CR 12, still it is lower than the standard permissible emissions. Thus, the advantage of higher performance and permissible emissions level proposed CR 12 as recommended setting for the biogas fueled SI engines for the above-mentioned operating conditions.

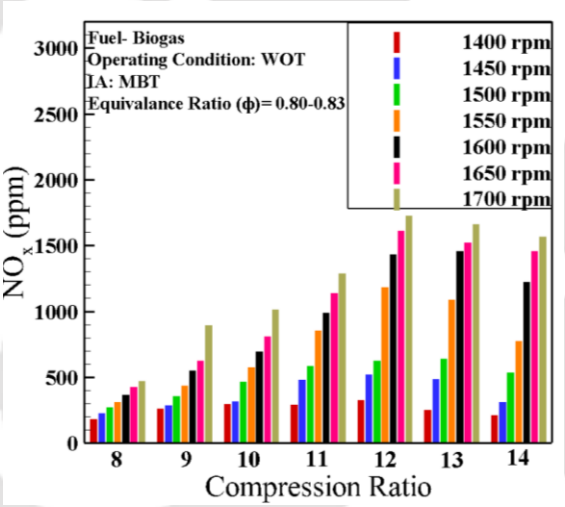

Fig. 5. 35: Effect of CR and engine speed on the NO_X emission of the biogas fueled SI engine

5.4 Effect of Equivalence Ratio (ER)

The engine performance evaluation is mostly influenced by the operating equivalence ratio of the fuel/air mixture supplied to the engine. The ratio of these mass flow rates is useful in defining the limit of the engine operating conditions. Further, the combustion characteristics of the fuel/air mixture and combustion products govern the performance and emission of the engine and can be corelated best for wide range of fuel relative to the stochiometric mixture proportion. In order to meet the current low emission technology standards, precisely

controlled air/fuel ratio is desirable. Hence, in the present section of the investigation the biogas fueled VCR SI engine (*Engine 3*) is operated at the optimum CR (12) and MBT (33º CA bTDC) setting at WOT and 1650 rpm over an operating ER (Φ) limit of 0.744 to 1.109. The detailed experimental matrix and operating procedure for conducting this investigation are mentioned respectively in *Sections 5.1.1 and 5.1.2*. The performance, combustion and emission analysis are carried out to propose the recommended range and optimum ER setting for the biogas fueled SI engine for the mentioned operating condition of the engine.

5.4.1 Performance analysis

As referred from the literature (Heywood, 1988 and Stone, 2012), the performance parameters such as BT, BP, BSFC, BTE and the operating ER are evaluated from the Eqs. D1 to D8 of Appendix D. The average values of these parameter obtained from the repeated experimental data points are considered for the further analysis.

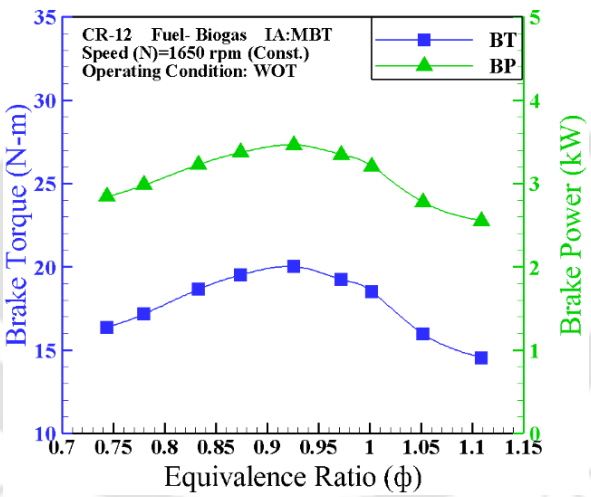

Fig. 5. 36: Variation of brake power with equivalence ratio at WOT condition

Fig. 5. 36 depicts the influence of operating ER on the BT and BP of the biogas fueled SI engine operating at CR 12, IA of 33º CA bTDC, 1650 rpm and WOT condition. As observed, the induced BT and BP of the engine are increasing steadily with progressive enhancement of ER up to 0.926. However, with further progressive ER (Φ>0.93), the BT and BP followed an opposite trend and drops down. This may be attributed due to the lower combustion efficiency beyond the ER of 0.93 on the stochiometric and richer side of air-fuel

mixture. However, with the air-fuel mixture leaner than 0.93, the decreased engine power is attributed due to the lower volumetric heating value of the inducted air-fuel mixture. It has been observed that, operating the engine at leaner and richer mixture reduced the output power. Similar observations are also reported in open literature for hydrogen operated SI engines (Sadiq Al-Baghdadi, 2004). The BT and BP induced at Φ=0.93 are reported 20 N-m and 4.46 kW, respectively at CR 12 and 1650 rpm. The BT and BP are reported 7.2% higher compared to the induced BT and BP against Φ=0.83 (ER maintained for CR and IT optimization) at CR 12 and 1650 rpm. As shown in **Fig. 5. 36**, at the operating CR, the induced BT and BP of the engine followed an increasing trend along with the progressive advance of the equivalence ratio and deviates from the trend at a point very close to the stoichiometric mixture (Φ=1). The range of ERs covered the lean misfire limit (Φ=0.74) on one side to the knock limit (Φ=1.11) on the rich side. The leanest point shown in this plot corresponds to the condition just before the onset of misfire beyond which it was difficult to run the engine smoothly. It was also observed that, on rich side there is a drop in BP of the engine. This may be due to the enriched mixture supplied to the engine which onset knocking during combustion with the present operating condition of the engine.

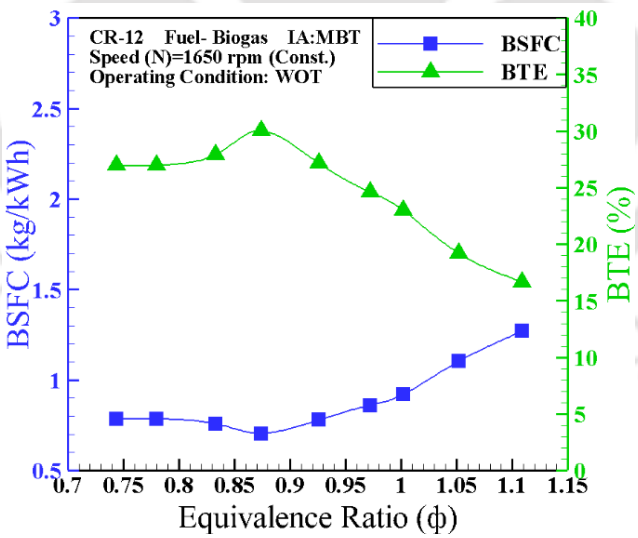

Fig. 5. 37: Variation of brake thermal efficiency with equivalence ratio at WOT condition

Fig. 5. 37 shows the effect of ER on the BSFC and BTE of a biogas fueled SI engine operated at WOT, CR12 and IA of 33º CA bTDC. It was observed that, as the air-fuel ratio

changed from the lean misfire limit to the rich side (moving left to right in the figure), the BSFC followed a decreasing trend and found minimum at Φ=0.874 and increases steadily up to the knock limit. Similarly, with progressive ER, the BTE followed an increasing trend and deviates at Φ=0.874. The minimum BSFC and the maximum BTE are reported 0.705 kg/kW-h and 30.04% at Φ=0.874 and 1650 rpm for the engine. The BSFC and BTE attained with the current operating ER is 7% lower and higher, respectively with respect to the reported BSFC and BTE where Φ was maintained 0.83 (ER maintained for CR and IT optimization) at CR 12 and 1650 rpm. Mixture richer and leaner than this point causes incomplete combustion due insufficient oxygen and slower the burning rate, respectively and hence lead to a drop in thermal efficiency (Heywood, 1989).

5.4.2 Combustion analysis

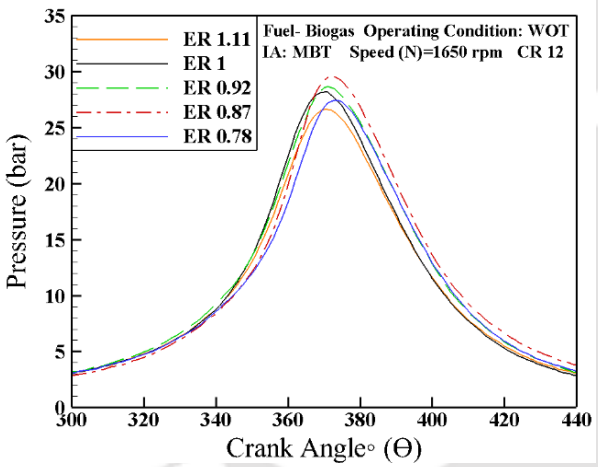

Fig. 5. 38: Effect of ER on the average peak pressure of the cylinder of the biogas fueled SI engine

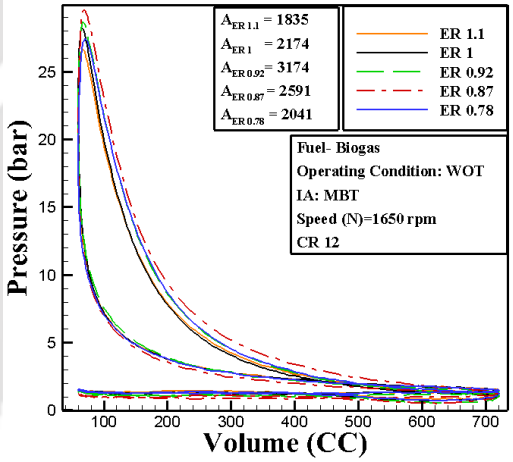

Fig. 5. 39: Effect of ER on the p-v plot area of the biogas fueled SI engine

As a fuel, biogas has an extremely low energy density on the volume basis on account of its higher CO_2 content. The lager quantity of CO_2 content reduces it calorific value, flame velocity and flammability limit. The combustion process is completely dependent on the flame propagation, which ultimately depends on the flame speed (25 cms^{-1} in biogas) and auto ignition temperature (650°C in biogas). **Fig. 5. 38** explains the effect of air-fuel ratio on the average cylinder pressure for a biogas fueled SI engine at WOT condition. The ignition advance, speed and compression ratios are remained constant for the particular study. This

particular plot explains the effect of air-fuel ratio on the average cylinder pressure of the engine operated at a CR12 and IA 33º bTDC. It is observed that with progressive equivalence ratio (as the fuel-air ratio changed from the lean misfire limit to the rich knock limit) the average peak cylinder pressure (PCP) increases and shift closer the top dead center. However, maximum PCP is reported 29.5 bar at Φ=0.874 and the LPCP is observed at 372º CA. This is because of the faster flame propagation, which results in improved thermal efficiency at this condition. Because of this pressure rise, the BTE is found maximum at Φ = 0.874 while the engine was operated at CR 12 and 1650 rpm. The PCP at the operating ER (Φ=0.926), at the point of maximum BP is observed 28.67 bar. It was also observed from **Fig. 5. 39** that, the area under the *P-V* curve is maximum (3174) at Φ=0.926. Hence, it may be inferred, the biogas fueled engine will operate efficiently in between the ER range of 0.874 and 0.926. At lower ERs the average PCPs are lower and as expected it increases with the richer configuration of the air-fuel mixture. However, beyond stochiometric condition the PCP drops due to inefficient combustion in the engine. The best observable ER at CR 12 with an IA of 33º CA bTDC is noticed 0.874.

The variation of NHRR with progressive advance of ER of a biogas fueled SI engine is shown in **Fig. 5. 40** at WOT operating condition. The heat release analysis evaluates the data on differential basis and this led to noise in the computed result, especially at the lower pressure regions where the discretization is a larger proportion of the signal. The negative NHRR implies that there is heat transfer to the cylinder wall and ignition should be close to the minimum NHRR. It has been noticed that with progressive ERs, the peak NHRR was increased up to Φ=0.926 and decreased with higher ERs (Φ=0.926). The peak NHRR was reported 26.53 J/ºCA at 12º aTDC. Similarly, The MGT profile shown in **Fig. 5. 41**, signifies the in-cylinder temperature profile during the combustion process. As noticed from the MGT profile, the peak MGT is also observed when the ER was maintained 0.926 (Φ=0.926). The peak MGT recoded was 1079 K at 35º aTDC. The effect of operating ER on the MFB of the biogas fueled SI engine is shown in **Fig. 5. 42** at CR 12 and 1650 rpm. As, observed, the with progressive advance of ER (as the fuel-air ratio changed from the lean misfire limit to the rich knock limit), the rapid burn angle (Δθb) followed a decreasing trend up Φ=0.926 and increased with further rise in ER. The minimum rapid burn angle (Δθb) with Φ=0.926 is recoded 24ºCA,

which signifies the faster fame propagation rate at this condition. Hence, it is evident from the combustion analysis that, due to the enhanced flame propagation rate the energy conversion efficiency is maximum when the biogas engine is operated with an ER of 0.92 (Φ=0.926). So, beyond this range of operating ER (0.926< Φ > 0926), the combustion event will not be efficient.

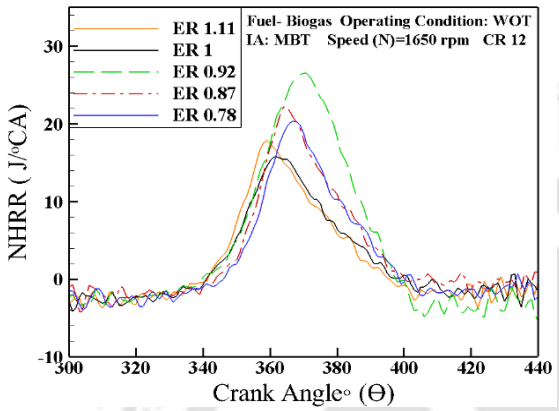

Fig. 5. 40: Effect of ER on the neat heat release rate of the biogas fueled SI engine

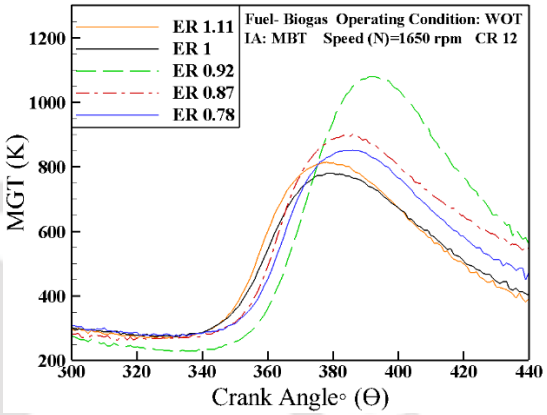

Fig. 5. 41: Effect of ER on the mean gas temperature of the biogas fueled SI engine

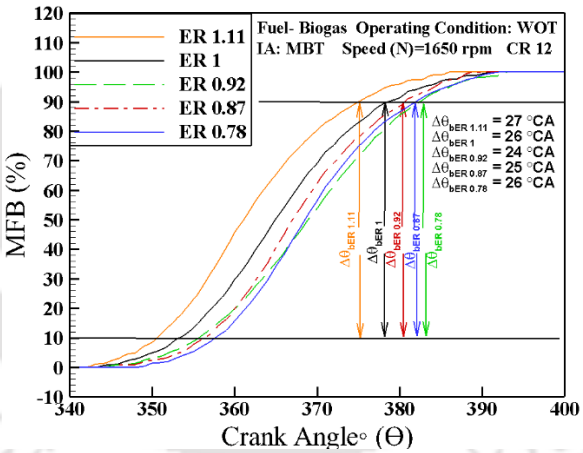

Fig. 5. 42: Effect of ER on the mass fraction burnt of the biogas fueled SI engine

5.4.3 Emission analysis

The effect of air-fuel ratio on the HC and NO_x concentration in the exhaust emission of a biogas fueled SI engine operated at 1650 rpm, WOT condition is shown in **Fig. 5. 43**. It was observed that, with the progressive rise in inducted ER (as the supplied fuel-air ratio changed from the lean misfire limit to the rich knock limit), the HC emission followed a

decreasing trend up to Φ=0.926 and increased with further rise in ER. The minimum HC emission was recoded 85 ppm (0.17 g/kWh) at Φ=0.926. The HC emission reaches the minimum value coinciding with the position of the best thermal efficiency. As the ER was varied from lean misfire limit (0.74) to reach knock limit (1.1), the HC emission was varied in between 85-165 ppm. The lean air-fuel mixture with insufficient oxygen promotes the incomplete combustion of fuel as a result misfire produces the unburnt HC. Mixture deviating from this point will have insufficient oxygen or lower combustion temperature, which will produce higher unburnt hydrocarbon. Fuel-air mixture leaner than 0.926 (Φ < 0.926) revealed an increase in HC level due the effect of flame quenching and incomplete combustion observed at the misfire limit. Similarly, the fuel-air mixture richer than 0.926 (Φ < 0.926) also revealed an increase in HC level due to insufficient oxygen which leads to incomplete combustion. Similar observations are also documented by researchers (Propatham et al., 2008; Huang and Crooks, 1998a) and proposed biogas engine operating at CR 13 and MBT at WOT releases minimum level of HC emission at ER ~0.95.

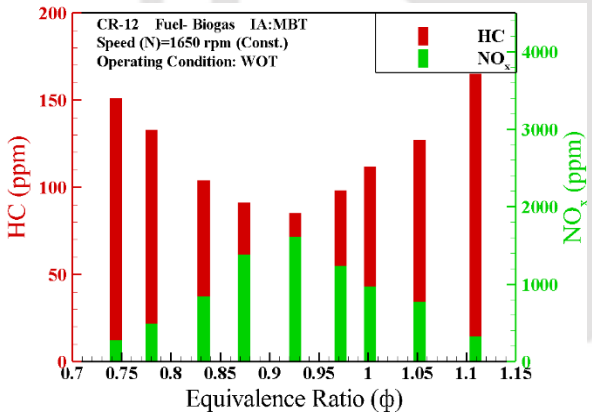

Fig. 5. 43: Effect of ER on the HC and NOx emission level of biogas fueled engine

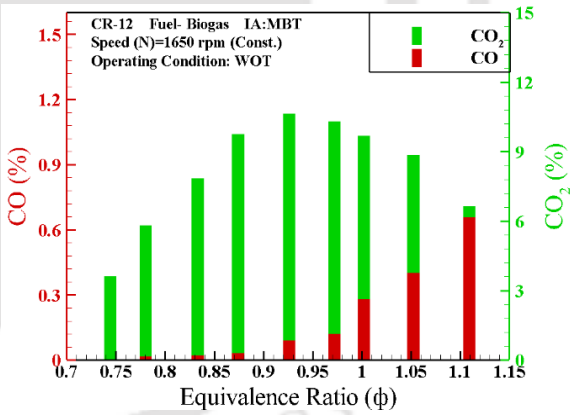

Fig. 5. 44: Effect of ER on the CO and CO2 emission level of the biogas engine

Similarly, the NO_x emission profile over the operating ER range of the engine is portrayed in **Fig. 5. 43.** As observed, the peak NO_x emission was observed at ER (Φ =0.926) leaner than the stoichiometric mixture and decreasing with linear and richer fuel-air mixture, respectively due to the abundance and insufficient oxygen at the respective condition. It has also observed that, NO_x formation is closely dependent on the MGT profile of the engine. The

NO_x emission is also reported maximum at the point of peak MGT (Φ = 0.926) and found 1609 ppm (10.68 g/kWh).

The effect of fuel-air ER on the CO and CO_2 emission of the biogas fueled SI engine is depicted in **Fig. 5. 44**. As observed, the CO concentration in the exhaust emission was gradually increased with increased ER and found maximum at ER= 1.1. This may be attributed because of incomplete combustion caused due to lack of oxygen and presence of unburnt HC when the engine is operated with richer than stochiometric fuel-air mixture. The minimum CO concentration was found 0.089% (3.19 g/kWh) at the point of maximum BP (Φ = 0.926). Whereas, the increased temperature of the combustion chamber (1079 K), oxidized the CO molecules and emits maximum CO_2 (at Φ =0.926) when the engine is operated with near stochiometric ER. The CO_2 concentration in the exhaust emission was also decreased for richer and leaner ERs. The maximum CO_2 emission was reported 10.63% (674.7 g/kWh) at Φ =0.926. The recorded CO, HC and NO_x emissions are converted to brake specific basis following *Eq. 4.1* and compared with the established emission standards and reported in **Table 5. 13**.

Table 5. 13: Summary of CO, HC and NOx emission at different ER

ER	Engine Speed (rpm)	CO			HC		NO_x		HC+ NO_x
		(vol %)	(g/kWh)	*Std.	(ppm)	(g/kWh)	(ppm)	(g/kWh)	*Std.
1.1	1650	0.658	23.62	≤ 250[#] ≤ 3.5[$] (The Gazette of India, 2016) (g/kWh)	165	0.33	321	2.13	≤ 12[#] ≤ 7.5[$] (The Gazette of India, 2016) (g/kWh)
1		0.281	10.09		112	0.22	972	6.45	
0.92		0.089	3.19		85	0.17	1609	10.68	
0.87		0.031	1.11		91	0.18	1380	9.16	
0.78		0.017	0.61		133	0.27	490	3.25	

*Emission standard set by the Govt. of India for the [#]genset run on petrol and natural gas (NG) or petrol and liquid petroleum gas (LPG) and [$] genset run on dedicated natural gas (NG) or liquid petroleum gas (LPG) as mentioned in GSR 281(E) dated 7th March 2016.

5.5 Summary

Experiments for the biogas operated VCR SI research engine are conducted at wide range of IA (23-53 ° CA bTDC), CR (8:1 – 14:1), engine speed (1400 – 1700 rpm), and ER (0.65 – 1.15). In lieu of that, performance, combustion and emission analysis was done which summarizes the following:

- Irrespective of the operating CR, the BSFC of the engine drops down consistently with the progressive advance of IA up to the MBT timing and ascends further with the over advanced IT along with the contrary behaviour for BTE.

- As the IA is progressed towards bTDC, the cylinder peak pressure increases significantly and shifts the location of peak pressure close to the TDC.

- The emission of CO and NO_x have similar trend being decreasing with IA advancement at specific CR. However, the trend is evident to be the reverse for CO_2 and HC level in the exhaust.

- VE of the biogas fueled SI engine increases steadily with the rise in CR up to a critical point of CR 12 and then remains almost a constant irrespective of the engine speed.

- Area under the P-V plot increases with increase in CR and decrease in engine speed.

- EGT decreases with increase in engine speed resulting in increased HC level and reduced CO level.

- BP follows an increasing trend with progressive advance of the equivalence ratio (ER) and deviates from a point very close to the stoichiometric mixture

- With increment in ER, the NHRR increases and shift towards TDC due to the enhanced flame propagation rate till $\Phi = 1.041$.

CHAPTER 6

Development and Performance Evaluation of a Biogas Fueled Retrofitted Gasoline Engine (Honda GX 200)

Overview

This chapter includes the overall performance assessment of the commercial gasoline engine (Honda GX 200) retrofitted for biogas application (Engine 3). The commercial gasoline engine is retrofitted with an venturi type biogas induction mechanism with multiple inlets as described in ***Appendix E****. The biogas induction mechanism is purposely designed and attached with the Honda GX 200 engine for enabling the engine to operate with biogas. The effectiveness of the biogas fueled Honda GX 200 engine (Engine 3) is assessed in the current chapter with biogas as the standalone fuel. In line with the previous findings, the best performance of the biogas fueled engine can be achievable when the engine is being operated at CR 12 with an ignition advance of 45°CA bTDC. However, because of the manufacturing constraints, the CR of the said engine could not be enhanced beyond 9.5:1. Hence, the CR and ignition advance of the commercial SI engine has been set to CR 9.5 and 50° CA bTDC (MBT corresponding to CR 9.5), respectively. Experiments are performed at varying engine speed in between 2200 to 2900 rpm with throttle position being WOT and PT. During these variations, performance, combustion and emission analysis was carried out and discussed in detail in this chapter.*

6.1 Experimental Design and Procedure

The experimental study, include testing of the retrofitted Honda GX 200 engine with GX 160 engine head at CR 9.53:1 over a speed range of 2200 to 2900 rpm with raw biogas and with IA of 50^{o} bTDC at WOT and PT condition. In each set of experiment, the engine is operated both in wide open and part throttle condition. The throttle position was maintained 90% of total throttle opening in wide open throttling (WOT) whereas, 50% of the total throttle is kept open in part throttle (PT) mode. The throttle position sensor attached to the throttle body unit was calibrated by the "PE3" monitor for accurately maintaining WOT and PT conditions during the experimentation. The load has been varied to achieve the entire speed range of the engine. The detail experimental matrix is depicted in **Table 6. 1**.

Table 6. 1: Experimental matrix

Fuel	CR	Throttle Position	Speed (rpm)	Performance Analysis	Combustion Analysis	Emission Analysis
Raw Biogas	CR 9.53:1	WOT PT	2200-2900	BT BP BTE BSFC VE	Variation P-θ NHRR MFB MGT	CO CO_2 NO_X HC

6.1.1 Testing the engine with raw biogas

At, first gasoline is used to ignite the engine, since the engine is not able to start with cold biogas. The diaphragm pump and the venture type biogas mixer as shown in **Fig. 3. 22** are the key components in the retrofitted Honda GX 200 engine setup which governs the flow of biogas to the engine. Further, the diaphragm pump is governed due to the pressure drop created at engine manifold during the suction stroke of the engine and thereby sucks and delivers biogas from the compressor storage to the heat exchanger for preheating the fuel. Further, the preheated biogas enters to the venturi type air- biogas mixer due to the pressure drop created at the throat of mixer and creates a homogenous mixture at the diverging section before entering to the engine. When, the engine is cranked fast enough, it creates adequate pressure drop at the intake manifold which in turn activate the diaphragm pump and supply

constant discharge of biogas to the engine. However, the inadequate cranking speed and cold biogas supply at starting condition do not create enough pressure drop in the intake manifold and the cold stating issue arises with raw biogas. Hence, for conducting the experiments, the retrofitted Honda GX 200 SI engine is initially started with gasoline by turning on the ignition switch with some load and throttle opening to achieve steady state. After the achieving the steady state condition the speed of the engine was set to 2200 rpm at WOT condition. Now, the IA in the "PE3" monitor was set to 50^{o}CA bTDC for the speed range in between 2200-2900 rpm. Then, the biogas fuel line valve is opened and the biogas is allowed to mix with air before entering to the inlet manifold of the engine. At the same moment the gasoline injector is turned off and the speed is allowed stabilized to 2200 rpm. From this moment on wards the retrofitted Honda GX 200 engine is solely running with raw biogas. After achieving the steady state condition, the "Enginesoft" was configured for particular CR (9.53:1), fuel calorific value (17000 kJ/kg), fuel density (1.2 kg/m^3) and the number of cycles (10) for which data has to be recorded. After configuring the software, the data has been logged on for 60 s time interval in the software itself. At the same time the exhaust gas composition was checked to quantify the corresponding emission of CO, CO_2, O_2, NOx and Unburnt Hydro Carbon (UHC) by inserting the probe of flue gas analyzer at the tail end of the exhaust pipe. Similarly, the speed of the engine was varied to 2300 to 2900 rpm by varying the load applied on the engine. The above-mentioned steps for data logging have been repeated for each speed. The same procedure is also repeated for part throttle (PT) condition.

6.2 Results and Discussion

In the present investigation a single cylinder, air cooled gasoline fueled commercial SI engine (Make: Honda GX 200), mostly used for stationary power production in Indian States are effectively retrofitted and operated by raw biogas by enhancing the CR (from 8.5:1 to 9.53:1) and by implementing a biogas induction mechanism. This section evaluates the performance, combustion and emission analysis of the retrofitted Honda GX 200 engine both at WOT and PT condition.

6.2.1 Performance analysis

The effect of speed on the variation of brake torque (BT) and brake power (BP) of a raw biogas fueled retrofitted Honda GX 200 SI engine at WOT and PT conditions ate plotted in **Fig. 6. 1**. The BT and BP follow a decreasing trend with increasing speed of the engine. This may be due to the only reason of increasing brake load at lower speed of the engine. The BT varies in between 8.71Nm to 11.97 Nm at WOT condition and 2.35 Nm to 6.53 Nm at PT condition. The maximum BP at WOT and PT conditions was found to be 2.94 kW, 1.57 kW at 2347 rpm and 2306 rpm respectively. The BP has been observed to be reduced by 46.4% in case of PT condition. This is due to the fact of more fuel consumption which in turn generates higher cylinder pressure at WOT condition.

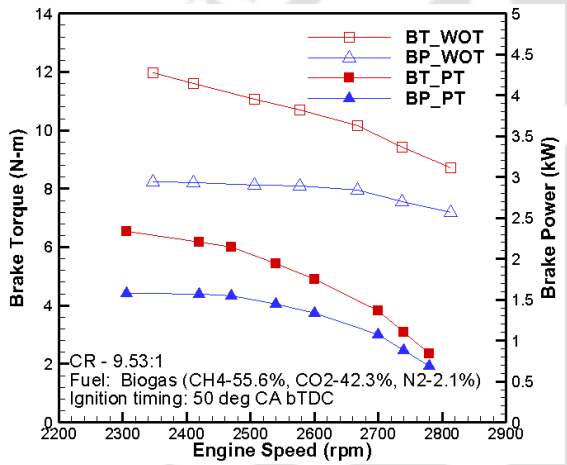

Fig. 6. 1: Engine speed Vs BT and BP [Retrofitted Honda GX 200 engine]

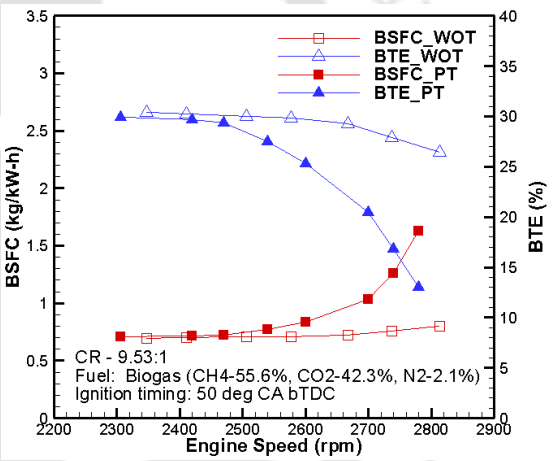

Fig. 6. 2: Engine speed Vs BSFC and BTE [Retrofitted Honda GX 200 engine]

Similarly, the variation of brake specific fuel consumption (BSFC) and brake thermal efficiency (BTE) along the speed range of a biogas fueled retrofitted Honda GX 200 SI engine at WOT and PT condition are plotted in **Fig. 6. 2**. The BSFC increases with increasing speed of the engine and found maximum for PT condition at 2780 rpm. The minimum BSFC is found to be 0.697 and 0.707 kg/kWh with WOT and PT conditions, respectively at 2347rpm and 2306 rpm of the engine. The maximum BSFC is found to be to 0.800 and 1.625 kg/kWh at WOT and PT conditions, respectively at the higher speed of the engine. The BSFC is found maximum in PT condition and increased by 50.78% and 12.76% at 2780 rpm and 2306 rpm, respectively. Since, BSFC is the function of mass of fuel consumed and BP at a particular

speed, and the mass flow rate of fuel is constant for WOT (2.051 kg/h) and PT (1.116 kg/h) conditions, the BP is the only function which varies BSFC at a particular throttle opening. So increased in BP reduces the BSFC at lower speed and vice versa. As observed, the BTE is decreasing with increasing speed of the engine both at WOT and PT condition. The maximum BTE was found to be 30.375% and 29.93% at WOT and PT conditions, respectively at 2347 and 2306 rpm. The minimum BTE was found to be 26.47% and 13.03% at WOT and PT conditions, respectively. With WOT condition the BTE was found be increased by 1.52% and 50.78% respectively at the lowest and highest speed of the engine. BTE is the function of BP, mass flow rate of fuel and calorific value of fuel. The mass flow rate of biogas is constant and are 2.05 kg/h and 1.116 kg/h, respectively at WOT and PT conditions. At WOT the BP and the mass flow rate of fuel consumed are higher as compared with PT condition, hence the BTE is comparatively higher in WOT condition.

Fig. 6. 3 describes the effect of speed on the volumetric efficiency and equivalence ratio of a biogas fueled SI engine. The volumetric efficiency is decreasing with increasing speed of the engine both in WOT and PT condition. As compared with PT condition, the volumetric efficiency is higher in WOT condition. At WOT the volumetric efficiency is found to be varied in the range of 69.9% to 70%. But, in PT operating condition the volumetric efficacy was only varied between 48.8 to 52.6%. This is may be due to the wider opening of throttle valve which induct more fresh charge to the engine intake manifold. The equivalence ratio was also followed the same trends as that of volumetric efficiency. This signifies, with increasing engine speed the charge consumed was comparatively rich in state. At WOT and PT condition the equivalence ratio varied between 0.867 to 1.0 and 0.683 to 0.764, respectively.

Fig. 6. 4, describes the effect of speed on the exhaust gas temperature (EGT) both in WOT and PT condition of a biogas fueled SI engine. The EGT is increases with increasing speed of the engine. At WOT condition EGT was found to be vary between 699^{o} C to 650^{o} C and the maximum temperature was observed at highest speed of the engine. Similarly, with increasing speed of the engine, the EGT at PT condition was also varied between 595^{o}C to 550^{o} C. This may be due to the deceasing volumetric efficiency at higher speed of the engine

which in turn consumed richer air-fuel mixture at the higher speed of the engine both in WOT and PT condition.

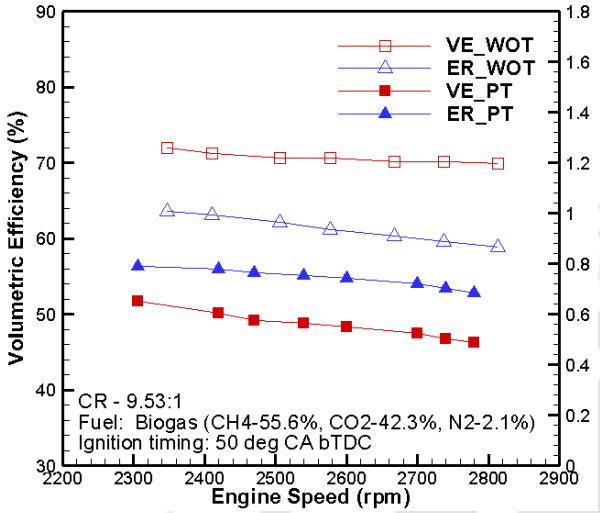

Fig. 6. 3: Engine speed Vs VE and ER [Retrofitted Honda GX 200 engine]

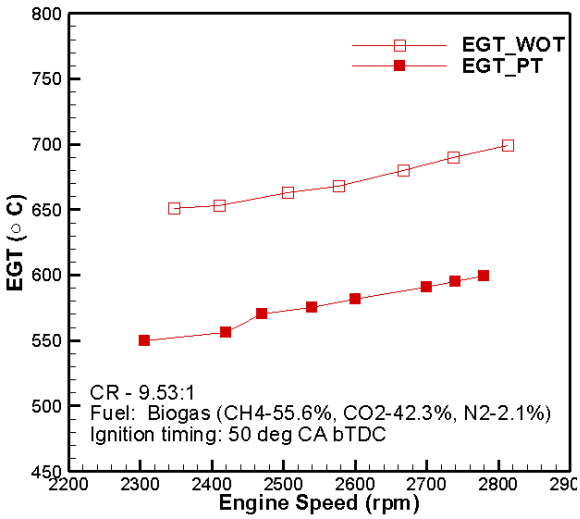

Fig. 6. 4: Engine speed Vs EGT [Retrofitted Honda GX 200 engine]

6.2.2 Combustion analysis

The variation of average cylinder pressure of a biogas fueled SI engine with WOT and PT operating conditions is shown in **Fig. 6. 5** at 2420 rpm. At WOT and PT conditions the average peak cylinder pressure were found 23.60 bar and 18.51 bar respectively. The Peak cylinder pressure was observed at 380^{o} CA and 383^{o} CA, respectively with WOT and PT conditions. However, the MBT timing was 50^{o}CA bTDC both for WOT and PT conditions. The average peak cylinder pressure in WOT condition is seeming closer to TDC where as in PT condition it is observed comparatively later in expansion stroke of the engine. This is because of the faster flame propagation, which results in improved thermal efficiency and power output at WOT condition.

Similarly, the variation of mean gas temperature (MGT) of a biogas fueled SI engine at WOT and PT condition is shown in **Fig. 6. 6**. The MGT is observed higher in case of WOT condition. The maximum temperature at WOT is found to be 1833^{o}K at 402^{o} CA where as it was observed be 1125^{o}K at 406^{o} CA. This may be because of the trend of average cylinder pressure, and mass burn fraction, where the combustion in initiated 4^{o}CA earlier in WOT

condition with reference to the PT condition. The main reason which falls behind is the faster flame front propagation rate at WOT condition.

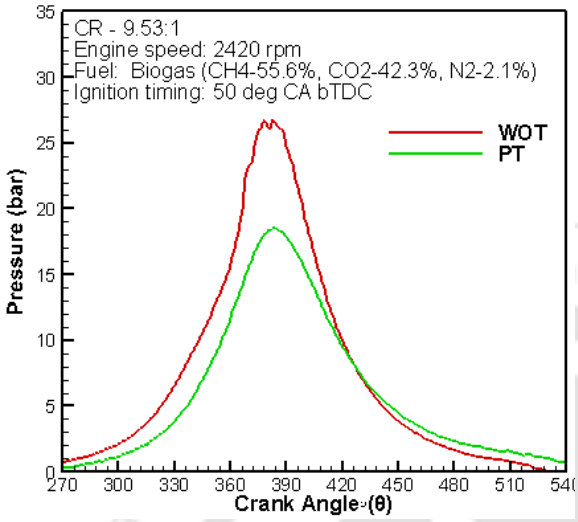

Fig. 6. 5: Crank angle Vs average cylinder pressure [Retrofitted Honda GX 200 engine]

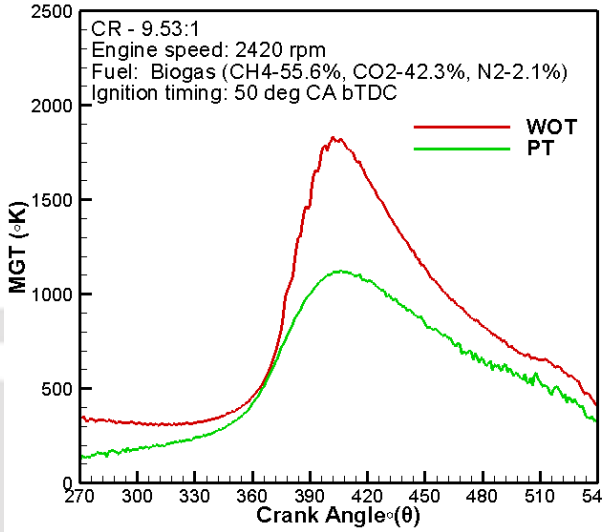

Fig. 6. 6: Crank angle Vs MGT [Retrofitted Honda GX 200 engine]

6.2.3 Emission analysis

The effect of engine speed on the concentration of CO and CO_2 in exhaust gas emission of biogas fueled SI engine at WOT and PT conditions are presented in **Fig. 6. 7** and **Fig. 6. 8**, respectively. The CO concentration was found to be decreasing with increase in speed of the engine. At PT condition the CO emission is considerably higher than WOT condition. Poor mixing of air and fuel, local rich regions and incomplete combustion produces CO, *(Jahirul et al., 2010).* At higher temperature CO converts to CO_2. At WOT and PT condition the CO concentration varies from 0.082`% to 0.01% and 0.099% to 0.005%. Since the MGT is higher at WOT condition, the CO converts in to CO_2 and the CO concentration is comparably lower in WOT condition. As shown in Fig. 5.17, the CO_2 concentration is found increasing with increasing speed of the engine. At WOT condition the CO_2 was noticeably higher than that of PT condition. Since the MGT is high in WOT condition, the CO is converted in CO_2 and because of this reason the CO_2 concentration in exhaust emission is higher as compared with PT condition. At WOT and PT condition the CO_2 concentration varies from 6.5% to 12.2% and 3.1% to 10.2%.

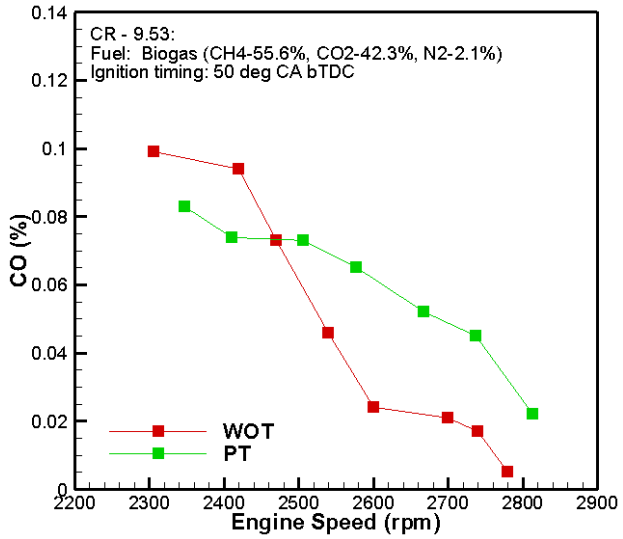

Fig. 6. 7: Engine speed Vs CO emission

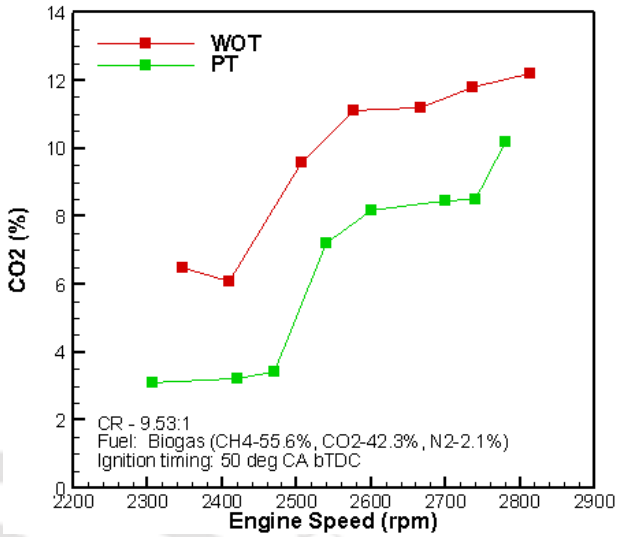

Fig. 6. 8: Engine speed Vs CO_2 emission

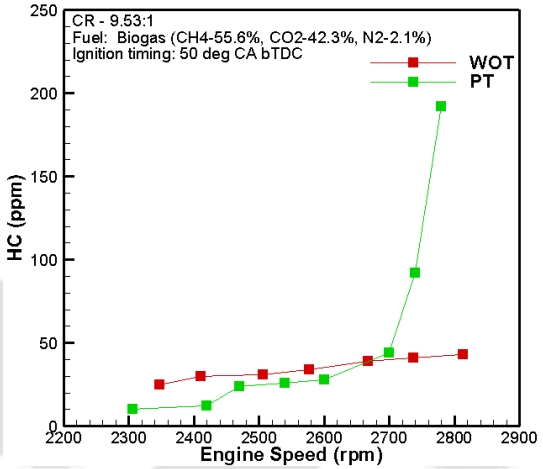

Fig. 6. 9: Engine speed Vs HC emission [Retrofitted Honda GX 200 engine]

Fig. 6. 9 explains the effect engine speed on HC concentration in the exhaust emission of a biogas fueled SI engine. The HC concentration in the exhaust emission increases with increasing speed of the engine. The HC concentration at WOT and PT condition in exhaust emission was varied in between 25 ppm to 43 ppm and 10 ppm to 192 ppm, respectively. Rich air fuel ratio with insufficient oxygen promotes the incomplete combustion of fuel as a misfire produces the UHC. Since the volumetric efficiency exactly follow the opposite trend and is comparatively lower in PT condition, the concentration of UHC is higher in PT condition and at higher speed of the engine.

6.3 Summary

A single cylinder, air cooled, gasoline fueled Honda GX 200 engine retrofitted with Honda GX 160 engine head and a biogas induction mechanism was successfully converted in to a biogas fueled SI engine. The operating CR of the engine was also enhanced from 8.5:1 to 9.53:1. The engine was operated efficiently in WOT condition. The maximum achievable BT and BP of the engine are 11.97 N-m and 2.94 kW, respectively at 2347rpm and WOT condition of the engine. Due to biogas mode operation, the rated power of the engine (3.7 kW@ 3600 rpm) was derated and dropped by 20.54%. However, the drop is quite acceptable due to the lower calorific value of biogas. The minim BSFC of the engine was found to be 0.697 kg/kWh and observed at 2347 rpm and WOT condition. The average fuel consumption of the engine was also estimated as 2.05 kg/h (1.84 m^3/h) and 1.16 kg/h (1.04 m^3/h) at WOT and PT operating condition of the engine, respectively. The maximum achievable brake thermal efficiency of the engine is 30.37% at 2347 rpm at WOT condition. The CO and HC emission of the engine is within the limiting range. However, the maximum CO2 emission was observed to be 12.2% and is the result of the CO_2 content in the raw biogas.

CHAPTER 7

Investigation of the Constant Speed Commercial Biogas Engine

Overview

*The motive behind the present investigation is to mark an bottom line by identifying the maximum BP, BTE, BSFC and deterioration of engine power along with the band of emission level from the commercial biogas engine at dynamic loading condition. Identification of the existing complication and compare the performance, combustion and emission characteristics of the commercial biogas engine, with the proposed VCR SI research engine (Engine 2) in Chapter 5, and retrofitted Honda GX 200 engine (Engine 2) in Chapter 6 at its optimized configuration are also the part of this investigation. In the present investigation a constant speed commercially customized biogas engine (Engine 1) (Make: Prakash Diesel Pvt. Ltd., Model: PN-1 BG) of rated capacity 6 HP (4.4 kW) and 1500 rpm was evaluated under different loading conditions following the standard guidelines as specified by the Bureau of Indian Standards (IS 10000: Part 6, 7 and 8)(Bureau of Indian Standards, 198*0). *Additionally, one of the key operating variables of the engine (compression ratio, CR) was also altered beyond the original configuration of the manufacturer, and the effect of operating CR on the performance, combustion and emission analysis of the biogas fuelled SI engine are also reported in this section.*

7.1 Experimental Matrix and Operating Procedure

The detail technical specifications and instrumentation of the commercially customized biogas fueled SI engine (*Engine 1*) are mentioned in *section 3.2* of **Chapter 3**. As mentioned, it's a 4.4 kW, constant speed, dedicated biogas engine with a fixed CR and CDI system. The schematic layout of the experimental facility is depicted in **Fig. 3. 2** of ***Chapter 3***. The rated CR of the engine is 13.94. However, to analyze the effect of CR on the performance, combustion and emission characteristics of the constant speed biogas operated SI engine, the operating CR of the engine was varied in between 10.52 to 15.29. The engine was tested at four different CRs (CR 10.52, CR 11.96, CR 13.94 and CR 15.29) under dynamic loading condition. The present experimental investigation consists of four folds. In the 1stfold, the CR of the engine was varied manually and set to 10.52 by method explained in the section *3.2.3* of CR variation control. The ignition timing of the engine was checked and found to be 15.88° bTDC. The H_2S scrubbed biogas (produced from anaerobic digestion of cow dung) is used as the standalone fuel for the engine. The Physico-chemical properties of the biogas used in this investigation are depicted in **Table 3. 1**. The engine is equipped with a starter motor which operates with the help of a 12 V battery connected to it. Once the engine is started, the spark timing of the engine was set MBT by manually adjusting the timing adjustment bolt and ignition switch. As soon as the engine gains its rated speed the coupled alternator produces 220 V at 50 Hz frequency. Once the output voltage of the alternator was found constant, the engine was allowed to achieve the steady state condition. The steady state is assumed to reach after operating the engine at idling condition approximately for 20 min. At this point of time there is no load on the engine. Hence to do the performance test, the engine is loaded progressively with the help of the resistive load panel by switching on a 200-Watt bulb. Once the engine is loaded, the corresponding reading of voltage output(v), current consumed (I), generated frequency (f), volume flow rate of the biogas consumed (m_f) and pressure difference across the orifice of the air box (mm of H_2O column) are recorded manually. At the same time, the pressure and crank angle signals are acquired by the piezo power unit through the lab view-based software 'Engine Soft'. For logging the P-Θ data the software was first configured for the particular setting of the engine. Similarly, for measuring the exhaust gas composition, the probe of the AVL Diagas analyzer was placed inside the tail pipe opening about 100 cm

from the exhaust port. The probe was placed inside the tail pipe for the duration of 30 s and the corresponding data are acquired by the AVL AECS software. Once the data acquisition process was completed, the load level of the engine was again varied steadily by increasing 200 watt on the base load. Similarly, the applied load was varied 15 times (200-3000 Watt in a set of 200 Watt) on the engine for a single CR ratio and the data acquisition process was repeated for each loading condition. In the 2^{nd}, 3^{rd}and4^{th}fold of the experiment, the CR of the engine was set to 11.9, 13.94 and 15.29, respectively. The above-mentioned steps for loading the engine and data acquisition were repeated for each fold of the experiment. *Table 7.1*illustrates the detailed experimental matrix for the test. The performance parameters evaluated are the air and fuel flow rates, air fuel ratio, brake power (BP), mean effective pressure (MEP), brake thermal efficiency (BTE), neat heat release rate (NHRR), mass fraction burnt (MFB), and mean gas temperature (MGT). The performance, combustion and emission characteristics of the constant speed biogas fueled SI engine was evaluated for varying load conditions at four different compression ratios ranging from CR 10.52 to CR 15.29.

Table 7.1: Experimental matrix for the commercial biogas engine *(Engine 1)*

Test	Ignition Advance	Electrical Load (Watt)	Performance Analysis	Combustion Analysis	Emission Analysis
CR 10.52:1 CR 11.96:1 CR 13.94:1 CR 15.92:1	MBT	200- 3000 (At a step of 200)	BP BSFC BTH Air-Fuel ratio Volumetric Efficiency	P-Θ NHRR MFB MGT	CO CO_2 HC NO_X

7.2 Results and Discussion

The performance, combustion and emission characteristics of the present engine (*Engine 1*) were evaluated for the varying load conditions; at the manufactures rated CR (13.94:1) and also at three other CRs (10.52:1, 11.96:1, 15.92:1) as listed in **Table 7.1**. The effect of the CR on the performance, and emission characteristics of the biogas fuelled SI engine were analysed carefully throughout the operating load range and explained in the below mentioned sections.

7.2.1 Performance analysis

Fig. 7. 1 explains the correlation between the brake load (%) and brake power (kW) developed by the biogas engine operated with CRs of 10.52, 11.96, 13.94 and 15.92. The spark timings were set to MBT before conducting each test. As observed, irrespective of the CR, the BP developed by the engine was increased with progressive development of the brake load on the engine. As shown in **Fig. 7. 2,** the developed speed of the engine remains almost constant (apart from CR 10.52:1) irrespective of the operating CRs and the developed brake torque increases with increasing brake load. As a result, the BP of the engine is also increased with progressive development of the brake load. Further, the additional explanation for this happening can also be drawn from **Fig. 7. 3** and **Fig. 7. 4**. These figures indicate that, with increasing brake load the fuel consumption rate and the volumetric efficiency of the engine are increasing to maintain the rated speed of the engine constant. This may be the key reason for the increased BP with increasing brake load on the engine. It was also observed that, with increasing CR the maximum BP output of the engine was increased with enhanced brake load carrying capacity. Higher CR increases the MGT and initiates the complete combustion and leads to higher energy conversion efficiency and develops more power.

The maximum and the minimum BP output of the engine were noticed at CR 15.29 and CR 10.52, respectively (**Fig. 7. 1)**. The maximum BP output of the engine operated at CRs 10.52, 11.96, 13.94 and 15.29 were found to be 1.94, 2.82, 2.88, and 2.93 kW with maximum brake load development of 50.40%, 73.33%, 74.80% and 76.27%, respectively. Increasing the operating CR from CR 10.52 to CR 11.96, CR 11.96 to CR 13.94 and CR 13.94 to CR 15.29 increased the maximum BP output by 45%, 2%, and 1.95%respectively. However, the observed power reduction of the engine when operated with raw biogas were found to be 55.9%, 35.9%, 34.5% and 33.4% at CR 10.52, CR 11.96, CR 13.94 and CR 15.29, respectively. Similar results have also been reported in the open literature i.e., the power of a CI engine was reduced by 46.3% when converted to a biogas fuelled SI engine operated at CR 12.65(Chandra et al., 2011; Kapdi et al., 2005).

The variations of the engine speed developed by the biogas fuelled SI engine operated at different CRs are shown in **Fig. 7. 2**. It was observed that with progressive development of the engine load, the speed of the engine starts deviating from its rated

speed. However, these deviations are quite acceptable in CRs 15.29, 13.96 and 11.94, where the maximum deviation is 9.3% from the rated speed of the engine. It was noticed that at CRs 15.29, 13.96 and 11.94 the engine speed remained almost constant (1500±50 rpm) up to 50% of the developed brake load and deviated after wards. The reason that could fit to explain the above fact may be the inefficiency of the governing system attached to the engine, which could not maintain the accurate air-fuel mixture to the engine beyond 50% of the engine load. But, at CR 10.52, the speed was drastically decreased with increase in brake load on the engine. The minimum speed observed was 1128 rpm at 50% engine load and was the maximum developed brake load at CR 10.52. Similar trends were also noticed in open literature which concludes enhanced stability and considerable deviation in engine speed at higher operating CRs (Chandra et al., 2011).

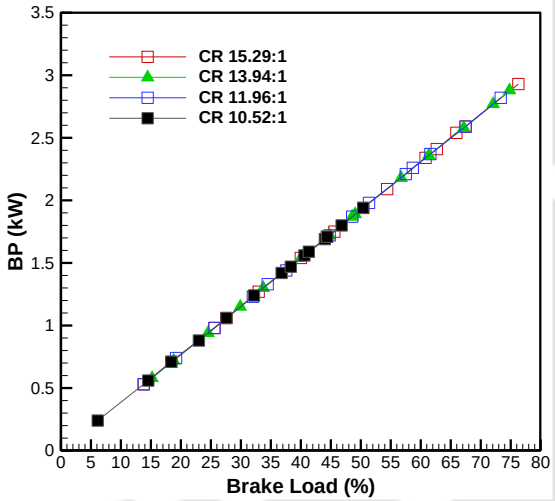

Fig. 7. 1: Effect of CR on the BP developed by the engine

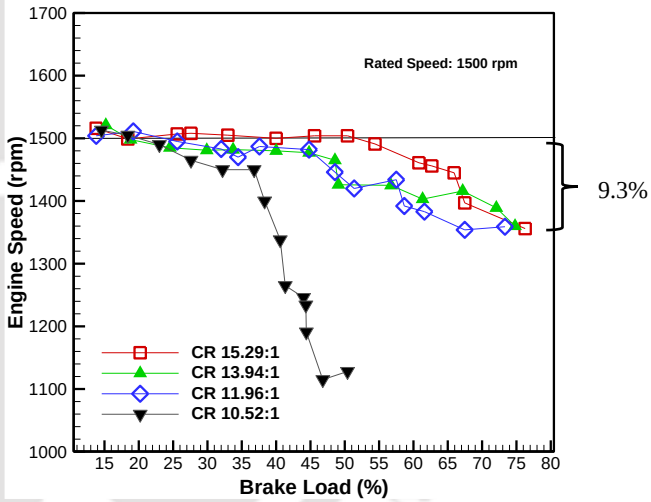

Fig. 7. 2: Effect of CR on the developed speed of the engine

Fig. 7. 4 depicts the variation of the VE of engine against the developed brake load when operated within the CR ranging from 10.52 to 15.29. It was observed that, irrespective of operating CR, the volumetric efficiency of the engine followed an increasing trend along with progressive development of the engine load. This is due to the fact that, with increasing brake load, the mass flow rate of the fuel consumed is increased (**Fig. 7. 3**) which interns induced more air to combustion chamber. It was also observed that, with increase in operating CR, the VE of the engine followed a decreasing trend. The VEs of the engine operated at CRs 10.52, 11.96, 13.94 and 15.29 were found to very between 34.6-51.1%, 32.7-48.8%, 29.1-48.3%, and 28.7-32.7% respectively. However, the maximum volumetric efficiency was observed at CR 10.52.

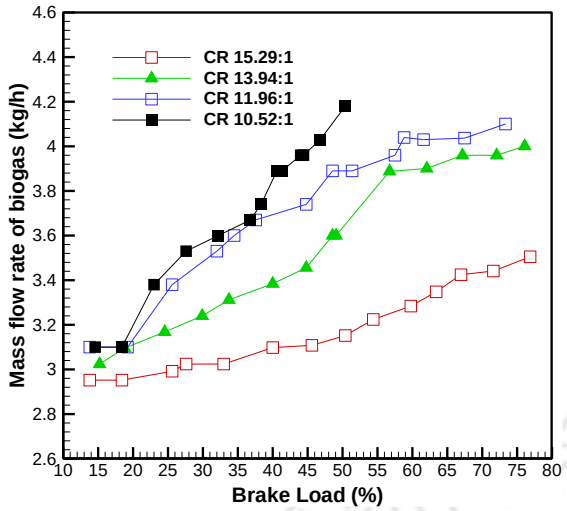

Fig. 7. 3: Effect of CR on the fuel consumption rate

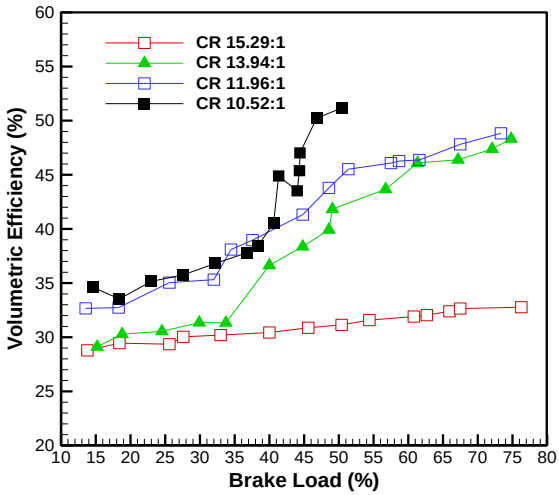

Fig. 7. 4: Effect of CR on the volumetric efficiency of the engine

Fig. 7. 5 shows the correlation between the BSFC and brake load of the engine at different operating CRs. It was evident from the figure that, irrespective of CR, the BSFC followed a decreasing trend with increase in brake load of the engine. This is because, with increasing brake load, the rate of rise in BP is higher than the rate of rise in mass of fuel consumed. It was also observed that the BSFC of the engine followed a decreasing trend with progressive development of the operating CR. The engine operated at CRs 15.29, 13.94, 11.96 and 10.52 exhibited the maximum BSFCs of 5.29 kg/kWh, 5.17 kg/kWh, 5.83kg/kWh and 5.53 kg/kWh at the brake loads of 13.8%, 15.20%, 13.8% and 14.57%, respectively. However, the minimum BSFCs of the engine operated at CRs 15.29, 13.94, 11.96 and 10.52 were found to be 1.15 kg/kWh, 1.43 kg/kWh, 1.46 kg/kWh and 2.15 kg/kWh at the brake loads of 76.2%, 74.8%, 73.3% and 50.4%, respectively. At a particular loading condition (50% brake load) increasing the CR from 10.52 to 11.96, 11.96 to 13.94 and 13.94 to 15.29 reduced the BSFCs by 8.37%, 4% and 21%, respectively, which concludes that the BSFC is reduced with increase in CR. This is because, with increase in CR, the rate of rise in BP is lesser than the rate of drop in mass of fuel consumed. Additionally, the mass of fuel consumed to generate unit BP is comparatively less at lower CRs.

The variation of BTE of the engine with progressive advancement of the developed brake load at different operating CRs are shown in **Fig. 7. 6**. It was observed that irrespective of CR, the BTE followed an increasing trend with increase in brake load of the engine. At all operating CRs the BSFC of the engine followed a decreasing trend against

the developed brake load (**Fig. 7. 5**). Hence the BTE followed an opposite trend to BSFC. It was also observed that the BTE followed an increasing trend with increase in operating CR of the engine. This is because of the enhanced BP and reduced fuel consumption rate of the engine at higher operating CRs. The engine operated at CR 15.29 revealed the maximum BTE of 18.35% at 76.2% of developed brake load. However, the maximum BTE of the engine operated at CRs 13.94, 11.96 and 10.52 were found to be 14.84%, 14.55% and 9.83%, respectively. Increasing the operating CR from 10.52 to 11.96, 11.96 to 13.94 and 13.94 to 15.92 enhanced the BTE of the engine by 48%, 2% and 23.6%, respectively.

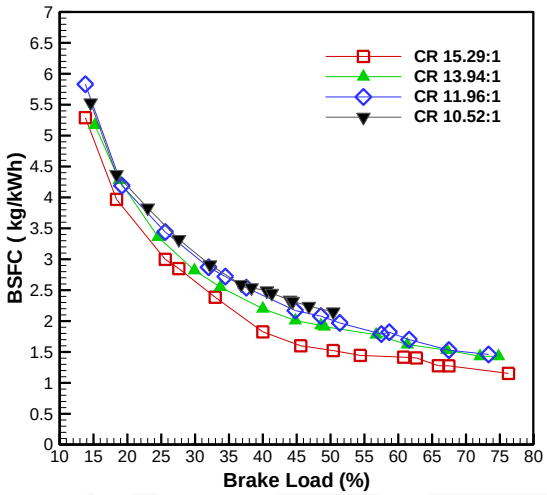

Fig. 7. 5: Effect of CR on the BSFC of the engine

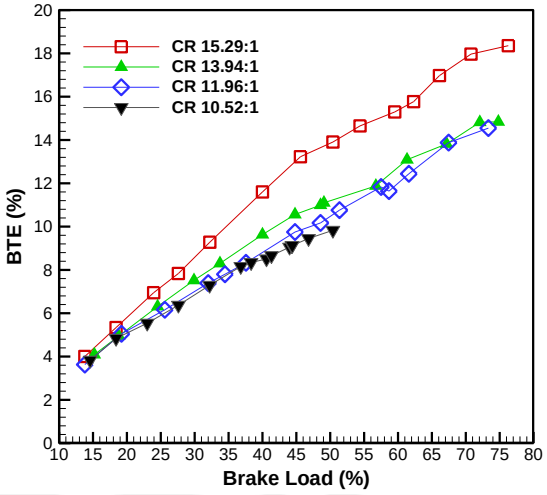

Fig. 7. 6: Effect of CR on the BTE of the engine

7.2.2 Combustion analysis

Cylinder pressure data analysis is an important tool to diagnose the engine combustion behavior. The cylinder pressure history directly influences the engine performance and the emission characteristics. In this study, the cylinder pressure data acquired through the data acquisition system is being used to draw the P-θ curves, the curves of NHHR, MFB and MGT for various loading condition and at different CRs of the engine. The biogas combustion in SI engine is much similar to gasoline combustion, where the combustion occurred in a premixed mode. The biogas air fuel mixture undergoes pre-ignition reaction during relatively long compression stroke. The pre-ignition phenomenon leads to the formation of active radicals and partial combustion products that greatly affect the combustion characteristics.

Fig. 7. 7 illustrate the effect of operating CR on the average cylinder pressure of the engine at 50% brake load condition. It was observed that, with increase in CR, the average peak cylinder pressure was increased and shifted towards TDC. The average peak cylinder pressure at CRs 15.29, 13.94, 11.96 and 10.52 were found to be 18.3, 15.9, 14.3 and 13.3 bar, respectively at 50% brake load condition of the engine. Increasing the CR from 10.52 to 11.96, increased the peak cylinder pressure by 7.9% at 50% brake load. Further, increasing the CR from 11.96 to 13.94, and 13.94 to 15.29 improved the average peak cylinder pressure by 10.9% and 14.6%, respectively at 50% brake load condition. Since biogas has high antiknock index, it could withstand the higher CR without knocking. There was no trace of knocking while operating the engine even at CR 15.29. The higher content of CO_2 (42%) in the raw biogas may be the reason behind accommodating such higher CR without traces of knock in the engine cylinder. It was also noticed that, progressive advancement of the CR from 10.52 to 11.96, 11.96 to 13.94, and 13.94 to 15.92 shifted the peak cylinder pressure by 0°, 4° and 2° crank angle (CA) and appeared at 387°CA, 383° CA, and 381° CA. Shifting of the peak pressure towards the TDC is an indication of better combustion. This is due to the faster flame front propagation which also results in improved thermal efficiency and power output at this condition (Stone et al., 1993)

Fig. 7. 8 explains the effect of operating CR on the variation of peak cylinder pressure (PCP) with the developed brake load of the biogas fueled SI engine. The PCP was increased with the increase in CR of the engine and the same was also noticed in **Fig. 7. 7**. As observed, the PCP followed an increasing trend along with the progressive development of the brake load on the engine. This is only due to the increase in consumed fuel mass at higher brake loads as depicted in **Fig. 7. 3**. The PCPs at CRs 10.52, 11.6, 13.94 and 15.29 were found to very between 11.2 to 13.9 bar, 10.9 to 21.2 bar, 12.6 to 21.5 bar and 15.6 to 23.3 bar, respectively in an increasing trend.

The effect of brake load on the average cylinder pressure of the engine operating with CR 15.29 at a rated speed of 1500 rpm was shown in **Fig. 7. 9**. It was clearly observed that, the peak cylinder pressure was increased steadily with progressive advancement of the developed brake load on the engine. But it was also observed that with progressive development of the brake load, the peak cylinder pressure was shifted away from the TDC. The shifting of PCP towards the expansion stroke is a clear indication of late combustion (Huang and Crookes, 1998a; Nirendra N Mustafi et al., 2006) of biogas at the increased

brake loading condition of the engine. The reason behind this fact is the increased fuel consumption at higher brake loading conditions of the engine as depicted in **Fig. 7. 3**. Because of this reason the combustion duration is also being increased with increasing brake load on the engine. The crank angles corresponding to the PCPs are 3˚, 5˚, 7˚, 11˚, 11˚, 13˚, 13˚, 19˚, 23˚, 23˚, 23˚, 23˚, 23˚, 23˚ and 23˚ aTDC (after TDC) at brake loading condition of 6.9%, 13.8%, 18.4%, 25.6%, 27.6%,32.9%, 40%, 45.6%, 50.4%, 60.8%, 62.6%, 65.9%, 67.4% and 76.3%, respectively.

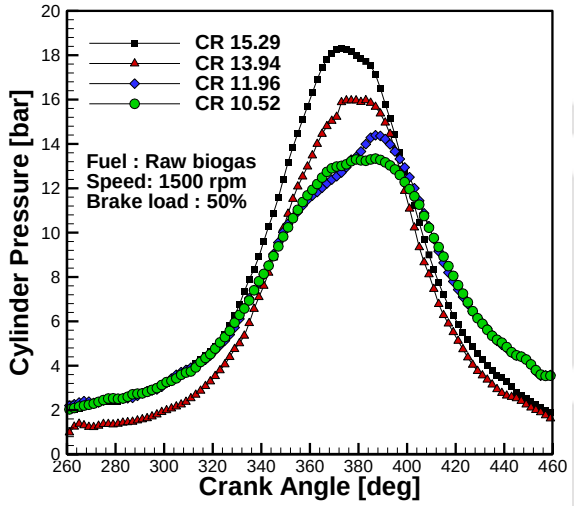

Fig. 7. 7: Effect of CR on the average cylinder pressure of the biogas fueled SI engine

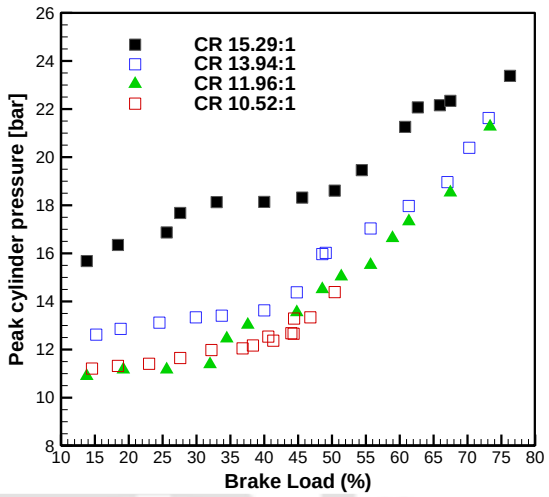

Fig. 7. 8: Effect of CR on the peak cylinder pressure of the biogas fueled SI engine

The effect of CR on the NHRR of the biogas fueled SI engine at 50% brake load condition is shown in **Fig. 7. 10**. It was observed that, the NHRR followed an increasing trend with increase in CR of the engine and found maximum at CR 15.29. The maximum NHRRs at CRs 10.52, 11.96, 13.94 and 15.29 were found to be 20.7 J/˚CA, 21 J/˚CA, 21.1 J/˚CA and 24.1 J/˚CA, respectively at 50% brake load condition. In the heat release analysis, the data were evaluated on differential basis which led to noise in the computed result of NHRR, especially at the lower pressure regions where the discretization are a larger proportion of the signal. Hence, the large variation in NHRR at low pressure regions may be neglected due to the uneven peak at that point. The negative NHRR implies a certain heat transfer to the cylinder wall and the CA close to the minimum value of NHRR signifies the point of ignition initiation in the combustion chamber. The increase in heat transfer rate is due to the increased temperature and density of the gas during combustion phenomena. But once the combustion completes, the heat release rate will start adding negative value

to the heat transfer. It was also observed that, with increase in CR, the peak NHRR was shifted towards TDC and appeared at CA of 27°, 2°, 23° and 21° aTDC at CRs 10.52, 11.96, 13.94 and 15.29, respectively. Shifting of peak NHHR with increase in CR is an indication of better combustion. This is due to the enhanced flame propagation rate where the energy conversion efficiency is maximum.

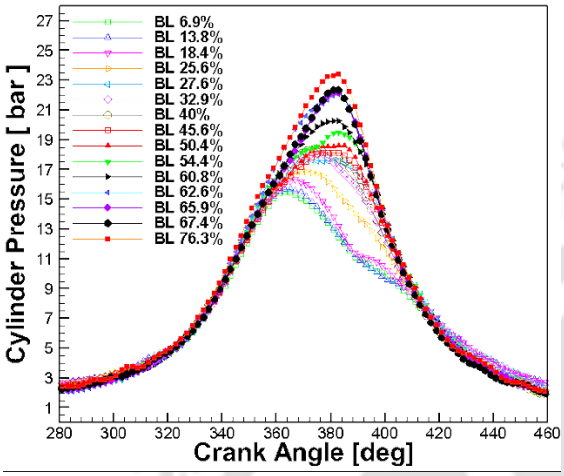

Fig. 7. 9: Effect of BL on the average cylinder pressure of the biogas fueled SI engine at CR 15.29

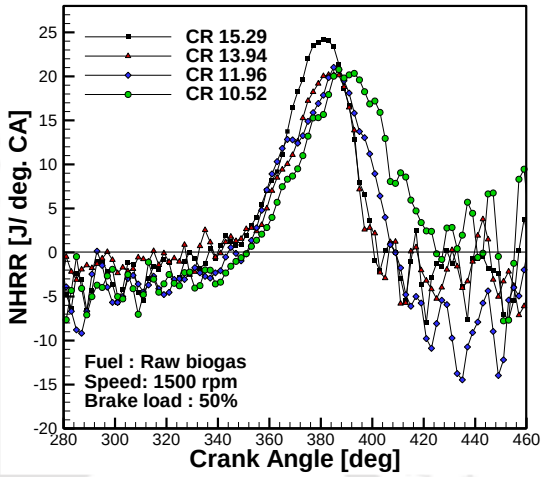

Fig. 7. 10: Effect of CR on the NHRR of the biogas fueled SI engine

Fig. 7. 11 illustrates the effect of CR on the variation of the MFB of the biogas operated SI engine at 50% brake load condition. It was observed that with increase in CR, the combustion of the biogas was started earlier and the flame was developed much before TDC. At CR 10.52, the combustion was initiated at 357° CA and terminated at 417° CA. Similarly, at CRs 11.95, 13.94 and 15.92 the flame development was initiated at CAs 355°, 351° and 349°, respectively. It was concluded that, the duration of combustion was reduced with increase in CR of the engine. The combustion durations at CRs 10.52, 11.95, 13.94 and 15.92 were found to be 60° CA, 56° CA, 54° CA and 50° CA, respectively. Hence, it was confirmed that with increase in CR, the rate of flame front propagation became faster and was higher in CR 15.29 for the biogas fueled SI engine.

The effect of CR on the MGT of the engine at 50% brake load condition is shown in **Fig. 7. 12**. It was observed that the MGT was increased with increase in CR of the engine. This is due to the fact that, with increasing CR the total volume of the engine decreases by reducing the clearance volume. The MGT is the function of volume and pressure at a particular CA. Hence, the MGT was increased with the increased CR. The maximum MGTs

at CRs 10.52, 11.96, 13.94 and 15.29 were observed to be 666° C, 679° C, 740°C and 789° C, respectively at CAs 419°, 407°, 405° and 397°.

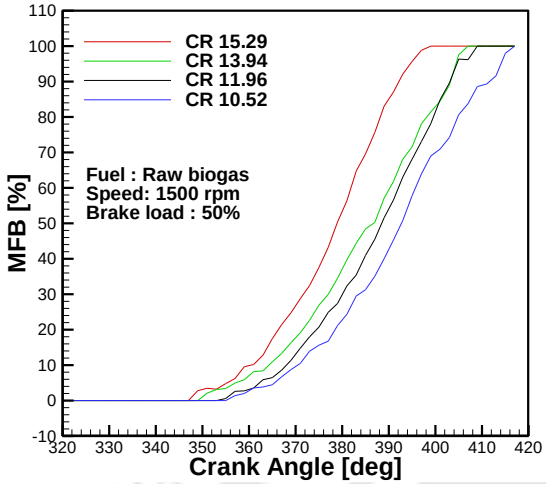

Fig. 7. 11: Effect of CR on the MFB of the biogas fueled SI engine

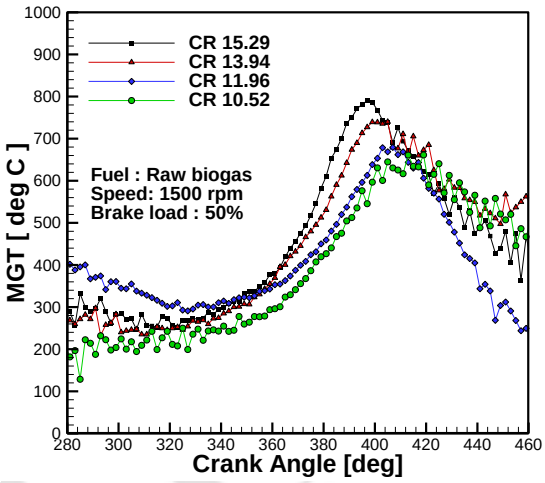

Fig. 7. 12: Effect of CR on the NHRR of the biogas fueled SI engine

7.2.3 Emission analysis

Carbon monoxide (CO) forms partially due to deficiency of oxygen in the fuel air mixture leading to incomplete combustion. In the current investigation as depicted in **Fig. 7. 13,** the CO emission was decreased with increase in CR of the engine. The phenomena can be related to the fuel mass consumed and the oxidation process of fuel. At lower CRs, the quantity of fuel mass consumed is comparatively higher. However, incomplete combustion takes place due to deficiency of oxygen ultimately restricting CO getting oxidized. On the contrary, with increase in CR, the flame front propagation becomes faster and consumes enough biogas-air mixture to bring down the CO level. It was also observed that, the CO emission followed an increasing trend with progressive development of brake load on the engine. The minimum CO emission was observed with CR 15.29 and found to very between 0.016 - 0.091%. The maximum CO emission was found with CR 10.52 and varies between 0.022 - 0.17%. Similarly, the effect of CR and brake load on the CO_2 emission of the commercial biogas engine is shown in **Fig. 7. 14**. As observed the CO_2 emission was found increasing with enhanced CR of the engine. This happening may due to the higher mass of fuel consumed and lower oxidization rate at lower operating CR of the engine. This happening can also be correlated with the MGT maintained during higher operating CR of the engine. Hence it positively affects the CO oxidization rate, which

reduced the CO level and increased the CO_2 level at higher operating CR of the engine (Papagiannakis and Zannis, 2013).It was also observed that irrespective of operating CR, the CO_2 emission followed a decreasing trend with increasing break load on the engine. The maximum CO2 emission was observed with CR 15.29 and found to very between 12.2–6.4 %. The minimum CO emission was found with CR 10.52 and varies between 8.2–6.2%.

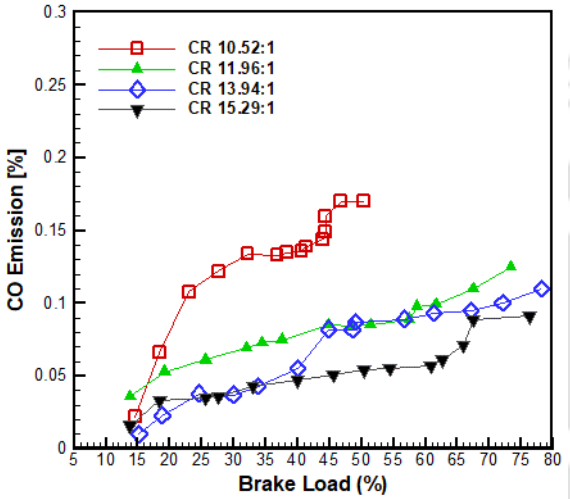

Fig. 7. 13: Effect of CR on the CO emission of the biogas fueled SI engine

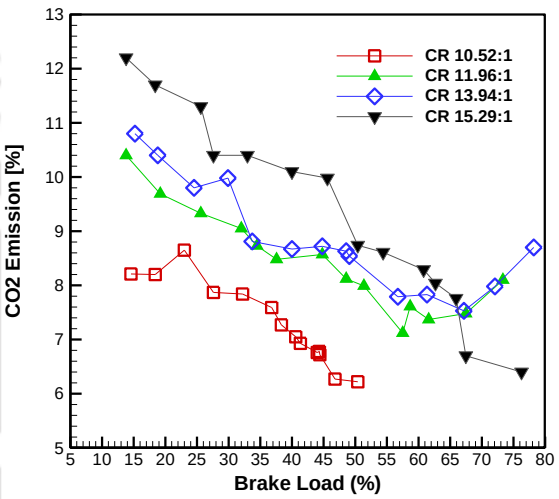

Fig. 7. 14: Effect of CR on the CO_2emission of the biogas fueled SI engine

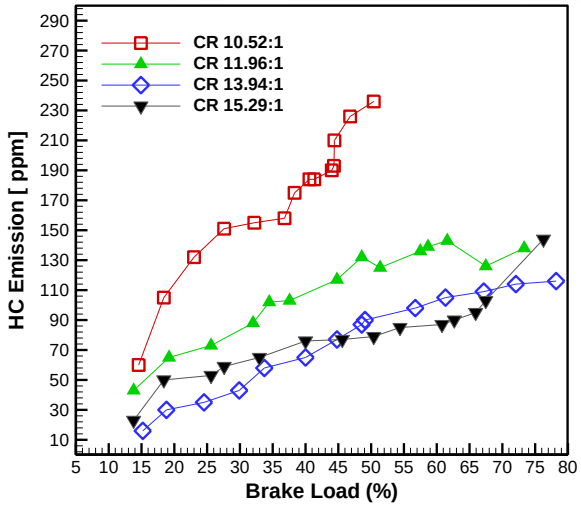

Fig. 7. 15: Effect of CR on the HC emission of the biogas fueled SI engine

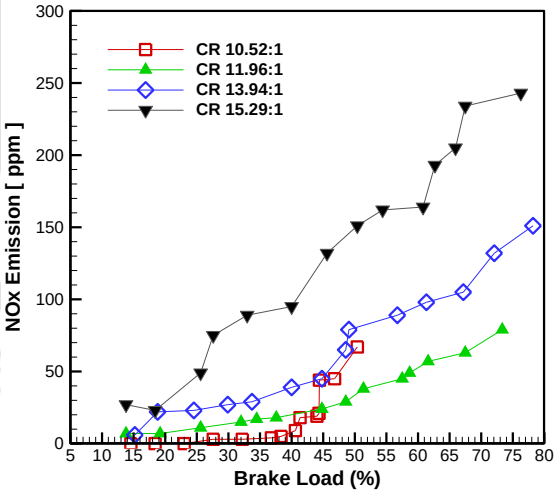

Fig. 7. 16: Effect of CR on the nitric oxide emission of the biogas fueled SI engine

The variation of HC emission at different CRs of the engine is shown in **Fig. 7. 15**. It was observed that the HC content in the exhaust emission of the SI engine was decreasing

with increasing CR of the engine. It was also observed that, irrespective of CR, the HC emission followed an increasing trend with increasing brake load on the engine. The unburnt hydro carbon is the product of incomplete combustion. Irrespective of engine loading condition, the minimum HC emission was observed at CR 15.29 and was found to very between 23-144 ppm.

Table 7. 2: Data of engine performance parameters at different operating CR

Operating CR	Performance parameter						Combustion parameter			Emission parameter		
	Maximum Achievable brake load	BP (kW)	BTE (%)	BSFC (kg/kW-h)	Fuel consumed (kg/h)	VE (%)	PCP (bar)	MFB duration (° CA)	MGT (K)	CO (%)	HC (ppm)	NOx (ppm)
10.52	50.40	1.94	9.83	2.15	4.18	51.1	13.9	60	666	0.17	236	67
11.96	73.33	2.82	14.55	1.46	4.10	48.8	21.2	56	679	0.12	138	79
13.94*	74.80	2.88	14.84	1.43	3.99	48.3	21.5	54	740	0.11	116	151
15.29	76.27	2.93	18.35	1.15	3.50	32.7	23.3	50	789	0.09	144	243

* Rated compression ratio of the engine

Fig. 7. 16 shows the effect of CR on the NO_x emission of the engine. It was observed that with increasing CR and brake load on the engine, the NO_x concentration in the exhaust emission of the engine followed an increasing trend. The maximum NO_x emission was detected at CR 15.29 and was found to very between 27-243 ppm. The NO_x emission is strongly related to the lean fuel with high cylinder temperature or high combustion temperature. The cylinder temperature and combustion temperature were increased with increase in CR and was higher in case of CR 15.29 as compared to other CRs. Because of this reason, the NO_x concentration was comparatively higher at CR 15.29. **The variation of** HC emission at different CRs of the engine is shown in **Fig. 7. 15.** It was observed that the HC content in the exhaust emission of the SI engine was decreasing with increasing CR of the engine. It was also observed that, irrespective of CR, the HC emission followed an increasing trend with increasing brake load on the engine. The unburnt hydro carbon is the product of incomplete combustion. Irrespective of engine loading condition, the minimum HC emission was observed at CR 15.29 and was found to very between 23-144 ppm.

Table 7. 2 shows the consolidated data of performance, combustion and emission parameters of the commercially customized biogas engine at the rated and other attainable operating CRs at maximum achievable brake load condition.

7.3 Summary

Based on the experimental investigation carried out to investigate the effect of CR on the performance and emission characteristics of the raw biogas fueled, constant speed SI engine, the following conclusions are drawn.

- Operating the engine at the rated CR (13.94) and maximum brake load condition (74.8%) declined the rated speed of the engine by 9.3% and deteriorated the engine power by 34.5%. The maximum achievable BP and BTE of the commercial biogas engine were 2.88 kW and 14.84%, respectively at the rated CR. The CO, HC and NOx concentration in the exhaust emission of the engine at the rated operating CR were 0.11%, 116 ppm, and 151 ppm, respectively at the maximum brake load condition.
- Higher CR increased the MGT (which helped in complete combustion) that led to higher energy conversion efficiency and ultimately more power. The maximum achievable brake load and brake power of the engine were observed at CR 15.29 and found to be 2.93kW and 76.27%, respectively. The stability of the engine was enhanced and the deviation of the operating speed was acceptable at higher operating CRs.The biogas engine operating with CR 15.29 revealed the minimum BSFC (1.15 kg/kWh) and the maximum BTE (18.35%) at 76.2% of brake load.
- The CO and HC concentration in the exhaust emission of the engine were decreased with increasing CR. Whereas, the NOx concentration was increased with increasing CR. The minimum CO and HC emission were observed at CR 15.29 and found to vary between 0.016 - 0.091% and 23-144 ppm, respectively. The maximum NOx emission was detected at CR 15.29 and found to vary between 27-240 ppm.

CHAPTER 8

Comparative Assessment of the Biogas Fueled SI Engines

Overview

The present Chapter includes the comparative assessment of the biogas fueled SI engines on the basis of performance, combustion and emission analysis. The performance, combustion and emission characteristics of the biogas fueled SI engines at their respective optimum operating condition are considered for this assessment. As mentioned, in ***Chapter 3,*** three SI engines are used for the present investigation. **Engine 1** is a commercially customized, constant speed biogas fueled SI engine having rated power 4.4 kW at CR 13.94, IT 15.88º CA bTDC and 1650 rpm. **Engine 2,** is a variable speed, VCR SI research engine having rated power output of 4.5 kW at 1800 rpm in gasoline mode operation. However, The VCR SI engine is retrofitted and fueled with biogas and produced maximum output power of 3.52 kW at CR 12, MBT 33º CA bTDC, WOT condition and 1400 rpm. Similarly, **Engine 3,** is a variable speed commercial SI engine (Honda GX 200), retrofitted with the optimized operating parameters obtained from **Chapter 5** to enable the engine for biogas operation. The rated output power of **Engine 3** is 4.1 kW at CR 8.5 and 3600 rpm in gasoline mode operation. Whereas, the retrofitted engine produced 2.9 kW at CR 9.54, MBT 33º CA bTDC, WOT condition and 2347 rpm. The biogas operated engines mentioned above are compared here in this chapter to justify the possibility of using the retrofitted **Engine 3** for biogas application under the specified operating condition.

8.1 Result and Discussion

The performance, combustion and emission characteristics of the biogas fueled engines are compared here in this section at their optimum operating condition. ***Engine 1*** is a commercially customized, constant speed biogas fueled SI engine having rated power 4.4 kW at CR 13.94, MBT 15.88^{o} CA bTDC and 1650 rpm. However, the maximum BP of the engine was reported 2.87 kW at CR 13.94, IT 15.88^{o} CA bTDC and brake load of 74.8% in **Chapter 7**. Similarly, the optimum operating condition for the VCR SI engine, ***Engine 2*** for biogas operation was reported CR 12, MBT 33^{o} CA bTDC, WOT condition and 1400 rpm in ***Chapter 5.*** Whereas**,** the optimum operating condition for the biogas fueled retrofitted Honda GX 200 engine, **Engine 3** was reported CR 9.54, MBT 33^{o} CA bTDC, WOT condition and 2347 rpm in ***Chapter 6.*** The biogas fueled engines are operated with the above mentioned optimum operating conditions and the BP, BTE, BSFC, CO, CO_2, HC and NOx emission from these engines are analyzed here along with the in-cylinder pressure and temperature profile.

8.2 Comparative Assessment

Fig. 8. 1 depicts the comparative assessment of the biogas fueled SI engines based on their BP, BTE and BSFC. As noticed, the induced BP was found maximum for Engine 2, followed by Engine 3 and Engine 1 respectively. The BP produced was recorded 3.52 kW, 2.94 kW and 2.87 kW, respectively for engine 2, 3 and 1. Although the operating CR of the Engine 1 is higher than that of Engine 2 and Engine 3, the IT set was not optimum for the operating CR (13.94) of the engine. Hence, the BP induced was minimum for Engine 1 (Jaramillo et al., 2018). The BP of the VCR SI engine at their optimum configuration found 22% higher than that of the commercial biogas engine. Similarly, the BP of the retrofitted Honda GX 200 engine at their optimum configuration is found 2.3% higher than that of the commercial biogas engine. Similarly, the BTE of the VCR SI engine at its optimum configuration is also found maximum among the three used engines. Similar observations while operating the biogas engine at its optimum configuration are also reported in open literatures (Crookes, 2006; Porpatham et. al.,2012, 2013). The maximum BTE observed with Engine 1, 2 and 3 are recorded 14.8%, 31,9% and 30.3%, respectively. The BTE in case of Engine 2 and 3 were increased by 114% and 104%, respectively with respect to the commercial biogas engine (Engine 1). Likewise, the BSFC is also observed minimum for Engine 2 followed by Engine 3 and Engine 1, respectively. The BSFC recoded for Engine 1, 2 and 3 are reported 1.43, 0.66 and 0,70 kg/kW-h. As recoded,

the biogas consumption rates are found 4.10, 2.34 and 2.05 kg/h respectively for Engine 1, 2 and 3.

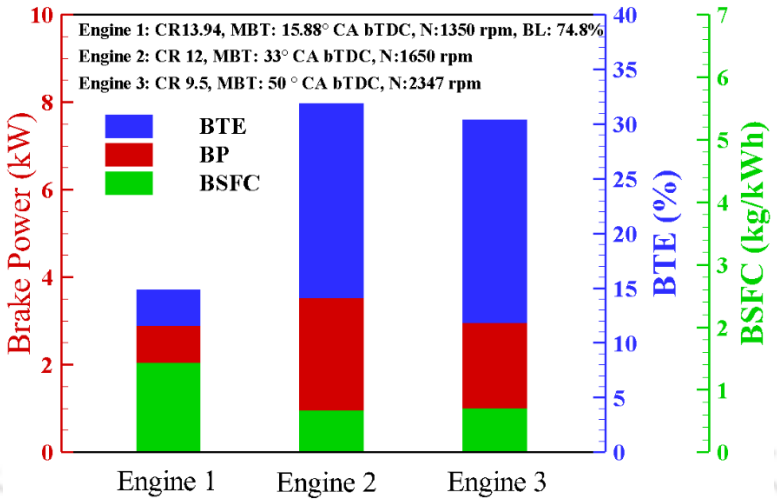

Fig. 8. 1: Comparative assessment of performance parameters of the biogas fueled engines

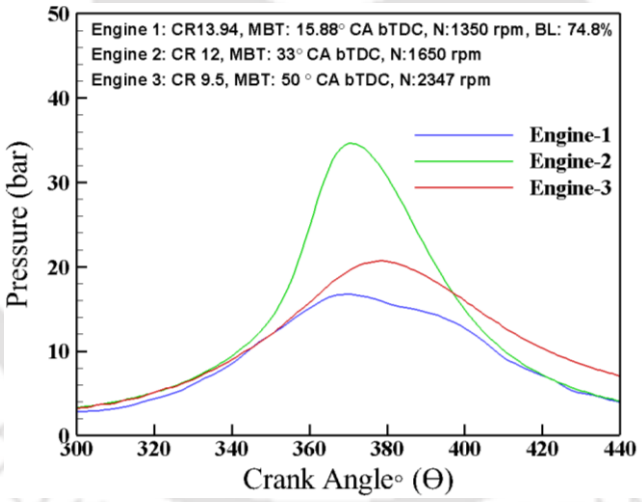

Fig. 8. 2: Comparative assessment of cylinder pressure profile of the biogas fueled engines

Fig. 8. 2 describes the in-cylinder pressure profile of the biogas fueled SI engines. As observed, the PCPs are recorded 16.7, 24.6 and 20.6 bar at 369ºCA, 375ºCA, and 389ºCA, respectively for Engine 1, 2 ad 3. It has been noticed that, the PCP in the engine cylinder is very low even though, the operating CR of Engine 1 is 13.94. Further, the LPP in Engine 1 is also observed very close to the TDC. Hence, there may be preignition or the rate of pressure

rise is too intense before the end of compression stroke. This may be the key reason to have lesser output BP for Engine 1 (Huang and Crookes, 1998a; Stone, 2012).

The comparative assessment of CO and CO_2 concentration in the exhaust emission of the biogas fueled SI engines are portrayed in **Fig. 8. 3**. The in-cylinder temperature (average MGT) and the operating ER plays key role to control the CO concentration in the exhaust emission. The operating ERs for the current operating condition of the engine are recorded 1.12, 0.82 and 1 respectively for Engine 1, 2 and 3. With increased ER, CO concentration in the exhaust emission increases gradually for biogas rich mixture due to the absence of oxygen and unburnt HC (Mokrane, 2018). Hence, the CO emission was minimum and recorded 0.03% for Engine 2. The CO emission recorded for Engine 1 and 3 are also with in the acceptable limit and found 0.11% and 0.22 %, respectively. As the average MGT is higher for Engine 2, the CO molecules are oxidized and reflected in the exhaust emission (Pulkrabek, 1997). The CO_2 emission was recorded 9.1% higher and 25.2% lower for Engine 2 and 3 with respect to Engine 1

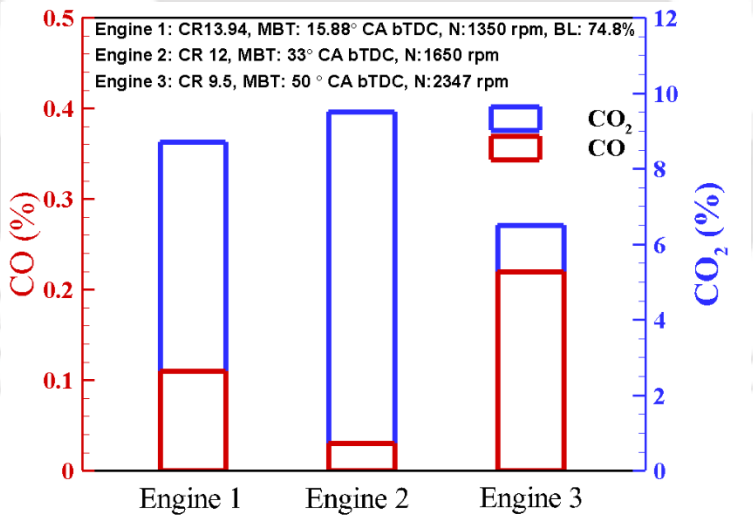

Fig. 8. 3: Comparative assessment of CO and CO_2 emission from the biogas fueled engines

The comparative assessment of HC and NO_x emission of the biogas fueled engine are depicted in **Fig. 8. 4**. As observed, the HC emission of Engine 1, 2 and 3 are recoded 116, 45 and 25 ppm respectively. The HC emission was harshly increased for Engine 1 due to incomplete combustion and preignition in the engine cylinder initiated because of higher operating CR (CR 13.94) (Huang and Crookes, 1998). Similarly, NOx emission reported was

found maximum for Engine 3. Since, the NOx emission is temperature dependent (Chandra et al., 2011) and the peak MGTs for Engine 1,2 and 3 are recoded 711.5, 1017.2, 1311.6 K, the NOx emission was found 151, 325, and 1472 ppm, respectively.

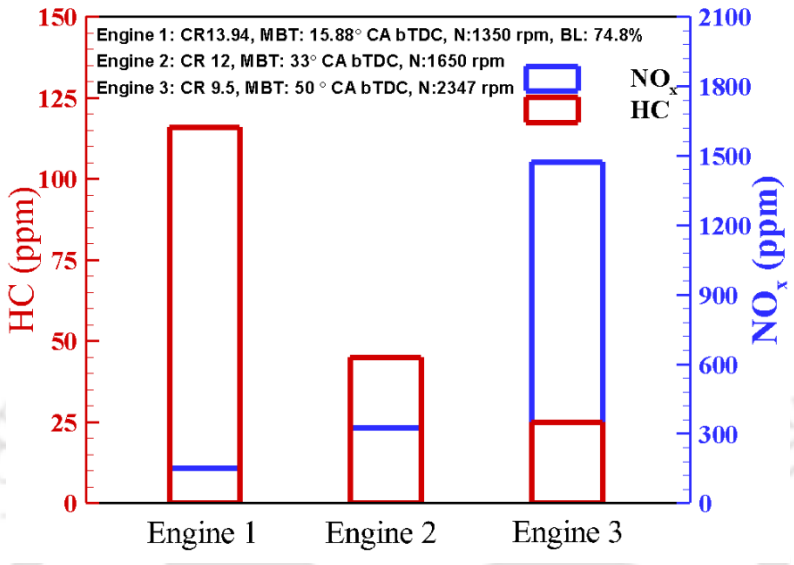

Fig. 8. 4: Comparative assessment of the HC and NO_x emission from the biogas fueled SI engine

8.3 Summary

The comparative assessment of the biogas fueled SI engines are summarized and the following conclusion were drawn.

The BP output of the commercial biogas engine (Engine1) is 22% and 2.3% lower than the VCR SI engine (Engine 2) and retrofitted Honda GX 200 engine (Engine 3), respectively at their optimum configuration. The BP produced was recorded 3.52 kW, 2.94 kW and 2.87 kW, respectively for engine 1, 2 and 3.

The BTE of the commercial biogas engine (Engine1) is 114% and 104% lower than VCR SI engine (Engine 2) and retrofitted Honda GX 200 engine (Engine 3), respectively at their optimum configuration. The maximum BTE observed with Engine 1, 2 and 3 are recorded 14.8%, 31,9% and 30.3%, respectively.

The HC emission was harshly increased for the commercial engine (Engine 1) and reported 116 ppm against 45 and 25 ppm for Engine 2 and 3. However, the NO_x emission was recorded 151, 325, and 1472 ppm respectively for Engine 1, 2 and 3.

CHAPTER 9

Conclusion and Scope of Future Work

9.1 Conclusion

The current research is mainly focused on the biogas fueled retrofitted SI engines. It is highly desirable to improve the performance of a variable speed SI engine if it is operated with biogas. The theme of the thesis is framed to determine the near optimal operating parameters (optimum compression ratio, maximum brake torque timing, throttle position and optimum air-fuel ratio) of a biogas fueled SI engine through a multi fuel, variable compression ratio (VCR), spark ignited research engine setup for effective implementation in a commercial SI engine. Moreover, baseline experiments are also carried out towards comparative assessment of the VCR SI engine fueled with gasoline, methane and biogas. Further, in the process of developing a dedicated biogas fueled SI engine, the optimized operating parameters (CR, IT, TP and AFR) attained through the series of experimentation in the VCR SI research engine setup were incorporated in a commercial SI engine with due modification in the fuel induction system. Finally, the performance of the dedicated biogas fueled variable speed SI engine is compared with an existing commercial biogas engine. As a result of this experimental campaign following conclusions have been derived.

- Biogas fueled VCR SI engine produced an average of 17.5% and 4.5% less BP than that of the gasoline and methane fueled SI engine at WOT operating condition at CR 10.
- With IT progressively advanced from the TDC, the induced BT and BP of the engine consistently improved up to 40° CA bTDC both for WOT and PT conditions due to faster flame propagation speed. Further advancement of the IT, reduced the BT and BP of the engine at CR 10.
- For the operating speed range (1400-1700 rpm), 40° CA bTDC is considered as the optimum IT for both WOT and PT conditions
- Irrespective of operating condition, the BSFC for the biogas fueled SI engine is always higher than that of the gasoline and methane fueled SI engine throughout the speed range.

- The duration of RBA is detected minimum for the methane fueled SI engine (21° CA at WOT and 23° CA at PT) and indicates the higher flame front propagation rate at the MBT timing.
- The early flame development and propagation rate resulted in maximum energy conversion efficiency at 45° CA bTDC for biogas fueled engine.
- At WOT conditions, the PCPs and LPPs of the biogas fueled SI engine are dropped by 31-34% and shifted by 3-4° CA, respectively with reference to the gasoline fueled engine.
- The average CO and NO_x emission of the biogas fueled SI engine is reduced by 45.5% and 67.5% than that of gasoline fueled SI engine at WOT condition.
- Irrespective of the operating CR, the progressive advance of IT for the biogas fueled VCR SI engine recorded a satisfactory development of the induced BT and achieves the MBT followed by the declined BT at the over advanced Its due to higher peak pressure and NHRR to produce maximum expansion work.
- MBT timing shift towards TDC as the operating CR increases due to the increased pressure and temperature at the end of compression stroke along with reduced fraction of residual gas at higher CR.
- MBT timings are progressively advanced by certain CA with increasing engine speed irrespective of the operating CR due to the shorter time interval of combustion process as a result of turbulence.
- Irrespective of the operating CR, the progressive advance of IT enhanced the BTE of the engine up to the MBT timing and declined further with the over advanced IT.
- With the progressive IA, the slope of the pressure and temperature gradients are constantly increasing just before the TDC.
- The area under the P-V curve which represents the network output during the cycle found improving up to the MBT timing due to the faster flame propagation, thereby resulting improved thermal efficiency and power output at 33° CA bTDC.
- The LPNHRR shifts closer to the TDC with the progressive advance of IT bTDC with maximum NHRR being at 33° CA bTDC.
- The maximum BT and BP of the engine are observed at CR 12 and found to be 22.5 N-m and 3.29 kW at 1400rpm.
- VE of the engine follows an increasing trend with increased operating CR of the engine.

- The PCP is found to be maximum at the lower speed of the engine because decrement in speed results in higher brake load and BT on the engine.
- The optimum CR is considered to be 12 because of the trend of mean gas temperature (MGT) and in-cylinder pressure just before the completion of compression stroke (355°CA) as well the pressure at TDC position (360°CA)
- The peak cylinder pressure increases and shifts towards TDC and ensures better combustion at reduced engine speed.
- With increase in CR the combustion event and flame development are initiated progressively before the TDC and thus, the RBA (actual burn duration) reduces due to faster flame propagation.
- Maximum CO concentration in the exhaust emission of the biogas fueled SI engine is only observed at CR 12, irrespective of the operating speed of the engine.
- The minimum value of HC concentration in the exhaust emission at CR 10 is 28 ppm which was reduced by 32% compared to HC emission at CR 8.
- At higher operating speed, the air fuel mixture with insufficient oxygen experiences the incomplete combustion of fuel and leads to greater unburnt HC because of lower volumetric efficiency.
- Irrespective of the ERs the BP output of the engine increases with increasing CRs.
- As the air-fuel ratio changed from the lean misfire limit to the rich side for the raw biogas, the BTE follows an increasing trend and deviates at a point very nearer to the stoichiometric condition.
- Higher CRs increases the CO emission and is quite noticeable in the rich region of the air-fuel mixture.
- Due to biogas mode operation, the rated power of the Honda GX 200 engine (3.7 kW@ 3600 rpm) was derated and dropped by 20.54%. However, the drop is quite acceptable due to the lower calorific value of biogas.
- The maximum achievable brake thermal efficiency of the engine is 30.37% @ 2347 rpm at WOT condition.
- The CO and HC emission of the engine is within the limiting range. However, the maximum CO_2 emission was observed to be 12.2% which is the result of the higher CO_2 content in the raw biogas.

- Operating the constant speed biogas fueled customized commercial SI engine at the rated CR (13.94) and maximum brake load condition (74.8%) declines the rated speed of the engine by 9.3% and deteriorate the engine power by 34.5%.
- The maximum achievable BP and BTE of the commercial biogas engine are observed to be 2.88 kW and 14.84%, respectively at the rated CR
- The CO, HC and NOx concentration in the exhaust emission of the engine at the rated operating CR are 0.11%, 116 ppm, and 151 ppm, respectively at the maximum brake load condition.
- The BP, BTE, BSFC, and the VE of biogas fueled retrofitted Honda GX 200 SI engine (**Engine 3**) is improved by 2.25%, 51%, 51% and 32%, respectively in comparison to the biogas fueled customized commercial SI engine (**Engine 1**).
- **Engine 3** produced lesser CO_2 and HC emission with respect to the **Engine 1.**

9.2 Future Scope

The present investigation mainly focused on the prospects of improving the performance of a variable speed biogas fueled SI engine through experimental optimization of operating parameters. Successful implementation of these optimized operating parameters in a commercial SI engine (Honda GX 200) available in global market is also the part of this investigation. The importance of this work lies behind the fact that, any gasoline fueled SI engine operating with any CR between CR 8 to 14 can be efficiently converted to a biogas engine by implementing the optimized data achieved through the current investigation. However further studies could be extended in the following directions.

- The optimized operating parameters obtained through the exhaustive experimental investigation are valid with in the maximum operating speed range and present configuration of the fuel used in the engine. Hence, further computational investigation can be planned through artificial neural networking and the generated ANN predicted model can be validated with the experimental data obtained through the current investigation.
- The main aspect of the engine conversion from gasoline to biogas mode operation is the fuel induction mechanism. The current fuel induction mechanism is purely working on the concept of pressure drop in the chamber. The mass of fuel inducted for entire speed and load range of the engine plays a vital role to deliver better economy and

efficiency. Hence, as a future work, the current engine may be tested with gaseous fuel injection system directly at the cylinder and on the throttle body. Further, the fuel mass that should be injected (in to the cylinder or to the throttle body) can be optimized through further experimentation and incorporated in the engine control system.

- Along with the optimized engine operating parameters, the location of spark plug in the combustion chamber reveals the behavior of flame after initiation and corresponding development of flame kernel in detail. Hence, further investigation can also be planned to optimize the location and effect of dual spark plug in the combustion chamber.
- Further improvement in the efficiency and emission level of the present engine can be achieved by implementing turbocharges to introduce compressed air to the engine. Further, the studies can be extended to multi cylinder engines to make it commercially viable.

References

Abu-Zaid, M., Badran, O., Yamin, J., (2004). Effect of methanol addition on the performance of spark ignition engines. Energy & Fuels, 18, 312–315.

Agbulut, U., Sarıdemir, S., Albayrak, S., (2019). Experimental investigation of combustion, performance and emission characteristics of a diesel engine fuelled with diesel–biodiesel–alcohol blends. Journal of the Brazilian Society of Mechanical Sciences and Engineering, 41, 1-12.

Alagumalai, A., (2014). Internal combustion engines: Progress and prospects. Renewable and Sustainable Energy Reviews, 38, 561–571.

Alasfour, F.N., (1998). NOx Emission from a spark ignition engine using 30% Iso-butanol–gasoline blend: Part 1—Preheating inlet air. Applied Thermal Engineering, 18, 245–256.

Anand, G., Gopinath, S., Ravi, M.R., Kar, I.N., Subrahmanyam, J.P., (2006). Artificial neural networks for prediction of efficiency and NOx emission of a spark ignition engine. SAE Technical Paper, 2006-01-1113.

Ando, Y., Yoshikawa, K., Beck, M., Endo, H., (2005). Research and development of a low-BTU gas-driven engine for waste gasification and power generation. Energy, 30, 2206–2218.

Aoyama, S., Moteki, K., Ushijima, K., Takemura, S., Mizuno, H., (2013). Internal combustion engine. EP 1911952A2. European patent office.

Arunachalam, A., Olsen, D.B., (2012). Experimental evaluation of knock characteristics of producer gas. Biomass and Bioenergy, 37, 169–176.

Aslam, M.U., Masjuki, H.H., Kalam, M.A., Abdesselam, H., Mahlia, T.M.I., Amalina, M.A., (2006). An experimental investigation of CNG as an alternative fuel for a retrofitted gasoline vehicle. Fuel, 85, 717–724.

Assanis, D.N., Cho, W., Choi, I., Ickes, A., Jung, D., Martz, J., Nelson, R., Sanko, J., Thompson, S., (2018). Pressure reactive piston technology investigation and

development for spark ignition engines. SAE Technical Paper, No. 2005-01-1648.

Asthana, S., Bansal, S., Jaggi, S., Kumar, N., (2016). A comparative study of recent advancements in the field of variable compression ratio engine technology. SAE Technical Paper, 2016-01-0669.

Aydin, H., Bayindir, H., İlkiliç, C., (2010). Emissions From an Engine Fueled With Biodiesel-kerosene Blends. Energy Sources, Part A: Recovery, Utilization, and Environmental Effects, 33(2), 130–137.

Azpiazu, M.N., Bustamante, C., Morquillasz, J.M., (1990). Effect of air preheating on automotive emissions. Water, Air, and Soil Pollution, 51, 231–237.

Bae, C., Kim, J., (2017). Alternative fuels for internal combustion engines. Proceedings of the Combustion Institute, 36(3), 3389–3413.

Balki, M.K., Sayin, C., (2014). The effect of compression ratio on the performance, emissions and combustion of an SI (spark ignition) engine fueled with pure ethanol, methanol and unleaded gasoline. Energy, 71, 194–201.

Bari, S., (1996). Effect of carbon dioxide on the performance of biogas/diesel duel-fuel engine. Renewable energy, 9 (1-4), 1007–1010.

Bauer, H., Automotive handbook 4th edition, Robert Bosch GmBH, (1996). ISBN 0-8376-0333.

Bilgin, A., Sezer, I., (2008). Effects of methanol addition to gasoline on the performance and fuel cost of a spark ignition engine. Energy & Fuels, 22, 2782–2788.

Birlo, F., (2018). CO_2 emmisions from fuel combustion. International Energy Agency, Paris, France, https://www.iea.org/data-and-statistics/charts/fuel-share-of-co2-emissions-from-fuel-combustion-2018.

Birol, F., (2006). World energy outlook. International Energy Agency, Internal Energy Agency, Paris, France, https://www.iea.org/reports/world-energy-outlook-2006.

Bora, B.J., Debnath, B.K., Gupta, N., Saha, U.K., Sahoo, N., (2013). Investigation on the

Flow Behaviour of a Venturi Type Gas Mixer Designed for Dual Fuel Diesel Engines, 3, 202–209.

Bora, B.J., Saha, U.K., (2015). Improving the Performance of a Biogas Powered Dual Fuel Diesel Engine Using Emulsified Rice Bran Biodiesel as Pilot Fuel Through Adjustment of Compression Ratio and Injection Timing. Journal of Engineering for Gas Turbines and Power, 137 (9), 091505.

Bora, B.J., Saha, U.K., (2016). Optimisation of injection timing and compression ratio of a raw biogas powered dual fuel diesel engine. Applied Thermal Engineering, 92, 111–121.

Bora, B.J., Saha, U.K., Chatterjee, S., Veer, V., (2014). Effect of compression ratio on performance, combustion and emission characteristics of a dual fuel diesel engine run on raw biogas. Energy conversion and management, 87, 1000–1009.

Boretti, A., (2013). Conversion of a heavy duty truck diesel engine with an innovative power turbine connected to the crankshaft through a continuously variable transmission to operate compression ignition dual fuel diesel-LPG. Fuel processing technology, 113, 97–108.

Brinkman, N.D., (1977). Effect of compression ratio on exhaust emissions and performance of a methanol-fueled single-cylinder engine. SAE Technical Paper, 770791.

BS EN ISO 5167-1, (1997). Measurement of fluid flow by Means of pressure differential devices. BS EN ISO 5167-1 1997 5, 63.

Bureau of Indian Standards, 1980. IS 10000-7 (1980): Methods of tests for internal combustion engines, Part 7: Governing tests for constant speed engines and selection of engines for use with electrical generators, https://archive.org/details/gov.in.is.10000.7.1980

Carrera, J.L.E., Riesco, J.M.A., Martinez, S.M., Sanchez, F.A.C., Gallegos, A.M., (2013). Numerical study on the combustion process of a biogas spark-ignition engine. Thermal Science, 17(1), 241-254.

Cerri, T., D'Errico, G., Onorati, A., (2013). Experimental investigations on high octane number gasoline formulations for internal combustion engines. Fuel, 111, 305–315.

Chandra, R., Vijay, V.K., Subbarao, P.M. V, Khura, T.K., (2011). Performance evaluation of a constant speed IC engine on CNG, methane enriched biogas and biogas. Applied energy, 88(11), 3969-3977.

Chaudhari, A.J., (2017). Design, Installation and assessment of a novel VCR mechanism for multifuel spark ignition engine (Doctoral dissertation). Indian Institute of Technology Guwahati, Guwahati, India.

Chaudhari, A.J., Hotta, S.K., Sahoo, N., Kulkarni, V., (2019). Combined impact of compression ratio and re-circulated exhaust gas on the performance of a biogas fueled spark ignition engine. Journal of Renewable and Sustainable Energy, 11, 13104.

Chaudhari, A.J., Sahoo, N., Kulkarni, V., (2014). Simulation Models for Spark Ignition Engine : A Comparative Performance Study. Energy Procedia 54, 330–341.

Cho, H. M., & He, B. Q. (2007). Spark ignition natural gas engines—A review. Energy conversion and management, 48(2), 608-618

Cholakov, G.S., (2010). Control of exhaust emissions from internal combustion engine vehicles. Pollut Control Technol, 3, 1–8.

Clarke, J.R and Tabaczynski, R.J., (1943). Internal combustion engine with adjustable compression ratio and knock control. U.S. Patent No. 6,135,086, Washington, DC: U.S. Patent and Trademark Office.

Corti, E., Cavina, N., Cerofolini, A., Forte, C., Mancini, G., Moro, D., Ponti, F., Ravaglioli, V., (2014). Transient spark advance calibration approach. Energy Procedia, 45, 967–976.

Crookes, R. J., (2006). Comparative bio-fuel performance in internal combustion engines. Biomass and Bioenergy, 30, 461–468.

Cui, G., Li, Z., Yang, C., (2016). Experimental study of flammability limits of methane/air mixtures at low temperatures and elevated pressures. Fuel, 181, 1074–1080.

Cullen, B., McGovern, J., (2009). The quest for more efficient industrial engines: a review of current industrial engine development and applications. Journal of Energy Resources Technology, 131, 21601.

Dagaut, P., Cathonnet, M., (2006). The ignition, oxidation, and combustion of kerosene: A review of experimental and kinetic modeling. Progress in energy and combustion science, 32(1) , 48–92.

Das, L.M., (1990). Hydrogen engines: a view of the past and a look into the future. International Journal of Hydrogen Energy, 15(6), 425-443.

Das, L. M. (2002). Hydrogen engine: research and development (R&D) programmes in Indian Institute of Technology (IIT), Delhi. International journal of hydrogen energy, 27(9), 953-965.

Das, L. M., Gulati, R., & Gupta, P. K. (2000a). Performance evaluation of a hydrogen-fuelled spark ignition engine using electronically controlled solenoid-actuated injection system. International Journal of Hydrogen Energy, 25(6), 569-579.

Das, L. M., Gulati, R., & Gupta, P. K. (2000b). A comparative evaluation of the performance characteristics of a spark ignition engine using hydrogen and compressed natural gas as alternative fuels. International journal of hydrogen energy, 25(8), 783-793.

Das, L. M. (1991). Exhaust emission characterization of hydrogen-operated engine system: Nature of pollutants and their control techniques. International Journal of Hydrogen Energy, 16(11), 765-775.

Dudley, B., (2019). BP Energy Outlook, London, United Kingdom. https://www.bp.com/en/global/corporate/news-and-insights/press-releases/bp-energy-outlook-2019.html

El-Emam, S.H., Desoky, A.A., (1985). A study on the combustion of alternative fuels in spark-ignition engines. International Journal of Hydrogen Energy, 10, 497–504.

Elfasakhany, A. (2015). Investigations on the effects of ethanol–methanol–gasoline blends

in a spark-ignition engine: Performance and emissions analysis. Engineering Science and Technology, an International Journal, 18(4), 713-719.

Emission Standars, India, (2019), Diesel Net, https://www.dieselnet.com/standards/in.

Ferguson, C.R., Keck, J.C., (1977). Spark Ignition Engines 205, 197–205.

Fischer, M., Jiang, X., (2015). An investigation of the chemical kinetics of biogas combustion. Fuel, 150, 711–720.

Fleming, R. D., & O'Neal, G. B. (1985). Potential for improving the efficiency of a spark ignition engine for natural gas fuel. SAE transactions, 461-471.

Ganesan, V., (2012). Internal combustion engines. McGraw Hill Education (India) Pvt Ltd.

Gong, C., Liu, F., Sun, J., Wang, K., (2016). Effect of compression ratio on performance and emissions of a stratified-charge DISI (direct injection spark ignition) methanol engine. Energy, 96, 166–175.

Gorjibandpy, M., & Sangsereki, M. K. (2010). Computational investigation of air-gas venturi mixer for powered bi-fuel diesel engine. International Journal of Mechanical and Mechatronics Engineering, 4(11), 1197-1201.

Govil, G.P., (2006). Investigations on a dual fuel engine using diesel and biogas for performance optimization and conversion kits (Doctoral dissertation), IIT Delhi.

Hallgren, B. E. (2005). Impact of retarded spark timing on engine combustion, hydrocarbon emissions, and fast catalyst light-off (Doctoral dissertation), Massachusetts Institute of Technology.

Haraldsson, G., Tunestål, P., Johansson, B., Hyvönen, J., (2002). HCCI Combustion Phasing in a Multi Cylinder Engine Using Variable Compression Ratio. SAE Transaction,111, 2654–2663.

Hassaneen, A.E., Varde, K.S., Bawady, A.H., Morgan, A.A., (1998). A study of the flame development and rapid burn durations in a lean-burn fuel injected natural gas S.I. Engine. SAE Technical paper, 981384.

Heilig, G. K. (1994). The greenhouse gas methane (CH_4): Sources and sinks, the impact of population growth, possible interventions. Population and environment, 16(2), 109-137.

Heseding, M., Daskalopoulos, P., (2006). Exhaust emission legislation-diesel-and gas engines. VDMA, Frankfurt am Main.

Heywood, J. B. (2018). Internal combustion engine fundamentals.McGraw-Hill Education.

Huang, J., Crookes, R.., (1998a). Assessment of simulated biogas as a fuel for the spark ignition engine. Fuel, 77, 1793–1801.

Huang, J., & Crookes, R. J. (1998). Spark-ignition engine performance with simulated biogas-a comparison with gasoline and natural gas. Journal of the Institute of Energy, 71(489), 197-203.

Hussain, S. M., Kumar, D. B. S. P., & Reddy, K. V. K. (2012). CFD analysis of combustion and emissions to study the effect of compression ratio and biogas substitution in a diesel engine with experimental verification. International Journal of Engineering Science and Technology, 4(2), 473-492.

ICCT, (2016). India Bharat Stage VI Emission Standards. https://theicct.org/publication/india-bharat-stage-vi-emission-standards

IEO, (2017). International Energy Outlook, U. S. Enrgy Information Administration. https://www.eia.gov/outlooks/ieo/pdf/0484(2017).pdf

Jahirul, M.I., Masjuki, H.H., Saidur, R., Kalam, M. a., Jayed, M.H., Wazed, M. a., (2010). Comparative engine performance and emission analysis of CNG and gasoline in a retrofitted car engine. Applied Thermal Engineering, 30, 2219–2226.

Jang, D.H., Kim, H.T., Lee, C., Kim, S.H., Doherty, W., Reynolds, A., Kennedy, D., Kong, X., Zhong, W., Du, W., Qian, F., Zheng, H., Kaliyan, N., Morey, R.V., Abdelouahed, L., Authier, O., Mauviel, G., Corriou, J.P., Verdier, G., Dufour, a, Ramzan, N., Ashraf, A., Naveed, S., Malik, A. a., Damartzis, T., Michailos, S., Zabaniotou, a., Nikoo, M.B., Mahinpey, N., Bryden, K.M., Hagge, M.J., Jayah, T.H., Aye, L., Fuller,

R.J., Stewart, D.F., Zainal, Z. a., Ali, R., Lean, C.H., Seetharamu, K.N., Rifau, A., Quadir, G. a., K. G. Mansaray, A. M. Al-Taweel, A., Dogru, M., Howarth, C.R., Akay, G., Keskinler, B., 2002. Gasification of hazelnut shells in a downdraft gasifier. Energy, 27, 415–427.

Jaramillo, J., Zapata, J., & Bedoya, I. D. (2018). Interactive control of combustion stability and operating limits in a biogas-fueled spark ignition engine with high compression ratio. International Journal on Interactive Design and Manufacturing (IJIDeM), 12(3), 929-942.

Jatana, G. S., Himabindu, M., Thakur, H. S., & Ravikrishna, R. V. (2014). Strategies for high efficiency and stability in biogas-fuelled small engines. Experimental thermal and fluid science, 54, 189-195.

Jeong, C., Kim, T., Lee, K., Song, S., Chun, K.M., (2009). Generating efficiency and emissions of a spark-ignition gas engine generator fuelled with biogas-hydrogen blends. International Journal of Hydrogen Energy, 34, 9620–9627.

Kakaee, A. H., Shojaeefard, M. H., & Zareei, J. (2011). Sensitivity and Effect of Ignition Timing on the Performance of a Spark Ignition Engine: An Experimental and Modeling Study. Journal of Combustion, 2011, 242-249.

Kapdi, S.S., Vijay, V.K., Rajesh, S.K., Prasad, R., (2005). Biogas scrubbing, compression and storage: Perspective and prospectus in Indian context. Renew. Energy, 30, 1195–1202.

Karim, G.A., Wierzba, I., (2010). Methane-Carbon Dioxide Mixtures as a Fuel. SAE Technical Paper. 921557.

Kemal, M., Sayin, C., (2014). The effect of compression ratio on the performance, emissions and combustion of an SI (spark ignition) engine fueled with pure ethanol, methanol and unleaded gasoline. Energy, 71, 194–201.

Kline, S., McClintock, F., (1953). Describing uncertainties in single-sample experiments. Mechanical Engineering, 75, 3–8.

Korakianitis, T., Namasivayam, A. M., & Crookes, R. J. (2011). Natural-gas fueled spark-ignition (SI) and compression-ignition (CI) engine performance and emissions. Progress in energy and combustion science, 37(1), 89-112.

Krylov, I. F., & Tonkonogov, B. P. (2005). Natural gas as motor fuel. Chemistry and technology of fuels and oils, 41(3), 165-174.

Kwon, E., Song, K., Kim, M., Shin, Y., Choi, S., (2017). Performance of small spark ignition engine fueled with biogas at different compression ratio and various carbon dioxide dilution. Fuel, 196, 217–224.

Larsen, G.J., (1991). Reciprocating piston engine with a varying compression ratio. U.S. Patent 5,025,757.

Lee, K., Ryu, J., (2005). An experimental study of the flame propagation and combustion characteristics of LPG fuel. Fuel, 84, 1116–1127.

Leiker, M., Christop., K., Cartelli., W., Pfeifer, U., Rankl, M., (1972). Evaluation of anti-knocking property of gaseous fuels by means of methane number and its practical application to gas engines. Mechanical Engineering, 94(7), 55.

Li, J., Gong, C.-M., Su, Y., Dou, H.-L., Liu, X.-J., (2010) . Effect of injection and ignition timings on performance and emissions from a spark-ignition engine fueled with methanol. Fuel, 89, 3919–3925.

Liu, S., Clemente, E.R.C., Hu, T., Wei, Y., (2007). Study of spark ignition engine fueled with methanol/gasoline fuel blends. Applied Thermal Engineering, 27, 1904–1910.

Ma, F., Li, S., Zhao, J., Qi, Z., Deng, J., Naeve, N., He, Y., Zhao, S., (2012). Effect of compression ratio and spark timing on the power performance and combustion characteristics of an HCNG engine. International Journal of Hydrogen Energy, 37, 18486–18491.

Malenshek, M., Olsen, D.B., (2009). Methane number testing of alternative gaseous fuels. Fuel, 88, 650–656.

Masi, M., (2012). Experimental analysis on a spark ignition petrol engine fuelled with LPG

(liquefied petroleum gas). Energy, 41, 252–260.

Mehrnoosh, D., Asghar, H. A., & Asghar, M. A. (2012). Thermodynamic model for prediction of performance and emission characteristics of SI engine fuelled by gasoline and natural gas with experimental verification. Journal of mechanical science and technology, 26, 2213-2225.

Mello, P., Pelliza, G., Catalun, R., (2006). Evaluation of the maximum horsepower of vehicles converted for use with natural gas, Fuel, 85 (14-15), 2180–2186.

Midkiff, K. C., Bell, S. R., Rathnam, S., & Bhargava, S. (2001). Fuel composition effects on emissions from a spark-ignited engine operated on simulated biogases. J. Eng. Gas Turbines Power, 123(1), 132-138.

Mihic, S., (2004). Biogas fuel for internal combustion engines. Annals of Faculty Engineering Hunedoara, 2(3), 179-190.

Min, B.H., Kim, H.Y., Park, S., Composition, G., (2002). Effects of Gas Composition on the Performance and Emissions of Compressed Natural Gas Engines, 16, 219–226.

Mittal, V. (2009). A study of the physics and chemistry of knock in modern SI engines and their relationship to the octane tests (Doctoral dissertation), Massachusetts Institute of Technology.

Moffat, R.J., (1982). Contributions to the theory of single-sample uncertainty analysis. J. Fluids Eng. Trans. ASME 104, 250–258.

Mohammadi, A., Manzie, C. and Nešić, D., (2014). Optimization of spark advance in alternative fueled engines using extremum seeking control. Control Engineering Practice, 29, 201-211.

Mokrane, C., Adouane, B., & Benzaoui, A. (2018). Composition and stoichiometry effects of biogas as fuel in spark ignition engine. International Journal of Automotive and Mechanical Engineering, 15(1), 5036-5052.

Montoya, J.P.G., Amell Arrieta, A.A., Zapata Lopez, J.F., (2015). Spark ignition engine performance and emissions in a high compression engine using biogas and methane

mixtures without knock occurrence. Thermal Science, 19, 1919–1930.

Moreno, F., Muñoz, M., Arroyo, J., Magén, O., Monné, C., Suelves, I., (2012). Efficiency and emissions in a vehicle spark ignition engine fueled with hydrogen and methane blends. International Journal of Hydrogen Energy, 37, 11495–11503.

Moteki, K., Aoyama, S., Ushijima, K., Hiyoshi, R., Takemura, S., Fujimoto, H., Arai, T., (2003). A study of a variable compression ratio system with a multi-link mechanism. SAE Technical Paper, 2003-01-0921.

Mustafi, N. N., Miraglia, Y.C., Raine, R.R., Bansal, P.K., Elder, S.T., (2006). Spark-ignition engine performance with "Powergas" fuel (mixture of CO/H2): A comparison with gasoline and natural gas. Fuel, 85, 1605–1612.

Mustafi, N. N., Raine, R. R., & Bansal, P. K. (2006). The use of biogas in internal combustion engines: a review. In Internal Combustion Engine Division Spring Technical Conference, 42061, 225-234.

Neame, G.R., Gardiner, D.P., Mallory, R.W., Rao, V.K., Bardon, M.F., Battista, V., (1995). Improving the fuel economy of stoichiometrically fuelled SI engines by means of EGR and enhanced ignition-a comparison of gasoline, methanol and natural gas. SAE Trans. 1062–1076.

Niaz, S., Manzoor, T., & Pandith, A. H. (2015). Hydrogen storage: Materials, methods and perspectives. Renewable and Sustainable Energy Reviews, 50, 457-469.

Nindhia, T.G.T., Surata, I.W., Atmika, I.K.A., Negara, D.N.K.P. and Wardana, A., (2013). Method on conversion of gasoline to biogas fueled single cylinder of four stroke engine of electric generator. International Journal of Environmental Science and Development, 4(3), 300-303.

O'sullivan, A., Sheffrin, S.M., (2002). Survey of economics: Principles and tools. Prentice Hall.

Ozcan, H., & Yamin, J. A. (2008). Performance and emission characteristics of LPG powered four stroke SI engine under variable stroke length and compression ratio.

Energy Conversion and Management, 49(5), 1193-1201.

Pan, L., Hu, E., Deng, F., Zhang, Z., & Huang, Z. (2014). Effect of pressure and equivalence ratio on the ignition characteristics of dimethyl ether-hydrogen mixtures. international journal of hydrogen energy, 39(33), 19212-19223.

Pana, C., Negurescu, N., Popa, M.G., Cernat, A., (2010). Experimental aspects of the use of LPG at diesel engine. Scientific Bulletin of UPB,72(1).

Papacz, W., (2011). Biogas as vehicle fuel. Journal of KONES, 18(1), 403–410.

Papagiannakis, R.G., Zannis, T.C., (2013). Thermodynamic analysis of combustion and pollutants formation in a wood-gas spark-ignited heavy-duty engine. International Journal of Hydrogen Energy, 38, 12446–12464.

Park, C., Park, S., Lee, Y., Kim, C., Lee, S., Moriyoshi, Y., (2011). Performance and emission characteristics of a SI engine fueled by low calorific biogas blended with hydrogen. International Journal of Hydrogen Energy, 36, 10080–10088.

Pilusa, T.J., Mollagee, M.M., Muzenda, E., (2012). Reduction of Vehicle Exhaust Emissions from Diesel Engines Using the Whale Concept Filter. Aerosol and Air Quality Research, 12(5), 994-1006.

Porpatham, E., Ramesh, a., Nagalingam, B., (2007). Effect of hydrogen addition on the performance of a biogas fuelled spark ignition engine. International Journal of Hydrogen Energy, 32, 2057–2065.

Porpatham, E., Ramesh, A., Nagalingam, B., (2008). Investigation on the effect of concentration of methane in biogas when used as a fuel for a spark ignition engine. Fuel, 87, 1651–1659.

Porpatham, E., Ramesh, A., Nagalingam, B., (2013). Effect of swirl on the performance and combustion of a biogas fuelled spark ignition engine. Energy conversion and management, 76, 463–471.

Porpatham, E., Ramesh, A., Nagalingam, B., (2012). Effect of compression ratio on the performance and combustion of a biogas fuelled spark ignition engine. Fuel, 95, 247–

256.

Pulkrabek, W.W. (1997) Engineering Fundamentals of the Internal Combustion Engine. Prentice Hall, Upper Saddle River, New Jersey, 07458.

Pundir, B, P., (2010). IC engines: combustion and emissions. Narosa Publishing House, New Delhi, India

Qian, Y., Sun, S., Ju, D., Shan, X., Lu, X., (2017). Review of the state-of-the-art of biogas combustion mechanisms and applications in internal combustion engines. Renewable and Sustainable Energy Review, 69, 50–58.

Rassweiler, G.M., Withrow, L., (1938). Motion pictures of engine flames correlated with pressure cards. SAE Transactions, 33, 185–204.

Ravi, K., Bhasker, J.P., Porpatham, E., (2017). Effect of compression ratio and hydrogen addition on part throttle performance of a LPG fuelled lean burn spark ignition engine. Fuel, 205, 71–79.

Roberts, M. (2003). Benefits and challenges of variable compression ratio (VCR). SAE Technical Paper, 2003-01-0398.

Roethlisberger, R.P., Favrat, D., (2002a). Comparison between direct and indirect (prechamber) spark ignition in the case of a cogeneration natural gas engine , part I : engine geometrical parameters. Applied Thermal Engineering, 22(11), 1217-1229.

Roethlisberger, R.P., Favrat, D., (2002b). Comparison between direct and indirect (prechamber) spark ignition in the case of a cogeneration natural gas engine,: part II: engine operating parameters and turbocharger characteristics. Applied Thermal Engineering, 22, 1231–1243.

Rogelj, J., Elzen, M. Den, Höhne, N., Fransen, T., Fekete, H., Winkler, H., Schaeffer, R., Sha, F., (2016). Paris Agreement climate proposals need a boost to keep warming well below 2 ° C. Nature, 534(7609), 631-639.

Roubaud, A., Favrat, D., (2005). Improving performances of a lean burn cogeneration biogas engine equipped with combustion prechambers. Fuel, 84, 2001–2007.

Roubaud, A., Röthlisberger, R., Favrat, D., (2002). Lean-burn cogeneration biogas engine with unscavenged combustion prechamber: Comparison with natural gas. International Journal of Applied Thermodynamics, 5, 169–175.

Ryan III, T.W., Lestz, S.S., (1980). The laminar burning velocity of isooctane, n-heptane, methanol, methane, and propane at elevated temperature and pressures in the presence of a diluent. SAE Transaction, 652–664.

Sadiq Al-Baghdadi, M.A.R., (2004). Effect of compression ratio, equivalence ratio and engine speed on the performance and emission characteristics of a spark ignition engine using hydrogen as a fuel. Renewable Energy, 29, 2245–2260.

Sahoo, B.B., (2010). Clean development mechanism potential of compression ignition diesel engines using gaseous fuels in dual fuel mode. PhD Thesis. IIT Guwahati,Guwahati, India.

Sahoo, B.B., Sahoo, N., Saha, U.K., (2009). Effect of engine parameters and type of gaseous fuel on the performance of dual-fuel gas diesel engines-A critical review. Renewable and Sustainable Energy Review, 13, 1151–1184.

Sayin, C., Hosoz, M., Canakci, M., Kilicaslan, I., (2007). Energy and exergy analyses of a gasoline engine. International journal of energy research, 31 (3), 259–273.

Seko, T., Yoshida, Y., Yamaguchi, I., Sakai, T., Hori, M., & Kim, Y. K. (1986). Combustion exhaust emissions of the spark-assisted methanol diesel engine. SAE transactions, 679-690.

Selim, M.Y.E., Radwan, M.S., Saleh, H.E., (2008). Improving the performance of dual fuel engines running on natural gas/LPG by using pilot fuel derived from jojoba seeds. Renewable energy, 33, 1173–1185.

Shah, A., Srinivasan, R., To, S. D. F., & Columbus, E. P. (2010). Performance and emissions of a spark-ignited engine driven generator on biomass-based syngas. Bioresource technology, 101(12), 4656-4661.

Shaik, A., Moorthi, N. S. V., & Rudramoorthy, R. (2007). Variable compression ratio

engine: a future power plant for automobiles-an overview. Proceedings of the Institution of Mechanical Engineers, Part D: Journal of Automobile Engineering, 221(9), 1159-1168.

Sridhar, G., Paul, P. J., & Mukunda, H. S. (2001). Biomass derived producer gas as a reciprocating engine fuel—an experimental analysis. Biomass and Bioenergy, 21(1), 61-72.

Stewart, J., Clarke, A., & Chen, R. (2007). An experimental study of the dual-fuel performance of a small compression ignition diesel engine operating with three gaseous fuels. Proceedings of the Institution of Mechanical Engineers, Part D: Journal of Automobile Engineering, 221(8), 943-956.

Stewart, M.C., (1997). Design and analysis of a variable-compression, ratio internal-combustion engine: the Alvar engine concept (Doctoral dissertation, Massachusetts Institute of Technology).

CR, S., Gould, J., & Ladommatos, N. (1993). Analysis of bio-gas combustion in spark-ignition engines, by means of experimental-data and a computer-simulation. Journal of the Institute of Energy, 66(469), 180-187.

Stone, R., (2012). Introduction to internal combustion engines, 4, Springer, London: Macmillan

Surata, I.W., Nindhia, T.G.T., Atmika, I.K.A., Negara, D.N.K.P., Putra, I.W.E.P., (2014). Simple Conversion Method from Gasoline to Biogas Fueled Small Engine to Powered Electric Generator. Energy Procedia, 52, 626–632.

The Gazette of India, (2016). G.S.R.281(E), Environment Standards for Genset engines Dedicated LPG/CNG,Diesel and LPG/CNG and Petrol and LPG/CNG, The Environment (Protection) Third Amendment Rules.

Thipse, S.S., (2010). Alternative Fuels: Concepts, Technologies and Developments. Jaico Book Distributors, India.

Thurnheer, T., Soltic, P., & Eggenschwiler, P. D. (2009). SI engine fuelled with gasoline,

methane and methane/hydrogen blends: heat release and loss analysis. International journal of hydrogen energy, 34(5), 2494-2503.

Türköz, N., Erkuş, B., Karamangil, M.I., Sürmen, A., Arslanoğlu, N., (2014). Experimental investigation of the effect of E85 on engine performance and emissions under various ignition timings. Fuel, 115, 826–832.

Umesh, K.S., Pravin, V.K., Rajagopal, K. and Veena, P.H., (2012). Development of a CFD 3D model to determine the effect of the mixing quality on the CNG-Diesel engine performance. International Journal of Engineering Research and Technology (IJERT), 1(5), 2278-0181.

Urdhwareshe, R., (2017). Indian Emission Regulations: Limits, Regulation, Measurement of Exhaust Emissions and Calculation of Fuel Consumption. AIS: Automot Res Assoc India, 137, 1-118

Usman, M., Hayat, N., & Bhutta, M. M. A. (2021). SI engine fueled with gasoline, CNG and CNG-HHO blend: comparative evaluation of performance, emission and lubrication oil deterioration. Journal of Thermal Science, 30, 1199-1211.

Vancoillie, J., Demuynck, J., Sileghem, L., Van De Ginste, M., Verhelst, S., Brabant, L. V. H. L., & Van Hoorebeke, L. (2013). The potential of methanol as a fuel for flex-fuel and dedicated spark-ignition engines. Applied Energy, 102, 140-149.

Vancoillie, J., & Verhelst, S. (2010). Modeling the combustion of light alcohols in SI engines: a preliminary study. In FISITA 2010 World Automotive Congress. International Federation of Automotive Engineering Societies.

Verhelst, S., & Wallner, T. (2009). Hydrogen-fueled internal combustion engines. Progress in energy and combustion science, 35(6), 490-527.

Vijay, V.K., Chandra, R., Gaur, R.R., Subbarao, P.M. V, (2005). Conversion of Diesel Engine for 100 percent Utilization of Raw as well as Enriched Biogas – Rural Electricity Generation. 47–52.

Von Mitzlaff, K., (1988). Engines for Biogas- Theory, Modification, Economic Operation.

A publication of German Center for Development Technologies, GTZ – GATE, Germany.

Whiston, P. J., Abdel-Gayed, R. J., Girgis, N. S., & Goodwin, M. J. (1992). Turbulent burning velocity of a simulated biogas combustion in a spark ignition engine. SAE Technical Paper, 922166.

White, C. M., Steeper, R. R., & Lutz, A. E. (2006). The hydrogen-fueled internal combustion engine: a technical review. International journal of hydrogen energy, 31(10), 1292-1305.

Williams, M., Minjares, R., (2016). A technical summary of Euro 6/VI vehicle emission standards. The International Council on Clean Transportation. The International Council on clean transportation, 1-12.

Xie, F.-X., Li, X.-P., Wang, X.-C., Su, Y., Hong, W., (2013). Research on using EGR and ignition timing to control load of a spark-ignition engine fueled with methanol. Applied Thermal Engineering, 50, 1084–1091.

Yanju, W., Shenghua, L., Hongsong, L., Rui, Y., Jie, L., Ying, W., (2008). Effects of methanol/gasoline blends on a spark ignition engine performance and emissions. Energy & Fuels, 22, 1254–1259.

Yousufuddin, S., Nawazish, M.S., (2008). Effect of ignition timing, equivalence ratio, and compression ratio on the performance and emission characteristics of a variable compression ratio SI engine using ethanol-unleaded gasoline blends. IJE Transactions B: Applications, 21(1), 97-107.

Yuksel, F., Yuksel, B., (2004). The use of ethanol–gasoline blend as a fuel in an SI engine. Renewable energy, 29, 1181–1191.

Zareei, J., Kakaee, A.H., (2013). Study and the effects of ignition timing on gasoline engine performance and emissions. European Transport Research Review, 5, 109-116.

भारतीय प्रौद्योगिकी संस्थान गुवाहाटी
Indian Institute of Technology Guwahati

Appendix-A

Characterization of Biogas

The raw biogas produced by anaerobic digestion varies in the composition of gases and are greatly influenced by surrounding environment and atmospheric conditions as discussed in chapter 1. The composition of the biogas was analyzed on site by using a portable gas analyzer (Make: Gas data, Model: GFM 406). It is an ATEX certified hand-held gas analyzer configured for biogas and suitable for monitoring biogas plants onsite. GFM 406 can detect and record the content of CH_4, CO_2, O_2 and H_2S in biogas. The data recorded on GFM406 can be transferred to computer using USB through the *Site man 5* software installed in the instrument. The detailed specifications of GFM406 are shown in **Table A- 1**. The onsite sample compositions were recoded repeatedly by GFM406 and are shown in **Table A- 2**. The portable gas analyzer could not analyze the content of N_2 present in biogas. Hence, prior to the use of biogas as a fuel in SI engine, the samples are further analyzed in a Thermo Scientific Made TRACE 1110 EPC series gas chromatograph. The gas chromatograph was equipped with a thermal conductivity detector (TCD) and porapak Q column. Helium was used as the carrier gas for this analysis. Before injecting the biogas sample at the injector port, the column temperature and TCD temperature of the gas chromatograph was set to 45^o C and 180^o C, respectively. The detailed specification of the Thermo Scientific Made TRACE 1110 series gas chromatograph and sample report are given in **Table A- 3**. There were no substantial changes in the composition of the produced biogas unless there was a drastic change in environmental operating parameters or change in feed materials to the biogas digester. Hence, the average compositions of its constituents were taken in to consideration. Based on the series of sample reports produced by Thermo Scientific Made TRACE 1110 series gas chromatograph, the average CH_4, CO_2 and N_2 content of the used biogas were 55.6 %, 42.3% and 2.1% respectively. Further, the LHV of the biogas was determined by using a Junker's gas calorimeter. The technical specification of the Junkers gas calorimeter is depicted in **Table A- 4**. **Fig. A- 1**shows the experimental setup used to find out the LHV of biogas. The Junker's gas calorimeter setup mainly consists of a mechanical governor, a fuel metering unit, Bunsen burner and the calorimeter along with thermocouples and temperature display unit as shown in **Fig. A- 1.** Biogas stored

in a neoprene coated rubber fabric balloon was sucked and compressed in a reciprocating compressor up to 3 bar and then sent to the Bunsen burner placed beneath the calorimeter through the mechanical governor and fuel metering unit. The inner tube of the calorimeter consists of copper to effectively transfer the generated heat due to combustion of biogas. The generated heat gets transferred to the water flowing in the water jacket of the outer tube. Thus, the heat generated by the combustion of biogas is transferred to the flowing water and increase its outlet temperature. So, the above depicted concept ensured the following by assuming no heat loss from the outer tube. The Junkers gas calorimeter works on the basic principle of energy conservation and governed by *Eq. A1*. The LHV of the biogas was calculated by *Eq. A3* and the sample calculation report was shown in **Table A-5.**

Heat generated by the biogas flame = Heat gained by the cooling water

$$C_v m_{bg} = m_w c_{pw} \Delta T_w \quad \text{(A1)}$$

$$C_v = \left(\frac{m_w}{m_{bg}} \right) c_{pw} \Delta T_w \quad \text{(A2)}$$

$$C_v = \left(\frac{V_w \rho_w}{V_{bg} \rho_{bg}} \right) c_{pw} \Delta T_w \quad \text{(A3)}$$

Table A- 1:GFM 406 for biogas technical specification

Gas Measurement	Range (Resolution)	Typical Accuracy
Methane	0-100% v/v	0.3%@5% 1.0%@60% 2.0%@100%
Carbon Dioxide	0-100% v/v	0.3%@5% 1.0%@60% 2.0%@100%
Oxygen	0-25% v/v	0.1%
Hydrogen Sulphide	0-5000 ppm v/v	10 ppm
Differential pressure measurement	+/-30 mB	0.5 mbar
Vane anemometer	0-40 m/s(0.1)	0.5 m/s
Temperature probe	-10-100 ^{O}C	0.2 ^{O}C

Table A- 2: Onsite sample report recoded by GFM 406 portable bio gas analyzer

Sample	Composition			
	CH_4 (% v)	CO_2 (% v)	O_2 (% v)	H_2S (ppm)
Feb 2016	56.621	42.912	0.1	580
Mar 2016	56.411	43.277	0.1	526
April 2016	54.447	42.139	0.2	435
May 2016	56.698	44.971	0	560
Jun 2016	53.601	42.744	0.1	456
July 2016	57.226	44.79	0	557
Aug 2016	56.038	41.975	0.1	554
Sep 2016	57.38	42.473	0.1	575
Oct 2016	53.235	40.691	0.2	449
Nov 2016	55.117	41.508	0.1	516

Table A- 3: Detailed specification and sample report of biogas composition tested in the Thermo Scientific Made TRACE 1110 series gas chromatograph

Performance Specifications	
Typical Retention Time Repeatability:	0.008 minute
Typical Peak Area Repeatability:	< 2% RSD
Oven Specifications	
Column Oven (H × W × D)	30.9 x 29.0 x 26.0 cm; 22.6 L
Operating Temperature Range:	+5 °C to 500 °C
Cryogenic Option Minimum Temperature:	-99 °C with liquid Nitrogen
Temperature Set Point Resolution:	1 °C
Number of Ramps/Plateaus:	7/8
Maximum Heating Rate:	50 °C/min
Oven Cool-Down (22 °C ambient):	400 °C to 50 °C in < 6 min
EPC (Electronic Pressure Control) Injectors	Injectors Pressure Range:0–1000 kPa
Packed Colum	Temperature Range: 50 ^oC – 450 ^oC

Split/Splitless	Temperature Range: 50 °C – 450 °C with EPC Carrier Flow Setting: 0.1 ml/min to 100 ml/min Split Flow Setting: 1 ml/min to 400 ml/min Purge Flow Setting: 0 to 50 ml/min Split Ratio: Up to 9999:1
PTV (Programmed Temperature Vaporizer)	Temperature Range: 50 °C – 450 °C with EPC Split Carrier Flow Setting: 0.1 ml/min to 100 ml/min Split Flow Setting: 1 ml/min to 400 ml/min Purge Flow Setting: 0 to 50 ml/min Temperature Programming Rate: 1 °C/min to 0600 °C/min
Detectors	
Flame Ionization Detector (FID)	MDL: <3 pg C /Sec for C9 hydrocarbon7 Linear Dynamic Range: $>10^7$ Maximum Temperature: 450 °C Flow Setting: - Air: 0-400 ml/min – H2: 0-150 ml/min- Makeup gas 0-150 ml/min
Thermal Conductivity Detector (TCD)	MDL: <800 pg C12/ml He Sensitivity: 10 µV /ppm for Nonane Linear Dynamic Range: $>10^5$ Maximum Temperature: 400 °C
Electron Capture Detector (ECD)	Radioactive Source: 370 MBq equal to 6310 mCi, Ni Cell Volume: <350 µl-13 MDL: <1×10 g/s Lindane Sensitivity: 0.1 pg/s Lindane Linear Dynamic Range: $>10^4$ Maximum Temperature: 400^0 C Makeup Gas: Nitrogen or 5% Methane in Argon Makeup Gas flow: 0-50 ml/min

Nitrogen Phosphorus Detector (NPD)	MDL: < 0.1pg N/sec for Azobenzene < 0.5pg P/sec for Methyl-Parathion Selectivity: gN/gC = 20,000; gP/gC = 40,000 Linear Dynamic Range: $>10^4$ Current Setting: 1 to 3.5 A Maximum Temperature: 450 ^oC Flow Setting: - Air: 0-100 ml/min, H: 0-50 ml/min, Makeup Gas: 0-50 ml/min

Sample gas chromatography report of biogas

Center for Energy
Technology complex
Guwahati, IIT, Assam

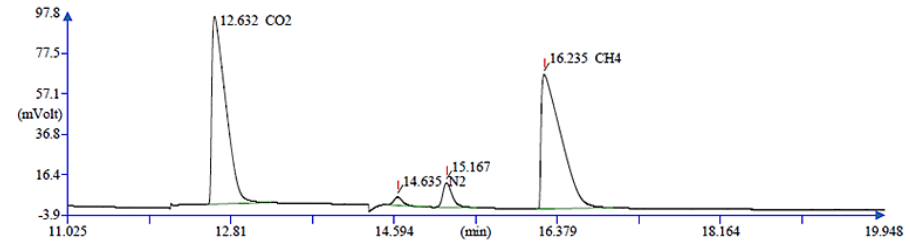

Operator ID: DEEP BORA
Analysed: 19-08-2016 17:03
Sample ID: SAMPLE
Chromatogram filename: C:\Thermo\Chemito Chrom-Card\data\First Run\S3_190816.dat

Retention Time (min)	Area (.1*uV*sec)	Amount (%Vol)	Component
12.632	9903753	43.975	CO2
14.635	277251	1.136	N2
15.167	875647	0.000	
16.235	10082870	56.058	CH4
	21139520	101.169	

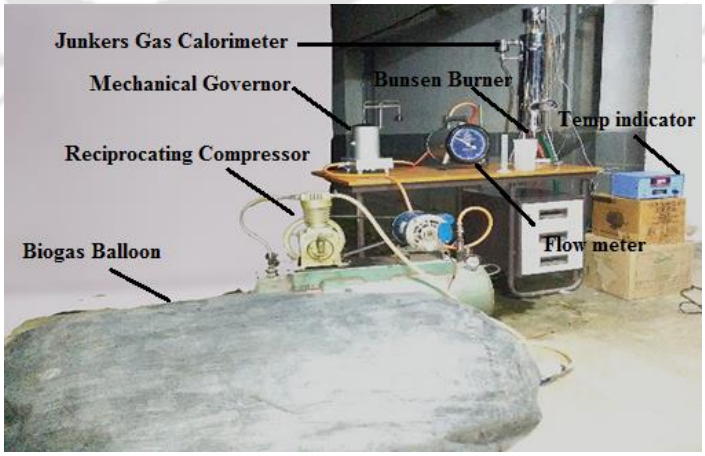

Fig. A- 1: Junkers gas calorimeter setup to find out the LHV of gaseous fuel

Table A- 4: Technical specification of the Hardson Co. made Junkers gas calorimeter

Hardson Co. made Junkers gas calorimeter	
Governor type	Mechanical, Pressure governor
Water flow measurement	Non recording 1 liter flow meter
Gas flow measurement	Volumetric gas meter with gas pressure regulator
Temperature measurement	T type, thermocouples with 6 channel display unit
Calorific value range	1000-26000 kcal/m^3
Burner	Bunsen burner

Table A- 5: Sample experimental data for LHV calculation

V_w (ml)	V_{bg} (ml)	ρ_w (kg/m_3)	ρ_{bg} (kg/m_3)	C_{pw} (kJ/kgK)	T_{w2}-T_{w1} (K)	CV_{bg} (kJ/kg)	CV_{bg} (kJ/m^3)
735	652	1000	1.11	4.184	4	16996.84	18866.50
490	650	1000	1.11	4.184	6	17049.14	18924.55
415	652	1000	1.11	4.184	7	16794.50	18641.90
328	650	1000	1.11	4.184	9	17118.73	19001.79
294	652	1000	1.11	4.184	10	16996.84	18866.50
Average calorific value (CV)						**16991.21**	**18860.25**

Appendix-B

Technical Specifications of the Customized Biogas Engine (Engine 1) and Associated Instrumentation

The detailed technical specification of the biogas fueled commercially customized SI engine test facility (*Engine 1*) developed by *Prakash Diesel Pvt. Ltd.* is depicted here in **Table B- 1**. The setup is commercially available as a biogas generator in the Indian market and mostly used by the community centres having availability of biogas. Further, the manufacturer has a clear guideline to operate the engine with scrubbed biogas (CO_2, H_2S and Moisture free). The biogas generator (*Model: PN-1 BG)* is procured from the manufacturer and customized as per the requirement of the experimental facility. **Table B-1**contains the technical specifications of the engine, braking system, sensors and indicators mounted on the experimental setup. The *AVL DIAGAS 444N* five gas analyzer is used to quantify the exhaust emission of the liquid and gaseous fuels. The gas analyzer uses different measuring principles to determine the concentration of different gases in a gas mixture. A NDIR sensor is used to measure the CO_2 concentration, whereas a HC heat effect sensor is used to determine the HC concentration bythe catalytic filament method. Similarly, a solid-state electrolyte sensor is used for the detection of O_2 by the principle of solid-state conductivity. The electrochemical sensors used to detect the CO and NO concentration by following the principle of ion selective potentiometry. The resolution, accuracy, and the range of these parameters are shown in the **Table B-2**. The consumption of the biogas in *Engine 1* is traced by a low-pressure biogas flow meter (*Make: Siya Instrumentation Pvt. Ltd., Model: SI-6*). **Table B- 3**represents the technical specification of the flow meter used for the biogas fueled commercially customized SI engine.

Table B- 1: Specifications of the commercial biogas engine (Engine 1) and accessories

System specifications	
Parameter	*Specification*
Product	Biogas Engine, Model: PN-1 BG
Type	Natural aspirated, 1 Cylinder, 4 stroke, Constant
Power	4.4 KW, Rated Speed 1500 rpm.
Type of cooling	Water cooled
CR range	Fixed, 13.94:1, Modified VCR range: CR10-CR16
Combustion chamber	Hemispherical bowl in piston type, Piston Cavity 51
Dynamometer	Alternator connected to a load bank
Air box	MS fabricated with orifice meter and manometer (100
Governing System	Cam operated, link controlled mechanical governor
Ignition System	Capacitive discharge spark ignition system
Data acquisition Software	'Engine soft' engine performance analysis software
Setup constants	
Bore × Stroke	102 mm× 115 mm
Capacity	990.6 cc
Orifice diameter	20 mm
Connecting rod length	310 mm
Braking system	
Product	Alternator, Model: PS350A
Rating	3.5 kVA
Output	230 V, 50 Hz
Phase	Single Phase
Power Factor	1
Load Bank	220 V, 3000 Watt
Sensors and indicators	
Pressure sensors	Piezo type, range 5000 PSI, with low noise cable
Speed sensor and indicator	Resolution 1º, range (5500 rpm) with TDC pulse
Data acquisition device	NI USB-6210, 16-bit, 250 kS/s
Theoretical constants	
Orifice coefficient of discharge	0.6
Specific heat of exhaust gas	1.00 – 1.25 kJ/kg-K
Specific heat of water	4.186 kJ/kg-K
Density of Air	1.174 kg/m3

Table B- 2: Technical specifications of AVL DIGAS 444N exhaust gas analyzer

Measured quality	Measuring range	Resolution	Accuracy	
CO	0 to 15 % vol	0.01% vol	0-10% ± 0.02% abs 10.01-15%	±3% rel ± 5% rel
CO_2	0 to 20% vol	0.01% vol	0-16% ± 0.3%abs 16.01-20%	± 3% rel ± 5% rel
HC	0 to 30000 ppm vol	≤ 2000: 1 ppm vol > 2000: 10 ppm vol	0-4000 ppm ± 8 ppm 4001-10000 ppm 10001-30000 ppm	±3% rel ± 5% rel ±10% rel
O_2	0 to 25 % vol	0.01 % vol	± 0.02% abs	± 1% rel
NO	0 to 5000 ppm vol	1 ppm vol	± 5ppm	± 1% rel
Engine speed	400 to 6000 rpm	1 rpm	± 1 % of ind. val.	
Oil temperature	0 to 125 °C	1 °C	± 4 °C	
Lambda	0 to 9.999	0.001		
Power Supply				
Voltage	19 V DC			
Power consumption	≈ 15 W			
System Constraints				
Warmup time	≈ 2 min			
Response time	≤ 15 s			
Operating temperature	5 to 45 °C			
Interface	USB interface, AECS software			

Table B- 3: Specification of the biogas flow meter (Make: Siya Instrument, Model: SI-6)

Product	Biogas flow meter for low pressure application,
Use	Biogas with minimum moisture content
Cycle volume	1.2 dm^3
Operating temperature	-20° C to 50° C
Storage temperature	-20° C to 50° C
Maximum operating pressure	0.5 bar
Line size	¾ Inch
Measuring range	0.04 m^3 to 6 m^3
Accuracy	± 0.4%

Appendix-C

Details of the VCR SI Research Engine (Engine 2) and Retrofitted HONDA GX 200 SI Engine (Engine 3) for Biogas Application

The VCR SI research engine test facility is a naturally aspirated, four stroke, water cooled, variable speed, manifold injected, single cylinder SI engine (*Make: Apex Innovation Pvt. Ltd., India, Model: 240 PE*) of rated power 4.5 kW at CR 10 and 1800 rpm in gasoline mode operation. The fuel induction and the VCR mechanism along with the ignition timing control of the VCR SI engine are further retrofitted for gaseous fuel (methane and biogas) application. The detailed technical specification of the engine along with the used transmitters, sensors and indicators are mentioned here in **Table C- 1**. In the current investigation a 'PE3' module is used for configuring the operating parameters of the engine with the alternative fuels. It is a completely adjustable ECU apposite for the single and multi-cylinder engines but need to have dedicated fuel injection and ignition engine control unit. The 'PE3' module also includes the 'PeMonitor and Tuning' software to configure the ECU as per the fuel and ignition specific controls. The detailed technical specification of the 'PE3' module is given in **Table C- 2**. Similarly, for measuring the liquid and gaseous fuel consumption the VCR SI engine is equipped with a DP transmitter (*Yokogawa, EJA110A*) and specially designed fuel specific float type rotameters (*Veskler Instruments, ABR-19-300A&B*). The EJA110A DP transmitter measures the flow rates and the pressure of the liquids, gases, steam, and also liquid levels. The detailed specification of the DP transmitter and fuel specific float type rotameters are given in **Table C- 3**and **Table C- 4**. The in-cylinder pressure and crank angle signals of VCR SI engine is traced by a piezo pressure sensor (*PCB Piezotronics, M111A22*) and crank angle encoder (*Kubler,8.3700.1321.0360*) mounted on the combustion chamber and crankshaft, respectively. The detailed specification of the piezo pressure sensor and crank angle encoder are given in **Table C- 5**and **Table C- 6**, respectively. The opening time of the fuel injector has been calibrated and configured by the manufacturer for the gasoline injection throughout the operating speed and throttle position range of the engine. The primary fuel

table with injector open time (ms) is shown in **Table C-7**. Further, the technical specification and instrumentation details of the Honda GX200 SI engine and retrofitted Honda GX 200 SI engine test rig used for biogas application are depicted in **Table C-8**.

Table C- 1: Specifications of the VCR SI research engine test rig and accessories

System specifications		
Parameter		*Specification*
Product		Research engine test setup, 240 PE
Type		Research engine test setup 1 cylinder, 4 stroke, multi fuel
Power		4.5 KW @ 1800 rpm, Speed range 900-1800 rpm.
Type of cooling		Water cooled
CR variation		Mechanically operated VCR system (Manual)
VCR range	Gasoline Mode	6:1-10:1(Manufacturer's Specification)
	Methane Mode	8:1-17.5:1 (Retrofitted Range)
	Biogas Mode	8:1-17.5:1 (Retrofitted Range)
Fuel injection		ECU controlled throttle body fuel injection system
Fuel Injector		Make Denso, Model: Maruti 800
Fuel pump		Make Denso, Model: Maruti 800
Throttle body		Make: Tata motors Model: used in TATA Nano car
Ignition system		ECU controlled variable ignition timing control
Combustion chamber		Hemispherical bowl in piston type
Dynamometer		Make: Saj test plant Pvt. Ltd., Model: AG10, Type: Eddy current, water cooled;
Dynamometer loading unit		Make Apex, Model AX-155. Type: constant speed, Supply 230V AC.
Air box		MS fabricated with orifice meter and manometer (100 -
Fuel tank		Capacity 15 lit with measuring tube (0-450 ml)
Calorimeter		Pipe in pipe type
Rotameters		Make: Eureka Model PG 5 and PG 6, Range: Engine cooling 40-400 lph, calorimeter 25-250 lph
Data acquisition Software		Make: Apex, Model: Enginesoft, Labview-based engine performance analysis software
ECU software		Make: Performance Electronics, PE Monitor & PE
Transmitters, sensors and indicators		
Piezo powering unit		Make-Apex, Model AX-409
Engine control unit		PE3 series ECU, full build sealed enclosure
Fuel flow transmitter		DP transmitter, Make Yokogawa, Model EJA110-EMS-5A-92NN, Calibration range 0-500 mm H_2O, Output
Air flow transmitter		Pressure transmitter, Make Wika, Model SL1 , (-) 250
Piezo pressure sensors		Make PCB Piezotronics, Model SM111A22, Range 5000 psi, Diaphragm stainless steel type & hermetic sealed with coaxial noise cancellation cable (Make PCB Piezotronics, Model 002C20)

Temperature sensors		Type RTD, PT100 and Thermocouple, Type K
Temperature sensors and transmitters		PT100 (RTD) type, range 0-100º C, output 4-20 mA (4 nos)
Load sensor		Make Sensotronics Sanmar Ltd., Model 60001, Type S beam, Universal, Capacity 0-50 kg, Type: Strain gauge type load cell with digital indicator
Load indicator		Model SV8 SERIES, 85 to 270VAC, Retransmission output
Crank angle encoder and Speed sensor		Make Kubler-Germany, Model 8.3700.1321.0360, Resolution 1º, Range (5500 rpm) with TDC pulse
Data acquisition device		NI USB-6210, 16-bit, 250 kS/s, Bus Powered M Series
Setup constants		
Pulse per revolution		360º
No. of cycles		50-100
Fuel measuring interval		60 s
Speed scanning intervals		2000 ms
Bore × Stroke		87.5 mm × 110 mm
Capacity		661 cc
Orifice diameter		20 mm
Dynamometer arm length		185 mm
Connecting rod length		234 mm
Piston cavity		34 cc
Valve timing	IVO	4.5º bTDC
	IVC	35.5º aBDC
	EVO	35.5º bBDC
	EVC	4.5º aTDC
Theoretical constants		
Orifice coefficient of discharge		0.6
Specific heat of exhaust gas		1.00 – 1.25 kJ/kg-K
Specific heat of water		4.186 kJ/kg-K
Density of Air		1.174 kg/m^3

Table C- 2: Important specifications of the PE3 module

General Specifications	
Manufacturer/ Model	Performance Electronics Ltd./ PE3 # ECU Series # Version # 1.1
Operating voltage:	6v-22v DC
Operating temperature range	Depends on loading: -22°F to 167°F (-30°C to 75°C)
Max. external current draw	For external sensors: 1.0 A
Specification of the Injector Driver	
Type of driver:	Saturated or Peak and Hold low side driver (software selectable)
Number of drivers	Up to 8
Driver protection:	Internally current limited to 10.0 amps per driver

Maximum current	10.0 amps before shutdown
Peak current	Maximum: 8.0 amps
Hold current	Maximum: 3.0 amps
Specification of the Ignition Coil Driver	
Type of driver	Inductive ignition driver
Number of drivers:	Direct coil driver: Up to 4 (external igniter not required) Smart coil or external igniters: Up to 8
Driver protection	Internally current limited to 10.0 amps per driver
Maximum current	10.0 amps before shutdown
Specification of the Trigger/Sync Input	
Configuration of Hall Effect Sensor	
Maximum input voltage	Up to Vbat
Threshold trigger voltage	Greater than 4.0 volts high side, less than 400 mv low side
Configuration of Variable Reluctance Sensor	
Max Input Voltage	100 volts
Min Input Voltage to trigger	+/- 250 mv (0 to peak)

Table C- 3: Detail specification of the EJA110A differential pressure transmitter

Parameters	**Specifications**
Manufacturer/ Model	Yokogawa/ EJA110A
Application	Measurement of flow rates and pressure of the liquids, gases, and steam
Output signal	4 to 20 mA DC
Operating pressure limit	1 to 100kPa (100 to 10000 mm H_2O)
Calibration range	0 to 200, 0 to 500 mm H2O
Input	10 to 24 VDC
Operating temperature	-40 to 120˚C
Wetted parts material	Body – SCS14A, Capsule – SUS316L
Installation	Horizontal impulse piping left side high pressure

Table C- 4: Detail specification of the fuel specific flow meters

Parameter	**Specifications**	
	CH_4 Rotameter	**Biogas Rotameter**
Make	Veskler Instruments	Veskler Instruments
Model No.	ABR-19-300 (A)	ABR-19-300 (B)
Fluid/Gas	Methane (CH_4)	Biogas (~60% CH4, ~40% CO_2)
Sp. Gravity	0.5538	0.939
Operating pr.	Atm.	Atm.
Flow range	10 – 50 LPM	10 – 50 LPM
Fitting MOC	SS 304	SS 304

Float	SS 316	SS 316
Metering tube	Drilled Acrylic Bar	Drilled Acrylic Bar
Gland packing	Neoprene	Neoprene
Scale engraved	on Body	on Body
Pressure rating	1.5 times of W. Pressure	1.5 times of W. Pressure
Accuracy	± 0.5 % FS	± 0.5 % FS

Table C- 5: Detail specification of the PCB Piezotronics made piezo pressure sensors

Parameters	Specifications
Sensor type	Dynamic pr. transducer with built in amplifier
Make/Model	PCB Piezotronics, Inc. / M111A22
Operating pressure Range, Useful range, Maximum	FS (5V output) 5000 psi, (10V output) 10000 psi, 15000 psi
Resolution, Sensitivity	0.1 psi, 1 mV/psi
Resonant frequency, Low frequency response	400 kHz, 0.001 Hz
Rise time, Discharge time constant, Linearity	2 µs, 500s, 2 %
Output polarity, Impedance, Bias	Positive, 100 ohms, 8-14 volt
Acceleration sensitivity	0.002 psi/g
Temperature coefficient, Temperature range Flash temperature	0.03 % / ^{o}F, -100 to 275 ^{o}F, 3000 ^{o}F
Vibration / Shock	2000 / 20000 g peak
Excitation, Voltage to current regulator	(Constant current) 2 to 20 mA, +18 to 28 VDC
Sensing geometry, Sensing element	Compression, Quartz
Housing material, Diaphragm, Sealing	17.4 SS, Invar, Welded hermetic
Electric connector	10-32 coaxial jack
Mounting thread, Weight (with clamp nut)	M7 x 0.75 pitches, 6 gm
Cable model	002C20 white coaxial cable

Table C- 6 Technical specification of the Kubler made crank angle encoder

Parameters	Specifications
Sensor Type	Crank angle sensor
Make	Kubler-Germany
Model	8.3700.1321.0360
Supply voltage	5-30VDC
Output	Push pull (AA, BB, OO)
PPR	360
Outlet cable type	Axial
Encoder Diameter Dia.	37
Shaft size	Dia.6mm x length12mm

Table C- 7: Primary fuel table with injector open time for gasoline fueled VCR SI engine at CR 10

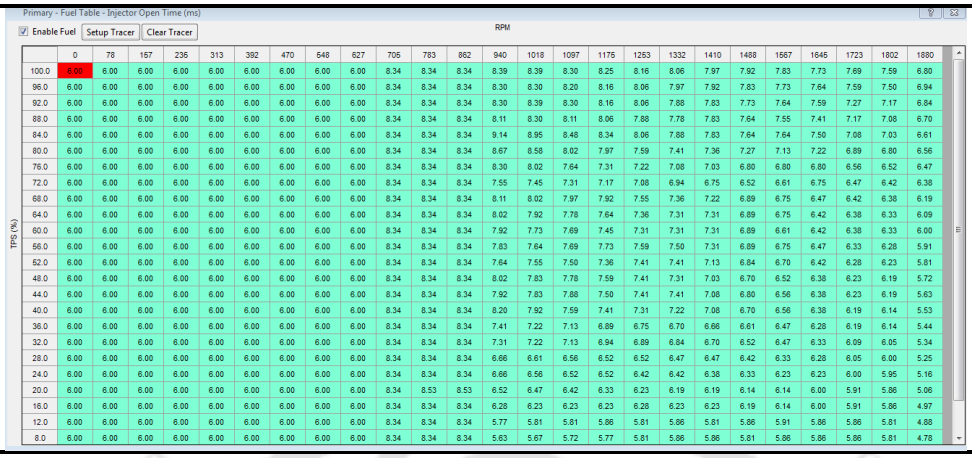

	0	78	157	235	313	392	470	548	627	705	783	862	940	1018	1097	1175	1253	1332	1410	1488	1567	1645	1723	1802	1880
100.0	6.00	6.00	6.00	6.00	6.00	6.00	6.00	6.00	6.00	8.34	8.34	8.34	8.39	8.39	8.30	8.25	8.16	8.06	7.97	7.92	7.83	7.73	7.69	7.59	6.80
96.0	6.00	6.00	6.00	6.00	6.00	6.00	6.00	6.00	6.00	8.34	8.34	8.34	8.30	8.30	8.20	8.16	8.06	7.97	7.92	7.83	7.73	7.64	7.59	7.50	6.94
92.0	6.00	6.00	6.00	6.00	6.00	6.00	6.00	6.00	6.00	8.34	8.34	8.34	8.30	8.39	8.30	8.16	8.06	7.88	7.83	7.73	7.64	7.59	7.27	7.17	6.84
88.0	6.00	6.00	6.00	6.00	6.00	6.00	6.00	6.00	6.00	8.34	8.34	8.34	8.11	8.30	8.11	8.06	7.88	7.78	7.83	7.64	7.55	7.41	7.17	7.08	6.70
84.0	6.00	6.00	6.00	6.00	6.00	6.00	6.00	6.00	6.00	8.34	8.34	8.34	9.14	8.95	8.48	8.34	8.06	7.88	7.83	7.64	7.64	7.50	7.08	7.03	6.61
80.0	6.00	6.00	6.00	6.00	6.00	6.00	6.00	6.00	6.00	8.34	8.34	8.34	8.67	8.58	8.02	7.97	7.59	7.41	7.36	7.27	7.13	7.22	6.89	6.80	6.56
76.0	6.00	6.00	6.00	6.00	6.00	6.00	6.00	6.00	6.00	8.34	8.34	8.34	8.30	8.02	7.64	7.31	7.22	7.08	7.03	6.80	6.80	6.80	6.56	6.52	6.47
72.0	6.00	6.00	6.00	6.00	6.00	6.00	6.00	6.00	6.00	8.34	8.34	8.34	7.55	7.45	7.31	7.17	7.08	6.94	6.75	6.52	6.61	6.75	6.47	6.42	6.38
68.0	6.00	6.00	6.00	6.00	6.00	6.00	6.00	6.00	6.00	8.34	8.34	8.34	8.11	8.02	7.97	7.92	7.55	7.36	7.22	6.89	6.75	6.47	6.42	6.38	6.19
64.0	6.00	6.00	6.00	6.00	6.00	6.00	6.00	6.00	6.00	8.34	8.34	8.34	8.02	7.92	7.78	7.64	7.36	7.31	7.31	6.89	6.75	6.42	6.38	6.33	6.09
60.0	6.00	6.00	6.00	6.00	6.00	6.00	6.00	6.00	6.00	8.34	8.34	8.34	7.92	7.73	7.69	7.45	7.31	7.31	7.31	6.89	6.61	6.42	6.38	6.33	6.00
56.0	6.00	6.00	6.00	6.00	6.00	6.00	6.00	6.00	6.00	8.34	8.34	8.34	7.83	7.64	7.69	7.73	7.59	7.50	7.31	6.89	6.75	6.47	6.33	6.28	5.91
52.0	6.00	6.00	6.00	6.00	6.00	6.00	6.00	6.00	6.00	8.34	8.34	8.34	7.64	7.55	7.50	7.36	7.41	7.41	7.13	6.84	6.70	6.42	6.28	6.23	5.81
48.0	6.00	6.00	6.00	6.00	6.00	6.00	6.00	6.00	6.00	8.34	8.34	8.34	8.02	7.83	7.78	7.59	7.41	7.31	7.03	6.70	6.52	6.38	6.23	6.19	5.72
44.0	6.00	6.00	6.00	6.00	6.00	6.00	6.00	6.00	6.00	8.34	8.34	8.34	7.92	7.83	7.88	7.50	7.41	7.41	7.08	6.80	6.56	6.38	6.23	6.19	5.63
40.0	6.00	6.00	6.00	6.00	6.00	6.00	6.00	6.00	6.00	8.34	8.34	8.34	8.20	7.92	7.59	7.41	7.31	7.22	7.08	6.70	6.56	6.38	6.19	6.14	5.53
36.0	6.00	6.00	6.00	6.00	6.00	6.00	6.00	6.00	6.00	8.34	8.34	8.34	7.41	7.22	7.13	6.89	6.75	6.70	6.66	6.61	6.47	6.28	6.19	6.14	5.44
32.0	6.00	6.00	6.00	6.00	6.00	6.00	6.00	6.00	6.00	8.34	8.34	8.34	7.31	7.22	7.13	6.94	6.89	6.84	6.70	6.52	6.47	6.33	6.09	6.05	5.34
28.0	6.00	6.00	6.00	6.00	6.00	6.00	6.00	6.00	6.00	8.34	8.34	8.34	6.66	6.61	6.56	6.52	6.52	6.47	6.47	6.42	6.33	6.28	6.05	6.00	5.25
24.0	6.00	6.00	6.00	6.00	6.00	6.00	6.00	6.00	6.00	8.34	8.34	8.34	6.66	6.56	6.52	6.52	6.42	6.42	6.38	6.33	6.23	6.23	6.00	5.95	5.16
20.0	6.00	6.00	6.00	6.00	6.00	6.00	6.00	6.00	6.00	8.34	8.53	8.53	6.52	6.47	6.42	6.33	6.23	6.19	6.19	6.14	6.14	6.00	5.91	5.86	5.06
16.0	6.00	6.00	6.00	6.00	6.00	6.00	6.00	6.00	6.00	8.34	8.34	8.34	6.28	6.23	6.23	6.23	6.28	6.23	6.23	6.19	6.14	6.00	5.91	5.86	4.97
12.0	6.00	6.00	6.00	6.00	6.00	6.00	6.00	6.00	6.00	8.34	8.34	8.34	5.77	5.81	5.81	5.86	5.81	5.86	5.81	5.86	5.91	5.86	5.86	5.81	4.88
8.0	6.00	6.00	6.00	6.00	6.00	6.00	6.00	6.00	6.00	8.34	8.34	8.34	5.63	5.67	5.72	5.77	5.81	5.86	5.86	5.81	5.86	5.86	5.86	5.81	4.78

Table C- 8: Technical specifications of Honda GX200 SI engine and Retrofitted Honda GX 200 SI engine experimental test rig with mounted accessories

Parameters	Original engine specification	Retrofitted engine Specification
Product	Honda GX 200	Retrofitted with milled head of Honda GX 160 over GX 200 engine assembly
Fuel	Gasoline	Gasoline/ Biogas
Type	1 Cylinder, 4 stroke Variable Speed	1 Cylinder, 4 stroke Variable Speed
Net power (IP)	5.5 HP (4.1 kW) @ 3600 rpm	3.21 kW @ 2350 rpm 3.84 kW @ 2800 rpm
Cont. rated power	3.7 kW @ 3600 rpm 3.3 kW @ 3000 rpm	2.56 kW @ 2800 rpm 2.94 kW @ 2350 rpm
Fuel consumption at cont. rated power	1.7 L/h @3600 rpm	2.05 kg/h @ 2800 rpm
Maximum net Torque (BT)	12.4 Nm @2500 rpm	11.97 Nm @ 2350 rpm
Type of cooling	Force air cooled	Force air cooled
CR range	Fixed, 8.5:1	Fixed, 9.54:1
Ignition system	Transistorized magneto coil	ECU controlled direct ignition system
Fuel induction System	Carbureted	EFI (Gasoline)/ Biogas induction system with venturi type mixer (Biogas)
	Setup constants	
Bore x Stroke	68 x 54 mm	68 x 54 mm
Capacity	196 cc	196 cc
Clearance volume	26.148 cc	22.97 cc
Orifice diameter	-	16 mm

Connecting rod length	105 mm	105 mm
Dynamometer arm	-	185 mm
Specification of the retrofitted Honda GX 200 SI engine test rig for biogas application		
Type	Retrofitted Honda GX 200 SI engine test rig, variable speed, 1 cylinder, 4 stroke, fixed CR (9.54:1), ECU controlled	
Fuel	Gasoline/ Biogas	
Power	4.1 kW @ 3600 rpm, Speed range 1400-3600 rpm. (Gasoline mode) 3.8.kW@ 2800 rpm, Speed range 900-2800 rpm (Biogas mode)	
Type of cooling	Force air cooled	
Operating CR	Fixed, 9.54:1 (after modification)	
Fuel induction	ECU controlled throttle body fuel injection system (Gasoline Mode) Diaphragm pump driven fuel induction system integrated with veturi type biogas mixer (Biogas mode)	
Heat Exchanger	Pipe in pipe type for preheating biogas	
Fuel Injector	Make Denso, Model: M 800	
Fuel pump	Make Denso, Model: M 800 (Gasoline Mode) Diaphragm Pump, Make: Lovato, Model: M200 (Biogas Mode)	
Throttle body	Make: Tata Motors, Model: used in TATA Nano car	
Ignition system	ECU controlled variable ignition timing	
Dynamometer	Make: Saj test plant Pvt. Ltd., Type: Eddy current, water cooled	
Dynamometer loading unit	Make: Apex, Model AX-155. Type: constant speed, Supply 230V AC.	
Air box	MS fabricated with orifice meter and manometer (100 - 10 -100)	
Data acquisition Software	Make: Apex, Model: Enginesoft, Labview based engine performance analysis software	
ECU and Software	Make: Performance Electronics, PE Monitor & PE Viewer	
Transmitters, sensors, indicators and software		
Piezo powering unit	Make-Apex, Model AX-409	
Engine control unit	PE3 series ECU, full build sealed enclosure	
Fuel flow transmitter	DP transmitter, Make Yokogawa, Model EJA110-EMS-5A-92NN	
Air flow transmitter	Pressure transmitter, Make: Wika, Model SL1, (-) 250 mm WC	
Piezo pressure sensors	Make PCB Piezotronics, Model SM111A22, Range 5000 psi	
Temperature sensors	Type RTD, PT100 and Thermocouple, Type K	
Load sensor	Make Sensotronics Sanmar Ltd., Model 60001,Type S beam	
Load indicator	Model SV8 SERIES, 85 to 270VAC, Retransmission output	
Crank angle encoder and Speed sensor	Make Kubler-Germany, Model 8.3700.1321.0360	
Data acquisition device	NI USB-6210, 16-bit, 250 kS/s, Bus Powered M Series	

Appendix-D

Correlations to Evaluate the Performance and Combustion Parameters

Data acquisition, processing and analysis are the major activates of any experimental investigation. Hence, in the present investigation, the evaluation of the performance, combustion and emission analysis of the biogas fueled commercially customized SI engine (Engine 1), VCR SI research engine (Engine 2) and the retrofitted Honda GX 200 SI engine (Engine 3) are done by capturing a large volume of raw data through a high-speed DAS (NI USB 6210, 16-bit, 250kS/s) at least for 50 to 80 consecutive engine cycles. The data captured in a single cycle include the engine speed, applied load, throttle position, air and fuel consumption, temperatures at different location, pressure signals, crank angle signals, ignition timing and emitted compounds. The recorded data are retrieved and preprocessed to evaluate the performance parameters (BT, BP, BSFC, BTE, VE, ER) and combustion parameters (P-θ, P-V, IP, LPP, NHRR, CHRR, MFB, $COV_{IMEP,}$ $COV_{PP}$and MGT) by using the following correlations as referred in the literatures (Heywood, 1988; Stone, 2012). The average values of the data points obtained are considered for further analysis

I. Performance analysis

a) Brake torque (BT):

$$BT\,(Nm) = F \times 9.81 \times r \qquad \text{(D1)}$$

Where F is the brake load applied on the engine shaft in Kg and r is the dynamometer arm length in meter.

b) Brake power (BP):

$$BP\,(kW) = \frac{2\pi NT}{60000} \qquad \text{(D2)}$$

Where, where N and T are the speed of the engine (rpm), brake torque acting on the engine shaft (Nm), respectively.

c) Brake specific fuel consumption (BSFC):

$$BSFC\ (kg/kWh) = \left[\frac{\dot{m}_{fuel}}{BP} \times 3600\right] \quad \text{(D3)}$$

$$\dot{m}_{fuel}\ (kg/h) = \left[\rho_{fuel} \times \dot{m}_{fuel}\ (cc/\min) \times 10^{-6} \times 60\right] \quad \text{(D4)}$$

Where, $\dot{m}_{fuel}$,BP and ρ_{fuel} are the mass flow rate of fuel consumption (kg/kWh), brake power (kW) and density of the fuel (kg/m^3), respectively.

d) Brake thermal efficiency (BTE):

$$\eta_{bte}\ (\%) = \frac{BP}{\dot{m}_{fuel} \times LHV_{fuel}} \times 100 \quad \text{(D5)}$$

Where, $\dot{m}_{fuel}$, LHV_{fuel} are the mass flow rate of fuel consumptions (kg/kWh) and lower heating value of the fuels consumed (kJ/kg), respectively.

e) Volumetric efficiency (VE):

$$\eta_{vol}\ (\%) = \frac{\dot{m}_a\ (kg/s) \times 3600}{(\pi/4) \times D^2 \times L \times N/n \times 60 \times K \times \rho_a} \times 100 \quad \text{(D6)}$$

$$\dot{m}_a\ (kg/h) = C_d \times \frac{\pi}{4} \times d^2 \times \sqrt{\left(2 \times 9.81 \times h \times \frac{\rho_w}{\rho_a}\right)} \times 3600 \times \rho_a \quad \text{(D7)}$$

Where, D, L, N, n, K,ρ_a ,C_d, d and ρ_w are the diameter of the cylinder (m), stroke length (m), engine speed (rpm), stroke per revolution (1/2), number of cylinders, density of air (kg/ m^3), coefficient of discharge of orifice (0.6), diameter of orifice plate (m) and density of water (kg/m^3), respectively.

f) Equivalence ratio (ER):

$$ER\ (\phi) = \frac{(F/A)_a}{(F/A)_s} \quad \text{(D8)}$$

Where, $(F/A)_a$, $(F/A)_s$are the actual and stoichiometric air/fuel ratio, respectively.

g) Stoichiometric Air/Fuel ratio $(A/F)_s$:

Assuming complete combustion of the fuel molecules in the presence of enough O_2, and considering complete conversion of the fuel into oxidized products, the chemically correct air fuel mixture was calculated.

For pure methane (100% CH_4):

$$CH_4 + 2(O_2 + 3.761N_2) \leftrightarrows CO_2 + 2H_2O + 7.522N_2 \quad \text{(D9)}$$

$$\left(\frac{A}{F}\right)_S = \left[\frac{(2\times 32)+(7.522\times 28.16)}{(1\times 12.011)+(4\times 1.008)}\right] = 17.19$$

For biogas (56% CH_4, 42% CO_2, 2% N_2):

$$0.56CH_4 + 0.42CO_2 + 0.02N_2 + 1.12(O_2 + 3.761N_2) \leftrightarrows 0.98CO_2 + 1.12H_2O + 4.232N_2 \quad \text{(D10)}$$

$$\left(\frac{A}{F}\right)_S = \left[\frac{(1.12\times 32)+(4.2123\times 28.16)}{(12.011\times 0.56)+(1.008\times 4\times 0.56)+(0.42\times 32)+(12.011\times 0.42)+(0.02\times 28.16)}\right] = 5.51$$

For biogas (56% CH4, 42% CO2):

$$0.56CH_4 + 0.42CO_2 + 1.12(O_2 + 3.761N_2) \leftrightarrows 0.98CO_2 + 1.12H_2O + 4.212N_2 \quad \text{(D11)}$$

$$\left(\frac{A}{F}\right)_S = \left[\frac{(1.12\times 32)+(4.212\times 28.16)}{(0.56\times 12.011)+(4\times 0.56\times 1.008)+(0.42\times 32)+(0.42\times 12.011)}\right] = 5.67$$

II. Combustion analysis

a) Pressure smoothing:

The raw signal captured by the DAS for the dynamic fluctuating pressure at each crank angle involves 540 – 864 kS data for a particular operating condition of the engine. The large volumes of data captured are originally a continuous analogue signal. Numerical differentiation of such signal shows a noisy trend between the successive values. Hence, the pressure signals must be post processed through higher order finite difference approach and smoothing algorithm (Stone, 2012). As suggested in literature, the following smoothing algorithm for (2b+1) values mentioned in Eq. D12 is widely accepted and is used for the post processing of captured pressure signals. The terms in Eq. D12 are only evaluated when the part of the subscript in bracket is not negative. This is illustrated by simplest case in Eq.D13 which was followed in the present case by considering b as 2 and '*P*' is the instantaneous pressure data.

$$P_n = \frac{1}{b^2}\left[P_{n-(b-1)} + 2P_{n-(b-2)} + 3P_{n-(b-3)} + ... + bP_n + .. + 3P_{n+(b-3)} + 2P_{n+(b-2)} + P_{n+(b-1)}\right] \quad \text{(D12)}$$

$$P_n = \frac{P_{(n-1)} + 2P_n + P_{(n+1)}}{4} \quad \text{(D13)}$$

b) Rate of pressure rise:

The rate of pressure rise is calculated by the 1st order finite differential equation with 4th order accuracy as mentioned in Eq. D14 from the smoothened pressure data obtained in Eq. D13. Here 'P' is the instantaneous pressure data and '$\Delta\theta$' is the corresponding crank angle interval.

$$\frac{dP}{d\theta} = \frac{P_{(n-2)} - 8P_{(n-1)} + 8P_{(n+1)} + P_{(n+2)}}{12(\Delta\theta)} \qquad \text{(D14)}$$

c) Rate of change of volume:

The rate of change of volume is calculated by using the Eq. D15. Where, 'V' is the volume of combustion chamber at crank angle 'θ'.

$$\frac{dV}{d\theta} = \frac{V_{(n+1)} - V_{(n)}}{\theta_{(n+1)} - \theta_{(n)}} \qquad \text{(D15)}$$

d) Net heat release rate (NHRR):

The NHRR is calculated by applying the 1st law analysis to the combustion chamber and considering the content of combustion chamber as a single zone model (which assumes the combustion products and reactants are fully mixed). The neat heat release rate is calculated by using Eq. D16 assuming there is no mass transfer across the control volume. Where, '$dQn/d\theta$' is the neat heat release rate in J/ºCA, 'γ' is the ratio of specific heat which normally varies in between 1.3 to 1.35 (Heywood, 1988; Pundir, B, 2010), '$dP/d\theta$' is the rate of pressure rise in bar/ ºCA and '$dV/d\theta$' is the rate of change of volume in CC/ ºCA.

$$\frac{dQ_n}{d\theta} = \left(\frac{\gamma}{\gamma - 1} \times P \times \frac{dV}{d\theta}\right) + \left(\frac{1}{\gamma - 1} \times V \times \frac{dP}{d\theta}\right) \qquad \text{(D16)}$$

e) The mass fraction burnt (MFB):

The MFB is calculated by following the method proposed by Rassweiler and Withrow (Rassweiler and Withrow, 1938) as shown in Eqs.D17-19. Here, $\sum_0^i \Delta p^*_c$ is the summation of referenced pressure rise due to combustion up to i[th] increments and $\sum_0^N \Delta p^*_c$ is the summation of referenced pressure rise due to combustion from 0 to N[th] increments (period of combustion). 'Δp_c' is the pressure rise due to combustion and the polytropic index (k) is taken as 1.2. For the present case, the rapid burn angle (RBA) '$\Delta\theta_b$' is considered as the crank angle interval between the end of flame development stage (mass fraction burnt of 10%) and the end of flame

propagation (mass fraction burnt of 90%). Similarly, the crank angle interval between the stage of spark initation (θ_{IT}) and end of flame developement (mass fraction burnt of 10%) is considered as the angle of ignition delay, $\Delta\theta_d = \left(\theta_{IT} - \theta_{10\%MFB}\right)$(Heywood, 1988; Stone, 2012).

$$mfb = \frac{\sum_{0}^{i} \Delta P_c^*}{\sum_{0}^{N} \Delta P_c^*} \tag{D17}$$

$$\Delta P_c^* = \Delta P_c \times \frac{V_i}{V_c} \tag{D18}$$

$$\Delta P_c = P_{i+1} - P_i \left(\frac{V_i}{V_{i+1}}\right)^k \tag{D19}$$

f) Mean gas temperature (MGT):

The mean gas temperature is calculated from Eq. D20 (Heywood, 1988). Where, 'P_θ'is the instantaneous cylinder pressure (N/m^2), 'V_C' isthe clearance volume (m^3), 'd' is the bore diameter (m), 'l' is the stroke length (m), 'r' is the crank radius (m), 'θ' is the crank angle (^{o}CA), 'ρ' is the density of air (kg/m^3) , 'V_θ'is the total cylinder volume at crank angle (m^3), 'R' is the specific gas constant (kJ/kg^{o}K)

$$MGT = \frac{P_\theta \times \left\{ V_C + \left[\frac{\pi d^2}{4} \left[l + r - r\left(\cos\theta + \frac{l}{r}\left(1 - 0.5 \times \left(\frac{r}{l}\right)^2 \times \left(0.5 - 0.5\cos 2\theta\right)\right)\right)\right]\right]\right\}}{\rho \times V_\theta \times R} \tag{D20}$$

g) Cycle-by-cycle variation (CCV):

The cycle-by-cyclic variation (CCV) is the difference in the combustion process on cycle by cycle. Since the cylinder pressure curve is uniquely related to the combustion process, variation in combustion process gets directly reflected in the cylinder pressure. The cyclic variability of the engine is derived from the pressure data are expressed in terms of coefficient of variation of indicative mean effective pressure (COV $_{IMEP}$) or coefficient of variation of peak pressure (COV$_{PP}$) and is generally expressed in percent. COV $_{IMEP}$ is the ratio of standard deviation in the indicated mean effective pressure (σ_{IMEP}) to the mean of indicated mean effective pressure (μ_{IMEP}) and are calculated from Eqs. D21, D23 and D24 (Heywood, 1988; Mittal et al., 2009). Similarly, the COV$_{PP}$ is calculated from the Eq.D22.

The IMEP is calculated by using Eq.D25 and is the ratio of network produced 'W_N' calculated from the P-V plot area (bar.cc) to the engine displacement volume 'V_d' (cc^3).

$$COV_{IMEP} = \frac{\sigma_{IMEP}}{\mu_{IMEP}} \times 100 \quad \text{(D21)}$$

$$COV_{PP} = \frac{\sigma_{PP}}{\mu_{PP}} \times 100 \quad \text{(D22)}$$

$$\sigma_{IMEP} \text{ or } \sigma_{PP} = \sqrt{\frac{1}{N}\sum_{i=1}^{N}\left(x_i - \mu\right)^2} \quad \text{(D23)}$$

$$\mu_{IMEP} \text{ or } \mu_{PP} = \frac{1}{N}\sum_{i=1}^{N}\left(x_i\right) \quad \text{(D24)}$$

$$IMEP = \frac{W_N}{V_d} \quad \text{(D25)}$$

Appendix-E

Optimizing Dimensions of the Biogas Induction Mechanism for the Retrofitted Honda GX 200 Engine

The major modification required for the conversion of a gasoline fueled SI engine for biogas application, is to attach a gas-air mixer in place of the carburetor. In this case, the engine control is performed by varying the mixer supplied which can be achieved by operating a butterfly valve in between the mixing device and the engine intake manifold. The mixing device has to ensure the provision of constant air/fuel ratio irrespective of the actual amount sucked into the engine. This is achieved by appropriate design of the mixing device along with the precise control of butterfly valve. The design of a gas mixer for a particular engine mainly depends on its rated power, specific fuel consumption, speed, volumetric efficiency, swept volume and manifold connection diameter (Von Mitzlaff, 1988). In most of the cases T-junction gas mixer are preferred for biogas powered dual fuel CI engines. The biogas inlet of the T-junction air-gas mixer makes an angle of 90^{o} with the air inlet as shown in **Fig. E- 1(a)**, which makes a huge energy loss due of the collision made by the two stream of fluid(Von Mitzlaff, 1988). Hence, in order to reduce the loss of collision, several other designs are proposed (Sahoo, 2010)where the gas inlet inclined at 45^{o} to the air inlet as shown in **Fig. E- 1(b)**. However, these designs are unable to asymmetric mixing of the two fluid streams. Further, to have a homogenous air/fuel mixing a new design is proposed with two fuel and one air inlet. The fuel inlets are inclined at 35^{o} with the air inlet, thereby, promoting a homogenous mixing of biogas and air (Bora et al., 2013). However, most of the above reported designs are applicable to dual fuel CI engines. Hence, in the direction of devising an effective air-biogas mixer and based on the present requirements mentioned in *Chapter 3* an air-biogas mixer is designed specifically for a retrofitted Honda GX 200 SI engine and is presented in this section. This variable speed SI engine has a fixed CR of 9.54:1 and an ECU controlled direct ignition system after modification.

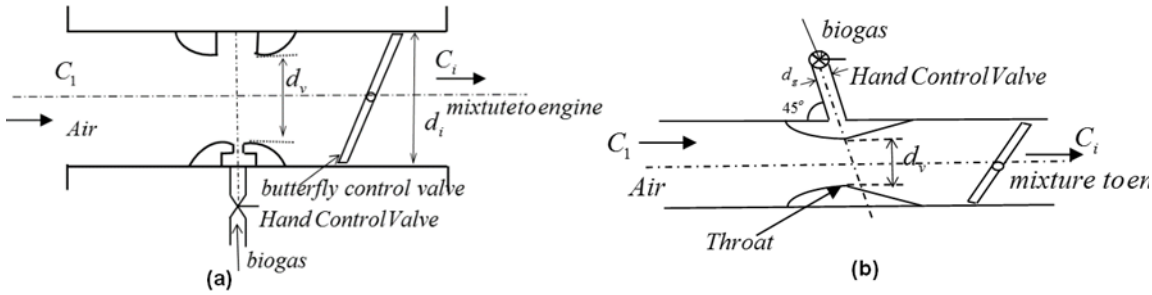

Fig. E- 1: Gas mixer for diesel engines proposed by researchers: (a) T-junction inlet; (b) Inclined inlets

E1. Design of the biogas mixer

The proposed design of the biogas mixer uses the concept of venturimeter and follows the Bernoulli's principle as mentioned in *Eq. E1*. It is clear from the *Eq. E3* that pressure drop is inversely proportional to the square of the area when all other parameter kept constant. Hence, at the throat the pressure is minimum and velocity is maximum. The venturi gas mixer composed of two gas inlet, one air inlet and one biogas-air outlet. As reported (Bora et al., 2014) it consists of a smooth contraction and expansion section which reduces the prominence of irreversible pressure loss. The function of the converging section is to enhance the velocity of the fluid by virtue of loss in its static pressure. The lower pressure region will drag in more biogas and enrich the turbulence with air. Hence there is a pressure difference created between the inlet and throat.

$$p_1 - p_2 = \frac{{v_2}^2 - {v_1}^2}{2}\rho \quad \text{(E1)}$$

Applying continuity equation, $A_1 v_1 = A_2 v_2 = Q$ (E2)

$$\Delta P = \frac{{A_1}^2 - {A_2}^2}{{A_1}^2 \times {A_2}^2}\rho Q \quad \text{(E3)}$$

Analytical method

The analytical method suggested by Mitzlaff (Von Mitzlaff, 1988) was adopted to obtain the base dimensions of the biogas mixer. The biogas mixer was designed for the 4-stroke, 1- cylinder SI engine of continuous rated power and speed of 3.3 kW and 3000 rpm, respectively. The swept volume and manifold connection diameter of the engine were 196 CC and 19 mm, respectively. The outlet diameter of the biogas mixer was fixed at 19 mm to easily attach with the engine intake. Due to dimensional constraint, the air inlet diameter

of the biogas mixer was also fixed and is 20 mm as shown in **Fig. E- 2**. The volumetric and the break thermal efficiency of the engine are consideredas70% and 30% respectively and was obtained while operating the engine at 3000 rpm with gasoline. The design of the biogas mixer is based on the methods reported in the literatures (BS EN ISO 5167-1, 1997; Von Mitzlaff, 1988). There are some critical designing parameters of the mixer namely converging angle, diverging angle, nozzle angle, nozzle diameter, number of nozzles, throat diameter and the length of the diverging section, which has also been considered carefully while designing the biogas mixer.

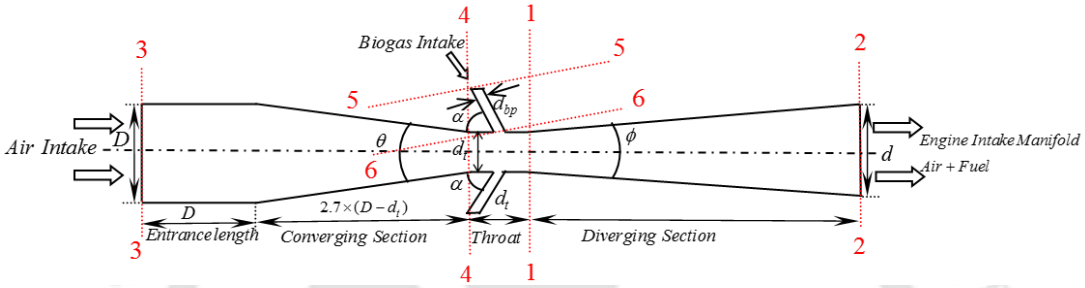

Fig. E- 2: Different parameters of venturi type biogas mixer

The flow in the mixer is assumed to be incompressible and unidirectional. The pressure is assumed to be constant throughout the length of the throat. The volumetric air intake to the engine was calculated from *Eq. E4* assuming the volumetric fuel demand of the engine is calculated from *Eq. E7*. V_d, V_2, N, η_{BTH},F_{cvol}, and C_V are the swept volume, volumetric air intake, engine speed, thermal efficiency, volumetric fuel intake, and calorific value of the fuel (17000 kJ/kg) respectively. The volumetric air and fuel intake to the engine were 0.00343 m^3/sec and 0.000575 m^3/sec, respectively at section 2 as shown in **Fig. E- 2**. As mentioned earlier, the outlet diameter of the biogas mixer was fixed to be 19 mm at section 2. Flow velocity at section 2 was calculated from the continuity equation as the volumetric air and fuel flow rate were calculated. The flow velocity at section 2 was found to be 14.12 m/sec.

The flow velocity at section 1 could not be lesser than or equal to the velocity at section 2 because there may be chances of back flow or no flow at the above-mentioned condition. The maximum velocity at section 1 could not cross 150 m/sec because the flow becomes compressible (Mach no exceeds 0.33) above this range. To determine the possible range of throat diameter, continuity equation is applied across section 1-2 with two imposed conditions. Since the volume flow rate at section 2 and the maximum and minimum

velocity at section 1 are known, the possible range of throat diameter at section 1 could be in the range of 6 to 19 mm as calculated from *Eqs. E5* and *E6*, respectively. The velocity of air flow at section 3 was calculated from the data obtained by the volumetric air consumption and was 10.91 m/sec. The air intake diameter was fixed to be 20 mm and the pressure was assumed to be atmospheric at section 3 and 5. The flow velocity just before the biogas inlet pipe (section 5) was found 11.439 m/sec by fixing the outlet diameter of the connecting biogas pipe as 8 mm.

$$V_2 = \eta_{vol} \frac{V_d}{2000 \times 60} \times N \quad \text{(E4)}$$

$$A_{1\min} v_{1\max} = V_2 \quad \text{(E5)}$$

$$A_{1\max} v_{1\min} = V_2 \quad \text{(E6)}$$

$$\eta_{BTH} = \frac{BP}{Fcvol \times Cv} \quad \text{(E7)}$$

The diameter of the throat (d_t) of the biogas mixer is lying in the range of 6 to 19 mm. Hence for each possible throat diameter the diameter of biogas pipe (d_{bp}) along with the pressure and velocity at each section was calculated and the required values are placed in the **Table E- 1**. As shown in **Table E- 1**, with increasing diameter of the throat, the velocity difference across section 1-4 is reduced. However, the throat pressure is increasing and approaching towards the atmospheric pressure. As observed from Table E1, the pressure (Pv) at throat diameter 11 mm is 100.94 kN/m^2 which is quite close to the pressure at section 3 i.e., 101.325 kN/m^2. Hence, beyond this point there will be possibility of no flow or back flow if the throat diameter is increased. Hence, the throat diameter of 10 mm is quite acceptable as the velocity difference across section 1 and 4 is minimum in this range. The corresponding diameter of biogas pipe was found 4.05 mm which is approximately 4 mm. But, as suggested in literature (Bora et al., 2013; Bora and Saha, 2015b) for asymmetric mixing of air and biogas or gaseous fuel, the venturi gas mixer should contain at least two gas inlets. Hence, the diameter of each biogas pipe has been proposed to be 2 mm for throat diameter of 10 mm. So d_t and d_{bp} are fixed to be 10 mm and 2 mm, respectively for further computational analysis using ANSYS 14.5. The converging angle (θ) of the biogas mixer was found as 21.34^o from the geometry by fixing the length of the converging section as 2.7*(D – d_t). Hence the obtained converging angle is considered to be optimized for the throat diameter of 10 mm. It was also reported (BS EN

ISO 5167-1, 1997) that, the diverging angle (ϕ) should vary in between 7-15°. So, the diverging angle was arbitrarily fixed to be 8°and the inclination angle of biogas pipe (α) along with its position at throat is optimized for the above fixed parameters by rigorous simulation and described in the section of computational method.

Table E- 1: Diameter of biogas pipe, velocity and pressure at required section at each throat diameter

Throat diameter (d_t) mm	Velocity at section 1 m/sec	Velocity at section 4 m/sec	Difference in velocity at section 1and 4 m/sec	Throat pressure (P_v) kN/m^2	Velocity of biogas pipe at section 6 m/sec	Diameter of biogas pipe (for two inlets) mm
6	141.74	121.31	20.43	92.86	123.57	1.22
7	104.14	89.13	15.01	96.79	90.86	1.42
8	79.73	68.24	11.49	98.69	69.65	1.62
9	63.00	53.92	9.08	99.71	55.13	1.83
10	51.03	43.67	7.36	100.29	44.76	2.03
11	42.17	36.09	6.08	100.94	37.11	2.23
12	35.44	30.33	5.11	101.26	31.32	2.42

Computational method

The converging angle and the throat dimeter of the biogas mixer were considered 21° and 10 mm respectively by analytical method in section E.1. But the diverging angle was fixed to be 8°, which was chosen arbitrarily from the specified range 7°-15° as suggested in the literature. The position and orientation of biogas pipe plays an important role in preparing the homogeneous mixture of air and biogas itself in the diverging section of the mixer. Hence, its position and orientation at the throat of the mixer was optimized for the above fixed parameters in this section. For the specified purpose, the position of the biogas pipe was evaluated at two different locations on the throat along with a range of orientation of biogas pipe from 30°-150°. The position of the biogas pipe was evaluated both at the inlet and middle of the throat. ANSYS Workbench 14.5 was chosen to study the effect of the position and orientation of biogas pipe on different parameters at each section of the biogas mixer. The 2-D geometry of the biogas mixer was modelled using the tool of Fluent (design modeler) and the 2-D geometry was divided into 1573 unstructured grids along with 1748 nodes while meshing using ANSYS ICEM CFD. The mesh file of the 2-d geometry is then analyzed in Fluent [ANSYS CFD]. The simulation is based on 2D space,

steady and pressure-based solver. The flow is considered to be 2D, viscous and incompressible. The realizable k-ϵ model with standard wall function and species transport model was used to solve the flow problem governing inside the gas mixer for three inlets; one was air inlet and other two were for biogas inlet. The TKE Prandtl number, TDR Prandtl number and Energy Prandtl number along with C2-Epsilon were fixed to be 1, 1.2 0.85 and 1.9 respectively. The basic *Eqs. (E8, E9 &E10)* governing the flow model along with the equation of mass conservation, momentum and energy were summarized in the conservative form of the Navier-Stokes equations (Stewart et al., 2007). Since in the present case the flow is steady and incompressible, density (ρ) is assumed to be constant and time variation of any property is zero. 'S_i' is the externa force per unit mass, 'h' is the thermal enthalpy, 'Q_H' is the heat source or sink per unit volume, 'S_{ij}' is the viscous shear stress tensor, 'q_i' is the diffusive heat flux. The subscripts are used to denote summation over the three coordinate directions.

$$\frac{\partial \rho}{\partial t}+\frac{\partial}{\partial x_i}\left(\rho U_i\right)=0 \tag{E8}$$

$$\frac{\partial \rho}{\partial t}\left(\rho U_i\right)+\frac{\partial}{\partial x_i}\left(\rho U_i U_j\right)+\frac{\partial p}{\partial x_i}=\frac{\partial}{\partial x_j}\left(\tau_{ij}+\tau_{ji}\right)+S_{ij}, i=1,2,3 \tag{E9}$$

$$\frac{\partial \rho}{\partial t}\left(\rho H\right)+\frac{\partial}{\partial x_i}\left(\rho U_i H\right)=\frac{\partial}{\partial x_i}\left(U_j\left(\tau_{ij}+\tau_{ji}{}^{R}\right)+q_i\right)+\frac{\partial P}{\partial t}-\tau_{ij}{}^{R}\frac{\partial U_i}{\partial x_j}+\rho\varepsilon+S_i U_j+Q_H \tag{E10}$$

$$H=h+\left(\frac{u^2}{2}\right) \tag{E11}$$

Boundary condition and initial condition

The boundary conditions shown in **Fig. E- 3**were used to represent the flow in the mixer for the CFD analysis. To match the flow at high speed with turbulent modeling, the boundary conditions should be appropriately defined (Gorjibandpy and Sangsereki, 2010). The turbulent intensity was considered to be 2%. The pressure and velocity at air inlet were considered to be 101325 N/m^2 and 10.91 m/sec respectively. The pressure and velocity at biogas inlet were considered to be 101325 N/m^2 and 177.67 m/sec, respectively. The mass fraction of CH_4, N_2, O_2, CO_2 and H_2O at biogas inlet were considered to be 0.6, 0.01, 0.005, 0.38 and 0.005. The outlet pressure was assumed to be atmospheric. The outer wall is assumed to be adiabatic.

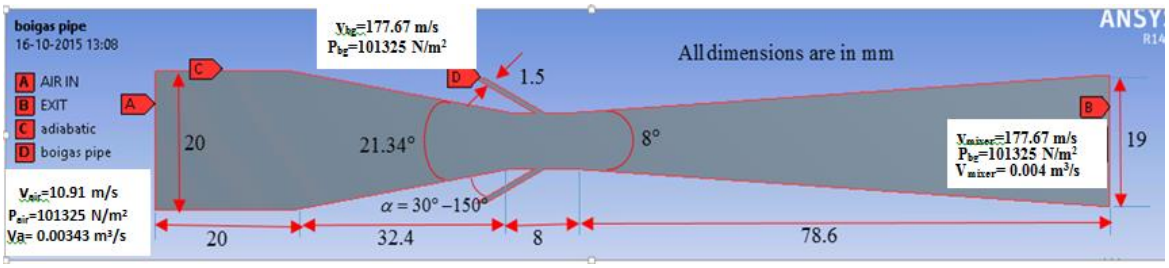

Fig. E- 3: Schematic diagram of the biogas mixer with Initial and boundary conditions

E2. Findings and discussion

To optimize the position and orientation of the biogas pipe with the defined parameters of the venturi type biogas mixer, the position and orientation of the biogas pipe has been varied and its effect on the pressure, velocity and mass fraction concentration at different sections has been analyzed and reported in this section. The position of the biogas pipe has been evaluated both at the inlet and middle of the throat. At each throat position the orientation of the biogas pipe has been varied in-between 30°-150°. After applying the boundary conditions for each geometrical modeling, the coupled scheme was adopted for the pressure velocity coupling and second order upwind scheme was chosen for spatial discretization in Fluent solution method. The solutions were converged to an accuracy of $1e^{-6}$ and the pressure, velocity and mass fraction contours were analyzed to find out the optimum position and orientation of biogas pipe. While the position of biogas pipe was at the inlet of the throat, the pressure and velocity of the biogas mixer at different sections were found out and reported in **Table E- 2**. Similarly, **Table E- 3** represents the variation of velocity and pressure at different section of the biogas mixer while the position of the biogas pipe was placed at the middle of the throat.

As it is clear from **Table E- 2** that, the difference of pressure and velocity across the throat is increasing along with increasing in orientation of biogas pipe at the throat which is not acceptable because of the constant cross section and low-pressure zone of the throat. The length of the throat is 8 mm and the stream of biogas entering with in the specified range will mostly diffuse near the boundary and will not affect much to the center line pressure and velocity. Hence, the orientation of the biogas pipe at which the pressure and velocity fluctuation is minimum across the throat may be treated as the optimized condition. It was also observed that at 30° and 40° orientation of the biogas pipe, the

pressure difference is negative which signifies the pressure at section 1 is higher than the pressure at section 4, which will initiate the back flow. Hence the orientations creating back flow were rejected and the orientation at which the pressure and velocity difference is minimum is proposed to be the optimized orientation for the corresponding position of biogas pipe. Similar trend is also observed when the position of the biogas pipe was placed at the middle of the throat. As observed from **Table E- 3**, the pressure and velocity difference were increasing along with the orientation of the biogas pipe at the throat which is undesirable. The pressure and velocity difference were also observed to be negative at an orientation of 30^o and 40^o of biogas pipe which is again not acceptable due to back flow. The minimum fluctuation of pressure and velocity were observed across the throat at an orientation of 50^o of the biogas pipe.

The fluctuation of pressure and velocity across the throat was observed to be minimum at an orientation of 50^o of the biogas pipe at both of the position of throat. Hence, the comparison of both cases at the same orientation was made to find out the optimized position. As observed from **Table E- 3**and **Fig. E- 4**minimum fluctuation of velocity and pressure across the throat were observed when the biogas pipe was placed at the middle of the throat. Hence the best possible orientation and position were proposed to be 50^o orientation of the biogas pipe at the middle of the throat. But the velocity, pressure and homogeneous mixing contours still need to be verified to approve the proposed condition to be optimized.

Table E- 2: Centre line pressure and velocity at different sections of the biogas mixer while the biogas pipe positioned at throat inlet

Orientation of Biogas Pipe	Pressure at different sections of Venturi type biogas mixer in N/m2				Velocity at different sections of Venturi type biogas mixer in m/sec				Pressure difference across throat N/m2	Velocity difference across throat m/sec
	S1	S 2	S 3	S 4	S 1	S 2	S 3	S 4	S 4-1	S 1-4
30^o	100205.8	101323.3	100176.3	100120	3.129	11.957	4.819	10.66	-85.86	-7.53
40^o	100750.5	101323.4	100792.9	100726.1	13.91	13.42	4.819	11.63	-24.45	2.28
50^o	100908.9	101323.4	101009.6	100952	21.44	14.81	4.819	11.24	43.08	10.2
60^o	100928.3	101321.8	101298	101215.4	31.25	18.88	4.819	12.91	287.1	18.33
70^o	100877.8	101323.1	101516.8	101428.9	38.22	18.2	4.819	13.15	551.1	25.06
80^o	100706.8	101323.1	101726.7	101639	46.64	18.47	4.819	13.06	932.18	33.57
90^o	100830.8	101323.2	101878.5	101797.3	42.78	15.66	4.819	12.74	966.5	30.04

140º	100329.7	101323	102387.3	102253.2	59.71	16.89	4.819	16.56	1923.4	43.15
150º	100106.3	101322.9	102603.4	102330.1	67.2	16.41	4.819	21.85	2223.83	45.35

Table E- 3: Centre line pressure and velocity at different sections of the biogas mixer while the biogas pipe positioned at middle of the throat.

Orientation of Biogas Pipe	Pressure at different sections of Venturi type biogas mixer in N/m^2				Velocity at different sections of Venturi type biogas mixer in m/sec				Pressure difference across throat N/m^2	Velocity difference across throat m/sec
	S1	S 2	S 3	S 4	S 1	S 2	S 3	S 4	S 4-1	S 1-4
30º	100207	101233.3	100205	100143.6	4.58	11.98	4.81	11.56	-64.1	-6.98
40º	100904	101233.2	100749	100683.8	20.4	15.41	4.81	11.59	-220.59	8.81
50º	100879	101233.4	100921	100882.1	16.19	14.74	4.81	11.39	2.55	4.8
60º	101226	101233.5	101209	101313.7	24.46	18.28	4.81	11.60	87.4	12.85
70º	100969	101233.3	101451	101382.8	34.62	19.13	4.81	11.84	413.44	22.77
80º	100759	101232.6	101807	101738.6	48.19	17.91	4.81	11.86	1453.47	36.33
90º	100555	101232.3	102080	102008.5	55.91	16.21	4.81	12.07	1453.47	43.83
140º	100500	101232.7	102445	102373.3	62.32	16.43	4.81	12.15	1873.29	50.17
150º	100266.1	101232	102736	102666.8	66.69	15.66	4.81	11.96	2400.65	54.73

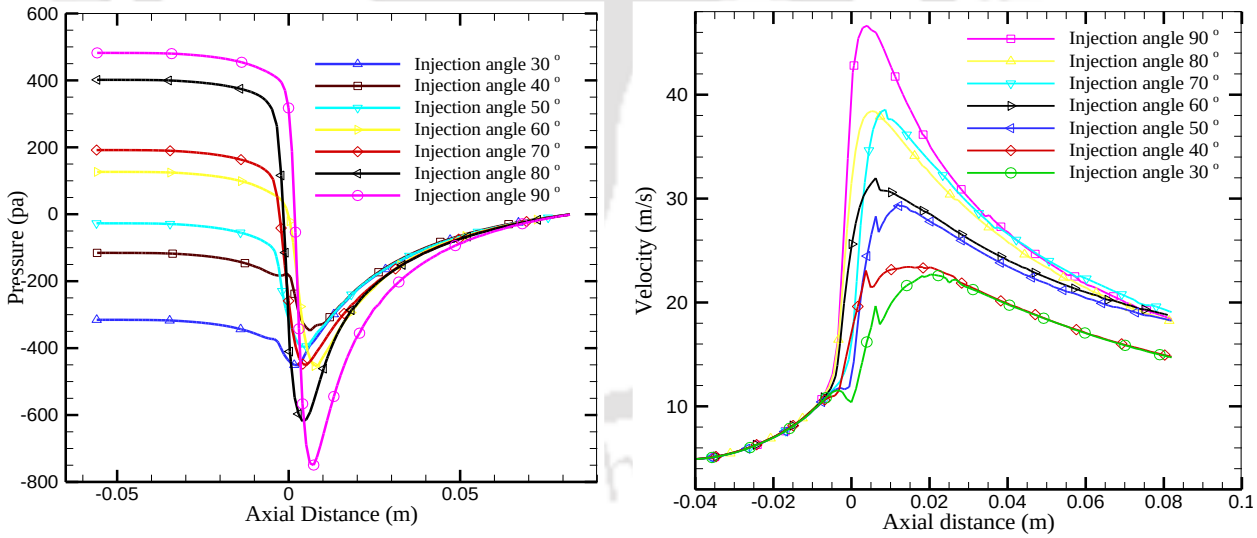

Fig. E- 4: Pressure and Velocity variation at the center line along length of the biogas venturi mixer with biogas pipe placed at the middle of the throat and at different orientation

Pressure analysis

Fig. E- 5(a) shows the pressure contour of the biogas venturi mixer when the biogas pipe is placed at the middle of the throat at an angle of 50º. **Fig. E- 5(b)** represents the

variation of static pressure across the length at the center line of the biogas mixer. The pressure shown in both of the figures are gauge pressures. For a venturi biogas mixer, the mixing of the air and biogas will be proper if the pressure drop is uniform throughout the throat of the biogas mixer. As shown in **Fig. E- 5(a),** the contour of static pressure is almost uniform in the throat section. However, the maxim pressure drop was observed at section 4 (inlet of the throat) and is 62.6 N/m^2 as shown in **Fig. E- 5(b)**. This improved pressure drop enhances the flow rate of biogas into the biogas mixer (Cullen and McGovern, 2009). This leads to the homogenous mixing of biogas and air which would result a proper combustion of air-fuel mixture. Similar kind of pressure distribution is also observed in the literature(Umesh et al., 2012).

Velocity analysis

The contour of velocity across the biogas mixer is shown in **Fig. E- 6(a)** when the biogas pipe is placed at the middle of the throat at an angle of 50^o. As shown in **Fig. E- 6(b)** the centerline velocity is increasing across the converging section and is maximum at the throat. The velocity fluctuation across the throat was found minimum compared to other cases enlisted in **Table E- 2**and **Table E- 3**. Since velocity of the mixing species is important from the point of view of fuel air transport which comprises an integral part of combustion. As shown in **Fig. E- 6(a),** the velocity profile of the biogas demonstrates the formation of wider velocity stream. With closure observation it has been noticed that due to the high stream velocity of biogas (177.6 m/sec) entering to the mixing zone, the flow becomes turbulent and the mixture becomes homogenous.

Analysis of mass fraction of CH_4

Figure E7(a) express the counter of CH_4 for the venturi type biogas mixer with biogas pipe inclination angle 50^o. For superior combustion, the air-fuel mixture needs to be homogeneous and uniform. As shown in **Fig. E-7 (a)** at the throat there are two distinct stream of biogas which slowly mixes with the air in the diverging section and disappears. It has been observed from **Fig. E-7 (b)** that the biogas is supplied at the throat and the CH_4 mass fraction starts diffusing slowly in the divergent section and became steady in the rest of the section. It signifies the homogenous mixing since the CH_4 is diffused completely in air along the diverging section.

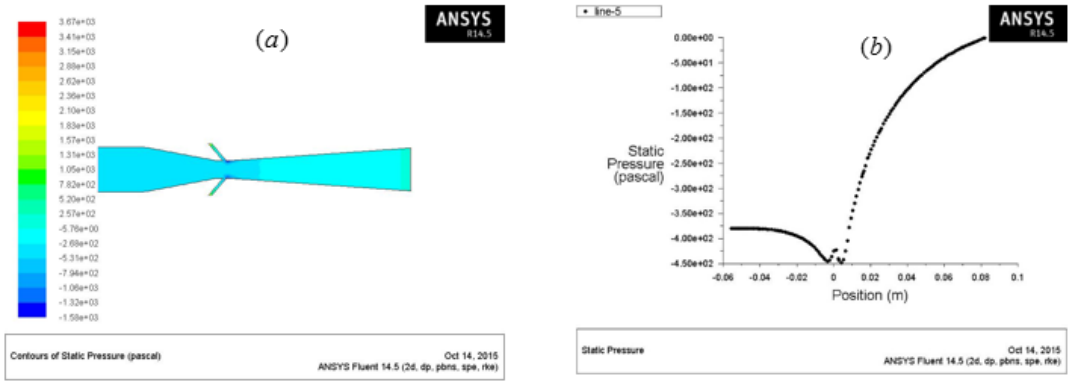

Fig. E- 5:(a) Pressure contour of the biogas venturi mixer (b) Static pressure variation at the center line along the biogas venturi mixer with biogas pipe placed at middle of the throat and oriented at 50^{o}

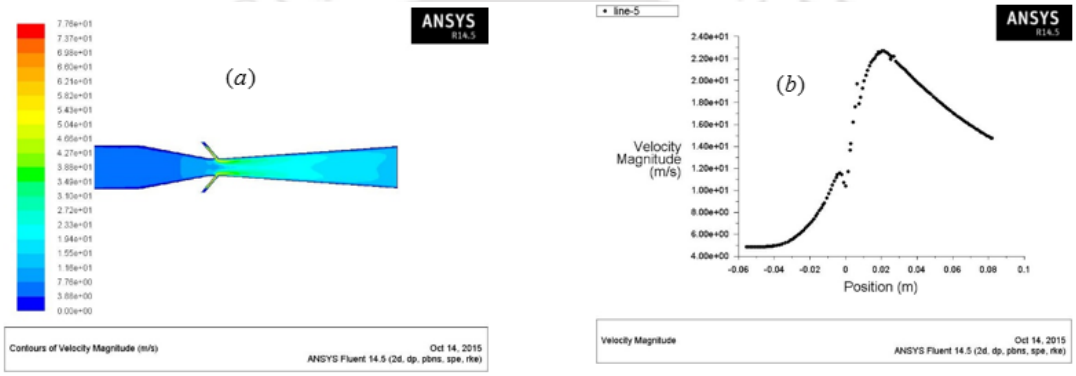

Fig. E- 6:(a) Velocity contour of the biogas venturi mixer (b) Velocity variation at the center line along the biogas venturi mixer with biogas pipe placed at middle of the throat and oriented at 50^{o}

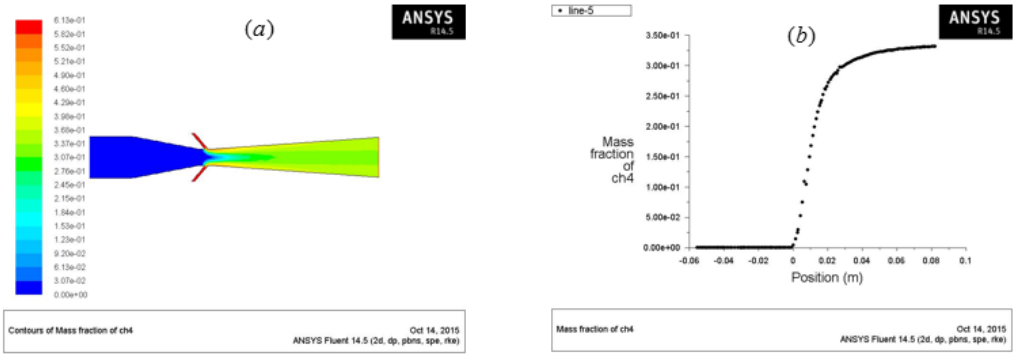

Fig. E- 7:(a) CH4 mass fraction contour of the biogas venturi mixer (b) Mass fraction of CH4 at the center line along the biogas venturi mixer with biogas pipe placed at middle of the throat and oriented at 50^{o}

E3. Conclusion

From the above enlisted observations, it has been proposed that the optimum throat diameter of the venturi type biogas mixer should be 10 mm provided that the inlet and out

let diameter of the biogas mixer are 20 and 19 mm, respectively. Depending on the throat diameter of the mixer, the diameter of the biogas supply pipe is optimized and found to be 2 mm with two biogas inlets at the throat. The position and orientation of the biogas pipe are also optimized in this study. The inclination angle of the biogas pipe is proposed to be 50^{o} and the middle position of the throat is suggested to utilize for superior mixing of air and biogas. The optimized dimensions of biogas mixer have been identified which is supposed to be attached to the engine intake system along with the existing carburetor so as to enable the engine to run with biogas and gasoline independently.

Appendix-F

Experimental Uncertainties

F1. Uncertainty analysis

It states the possible error or the uncertainty in the outcome based on the recorded experimental data. The current investigation involves three different experimental setup (*Engine 1, Engine 2, and Engine 3*) which further includes unlike measuring techniques and instrumentation for monitoring the performance parameters. The measuring instruments used in the current investigation are made by different manufacturers and follow different methodologies to measure several unlike parameters. Moreover, the accuracy of those measuring devices is instrument specific and dependent on the operating conditions as well as surrounding experimental environment. The systematic errors are dependent on the resolution of the measuring device, whereas the random errors are completely dependent on the operating condition and surrounding experimental environment such as mechanical vibration, electrical or magnetic interference, detector variation and data acquisition. Hence, the systematic and random errors associated with the measuring instruments not only develop a certain band of uncertainty in the measuring parameters, but also reflect in the derived parameter. Kline and McClintock along with Moffat (Kline and McClintock, 1953; Moffat, 1982) have proposed the most precise method to estimate the level of uncertainty in the experimental data. The proposed method uses the root mean square technique to evaluate the associated uncertainties in the experimental data by considering the random and systematic errors. The systemic errors of the measuring instruments are represented in **Table F- 1**and are obtained from the resolution and accuracy of the measuring instruments.

Let Y_1, Y_2, Y_3, Y_4… Y_n are the systematic errors corresponding to the instruments that get involved in deducing the performance parameter N and δN_1 is the resulted cumulative systematic uncertainty evaluated from *Eq. F1*. This systematic uncertainty remains unaltered irrespective of the operating condition of the engine**.** Similarly, the random uncertainty δN_2 associated with parameter N can be calculated using *Eq. F2* where X_1, X_2,

X_3 ,X_4,…X_n are the independent variables. The random errors associated with the independent variable (δX_n) are represented in **Table F-2.** The overall uncertainty of the measured parameters is represented as U_N which is calculated from *Eq. F3* that includes component of both the systematic and random uncertainty. The overall uncertainty corresponding to different performance parameters is presented in **Table F- 3**.

$$\delta N_1 = \left[(Y_1)^2 + (Y_2)^2 + (Y_3)^2 + ... + (Y_n)^2 \right]^{\frac{1}{2}} \quad \text{(F1)}$$

$$\delta N_2 = \left[\left(\frac{\partial N}{\partial X_1} \delta X_1 \right)^2 + \left(\frac{\partial N}{\partial X_2} \delta X_2 \right)^2 + ... + \left(\frac{\partial N}{\partial X_n} \delta X_n \right)^2 \right]^{\frac{1}{2}} \quad \text{(F2)}$$

$$U_N = \sqrt{(\delta N_1)^2 + (\delta N_2)^2} \quad \text{(F3)}$$

Table F- 1: Systematic error of the measuring instruments

Measuring Instruments		Systematic error of the measuring instruments (%)		
		Engine 1	Engine 2	Engine 3
Optical rpm sensor		± 0.3%	± 0.3%	± 0.3%
Optical crank angle encoder		± 0.3%	± 0.3	± 0.3%
Voltmeter		± 0.1%	-	-
Ammeter		±0.2%	-	-
Stain gauge type load cell		-	± 0.2%	± 0.2%
Open U-tube manometer		±0.2%	±0.2%	±0.2%
Air flow transmitter		-	± 0.5%	± 0.5%
Fuel flow transmitter (Liquid fuel)		-	± 0.1%	± 0.1%
Flow meters (Gaseous fuel)		±0.4%	± 0.5 %	± 0.5%
Piezo pressure sensor		±0.1%	±0.1%	±0.1%
Temperature sensors and transmitters		±0.3%	±0.3%	±0.3%
Exhaust gas analyzer	CO	± 3%		
	CO_2	± 3%		
	HC	± 3%		
	NO_x	± 1%		

Table F- 2: Random error of independent variables

Recorded parameters		Random error of independent variables		
		Engine 1	Engine 2	Engine 3
Engine speed		±3.3%	± 0.6%	± 0.6%
Engine load		±0.8%	± 1.3%	± 1.3%
Airflow rate		±1.1%	±0.4%	±0.4%
Biogas flow rate		±1.8%	±1.5%	±1.7%
LHV of biogas		±0.8%	±0.8%	±0.8%
LHV of gasoline		-	±0.9%	±0.9%
Temperature		± 0.1%	± 0.1%	± 0.1%
Cylinder pressure		± 0.2%	± 0.2%	± 0.2%
Cylinder volume		± 0.1%	± 0.1%	± 0.1%
Concentration in exhaust emission	CO	± 3.8		
	CO_2	± 1.8		
	HC	± 4.4		
	NO_x	± 3.6		

Table F- 3: Overall uncertainty corresponding to the performance parameters

Derived parameters		Systematic uncertainty (%)			Random uncertainty (%)			Overall uncertainty (%)		
		Engine 1	Engine 2	Engine 3	Engine 1	Engine 2	Engine 3	Engine 1	Engine 2	Engine 3
Performance Parameter	A/F	± 0.4	± 0.7	± 0.2	± 2.0	± 1.4	± 1.5	± 2.0	± 1.6	± 1.5
	BT	-	± 0.2	±0.4	-	± 0.1	± 1.8	-	± 0.3	± 1.9
	BP	± 0.4	± 0.4	±0.6	± 2.9	± 1.3	± 2.6	± 2.9	± 1.4	± 2.7
	BTE	± 0.5	± 0.8	±0.4	± 3.5	± 1.5	± 2.5	± 3.5	± 1.7	± 2.6
	BSFC	± 0.5	± 0.6	±0.6	± 2.4	± 1.9	± 1.4	± 2.8	± 2.1	± 1.6
	VE	± 0.4	± 0.6	±0.7	± 2.8	± 0.8	± 1.9	± 2.3	± 0.9	± 2.1
Combustion parameter	NHRR	± 0.3	± 0.3	±0.3	± 0.4	± 0.4	± 0.4	± 0.5	± 0.5	± 0.5
	MGT	± 0.4	± 0.6	±0.6	± 1.1	± 0.5	± 0.9	± 1.2	± 0.8	± 1.1
	MFB	± 0.3	± 0.3	±0.3	± 0.3	± 0.3	± 0.3	± 0.4	± 0.4	± 0.4
Emission parameter	CO	± 3	± 3	± 3	± 2.7	± 3.8	± 4.5	±4.1	± 4.9	± 5.4
	CO_2	± 3	± 3	± 3	± 1.2	± 1.8	± 1.6	± 3.2	± 3.5	± 3.4
	HC	± 3	± 3	± 3	± 4.3	± 4.4	± 4.6	± 5.3	± 5.3	± 5.1
	NO_X	± 1	± 1	± 1	± 3.3	± 3.6	± 3.6	± 3.3	± 3.7	± 3.7

F2. Sample uncertainty calculation

The sequential approach for the overall uncertainty estimation is explained in this section. As a sample calculation, the uncertainty associated with BP estimation of the biogas operated VCR SI research engine (Engine-2) at CR 12 has been elaborated. The overall uncertainty for the evaluation of BP can be calculated using *Eq.F4* where, U_{BP} is the overall uncertainty, $\left(\bar{U}_{BP}\right)_{Sys}$ is the average systematic uncertainty, $\left(\bar{U}_{BP}\right)_{Ran}$ is the average random uncertainty associated with the BP calculation for the engine over the operating speed range (1450-1700 rpm).

$$U_{BP} = \left[\left(\bar{U}_{BP}\right)_{Sys}^{2} + \left(\bar{U}_{BP}\right)_{Ran}^{2}\right]^{\frac{1}{2}} \quad \text{(F4)}$$

The BP of the engine is calculated using *Eq. F5*. Therefore, BP is the function of engine speed (N) and applied brake load (F) as shown in *Eq. F6.*

$$BP = \frac{2\pi NFr}{60,000} \quad \text{(F5)}$$

$$BP = f(N, F) \quad \text{(F6)}$$

The optical speed sensor and the strain gauge type load cell are the instruments used for the measurement of N and F, respectively. Therefore, the systematic errors (ε) associated with these measuring instruments are taken into consideration. In fact, the systematic error is instrument specific and hence, it is assumed to be constant for all operating condition of the engine. The systematic uncertainty of the BP can be obtained by considering the contribution from the systematic errors associated with both N and F by using *Eq. F7.*

$$(U_{BP})_{sys} = \left[(\varepsilon_N)^2 + (\varepsilon_F)^2\right]^{\frac{1}{2}} \quad \text{(F7)}$$

As mentioned in the **Table F- 1**, the systematic errors of optical RPM sensor (ε_N) and load cell (ε_F) are 0.3% and 0.25%, respectively. Therefore, the systematic uncertainty for the measurement of BP is calculated as mentioned in *Eq. F8.*

$$(U_{BP})_{sys} = [(0.3)^2 + (0.25)^2]^{\frac{1}{2}} = 0.39\% \quad \text{(F8)}$$

Since the systematic uncertainty is constant over the entire speed range of the engine at CR 12, the average systematic uncertainty $\left(\bar{U}_{BP}\right)_{Sys}$ is also having the same value i.e., 0.39%.

Similarly, the random uncertainties associated with the BP are the function of the random errors linked with the measurement of N & F. Therefore, random uncertainty of the BP can be calculated by using *Eq. F9*. The random uncertainty associated with BP at CR 12 and 1700 rpm is calculated by using *Eq. F10* and found to be 1.43%.

$$\delta_{BP} = \left[\left(\frac{\partial BP}{\partial N}\Delta N\right)^2 + \left(\frac{\partial BP}{\partial F}\Delta F\right)^2\right]^{\frac{1}{2}} \quad \text{(F9)}$$

$$\left(U_{BP}\right)_{Ran} = \frac{\delta_{BP}}{BP} = \left[\left(\frac{\Delta N}{N}\right)^2 + \left(\frac{\Delta F}{F}\right)^2\right]^{\frac{1}{2}} = \left[\left(0.58\right)^2 + \left(1.3\right)^2\right]^{\frac{1}{2}} = 1.43\% \text{ (For 1700 rpm)} \quad \text{(F10)}$$

Similarly, the random uncertainties associated with different operating speed (and corresponding load) of the engine are calculated by using *Eq. F9* and are found 1.36%, 1.31%, 1.26%, 1.24%, 1.22%, 1.2% for the speeds of 1650,1600,1550,1500 and 1450, respectively. The average random uncertainty $\left(\bar{U}_{BP}\right)_{Sys}$ associated with the BP measurement is evaluated considering the individual uncertainties related with the speed range of the engine by simple averaging technique and the value is found to be 1.27%. Therefore, the overall uncertainty for the measurement of BP is calculated by using the *Eq. F11* and is found within the uncertainty band of ±1.35%. The overall uncertainties of the other operating parameters are calculated by following the above-mentioned procedure and presented in **Table F- 3.**

$$U_{BP} = \left[\left(0.39\right)^2 + \left(1.27\right)^2\right]^{\frac{1}{2}} = 1.35\% \quad \text{(F11)}$$